UNIVERSITY OF SOUTHAMPTON

Multiwaveband studies of Be/X-ray binaries.

Nicholas Jonathan Haigh

Submitted for the degree of Doctor of Philosophy

DEPARTMENT OF PHYSICS AND ASTRONOMY
FACULTY OF SCIENCE

September 3, 2002

UNIVERSITY OF SOUTHAMPTON

ABSTRACT

FACULTY OF SCIENCE

DEPARTMENT OF PHYSICS AND ASTRONOMY

Doctor of Philosophy

Multiwaveband studies of Be/X-ray binaries.

by Nicholas Jonathan Haigh

Studies of three BeXRBs: A0535+262, AX J0051–733 and XTE J0111.2–7317 are presented. 15 years of spectroscopy and photometry of A0535+262 is analysed to reveal the global behaviour of a typical BeXRB in detail. The detection of the recently predicted varying resonant truncation, the simultaneity of truncation events with X-ray activity, and the governing rôle of a 1400 day cycle, probably a manifestation of precession of the circumstellar disc, are described. AX J0051–733, a recent SMC discovery, exhibits a coherent 0.7/1.4day photometric modulation, the period of which appears to be decreasing. Various possible explanations, none of them fully satisfactory, are discussed. XTE J0111.2–7317, also an SMC system, is embedded in a compact emission nebula. The nature of this nebula is examined and found to be an HII region ionised by the BeXRB.

Contents

List of Figures

List of Tables

Chapter 1

Background to Be stars and BeXRBs.

1.1 Introduction

This purpose of this Chapter is to provide both a summary of the state of knowledge regarding Be stars and BeXRBs in general and the relevant background to A0535+262, the only system studied within these pages which has a sizable quantity of literature associated with it.

1.1.1 Definitions and phenomena

The 1867 observation by Father A. Secchi that γ *Cas* exhibited Hα line emission marked the discovery of the **Be** star, though they were not labelled as such until 1922 when Fowler proposed that the suffix **e** be used to denote stars of a type which do not generally exhibit line emission, but which have been observed to do so.

The modern definition is that a Be star is a non-supergiant B star whose spectrum

exhibits, or has at some time exhibited, one or more Balmer lines in emission. Despite some similarities (mostly superficial) with the Herbig Ae/Be stars, these are fundamentally different in that their emitting regions arise from *accretion* as opposed to *mass loss* in the Be stars, and they also show strong IR dust emission.

1.2 Be stars

1.2.1 Photometric properties

Be stars possess a universal luminosity excess relative to B stars of the same spectral type and luminosity class (Briot et al., 1997; Fabregat et al., 1996), which increases towards longer wavelengths. Fabregat and Torrejon (1998) found a mean overluminosity of 0.3 in m_V for B0-5e stars, whilst a tight correlation with the equivalent widths (W_λ) of the Balmer lines is observed (Zorec and Briot, 1991), confirming that the two dominant observational characteristics (line emission and IR excess) of Be stars are due to the same material (see also Section 2.5). This excess frequently becomes the dominant source of flux longwards of several microns and continues into the IRAS bands.

Gehrz (1974) showed that the this excess emission is best explained as arising from a combination of free-free and bound-free (ff/bf) emission from a predominantly hydrogen plasma. This result critically showed that another dominant source of astrophysical IR excess, thermal emission from dust, was not responsible, thus enabling theories of the processes underlying the Be phenomenon to progress. Observations in the near IR (JHKL wavebands) where the disc excess and stellar contributions are of approximately equal importance therefore provide a sensitive measure of the global state of Be discs. At this point a possible connection of Be stars with the B[e] stars should be acknowledged (Allen and Swings, 1976); such objects are defined by their SEDs displaying strong thermal dust emission, and many also exhibit forbid-

den lines in their spectra. In many ways B[e] stars resemble extreme Be stars, to the extent that their spectra are forests of emission lines and few if any photospheric lines are visible. Be stars do not show forbidden line emission because the regions of their outer discs of sufficiently low density are simply too small, unlike B[e] stars which possess such high base densities that enormous low density regions exist. A subset of the heterogeneous B[e] stars, in particular the sgB[e], also contain disc-like circumstellar envelopes (Zickgraf, 2000), making their affiliation with Be stars all the more plausible.

Several works have commented on the overluminosity of Be stars relative to B stars of equivalent Sp/L class even after allowing for the continuum excess. Briot, Robichon and Hubert (1997) found that this overluminosity is greater for later Be stars despite their disc related emission characteristics being weaker. One might expect this result based upon the observation that Be stars represent a subset of *evolved* B stars (Section 1.3). However, as Zorec and Briot (1991) point out, the real stellar menagerie is populated by a continuum of luminosity classes, and our penchant for pigeonholing into several fixed luminosity bins necessarily leads to disagreement between 'theoretical' magnitudes for a Sp/L type and the range present in stars assigned to this type.

Negueruela et al. (1999) found that the circumstellar disc of V0332+53 was entirely optically thick in the JHK wavebands. This appears to be the case in most BeXRBs due both to their severe truncation and consequent higher base density than isolated Be stars, whilst these in general are probably only optically thick in their inner, denser regions (Dachs et al., 1988). X Per appears to be an exception, due to it's atypically large circumstellar disc amongst the BeXRBs (Clark, private communication).

1.2.2 Spectroscopic properties and physical structure

Observations in the optical/IR regions reveal Balmer and Brackett lines, particularly those lower in each series, to be in emission. Further lines, most notably those of He I and Fe II, also show emission, though not in all Be stars.

Most early work explained Be Balmer line profiles, in particular those which displayed double peaks, as due to a spherically symmetric expanding wind allied to the processes generating P Cyg profiles. Whilst this picture continued to be invoked until quite recently (Doazan et al., 1982; Doazan et al., 1988) and can indeed explain many observations albeit with increasingly contrived details, the modern consensus had first emerged in 1931 when Struve made the observation that stellar $vsini$ correlated with Balmer line FWHM. This led him to propose the geometry which is accepted today, that of a rotating, axially symmetric lenticular disc of material in the equatorial plane of a B star, the observed variation between stars arising primarily from differing inclination angles (Figure 1.1). Numerous further publications, for example the finding of Dachs et al. (1986) that $W_{\lambda H\alpha}$ scaled with the square of the calculated disc radius, have confirmed this geometry. Even this simple picture is able to explain many of the observational properties of Be stars.

The profiles of emission lines are primarily determined by the kinematic (Struve, 1931) and density structures of the emitting regions (Section 1.2.3); thermal broadening is generally negligible. The convolution of these factors leads to a variety of profile shapes, though most can be decomposed into pairs of V and R (Violet and Red) peaks displaced by $\pm v_{Kepler} sini$, though not necessarily of similar intensity. Thus most often profiles are variations upon double or single peaked profiles, with widths of several hundred $\mathrm{km\,s^{-1}}$. The radial velocities are $< 1\,\mathrm{km\,s^{-1}}$, which is confirmed for A0535+262 in Chapter 2. Lines of Fe II are particularly valued as being optically thin they display almost purely kinematically derived structure, whereas Hα may be altered considerably by optical depth effects.

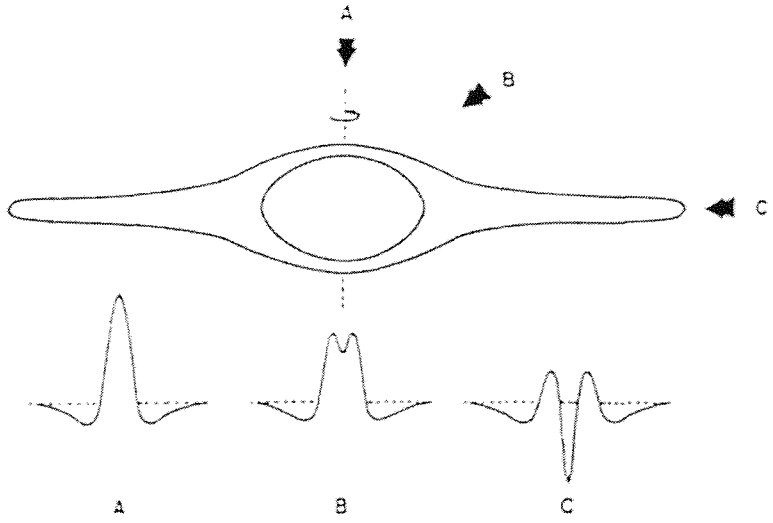

Figure 1.1: Otto Struve's model for the origin of single peaked, double peaked and shell profiles in a flattened circumstellar disc. From Struve (1931).

The consensus of opinion therefore has converged on the concept of the emitting region taking the form of an equatorial disc. This geometry was finally put beyond doubt by direct interferometric imaging (Stee et al., 1998; Quirrenbach et al., 1997) which showed that while the stars were not resolved in continuum wavelengths, Hα and He I revealed an extended and non-spherical appearance (Figure 1.2), and most showed significant asymmetries in Hα emission. The elongation position angles were fully consistent with the expected orientations of circumstellar discs from polarimetric observations. Furthermore, in cases like ζ Tau, the asymmetry is sufficient to restrict the disc opening angle to less than 20 degrees. ϕ Per has also been spatially resolved at radio wavelengths (Dougherty and Taylor, 1992).

The presence or absence of various lines informs us of the physical conditions (for example temperature and density) in the emitting material. Combined with line profile analysis this can reveal information regarding the spatial distribution of the conditions within the disc.

Some Be stars, most famously Pleione (Gulliver, 1977) display narrow absorption cores in the same lines which display emission. This is interpreted as absorption by

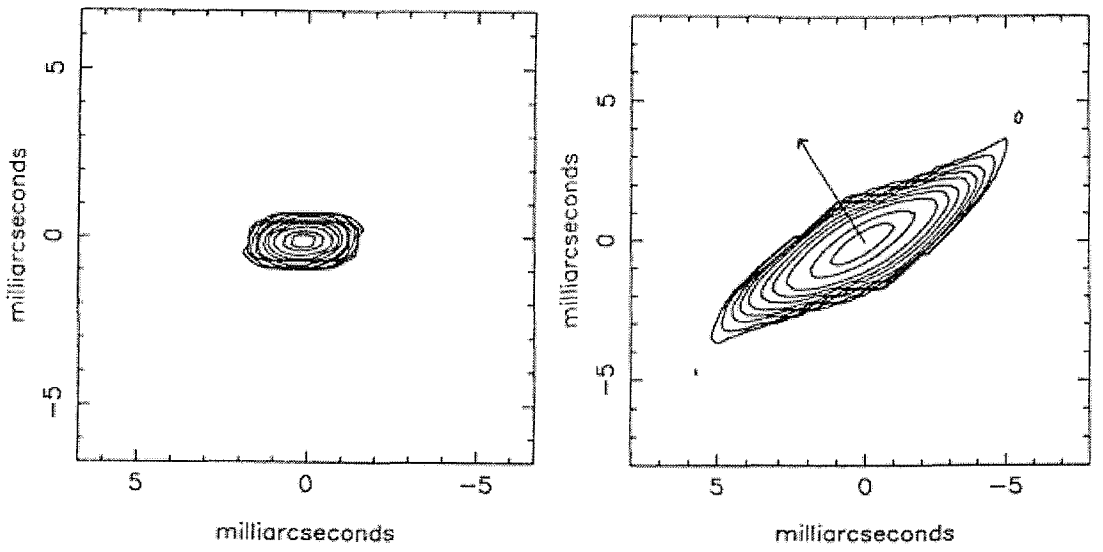

Figure 1.2: Reconstructed image of the Be star ζ Tau with the Mk III interferometer. 550nm continuum (left) and Hα (right). From Quirrenbach et al. (1994).

the same material responsible for emission seen in projection against the photosphere (Figure 1.1). These absorptions are often highly variable, and range from a central intensity of almost zero to complete disappearance, in which case the star has undertaken a transition Be-shell$\rightarrow$Be, presumably reflecting changes in the quantity of material along the line of sight. However, in view of the equatorial concentration of material in the Be stars, in order for a star to show shell lines it's inclination must be close to 90°, and thus $v \sin i \approx v$; such stars thus acquire considerable import (see also Section 2.4.0.3). For example observations universally reveal $\omega (= v_{rot}/v_{crit}) \sim 0.7$ (Porter, 1996) thus demonstrating that Be stars are, without exception, very fast rotators.

In contrast to the high densities, low ionisation and moderate velocities observed from the equatorial regions, UV observations reveal an altogether different environment. P Cyg profiles, regardless of system inclination, in the lines of highly excited species such as C IV and Si IV inform us of a quasi-spherical hot wind moving at up to 1500 km s^{-1}. These velocities and implied temperatures cannot exist in the same regions that gives rise to the Balmer emission and IR excess, and are thus attributed

to a high velocity polar wind, though by 'polar' the sense is more of 'non-equatorial' than restricted to very high latitudes.

A challenge to this theory has come from a short section in Rivinius et al. (2001). He cites the case of θ CrB, which declined from Be-shell status to become a B star, so far as optical spectroscopy is concerned, by the end of 1980. However, IUE continued to show a high (though declining) velocity wind until March 1982, following which the star resembled a B star in every respect. His interpretation is that the UV wind arose from ablation of the disc by the stellar radiation; the higher optical depth in the IUE lines enabled these characteristics to remain visible after Balmer emission had vanished but a vestige of disc remained. Subsequent sporadic enhanced UV wind episodes were then explicable as failed disc formation. He additionally notes that pole-on Be stars tend to display substantially weaker UV winds than moderately inclined or Be-shell objects. This could arise from the direct line of sight to the star intercepting little of the regions above the disc. Though this is a circumstantial theory with few hard facts to support it, it is sufficiently intriguing to be worthy of further study. However, in the absence of IUE this will probably have to wait some years.

1.2.3 Line profile formation

The derivation of physical parameters from spectral line profiles is critical to this work, and the work of Huang (1972) was instrumental in establishing this field.

Optically thick discs that span a relatively narrow radius range of a factor 2-3 are characterized by a relatively sharp emission edge (Figure 1.3), whilst discs that span a wider radius range, e.g. a factor 5 or more, should have a quite gradual edge. As can be seen, in this case line-profiles are not well-suited to determining whether the inner disc radius is detached significantly from the stellar surface.

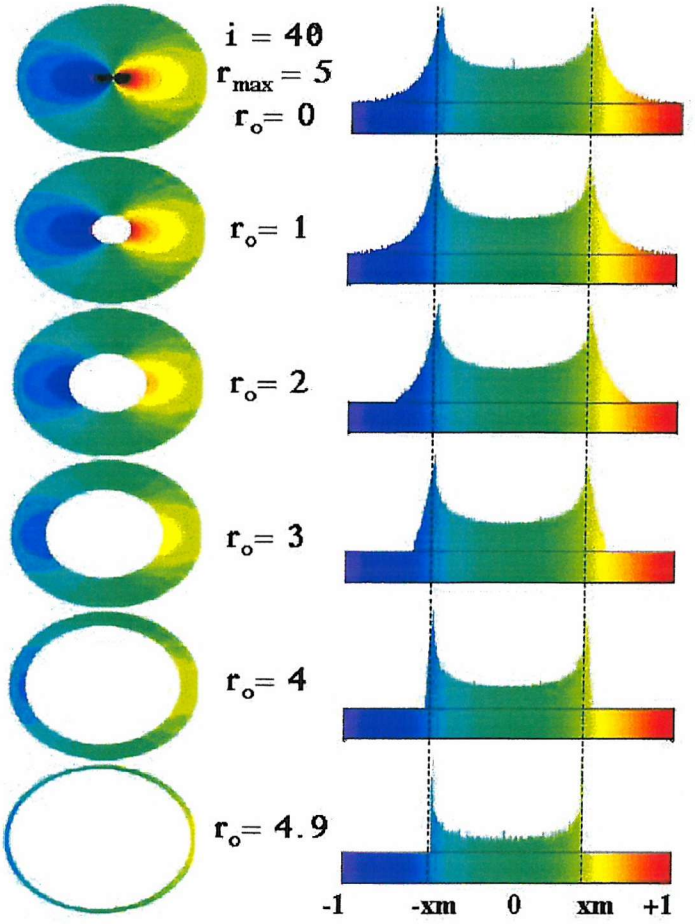

Figure 1.3: Theoretical line profiles from rotating annuli/discs delimitted by constant r_{outer} and variable r_{inner}. Top : $r_{inner} \ll r_{outer}$. Bottom: $r_{inner} \approx r_{outer}$.

In general, the velocity of the emission peaks ($\frac{1}{2}\Delta V_{peak}$) provides the projected orbital velocity at the outer edge of the disc. This is because the largest contribution to each velocity interval in the line profile comes from the region (Figure 1.3) at the furthest edge of the isovelocity contours, the 'bulk' radius (Rivinius et al., 2001). This approximation can fail in the case of steep density gradients combined with optically thin emission, where the large surface area of these outer regions is offset by the weak emission therefrom. The success of the Keplerian rotating disc in generating realistic line profiles, and it's ability to provide meaningful astrophysical results (see Chapter 2) in numerous studies provides overwhelmingly strong evidence for it's validity.

1.2.4 Variability

1.2.4.1 Photometric

Roche et al. (1993) noted cessation of all optical variability during periods of disc-loss ('faint states') in the BeXRB system X Per, when it's photometric properties converged with those of the underlying B star. This observation has been made for several systems, and it seems probable that all photometric variability in Be stars is attributable to changes in the disc (Roche et al., 1993; Negueruela et al., 1997; Clark et al., 1999a; Lyuty and Zaĭtseva, 2000), at least down to the minimal levels of variation observed in B stars. Thus the topic of photometric variability is primarily a study of the timescales and amplitudes of disc variability. As with the single-epoch studies of Be stars, a close correlation between line emission and photometric excess is seen within episodes of variability. However, by observing the changes in photometry and line emission simultaneously subtle properties of the Be disc may be divulged (see for example Section 2.6.3).

Substantial variability appears to be a characteristic of all Be stars. The timescale for gross changes in the overall disc properties are from several weeks to a year,

though at times of near disc-loss significant changes can be observed in hours-days. Long term photometry may also reveal longer term fluctuations over decades. Such variation can be seen in Figure 1.14, though NS effects could a factor in this case.

1.2.4.2 Spectroscopic

In addition to the changes described above manifesting themselves spectroscopically (i.e. as $W_{\lambda H\alpha}$), spectroscopy reveals many more subtle changes.

Phase changes Be stars may in general exhibit changes between Be and B phases on timescales of weeks to years, for example A0535+262 (Chapter 2). Such changes are simply explicable (symptomatically if not causally) as the loss of the circumstellar disc which gives Be stars their unique properties. These events thus show us the timescales involved in the distribution of material into a disc, and allow us a glimpse of the underlying B star.

High inclination systems may in addition to these states exhibit transient Be-shell phases (see Section 1.7).

V/R cycles. Probably the commonest form of spectral variability, excluding global W_λ changes, is the cyclical variation in intensity of the V and R peaks, usually expressed as the ratio V/R. The logical inference, that there is an asymmetry in emission between the appraching and receding lobes of the disc, has long caused confusion in that the *orbital* period of such material is of the order of days, whereas V/R variations have periods of years.

Mennickent and Vogt (1991) find, in their survey of 33 southern Be stars, that 76% display V/R cycles with a mean period of 7years, mostly from 2-13years, though 6 objects were found which show changes from $V < R$ to $V > R$ in 6-100 days.

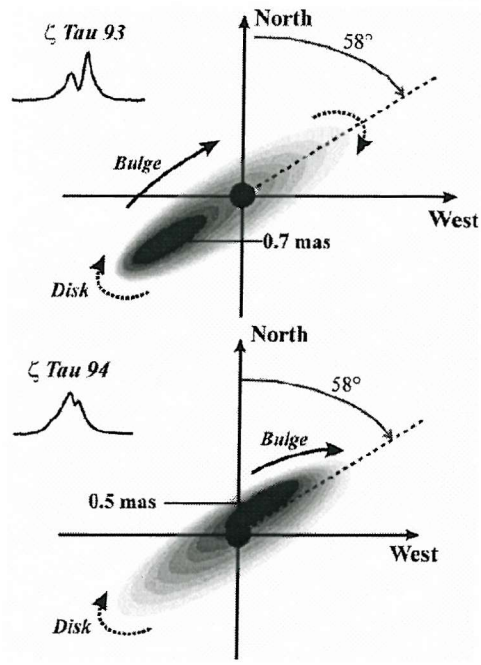

Figure 1.4: Schematic representation of ζ Tau in Hα from interferometric data showing agreement with asymmetries inferred from Hα spectra. From Vakili et al. (1998).

No correlation exists between V/R period and spectral/luminosity class or $v \sin i$, though only stars with $r_{H_\beta} < 4R_*$ showed the short term variations.

Such oscillations have in general been successfully explained as manifestations of Global One Armed Oscillations or GOAOs (Okazaki, 1991), which naturally gives the result that smaller discs exhibit shorter periods and also predicts the loose correlation with stellar properties. Impressive support has recently come from interferometric imaging achieving sub-mas resolution, which has detected enhancements in emission in precisely the locations suggested by spectra in the context of GOAOs (Figure 1.4), rotating in a prograde sense (as predicted for GOAOs) with a period of $\sim$ 3.1years.

Outbursts Rivinius et al. (2001) describe the appearance in profiles of Balmer, Fe II and He Iλ6678 lines of 'outbursts' in several well studied Be stars. As an example, they describe the appearence in He Iλ6678 of η *Cen* of high velocity components which propogate outwards from 1.2 to 3.3R_* over two months, the latter being a

typical value for the inner disc radius. In general these events are characterised by a 'plateau of emission' appearing across the line profile to significantly greater velocities than are seen for typical emission, or of well defined peaks at similarly high velocities. This maximum observed velocity, corresponding to the disc inner edge, gradually decreases until it reaches typical values. By a simple extension of the work of Huang (1972) this can be understood as the superposition of two annuli or discs of emitting material at differing radii, though the structures are probably better described as radially quasi-symmetric density enhancements than distinct rings of material. At times when no such outbursts are visible, an inner cavity of low density extending from the photosphere to $\sim 3R_*$ is invoked.

These events are at best extremely difficult to observe in Hα and to a lesser extent the entire Balmer series not only due to overwhelming emision from outer regions but because of scattering effects. Thus optically thin lines are preferred, and with it's strong radial dependence (Stee et al., 1998) He I 6678 emission enables relatively weak emission from small inner regions to be clearly seen.

Detailed analysis of line profiles in some early, active, Be stars has shown that the outer disc radius remains almost constant, whilst successive waves of material travel outward from close to the stellar surface. For ω CMa (B2IV-Ve) outbursts occur at a frequency of 200-330 days, with major outbursts seen in 1996 and 2000. Other stars have shown outbursts at intervals from weeks to years apart. These phenomena may be closely allied to so-called 'bumpers', Be stars detected by the MACHO project which exhibit sudden brightenings and gradual fades with possible 100-300day periodicities (Baade, 2000). It appears that these events are at least partially, if not solely, responsible for feeding material into the disc.

1.3 Origin of the Be phenomenon

Clearly the most important question underlying the totality of Be/BeXRB research is, what phenomena or mechanisms give rise to the dense equatorial disc that is their defining feature? Studies of variability, both spectral and photometric, show us that beneath this disc lies a fundamentally unassuming B star; this point is made most clearly by observations of Be stars spanning episodes of complete disc loss and regrowth.

1.3.1 Comparison of B and Be stars.

Fabregat and Torrejón (2000) found a strong age dependance in studying the Be/B star fraction in open clusters. Clusters younger than 10Myr, despite possessing the expected distribution of early OB stars, included no Be stars. The fraction peaked in clusters aged from 13-25Myr. Their conclusion is that the Be phenomenon must be strongly tied to evolutionary effects which appear in the latter half of the MS lifetime of a B star; these are suggested to be the onset of strong convection with an associated enhancement of magnetic field.

The Be phenomenon is observed from 08 to A1, reaching a maximum of 34% of the stellar population at B1 (Zorec and Briot, 1997), in all luminosity classes; towards later classes, and declining luminosity, the frequency drops steadily. This apparent connection with stellar luminosity was also demonstrated by Briot (1986), who showed in a comparative analysis of B0e-B5e with B6e-B9e objects that the earlier spectral classifications display larger equivalent widths (W_λ) than the later stars. Yudin (2001) demonstrated much the same effect with IR (V-L) excess declining towards later spectral types.

Another critical discovery was that Be stars have on average a higher $v \sin i$ than their non-emission brethren, the B stars. This trend continues into the Be popula-

tion, wherein fast rotating objects tend to exhibit larger $W_{\lambda H\alpha}$(Briot, 1986). These facts show that the Be phenomenon is inextricably linked with rapid rotation and high luminosity. Referring back to the definition of Be stars which hinted at the transient nature of the phenomenon, Be stars are observed to display varying proclivities towards displaying the phenomenon, from briskly rotating B7 stars which occasionally show emission features in the wings of Hα, to whirling B1 stars which have consistently displayed a large $W_{\lambda H\alpha}$ over decades. Such observations show that a tendency toward the Be phenomenon is a property possessed by stars to different degrees; it is not a black and white matter.

1.3.2 Origin of the circumstellar disc

Whilst there is no widely-accepted model for Be disks, the viscous decretion disk model appears to be the most successful at present (Porter, 1999). This model redistributes angular momentum from the inner to the outer disc, enabling a slow outward, and highly subsonic, radial flow. The bulk of the disc, certainly as regards most photometric/spectroscopic observables, is quasi-Keplerian and characterised by an opening angle of at most a few degrees. Should this supply of angular momentum from the inner disc halt, the disc may be re-accreted by the star (Porter, 1999).

The mechanism by which matter arives above the surface of the star with sufficient velocity to remain there is far from being resolved; mechanisms similar to the energetic flare and CME events observed on the sun and dependant upon magnetic fields are popular. However, simplistic ad-hoc theories which eject clouds of material containing a range of velocities show that whilst much of the material will rapidly re-accrete, a fraction will attain orbital velocity and be capable of transferring angular momentum into the disc. In the broadest sense, magnetic events (see below) could provide the mechanism. Additionally, the higher the stellar rotational velocity, the larger will be the influx of mass and angular momentum to the disc, as observed.

In at least some stars such events are believed to be triggered, if not actually generated by, non-radial-pulsations as observed in line profile variations of μ Cen (Rivinius et al., 1998a). The distortions induced into the stellar surface velocity field modify the shape of the global line profile in excellent agreement with models. This star has shown emission line outbursts at times matching the superpositional maxima of observed non-radial pulsational frequencies. Non-radial pulsations have been observed in the form of 'travelling bumps' in line profiles of many early type stars, and also reveal themselves in multiperiodic radial velocity variations (Harmanec, 1998).

Smith (2000) describes the appearance in He I line profiles of λ Eri of discrete high velocity absorptions (*hvas*) which appear blue-shifted by several hundred $\mathrm{km\,s^{-1}}$. Such features can develop on timescales of minutes and last hours, and have been observed by Rivinius (1998b) to coincide with the start of emission line outbursts in μ Cen. Such features appear in observations of numerous Be stars, including those that show little evidence for NRPs, and thus are excellent candidates for the processes creating the mass outflow, though whether they represent the events themselves or are merely associated is unclear. Balona (2000) describes the appearance in trailed high resolution spectra of 'flare events' visible as bright features apparently corotating with the star for several rotations before declining. He conjectures that their characteristics are strong evidence for the involvement of magnetic fields; specifically the trapping of material in magnetic loops high above the photosphere can enable corotation to approach or exceed the orbital velocity, providing a mechanism for raising the material into orbit; the demise of such loops could powerfully eject material.

The episodic nature of these processes is a key conclusion reached by all authors. What is clear is that at present such work appears the most promising regarding an understanding of the Be phenomenon.

1.4 X-ray binaries

X-ray binaries can be divided into low mass $< 2M_{\odot}$ and high mass $> 10M_{\odot}$. LMXRBs are compact systems containing late type low mass stars accreting via Roche-lobe overflow and an accretion disc. Their optical flux is often dominated by the accretion disc; their disimilarity to the systems studied in these pages precludes further mention.

1.5 Be X-ray binaries

The generation of X-radiation in the BeXRBs is due to the phenomenally deep gravitational potential well possessed by the compact object. The fraction f of the rest energy mc^2 released by a mass m falling onto the surface is given by

$$f = \frac{GM_x m}{R_x} \frac{1}{mc^2} = \frac{GM_x}{R_x c^2} \tag{1.1}$$

Thus the efficiency with which energy is generated depends upon the ratio M_x/R_x, which is very much higher for neutron stars (NS) than white dwarves. This efficiency is $\sim 10^{-4}$ for a white dwarf, ~ 0.1 for a NS and ~ 0.4 for a black hole. Thus a collossal energy release occurs upon the accretion of modest quantities of matter onto a NS, making such objects visible across extra-galactic distances.

BeXRBs make up approximately 2/3 of all known HMXRBs, with more routinely discovered each year. Observationally they are distinguished from the supergiant X-ray binaries (which make up the remainder of the HMXRBs) by the extremely transient nature of their X-ray behaviour (though the X Per subclass differs, see below). The physical reason underying this is that whereas the NS in supergiant systems accrete steadily from the primary's dense stellar wind at all orbital phases,

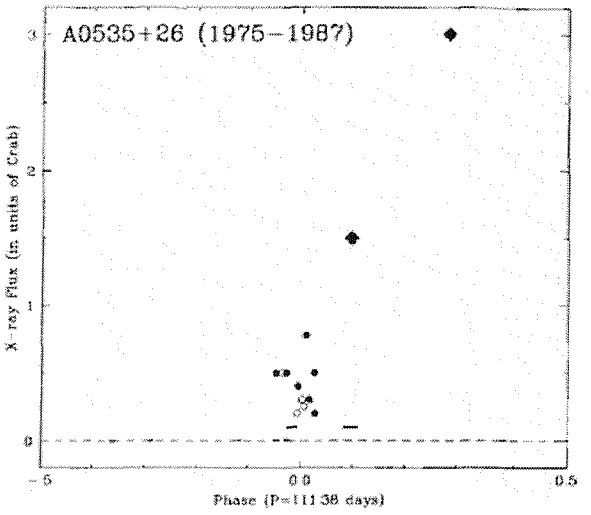

Figure 1.5: Figure 4 from Motch et al. (1991) showing outbursts from A0535+262 folded against their best orbital ephemeris ($111.^d38 \pm 0.11$, $T_{max} = JD2,446,743.3 \pm 2.3$). Note the tight clustering of normal Type I outbursts around phase 0 ± 0.05 with Type II outbursts delayed somewhat. Dashes denote upper limits of non-detections.

accretion from Be stars is generally restricted to passage of the NS through the equatorial plane and occurs primarily close to periastron (Figure 1.5); the orbit of the NS is generally wide ($P_{orb} = 10 \rightarrow 300$days) and eccentric (e=0.1→0.9). Thus BeXRBs display vast ranges of X-ray luminosity from quiescent levels of $10^{34} erg\ s^{-1}$ to $\approx 2 \times 10^{38} erg\ s^{-1}$, close to their Eddington luminosity. Outbursts fall into two types (Stella et al., 1986):

I Type I outbursts ($10^{36} - 10^{37} erg\ s^{-1}$) last a matter of days and occur at intervals of integer multiples of the orbital period, from a few tens to a few hundreds of days. They occur close to or shortly after periastron (Figure 1.5).

II Both XTE J0111.2–7317and A0535+262 were discovered when they underwent so-called 'Giant' or Type II outbursts of $\sim 10^{38} erg\ s^{-1}$. These are far more loosely correlated with periastron than are Type I events, generally occurring between phase 0 and 0.5, and lasting several tens of days.

The standard explanation for Type II outbursts is that they are the result of

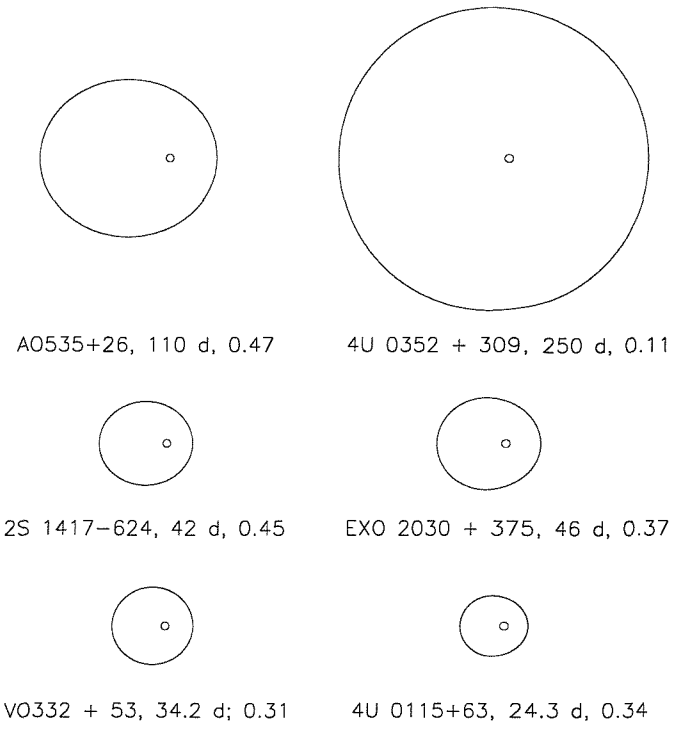

Figure 1.6: The orbits of six well-known BeXRBs to scale. Figure 11 from Delgado-Marti et al. (2000).

large mass ejection events from the Be star. Several authors (de Loore et al., 1984; Demartino et al., 1989) have observed $\sim$ 0.1 magnitude brightenings just prior to X-ray activity and have interpreted this as support for the above theory. However, the propagation of such a packet of material through the disc and directly at the NS offers problems for the theory, and large numbers of such brightenings must surely occur for each successul 'hit' on the NS. An alternative explanation for this apparent 'shell ejection' is offered in Chapter 2.

Whilst such systems make up most known BeXRBs, there exists a subclass of five systems (Reig and Roche, 1999; Israel et al., 2000) of which X Per (4U 0352+309) is the prototype, which display only persistent low level activity ($10^{34} erg\ s^{-1}$) with some restricted flaring. The physical reason for this apparent dichotomy lies in the ellipticity of the NS orbit; the X Per subclass are believed to feature orbits of low ellipticity and large radius (Delgado-Marti et al., 2000) so accretion occurs far from the Be star in a low density medium (see Figure 1.6). This low accretion rate is also

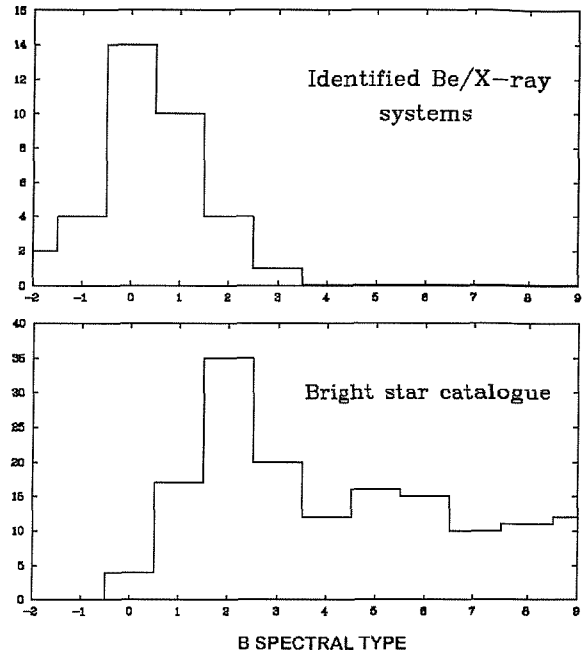

Figure 1.7: The narrow range of BeXRB primary spectral types compared to the range observed in isolated systems. From Negueruela (1998).

reflected in the long NS spin periods, X per has a pulsation period of 837secs and orbital period of 250days.

The Be stars in such systems are generally typical of Be stars in general. However there are two important points to make:

I Be stars in BeXRB systems possess discs that are both smaller (Zamanov et al., 2001), denser (Zamanov et al., 2001; Telting et al., 1998) than Be stars in general, and have lower $W_{\lambda H\alpha}$ (Reig et al., 1997) as seen in Figure 1.8.

II The primaries occupy a small range in spectral type, from O9-B2 (Figure 1.7) relative to the total Be population (Negueruela, 1998).

The high density factor could be a selection effect, if only binary systems with dense discs can cause X-ray activity. The truncation paradigm (Section 1.7) however naturally predicts that discs in BeXRBs will become denser than in isolated systems.

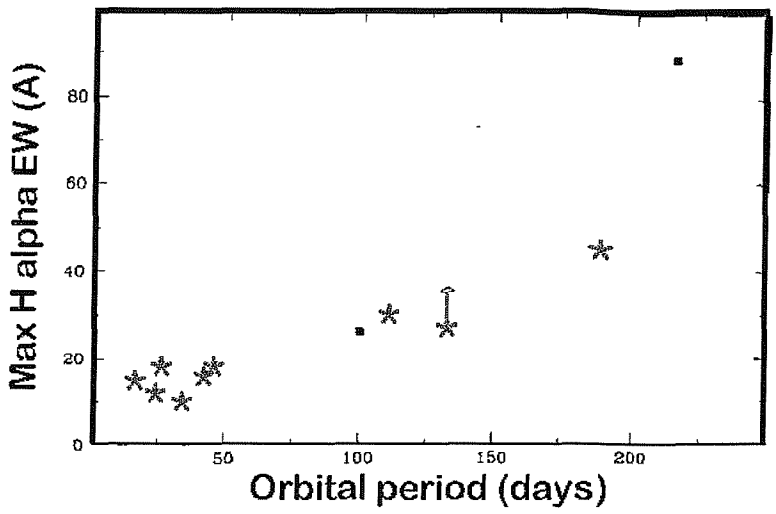

Figure 1.8: Comparison of the maximum observed $W_{\lambda H\alpha}$ for BeXRBs as a function of their orbital period. From Reig, Fabregat and Coe (1997).

Insofar as variability is concerned, BeXRBs display all the phenomena shown by Be stars in general. However, they also display additional behaviour attributable to interactions with the orbiting NS; the mass of the NS is approximately 10% of the Be star, and so whilst it does not dominate the system, it's perturbing effects become quite significant outside a few R_* from the Be star (see Section 1.7). The summary of A0535+262 below is typical of BeXRBs in general; there is no reason to suspect it to be unrepresentative of the group.

For a large number of years it has been the standard mantra of BeXRB astronomers that 'Neutron stars offer a probe of conditions within the Be star disc'. There has long been a feeling that X-ray activity is telling us something about the conditions in the disc, presumably at the point where the NS orbit intersects the Be disc. Thus the standard view evolved that accretion was taking place directly from the Be disc as the NS passed directly through it, with changing disc conditions playing a straightforward rôle in determining X-ray activity. Recent work though has changed this view, and it now appears that circumstellar discs in BeXRBs are radically altered by the presence of the NS (see point *I* above). These discrepancies arise as discs in BeXRBs are expected to be truncated at radii smaller than the periastron distance of the NS (Section 1.7), so that accretion never occurs directly

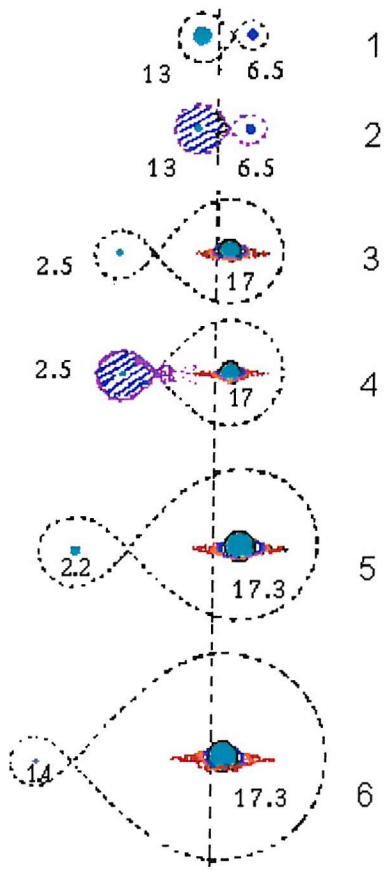

Figure 1.9: Evolutionary scheme for BeXRBs, adapted from Coe (2000). Numbered stages are described in the text.

from the disc.

1.5.1 Formation of BeXRBs and the Corbet diagram

The existence of BeXRBs posed a problem for theorists, due to the established fact that if a system loses more than half of it's mass in a supernova event, it will become unbound (Blaauw, 1961). A simplistic explanation of a BeXRB formation would hold that the more massive component simply exploded first to leave a Be+NS binary, but if the progenitor was indeed more massive it must have ejected more than half of the system mass in the SN. The theory of BeXRB formation therefore depends upon transfer of mass from the primary to the secondary prior to the supernova in a close binary.

Figure 1.9 shows the key stages in the evolution of a BeXRB, as described by van den Heuvel (1983). The evolution commences with the formation of two B stars of moderately unequal mass in a detached binary [1]. The detached nature arises because neither star fills it's Roche lobe, and thus both components are effectively unaware of their neighbour; thus no interaction occurs until the end of the MS lifetime of the primary (denoted as such regardless of subsequent mass exchange, shown on the left in Figure 1.9. Note that in the evolved BeXRB this object will ultimately become the NS, or secondary). At this point, commencement of He burning in the core triggers an expansion, the Roche lobe is filled, and mass starts to flow onto the secondary [2]. This continues until the primary consists of only the stripped down He core of the primary, a Helium star [3]. The flow of mass onto the secondary, and the associated transfer of angular momentum, has spun up the (now more massive) secondary which consequently becomes a Be star. Evolution of the primary may cause subsequent episodes of mass transfer [4-5], before the evolved He star explodes as a Type II supernova [5-6]. The loss of mass at this stage has two consequences; firstly the system acquires a net velocity due to the shedding of the ejecta's linear momentum (see Section 1.6), and secondly the loss of the ejecta's mass from the system induces an eccentricity. Possible kick's from asymmetric SN explosions may exacerbate this second effect, but only rarely cause disruption. The system has now become a BeXRB.

The realisation that ϕ Per is a formerly missing link, lying at stage [3] of the above evolutionary process with a Be star orbited by a hot He star, has provided confirmation that this process is accurate (Gies, 2000).

The formation of the system in the manner described above leaves the NS spinning with an arbitrary period, probably far shorter than the tens of seconds observed for BeXRBs.

The Corbet diagram (Corbet, 1986), a plot of NS pulse period against orbital period shown in Figure 1.10, shows that there is a well defined equilibrium spin-

period for a given system type and orbital period. Furthermore this provides a discriminatory tool for the different types of XRB if both periods are known, and a means of estimating the other period if just one is known.

The different areas occupied by subsets of the population arise from an equilibrium arising involving the accretion rate, which is indirectly a function of orbital period for a given XRB type and varies considerably between XRB types, and spin-down. In order to accretion to occur, the Alfven radius (at which the NS magnetic field dominates the proceedings over gravity) must be smaller than the co-rotation radius. If this criterion is not met, the effect of the magnetic field at the Alfven radius is to accelerate the material, preventing accretion and causing spin-down; the so-called propellor effect. If NS spin is slower than this balance point accretion occurs and the NS spins up until this mechanism becomes a factor, equilibrium occurring where $R_{Alfven} \approx R_{corotation}$. Smaller orbits generally accrete from denser winds enable higher accretion rates, reducing the Alfven radius and thus creating equilibrium at a shorter spin period.

1.6 Runaway systems and bowshocks

1.6.1 Runaway systems

Blaauw (1961) defined a runaway as a star/system with a space velocity above $40\,\mathrm{km\,s^{-1}}$; in the case of isolated OB stars this criterion isolates a clear excess of high velocity stars above the expected distribution (van Oijen, 1989). Such a clear cut definition is not applicable however to all systems, as BeXRBs possess mean runaway velocities of only $15\,\mathrm{km\,s^{-1}}$ (van den Heuvel et al., 2000) acquired during their evolution (Section 1.5.1). In essence the concept is one of a system or star which has been in some way accelerated from it's former location. Thus with regard to the OB runaways which concern us here, the two main observational characteristics are

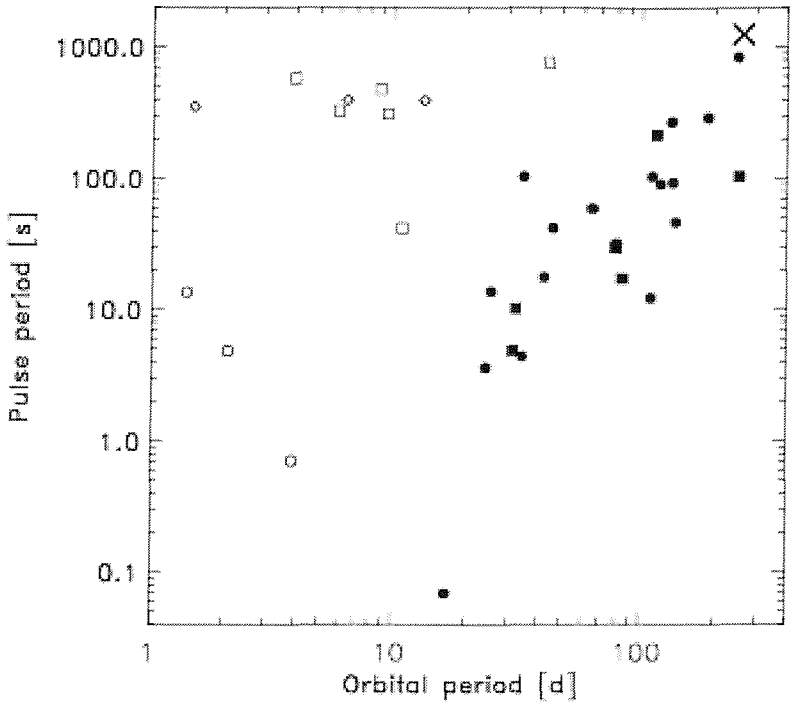

Figure 1.10: Corbet diagram from in't Zand et al. (2001). Open symbols are supergiant systems, filled symbols and x are Be systems. For the Be systems, the circles indicate optically identified cases and squares those that are not. The open squares refer to optically identified Roche-lobe underfilling supergiants and the open circles to Roche-lobe filling giants. The diamonds refer to systems without optical counterpart.

a location far from a star forming region, and an anomalously large space velocity. The short lifetimes of such massive stars ensure that without such a large velocity they will never drift significantly far from the OB association within which they were formed.

Blaauw's scenario High mass X-ray binaries are all, by virtue of their formation mechanisms, runaways to a greater or lesser extent. If one considers the progenitor binary system of a HMXRB to be at rest, it can be seen that at any instant the momentum of one of the components is balanced by the equal and opposite momentum of the other. The supernova explosion that subsequently occurs, forming the neutron star, asymetrically removes mass and orbital momentum from the system, causing an imbalance and a net spatial velocity for the system of $\sim 15\,\mathrm{km\,s^{-1}}$. Such a loss of mass also reduces the binding energy of the binary, but this will not lead to break-up provided that no more than half of the overall system mass is lost in the supernova event (Blaauw, 1961). Blaauw neglected the substantial effects of mass transfer during evolution and thus overestimated the fraction of systems disrupted in this way. In the absence of other effects disruption does not occur because most of the system mass is contained within the companion. The asymmetry of supernovae does impart an additional effect though, and in general imparts a random 'kick velocity' (Lai, 2000) of up to several hundred $\mathrm{km\,s^{-1}}$ to the nascent neutron star. The magnitude of this velocity relative to typical orbital velocities implies that only those NS born with small kicks can survive as a system. Furthermore, in those systems that remain bound, such characteristics as the probable coplanarity of the Be equator and NS (progenitor) orbit will be lost.

Cluster Ejection Scenario The complex gravitational interplay of the thousands of stars in dense clusters can occasionally lead to the ejection of individial members or binaries (Leonard, 1995), with the energy-donating binary sinking further into the cluster's gravitational well. Simulations have shown that such ejections are con-

siderably more efficient for binary-binary interactions than for single star-binaries. The systems involved will, in converting internal orbital energy into systemic kinetic energy, become significantly tighter following such an event.

Note that whilst the two processes described above are believed to be dominant, and of approximately equal importance in generating runaway systems, there may be further mechanisms; Graff and Gould (2000) describe how the cluster which gave rise to SN1987A was formed in the LMC plane with a perpendicular velocity of $50\,\mathrm{km\,s^{-1}}$. No explanation could be found.

1.6.2 Bowshocks

The formation of a bowshock arises from the ram pressure balance between an expanding stellar wind and the generally slowly moving ISM. When the stellar velocity exceeds the local sound speed the shock wave thus created is unable to propagate and sweeps up material in it's path. This high density material moves along the surface of the paraboloidal shock before dispersing behind the star. The presence of a bowshock is thus critically dependant upon the supersonic nature of the wind source. Such features provide an accurate measurement of the direction of travel and an estimate of the velocity, which can reveal the system age if the nascent association can be identified (Ankay et al., 2001). Such data are clearly useful for the SMC where proper motions are currently undetectable. Thus the case of XTE J0111.2–7317(Chapter 4) is of great interest as if confirmed as a bowshock it may be possible to determine the age of the system, as has been done for such systems as Vela X-1 (Kaper et al., 1997) and AE Aur using proper motions.

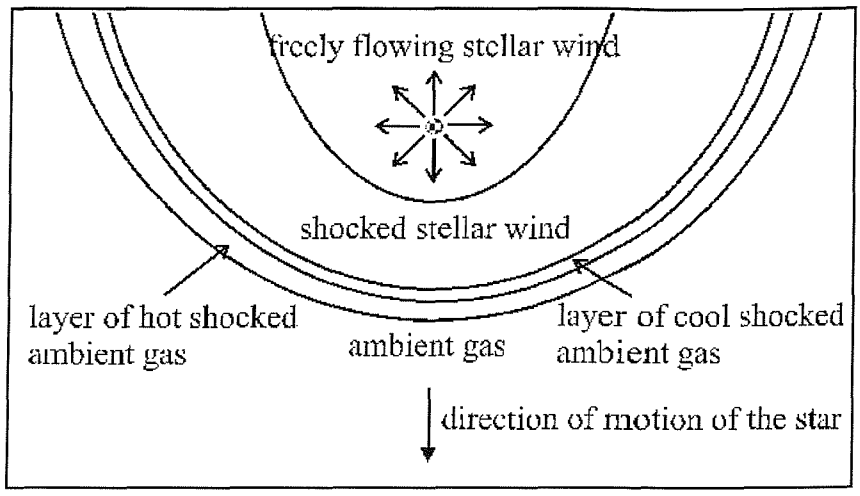

Figure 1.11: Schematic of the interaction of a supersonic star and the ISM to form a bowshock. Figure 1 from Comeron and Kaper (1998).

1.7 Truncation and the NS effects

Theoretical work and 3D SPH N-body simulations (Okazaki, 2001) have shed a great deal of light upon the interactions between a Be star's viscous decretion disc and an orbiting NS. Such modelling leaves no doubt that tidal truncation is critically important in determining the characteristics of the circumstellar disc. The primary consequence of considering the forces in detail is that in BeXRBs the Be disc is truncated by the NS at a radius where the tidal forces exceed the viscous forces. Such tidal forces are significant only where the outer disc is in resonance with the NS, eg a $P_{NS} : P_{disc}$ of 4:1.

This truncation of the Be disc inevitably causes a very large reduction in the accretion rate onto the NS relative to the rate if the NS were able to move directly through the dense Be disc. Additionally, the truncation results in an accumulation of matter in the outer disc, resulting in a flatter density distribution than in discs around isolated Be stars. It transpires that for a higher orbital eccentricity, the truncation radius is smaller, truncation less efficient and thus accretion rate higher, and orbital modulation in the continuum is more pronounced (see Section 2.6.6).

Thus we arrive at a picture of BeXRBs that differs markedly from the 'traditional'

view. The old picture of direct accretion from has been shown to be erroneous (Negueruela et al., 2001) due to truncation of the Be disc.

In two recent papers (Negueruela and Okazaki, 2001; Negueruela et al., 2001) a model of 4U0115+63 is presented based predominantly upon observations and the above work. They describe cycles of activity, incorporating the major observational features, both optical-IR and X-ray. Representative Hα profiles from three of these cycles are shown in Figure 1.13. The primary phases of these cycles are

I Disc-less state. Emission line outbursts cause emission wings to appear.

II Disc grows, W_λ increases, FWHM decreases as disc expands. Fast and slow V/R cycles. Truncation, ρ increases.

III Warping, precession lead to shell/single-peak transitions. Type II outbursts.

IV Dissipation of the disc.

Negueruela et al. (2001) see shell lines at the end of each cycle as the system fades into the disc-loss state that terminates each cycle. They suggest that perturbation of the disc leads to outbursts, but the direction of causality is uncertain. Overall this scenario is very successful in describing 4U0115+63 as a complete system. It's application to A0535+262, and possible variations to the phenomenology which might apply to BeXRBs generally, are discussed in Chapter 2.

1.8 A0535+262

1.8.1 System properties

On May 5 1975, IAUC 2774 (Eyles et al., 1975) announced that the Ariel V satellite had discovered a new X-ray nova. Designated A0535+262, it was detected from

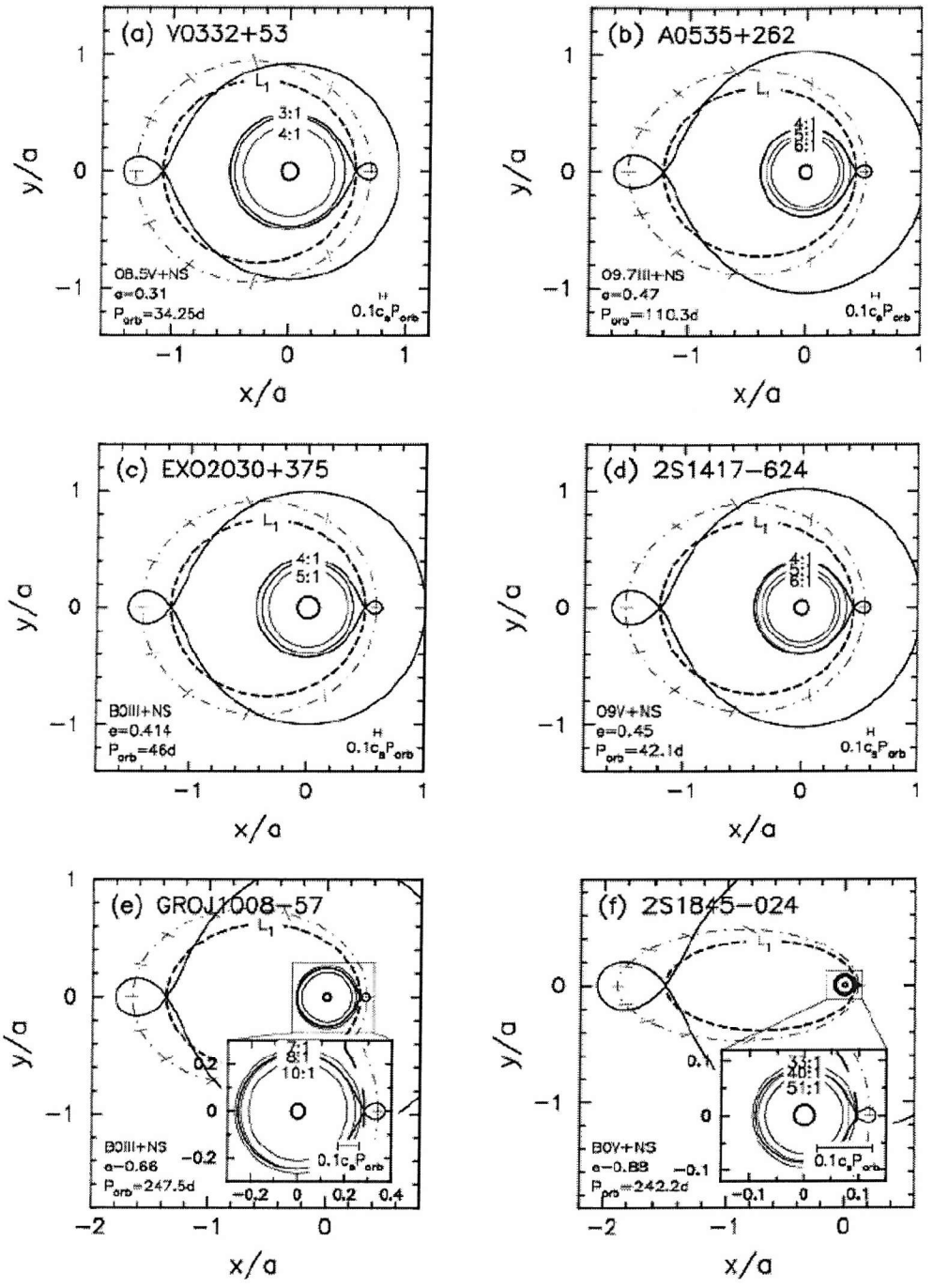

Figure 1.12: Figure 2 from Okazaki and Negueruela (2001) showing orbital resonances and orbits for 6 BeXRBs including A0535+262.

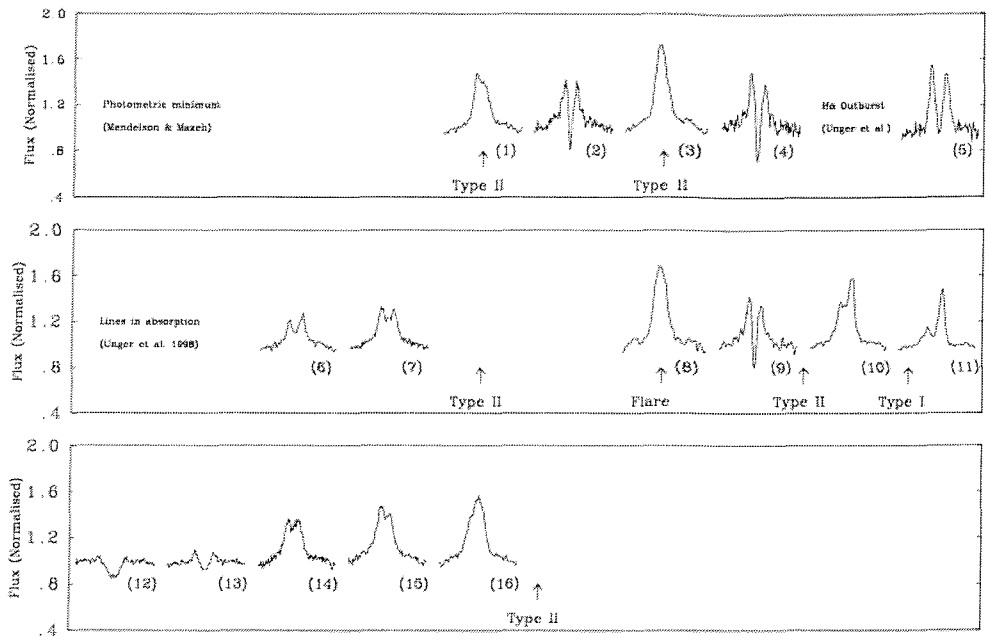

Figure 1.13: Figure 2 from N2001B. showing representative Hα profiles from three cycles.

April 13 onwards (Coe et al. 1975; Rosenberg et al. 1975). IAUC 2780 (Liller, 1975) shortly afterwards pointed out that 'a peculiar B emission star, BD +26 883 = HDE 245770 = SAO 077348, located 0m.1 west of the best position' had displayed optical photometric variability and varying line emission since the 1920s, and was a possible optical counterpart. Subsequent observations verified that this was indeed the case, and since then the Be star component of this HMXRB, HDE 245770 or V725 Tau, has been subject to intense scrutiny due to it's northern declination, optical/IR brightness, and variety of X-ray activity, most of which remains not only unpredictable but inexplicable.

Almost 3 decades later, the optical component of A0535+262 is classified as 09.7-B0IIIe (Steele et al. 1998). Wang and Gies (1998) found a projected rotational velocity of $v \sin i = 250 \pm 15\,\mathrm{km\,s^{-1}}$.

The system contains a 103s spin-period neutron star (Rosenberg et al., 1975). Analysis of the peak times of Type I outbursts, presumed to mark periastron, resulted in an orbital period of 111 days (Priedhorsky and Terrell, 1983) later refined to 111.38 ± 0.11 days (Motch et al., 1991) though pulse timing has given the marginally

incompatible result of 110.3 ± 0.3 (Finger et al., 1996).

Most studies have found distances of 2-3 kpc (Janot-Pacheco et al., 1987; Lyuty and Zaĭtseva, 2000) generally dependant upon the uncertain luminosity class.

1.8.2 Behaviour

1.8.2.1 Photometric

HDE 245770, in common with all Be stars, displays optically variability on many timescales, the vast majority attributable to changes in the circumstellar disc (Lyuty and Zaĭtseva, 2000; Roche et al., 1993). Photometry (Figure 1.14) suggests that the last 30 years since it's recognition as a BeXRB may be unrepresentative of the longer term behaviour. Prior data shows a considerably smaller ff/bf excess, if indeed any disc emission, from 1898 until the late 1960's (Figure 1.14) whereupon it's ff/bf excess, a good measure of the degree to which a star is displaying the Be phenomenon, strengthened greatly.

The observation of short period (days) brightenings, typically of ~ 0.1 magnitudes in m_V and termed 'shell ejection' events have been reported just prior to X-ray activity (Lyuty et al., 1989). Discussions of the mechanisms that lead to the X-ray outbursts have interpreted these as 'enhanced episodes of mass-loss', with modelling based upon the assumption of the subsequently accreted material being ejected directly from the Be star (Demartino et al., 1989), despite a lack of physical evidence for this. Clark et al. (1999a) and Larionov et al. (2001) have presented studies of the photometric timescales involved; the periods found can be seen in Figure 2.28. Whilst these timescales are typical of Be stars in general, a description of their probable cause is contained in Sections 2.6.4 and 2.6.6.

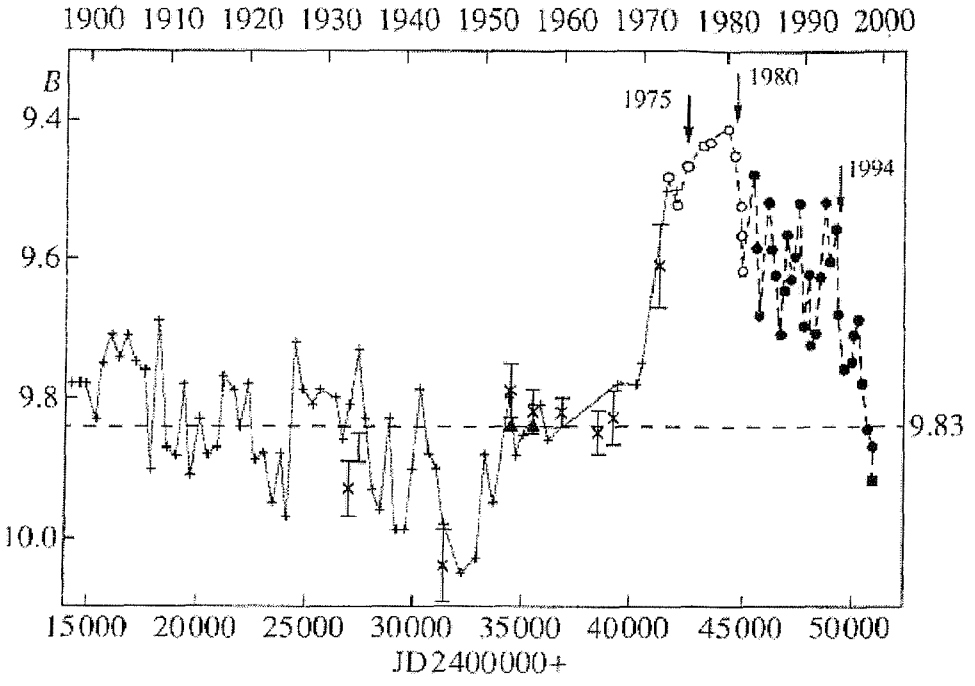

Figure 1.14: Figure 2 from Lyuty and Zaĭtseva (2000), showing the photometric history of A0535+262 since 1898. Most pre-1970 data is extracted from photographic plates and has errors of up to 0.3mag (Lyuty et al. 1989).

1.8.2.2 Spectroscopic

Since it's identification with A0535+262, optical and IR spectra of HDE 245770 have consistently exhibited emission in the H I lines, with Hα typically displaying W_λ from -5$\rightarrow$-15Å, suggesting the continuous presence of a circumstellar disc. Many of the expected Be variabilities have been seen. For example, the profile shape has varied widely, frequently being double peaked and displaying evidence for V/R cycles of around 1 year (Clark et al., 1998b). Before the regular monitoring of the last 3 decades began, isolated spectra in 1922 and 1926 showed a normal B0 star (Lyuty et al., 1989).

1.8.2.3 X-ray

A0525+262 displays the two types of outburst, in addition to quiescent emission, characteristic of BeXRBs.

Clark et al. (1999) has shown that the lack of correlation between photometric excess and X-ray activity prohibits a simple wind-fed accretion process. Finger et al. (1996) show that the detection and temporal evolution of QPOs provides strong evidence for an accretion disc, at least during the 1994 Type II outburst. Following discovery the system displayed Type I outbursts on most periastron passages until the early 1980s, when activity began to falter with many more 'missing' outbursts (see Table 2.7). A Type II event in 1989 followed by a single Type I heralded the end of activity until 1993-1994, when a series of Type I outbursts occurred with the Type II event in the midst of them. No outbursts have been seen since, though the system has been detected in quiescence.

The standard picture of accretion onto the NS from the Be circumstellar disc near perihelion has been invoked to explain the periodic 'normal' outbursts, and in common with most BeXRBs A0535+262 exhibits less predictable non-perihelic 'giant' outbursts, usually between phase 0 and 0.3 (Figure 1.5).

1.9 The SMC population.

The Small Magellanic Coud (SMC), which along with the LMC make up by far the brightest two of the Milky Way's eleven known satellite galaxies, is a small ($M \sim 0.01 M_{milkyway}$) object lying at a distance of approximately 63kpc (see Section 1.9.1).

The SMC has proved to be an abundant source of recent BeXRB discoveries (Haberl and Sasaki, 2000; Yokogawa et al., 2000), instigated by the impressive array of X-ray satellites which have been developed in recent years, most notably ASCA, RXTE, BeppoSAX, and ROSAT. Whilst it is further than the far side of our own galaxy, the minimal extinction, combined with a fairly well known and constant distance modulus and the development of powerful instrumentation in the

southern hemisphere have made this population very appealing for further study. This point is driven home by comparing A0535+262, the subject of Chapter 2, with XTE J0111.2-7317, studied in Chapter 4. The first is a nearby ($\sim 3kpc$) object, and thus bright both optically and in X-rays, seen through $A_v \sim 2.5$. Due to it's distance XTE J0111.2–7317, though a similar system, has 0.3% the observed brightness but only $A_v \sim 0.2$.

However this low mass belies a tumultous recent past which has led to the presence of large numbers of young and maturing massive stars relative to our galaxy. This hefty episode of recent star formation is usually attributed to tidal interactions with both the LMC and the milky way, invoking the principal that in such situations the less massive object invariably suffers greater disruption and deformation triggering star formation on a large scale, particularly in a galaxy as gas rich as the SMC (H I fraction is 30% of total mass, c.f. 1% for our galaxy). The Magellanic Stream, a tidal tail torn from the Magellanic Clouds by the Galaxy, exhibits asymmetry derived from the SMC/LMC relative masses, with a long tidal tail and weaker leading arm (Figure 1.15).

Both MCs are close to perigalacticon ($P_{orb} \sim 1.3Gyr$) and experienced a mutual encounter at only 7kpc $\sim 200Myr$ ago. Abundant evidence of recent enhanced interaction-driven star formation is thus to be expected. Indeed, due to the nature of BeXRBs (and other HMXRBs) as the middle-aged to elderly members of massive starburst populations, they can shed considerable light upon the star formation histories of their host galaxies. In this way it is noticeable that the LMC has a population of XRB systems relative to it's mass almost identical to the milky way, whereas the SMC has a far higher ratio particularly of BeXRBs (Haberl and Sasaki, 2000), with a BeXRB/sgOBXRB ratio an order of magnitude larger than our galaxy. However, the components of HMXRBs have lives of only $\sim 10^7 yrs$ and so are evidence of star formation considerably more recently than the MC interations would predict. The 'wing' of the SMC contains numerous associations less than 50Myr old (Kahabka and Pietsch, 1996). Whilst most galaxies accomodate

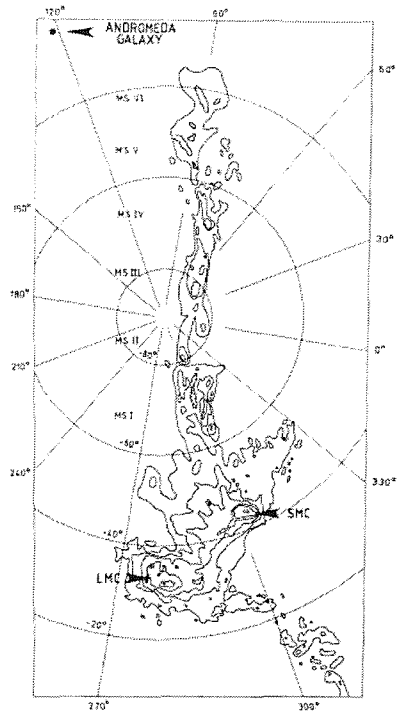

Figure 1.15: Neutral H I in the MC system from Mathewson (1985). The long structure traversing the image is the *Magellanic stream*, the *Bridge* links the MCs, while emission at lower right is the *leading arm*.

young and old stars in different regions with radial symmetry, in the SMC there is a large offset between the two (Cioni et al., 2000). Zaritsky et al. (2000) find that the fundamental morphology of the SMC, that shown by the oldest stars, is a conventional spheroid and only the highly asymmetric star formation has led to it's irregular classification. This may be attributable to the delayed interaction of material displaced by the encounters (both within and out of the galaxy) prompting formation of spiral arms. Interaction with the Magellanic stream may also play a rôle.

Numerous studies have emphasised the overabundance of Be to B stars in the SMC relative to the milky way (Coe et al., 2000). Metallicity effects may be important in this regard, as $Z_{SMC} \sim 1/8 Z_{M.W.}$. This has important consequences for line blanketting and mass loss in massive stars, producing higher luminosities and lower angular momentum loss through the main sequence of a massive star, ultimately favouring production of the rapidly rotating OB stars which lie at the heart

of Oe/Be systems (Maeder and Meynet, 2001). This may explain, at least in part, the prevalence of Be stars and BeXRBs in the SMC.

1.9.1 Distances to the Magellanic Clouds.

Clearly many of the quantities derived for Magellanic Cloud systems are dependant upon the assumed distance. The distances quoted below are used throughout.

Recent reviews of this subject (Gibson, 1999) point out that there exists a significant variation (at a $> 3\sigma$ level) in published values for μ_{LMC}. However, the relative distance modulus $\mu_{SMC} - \mu_{LMC}$ is found to remain far more consistent amongst publications at $\sim 0.50 \pm 0.05$ magnitudes. Most of these results come from comparisons of stellar populations in the two galaxies thus yielding accurate relative distances. The review of Gibson (1999), in common with the literature, provides more and better data for the LMC than the SMC, and is strongly suggestive of μ_{LMC} as 18.5 ± 0.1, yielding a suitable value for μ_{SMC} of 19.0 ± 0.1; corresponding distances are 50120 and 63100 pc respectively. Whilst some studies have detected the relative distance between the near and far sides of these inclined systems, these distances are assumed to hold for their entirety.

Chapter 2

Multiwaveband studies of variability in the BeXRB A0535+262

2.1 Introduction

The aim of this Chapter is to study all of the spectral and photometric observations gathered by the Southampton/Valencia collaboration since 1987 to create a coherent picture in which some light is shed upon its various states and behaviours. A background to the behaviour of this prototype of the Be X-ray binaries can be found in Section 1.8, whilst a description in terms of the framework developed here can be found in Section 2.6.4.

A0535+262 is of considerable interest to those studying BeXRBs for more than historical reasons; due to it's proximity it is relatively simple to obtain high quality data, whilst in many ways it is typical of BeXRBs in general. Thus the behaviour described here for A0535+262 may be applicable to BeXRBs in general.

Integral to this framework is the recent work by Okazaki, Negueruela and Rivinius. Whilst their recent works have provided a framework within which much of the phenomenology of BeXRBs has been explained (Section 1.7), the analysis of A0535+262 presented here has the advantage of a substantially larger dataset to draw upon, leading to the availability of many quasi-simultaneous spectral and photometric measurements.

Thus the phenomenology that has been described (Negueruela et al., 2001) regarding 4U0115+63 is applied to A0535+262 and some minor modifications are suggested. The integral role of a warped, precessing disc invoked in 4U0115+63 is supported in the case of A0535+262, though it is less of a transient feature than Negueruela et al. found in 4U0115+63 (and in all probability other BeXRBs).

Central to the interpretation and explanation of the data set is the observational verification of discrete disc 'states', apparently determined by truncation at orbital periods resonant with the NS and predicted by Negueruela et al. (Okazaki and Negueruela, 2001).

Additionally correlations between the photometric properties of the system and various spectral line parameters are investigated.

2.2 Observations

In studying the long term behaviour of any system which displays variability on timescales of weeks to decades (see Figure 1.14) a long term monitoring campaign proves critical; the ability to watch how a system such as A0535+262 enters an unusual state, such as is discussed here with the disc-loss episode, can prove as enlightening as studying it only during and after the event. To this end the long term IR photometric monitoring of A0535+262 (and most other known galactic BeXRB systems) at the TCS and SAAO 1.9m is an excellent indicator of the general status

of a Be star. Additional spectroscopic monitoring of these systems, mostly using the INT, shows in far greater detail the distribution of material in the circumstellar disc. Correlations of spectral properties with photometric (such as Figure 2.21) can only be done when appreciable numbers of quaisimultaneous data sets exist.

In addition to the data gathered in this way, several spectra have been obtained through the ING archive service. Summaries of all the observations in this work may be found in Tables 2.2 and 2.1. The vast majority of data reduction and data visualisation has been carried out using STARLINK software, except where noted.

2.2.1 Optical and IR Photometry

UBVRI photometry have been obtained from observations in service mode at the Jacobus Kapteyn Telescope (JKT) on 1998 December 15 using the JAG-CCD camera, and the SAAO 1.0m on 1999 January 23 using the standard Tek8 CCD camera. Image reduction was undertaken using the FIGARO package, whilst subsequent aperture photometry took place within GAIA.

UBV photometry has been obtained from the catalogue of Lyuty and Zaĭtseva (2000), presenting observations made at the Crimean Station of SAI in 1980 and 1988-1998.

The BeX group, based primarily at the universities of Southampton and Valencia, has maintained a programme of JHK photometry using the CVF photometer of the 1.5m Telescopio Carlos Sanchez (TCS) at Teide observatory, Tenerife which has been monitoring HDE 245770 since 1987. Data were reduced by means of the procedure described by Manfroid (1993), with instrumental values transformed to the TCS standard system (Alonso et al. 1998). SAAO IR photometry was reduced using standard SAAO software which is also based upon the methods described in Manfroid (1993).

Date	Telescope	Instrument	Filters
1987-1998	TCS	CVF	JHK
6/1/1999	SAAO 1.9m	Mk III Photometer	JHK
15/12/1998	JKT	JAG-CCD camera	UBVRI
23/1/1999	SAAO 1.0m	CCD camera	UBVRI

Table 2.1: Photometric observations of HDE 245770.

In addition to the TCS JHK photometry, data prior to 1991 has been obtained from the 0.6m and 2.6m telescopes at Byurakan, Armenia, and since 1993 from 0.7m telescope at CRAO. Details may be found in Clark (1997), p. 153.

2.2.2 Spectroscopy

2.2.2.1 IR

Infrared spectra of the system were obtained using the CGS4 spectrometer of the United Kingdom Infrared Telescope (UKIRT), Hawaii. The 256 × 256 array was used with the 1.70 – 2.40 μm grating position. *A* and a *G*-type standards were also observed in order to allow correction of the spectra for telluric absorption. *A* type IR spectra are nearly featureless except for H lines, whilst *G* star spectra have weak H lines but numerous other features, requiring a combination of each to allow an accurate interpretation.

Initial data reduction was carried out at the telescope using the CGS4DR software (Puxley, Beard & Ramsey 1992). Subsequent sky subtraction, optimal extraction, division by the standard star, and wavelength calibration using arc lamp observations were carried out using FIGARO.

Date	Telescope	Instrument	Details
13/12/1991	INT	IDS	EEV5, 500mm Cam., R1200R
8-10/3/1993	SAAO 1.9m	Spectrograph	RPCS
12/2/1995	JKT	AGB	EEV5, AGBX
4/4/1996	SAAO 1.9m	Spectrograph	RPCS
28/10/1997	JKT	AGB	TEK4, AGBX
6/2/1998	SAAO 1.9m	Spectrograph	SITe, 1200l/mm
30/8/1998	KPNO Coudé-Feed	Coudé Spectr.	F3KB, 108cm camera, 316 l/mm
10/9/1998	KPNO Coudé-Feed	Coudé Spectr.	F3KB, 108cm camera, 316 l/mm
26/11/1998	INT	IDS	TEK5, 235 camera, R600R
24/12/1998	WHT	ISIS	TEK2, R600R (Red)
24/12/1998	WHT	ISIS	EEV12, R600B (Blue)
11/1/1999	SAAO 1.9m	Spectrograph	SITe, 1200lmm^{-1}
4/2/1999	INT	IDS	TEK5, 235 camera, R1200R
22/2/1999	INT	IDS	TEK5, 235 camera, R1200R
4/3/1999	INT	IDS	TEK5, 500 camera, R1200Y
7/3/1999	INT	IDS	TEK5, 235 camera, R1200R
27/3/1999	WHT	ISIS	TEK2, R600R
24/4/1999	INT	IDS	TEK5, 235 camera, R1200Y
21/9/1999	INT	IDS	TEK5, 235 camera, R1200R
20/10/1999	WHT	UES	SITe1
29/1/2000	3.5m Calar Alto		Private communication, IND
22/3/2000	INT	IDS	TEK5, 235 camera, R1200R
10/4/2000	INT	IDS	TEK5, 500 camera, R1200Y
15/8/2000	INT	IDS	TEK5, 500 camera, R1200Y
16/10/2000	1.3m,Mt. Skinakas	Spectrograph	1302r lmm^{-1} +80μm + ISA 608
5/2/2001	INT	IDS	TEK5, 500 camera, R1200Y
11/11/2001	SAAO 1.9m	Spectrograph	SITe, 1200l/mm
10/11/1998	UKIRT	CGS4	K spectra, long cam., 40 l/mm
14/8/1999	UKIRT	CGS4	K spectra, long cam., 40 l/mm
21/11/2000	UKIRT	CGS4	K spectra, long cam., 40 l/mm

Table 2.2: Unpublished spectroscopic observations of HDE 245770.

2.2.2.2 Optical

A considerable effort has been made to collect every possible spectrum of HDE 245770 since 1987, in addition to those obtained by the BeX group through routine monitoring. Basic information is tabulated in 2.2. Optical spectra have largely been obtained from the ING service programme using the Intermediate Dispersion Spectrograph (IDS) on the Isaac Newton Telescope (INT) and ISIS and the UES (Utrecht Echelle Spectrograph) on the William Herschel Telescope (WHT), both located at the Observatorio del Roque de los Muchachos, La Palma, Spain. Further spectra (30/8/98 and 10/9/98) have been obtained at the Kitt Peak National Observatory (KPNO) Coudé-Feed Telescope by Douglas Gies, and the 1.9m at the South African Astrophysical Observatory (SAAO). In addition to the ING service spectra, the ING archive has provided several more.

Most spectra were de-biased, flat-fielded, extracted and wavelength calibrated (using CuAr and ArNe arc lamp spectra) with appropriate elements of the FIGARO package. Heliocentric velocity corrections were applied using VACHEL. Exceptions were the spectra of 4/3/1999, 5/2/2001 and 11/11/2001, which were reduced using the MOLLY package, and 30/8/98 and 10/9/98, which utilised IRAF. Further processing made use of DIPSO and in particular the ELF emission line fitting subpackage. Details of spectral line analysis can be found in Section 2.2.3.

Additional Hα W_λ measurements have been taken from Piccioni et al. (1998), IAUC 7293 (Giovannelli et al., 1999) and Lyuty and Zaĭtseva (2000).

All observations prior to the 1^{st} March 1996 not described above are in Tables 1 and 2 of Clark et al. (1998).

2.2.3 Line profile fitting

Whilst the overall strength (W_λ) of emission lines is a useful probe of the general state of Be circumstellar discs, the detailed shape of the line provides a wealth of information to study the velocity field and radial (and to a lesser extent azimuthal) emissivity of these discs.

The most important effect dominating the structure of Be star line profiles is the displacement of emission components from their rest wavelength by their Doppler shift. The similarity of the He I profile (Figure 2.1,bottom) with the calculated profile for a rotating disc (Figure 1.3) verifies that this structure arises from kinematic effects (Huang 1972). Thus information regarding distribution of emitting gas around the star can be inferred from the line profile. Broadly speaking, high velocity emission wings (such as are seen in outbursts) are the signature of a small, rapidly rotating inner disc whereas strong narrow lines are the signature of large robust discs.

In order to proceed with such an analysis, Hα and He I lines in all spectra have been fitted using the DIPSO ELF package. Strictly speaking the line profile components are not expected to be Gaussian as they arise from the convolution of non-Gaussian functions (velocity distribution around an orbit etc.). However the fits have in most cases been excellent, justifying this approximation (see Figure 2.1), probably due to the finite spectrograph resolution. Only in the case of the highest resolution spectra from the Shajn telescope, Ukraine, were the peaks in the spectra noticeably 'pointier' than Gaussian, as expected (see Figure 1.3).

It is clearly desirable to be able to determine the orbital radius of the emitting material from Doppler shifted features in line profiles. Under the assumption of circular Keplerian orbits, the observed velocity of such material is simply related to it's orbital radius by the equation

$$r = \frac{sin^2 i}{v_{obs}^2} GM_* \tag{2.1}$$

2.2.3.1 Hα

Whilst a 2 component Gaussian fit gives an acceptable fit to some data, exceptional fits were possible by introducing a third, much broader component (FWHM$\sim$ $350 - 550\,\mathrm{km\,s^{-1}}$) centred at $v \sim 0\,\mathrm{km\,s^{-1}}$, with 2 sharper peaks (typically FWHM $150\,\mathrm{km\,s^{-1}}$) superimposed on it. Whilst it might be argued that this gives too many degrees of freedom to provide a rigourously accurate (or meaningful) fit, a careful choice of initial conditions (line centres, FWHMa) ensured that the fit was repeatable and valid. Poor selection of choices can cause convergence on fits with no astrophysical significance, generally with larger residuals. The choice of line components is based strictly upon their astrophysical origins, thus weak circumstellar emission is most successfully modelled as a broad photospheric absorption line (FWHM$\sim 450\,\mathrm{km\,s^{-1}}$) with two emission peaks (FWHMa$\sim 150\,\mathrm{km\,s^{-1}}$) at $\pm \sim 250\,\mathrm{km\,s^{-1}}$. The shell interpretation of Piccioni et al. (2000), that the Hα line is a broad emission feature with a superposed absorption core, could also be fitted, though with less confidence and a FWHM atypically large for a shell profile. Selecting line centres inaccurately could cause convergence upon this solution however. An example of the success of this technique can be seen in Figure 2.17.

An unexpected result was that in fitting some spectra where the line was entirely in emission, a third component frequently emerged as being in absorption with FWHM$\approx 540\,\mathrm{km\,s^{-1}}$. The same FWHM ($539 \pm 7\,\mathrm{km\,s^{-1}}$) was found in fitting the almost purely photospheric Hβ profile obtained on 24/12/98. This reinforces the ability of the multi-component fitting technique to derive fits with physical meaning.

	Hα			He I λ6678				
JD	ΔV_{peak} $km\,s^{-1}$	V/R	W_λ $\AA$	ΔV_{peak} $km\,s^{-1}$	V/R	W_λ $\AA$	m_K	Int. *days*
1987								
2447144			-10.4± 0.4				0	
2447154			-9.5± 0.5				7.159	5
2447161			-10.5 ± 0.4				7.124	1
1988								
2447229			-13.8 ± 0.4				7.243	3
2447232			-13.1 ± 0.4			-0.6 ± 0.07	7.202	2
1990								
2447942	197	0.606	-10.6± 0.3			-0.38 ± 0.06		
2448209	189.7	1.031	-9 ± 0.1			-0.19 ± 0.08		
2448252	221.9	1.148	-11 ± 0.4				7.53	27
1991								
2448283	188.3	1.889	-9.9 ± 0.2	348.3	2.465	-0.62 ± 0.09	7.5	2
2448363	254.8	1.828	-7.3 ± 0.1	225		0.033 ± 0.015	7.25	1
2448497	251.2	0.784	-9.9 ± 0.2				7.07	0
2448604	239.3	0.637	-12.18± 0.05	227.7	0.936	-0.35 ± 0.15	7.11	11
1992								
2448669	219.3	0.927	-11 ± 0.2			-0.13 ± 0.05	7.16	0
2448851	250.9	2.424	-8.5 ± 0.25		1.239	-0.17 ± 0.08	7.06	7
2448852	254.3	2.378	-8.0 ± 0.5			0.06 ± 0.05	7.05	6
1993								
2449055	196.0	0.496	-15.7± 0.25			-0.33 ± 0.05		
2449057	200.0	0.518	-15.6 ± 0.2			-0.29 ± 0.09		
2449253	182.9	0.7272	-11.5 ± 0.11	220.7	1.159	-0.08 ± 0.01	7.2	19
2449254	179.2	0.825	-12.5 ± 0.25	222.7	1.546	-0.08 ± 0.09	7.2	18
2449327			-14.4 ± 0.3	265.8	2.314	-0.29 ± 0.03	7.196	14

	Hα			HeI λ6678				
JD	ΔV_{peak} $km\,s^{-1}$	V/R	W_λ $\AA$	ΔV_{peak} $km\,s^{-1}$	V/R	W_λ $\AA$	m_K	Int. *days*
1994								
2449398	264.3	5.076	-12.8 ± 0.2				7.39	2
2449399	248.6	4.39	-12.2 ± 0.8				7.39	1
2449400				347.3	4.001	-0.61 ± 0.02	7.39	1
2449410	202.1	1.712	-12.2 ± 0.5	253.6	2.01	-0.60 ± 0.03	7.52	6
2449413	201.8	1.7074	-13.05± 0.3				7.52	3
2449438	177.1	1.527	-10.5 ± 0.5	354.3	3.086	-0.60 ± 0.11	7.38	1
2449604	269.1	1.649	-10.3 ± 0.3				7.61	18
2449611	249.2	1.789	-10.0 ± 0.4	406.7	0.844	-0.90 ± 0.07	7.61	11
2449653	250.0	1.533	-8.7 ± 0.3	395.4	0.42	-0.49 ± 0.01	7.641	7
2449657				463.1	0.532	-0.51 ± 0.04	7.641	4
2449666	236.9	1.141	-11.5 ± 0.6				7.455	0
2449691	236.9	1.04	-8.0 ± 0.3				7.473	25
2449708	233.3	0.926	-8.7 ± 0.4	423.2	0.627	-0.68 ± 0.05	7.479	12
1995								
2449759	230.7	0.734	-9.1 ± 0.3	321.1	1.163	-1.04 ± 0.04	7.527	36
2449773	258.0	0.741	-9.2 ± 0.5			-0.60 ± 0.2	7.527	50
2449936	266.1	1.32	-8.0 ± 0.1	367.4	1.365	-0.66 ± 0.1		
2449937	275.2	1.349	-8.4 ± 0.3	343.9	1.23	-0.64 ± 0.12		
2449975	275.5	1.499	-8.4 ± 0.4	341.7	1.13	-0.79 ± 0.04		
2450007	266.6	1.118	-8.5 ± 0.3	342	0.898	-0.48 ± 0.22	7.475	1
2450039			-7.3 ± 0.4	233.2	1.04	-1.05 ± 0.2	7.591	3
2450040	280.7	0.884	-7.1 ± 0.4			-0.80 ± 0.4	7.591	4
2450041	278.7	0.892	-6.8 ± 0.3			-0.15 ± 0.5	7.591	4
2450050	261.5	0.896	-8.1 ± 0.4	411	0.7	-0.47 ± 0.03	7.591	14
2450051	266.0	0.856	-8.7 ± 0.3			-0.66 ± 0.13	7.591	15
2450070	281.5	0.9	-8.1 ± 0.3	392.8	0.662	-0.58 ± 0.08	7.349	27

	Hα			He I λ6678				
JD	ΔV_{peak} $km\,s^{-1}$	V/R	W_λ $\AA$	ΔV_{peak} $km\,s^{-1}$	V/R	W_λ $\AA$	m_K	Int. *days*
1996								
2450140	271.0	0.78	-8.7 ± 0.4	335.1	1.204	-0.46 ± 0.03	7.524	18
2450177	245.3	1.026	-8.1 ± 0.25			-0.75 ± 0.3	7.349	17
1997								
2450465			-12.4 ± 0.5					
2450496			-13.1 ± 0.5					
2450497			-12.4 ± 0.5					
2450498			-12.4 ± 0.5					
2450499			-11.9 ± 0.5					
2450502			-11.5 ± 0.5					
2450506			-12.0 ± 0.5					
2450749	279.6	1.136	-7.25 ± 0.1	387.7	1.004	-0.40 ± 0.04		
2450767			-7.09 ± 0.3					
2450795			-6.34 ± 0.3					
2450796			-6.37 ± 0.3					
1998								
2450849	271.5	1.057	-4.75 ± 0.15	351.7	1.901	0.231 ± 0.025		
2450889			-3.15 ± 0.2					
2450893			-2.79 ± 0.2					
2451056	528.2	1.16	1.7 ± 0.03	603	0.473	0.792 ± 0.005	8.423	50
2451066	485.29	1.063	0.83 ± 0.04	582.3	0.437	0.52 ± 0.01	8.423	49
2451123			2.2 ± 0.1				8.247	7
2451128			0.04 ± 0.02				8.247	12
2451129			0.05 ± 0.02				8.247	13
2451143	457.2	0.926	-0.68 ± 0.05	530	0.86	0.20 ± 0.02	8.247	27
2451171	441.3	1.209	-0.51 ± 0.03	499.5	1.259	0.46 ± 0.01	8.339	13
1999								

	Hα			He I λ6678				
JD	ΔV_{peak} $km\,s^{-1}$	V/R	W_λ Å	ΔV_{peak} $km\,s^{-1}$	V/R	W_λ Å	m_K	Int. *days*
2451189	433.0	1.04	-0.67 ± 0.04	536.2	1.107	0.20 ± 0.1	8.339	4
2451212	432.5	0.997	-0.50 ± 0.03	505.1	1.488	0.41 ± 0.02	8.339	27
2451230	438.6	0.969	-0.76 ± 0.05	520.4	1.542	0.24 ± 0.02		
2451243	431.3	1.024	-0.43 ± 0.03	556.6	1.311	0.38 ±0.01		
2451246	426.4	0.962	-0.38 ± 0.03	507.3	0.937	0.415 ±0.005		
2451266				510.2	0.678	0.325 ±0.05		
2451293	413.7	1.617	-0.29 ± 0.04	460.6	1.413	0.24 ±0.02		
2451442	346.2	0.993	-3.7 ± 0.2	454.6	0.813	-0.105 ±0.05	7.538	12
2451472	337.4	1.07	-3.5 ± 0.2	399.6	0.829	-0.15 ±0.01	7.559	13
2000								
2451572			-4.4 ± 0.3				7.388	5
2451626	295.5	1.011	-5.5 ± 0.3	387.9	1.132	-0.08 ±0.03		
2451644	293.3	1.08	-5.9 ± 0.3	343.3	0.977	0.05 ±0.02		
2451771	288.4	1.047	-5.8 ± 0.15	327.8	0.85	0.18 ±0.01		
2451833	289.3	0.9728	-8.6 ± 0.1			-0.08 ±0.06	7.128	1
2001								
2451944	221.6	0.974	-8.75 ± 0.05	291.6	0.971	0.09 ±0.03	7.003	17
2452224	217.7	1.05	-11.3 ± 0.2	283.9	0.628	0.025 ±0.02		

Table 2.3: A0535+262 Hα and He I λ6678 line parameters 1987-2001. *Int.* denotes the elapsed time between the m_K photometry and the spectrum.

Strictly speaking the Hα profile is the sum of at least 4 components; the photospheric absorption profile, a broad circumstellar component of breadth corresponding to the orbital velocity at the scale size of the disc, and 1 or more narrower

Gaussians corresponding to brighter regions of emission, i.e. GOAOs or annuli of material (Rivinius et al., 2001). However, introducing 4 components requires data of remarkable quality, particularly in view of the photospheric component and the 'bulk' disc component possessing the same line centre and similar widths. Thus a 3 component fit is used, generally producing fits of an excellent quality.

Most work on V/R variability measures the peak intensities, but in the case of a Gaussian superimposed on the wings of another, the actual location of the peak differs from the location of the feature. Thus the positions of the Gaussian components that constitute the V-R pairs are used. In order to achieve consistency with previous work on V/R variations, the peak intensity of the line fits has been measured, rather than the W_λ, even though this would be a better measure of the amount of material emitting and thus more closely related to the physical state of the disc.

Line fitting proves valuable in several circumstances.

- Noisy spectra; locating line peaks manually is extremely subjective, and tends to be led astray by noise-induced peaks. Fitting uses the entirety of the profile in a manner hard to replicate manually.
- The presence of 2 Gaussian components does not guarantee a 2 peaked profile if one component strongly exceeds the other's intensity. Frequently only a shoulder is visible on a single-peaked profile (for example the Hα spectrum of 930310, Figure 2.8), but all except the weakest of shoulders can be fitted, allowing V/R parameters to be derived from single-peaked profiles that are clearly far from a simple Gaussian, and preserving the validity of the measurement. (As with all fits, the V and R intensity measurements are made at the location of the line centres of these components.) Profiles such as that of 16/10/2000 which have a broad base of emission only subtly altered by peaks on each side (appearing square) also benefit.

• the spectra of 30/8/1998 and 10/9/1998 display a photospheric absorption line with 2 weak peaks superimposed at $\sim \pm 260\,\mathrm{km\,s^{-1}}$ whose peaks are below/level with the continuum. V/R ratios of such spectra, and the ones that followed in the 'stable state' up to 24/4/1999, are the ratios of the peak intensities of the high velocity components. Subsequent data use intensities above continuum.

2.2.3.2 He I

In general, fitting the HeI profile is more problematic than Hα due to the lower W_λ exacerbating the problem of low S/N. Many spectra (in particular 980830 and 980910) are essentially photospheric profiles plus emission at high velocities of $\sim 200 - 300\,\mathrm{km\,s^{-1}}$. The spectrum of 980830 (weakest emission) was modelled as a Gaussian absorption profile with emission wings in order to determine the photospheric profile underlying all spectra (Figure 2.1). Even this profile certainly contains some weak emission between the emission peaks - indeed, noticeable infilling occurred between this epoch and a spectrum obtained only 11 days later - but at a level that can reasonably be neglected without consequence. This Gaussian profile was then subtracted from all other spectra before modelling, leaving a spectrum containing only the circumstellar emission. In this way the high S/N of the 980830 data is used to reduce the number of free parameters in the analysis of subsequent and previous data, enabling better fitting of the weak emission features.

The validity of this photospheric subtraction can be observed by comparing the post-subtraction He I profile of Figure 2.1(bottom) with a theoretical profile from a broad Keplerian disc (Figure 1.3). It is clear even from this comparison that the emitting region in this case is a broad disc as opposed to a thin ring.

A further benefit is the ability to determine V/R ratios when the peaks lie below the continuum. For consistency with previous work, the intensities at the location of

the V and R emission peaks is used, regardless of the FWHM of these components.

The strong IS feature at 6660.6Å(or -788.34 $\mathrm{km\,s^{-1}}$) was used as a check on the velocity scale; some archived spectra exhibited marked deviations (up to 100 $\mathrm{km\,s^{-1}}$) from the correct wavelength/velocity scale. Using this calibration $W_{\lambda HeI}$ was measured from -600 to 600 $\mathrm{km\,s^{-1}}$.

Where multiple peaks were visible (interpreted as multiple discs - Section 2.4.2), the dominant peak was used to derive ΔV_{peak}.

Measurements of the maximum velocity of emission in a line profile yields only a lower limit, due to the diminishing radius and thus size of emitting region from which such line components must eminate. In contrast to the line-fitting techniques used to measure ΔV_{peak} (disc outer radius), this measurement was done entirely by eye. In many cases the photospheric profile has been filled in to continuum level and no more, thus giving a result equal to the full-width of the photospheric profile. Most spectra yield inner radii velocities of similar magnitude to $v \sin i$.

2.3 Optical and IR Photometry

Photometry shows broadly the same patterns of brightening and fading in all wavebands (see Figures 2.21 and 2.22).

2.3.1 Interstellar reddening and intrinsic colour

2.3.1.1 Using DIBs

Following Steele et al. (1998), an attempt has been made to calculate the extinction to A0535+262 using Diffuse Interstellar Bands (DIBs) which correlate with E(B-

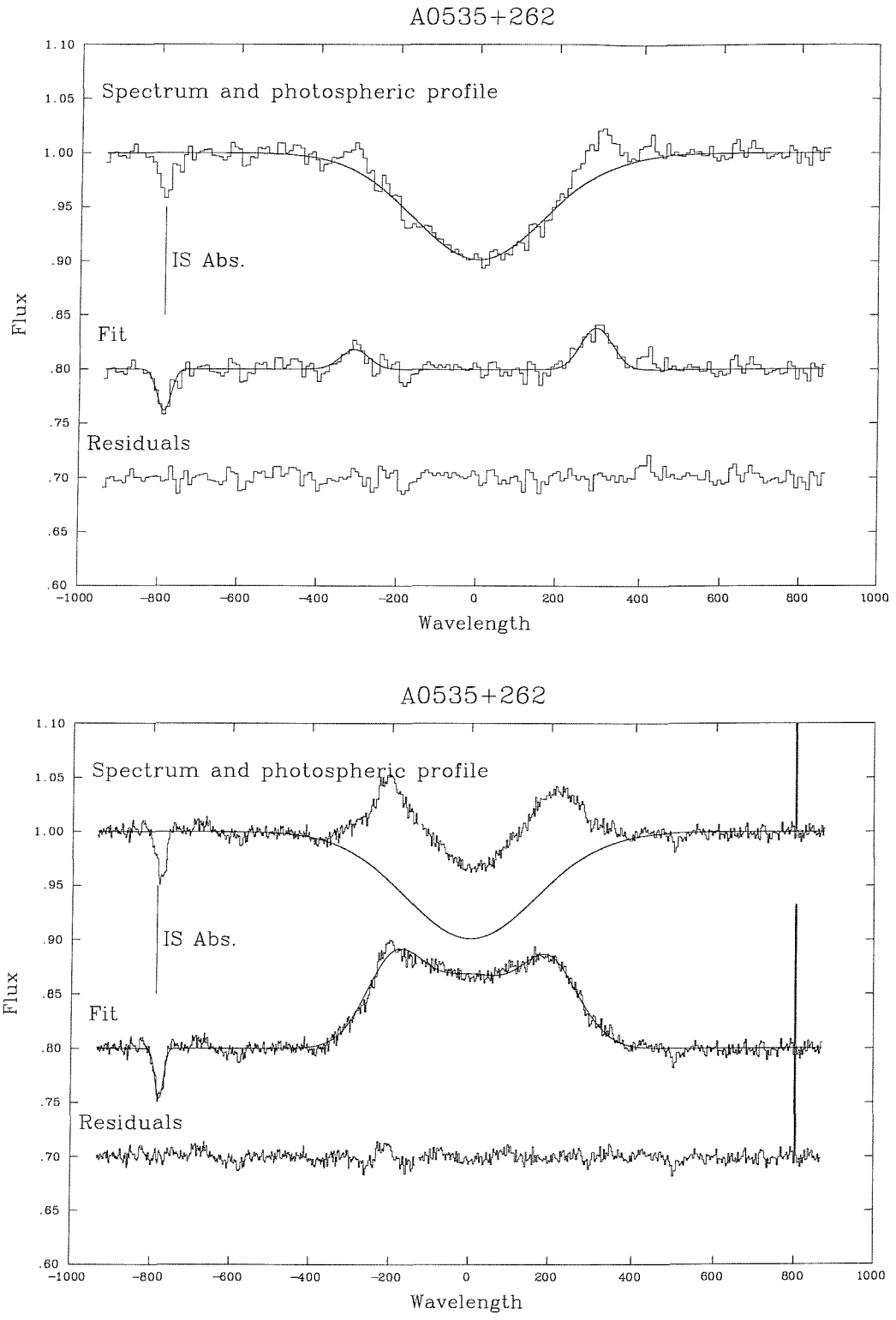

Figure 2.1: He I λ6678 profiles: 30/8/98 (top) and 20/10/99 (bottom).

Line	W/E(B-V)	W	E(B-V)	Spectrum
6613.72	0.231 ± 0.037	0.185 ± 0.004	0.80 ± 0.13	991020
6660.64	0.051 ± 0.029	0.031 ± 0.003	0.61 ± 0.35	991020
6699.37	0.041 ± 0.011	0.022 ± 0.001	0.54 ± 0.15	991020
6701.98	0.015 ± 0.002	0.015 ± 0.003	1.00 ± 0.24	991020
6196.19	0.061 ± 0.005	0.051 ± 0.005	0.84 ± 0.11	981224
4501.80	0.195 ± 0.020	0.146 ± 0.005	0.75 ± 0.08	981224
4762.57	0.079 ± 0.011	0.087 ± 0.004	1.10 ± 0.16	981224
6265-6295 blend	2.054 ± 0.095	1.678 ± 0.040	0.82 ± 0.04	981224
6203-6204 blend	0.296 ± 0.050	0.211 ± 0.005	0.71 ± 0.12	981224

Table 2.4: Equivalent widths of DIBs in the spectrum of HDE 245770, and derived reddening. W/E(B-V) values are taken from Table 3 of Jenniskens et al. (1994).

V) in a linear fashion. The Sodium D_2 λ5890 lines, which are oft used for such purposes, were not chosen due to the presence of strong (presumably terrestrial) emission on the blue edge and possible contamination of the absorption features on the few spectra in this region. The correlation of Herbig (1975) used by Steele has been superseded by that of Jenniskens et al. (1994) who provide accurate W_λ/E(B-V) for a large number of DIBs, obtained from observations of four OBA stars with well defined reddening. Only narrow (FWHM$<$ 4Å) features were used as these enable superior continuum determination and thus more accurate measurements. The highest quality (R and S/N) spectra, obtained with the WHT using UES (20 Oct. 1999) and ISIS (24 Dec. 1998) were used. Table 2.4 lists the lines observed and derived E(B-V).

The weighted mean of these measurements is $E(B-V) = 0.80 \pm 0.08$, which is close to the value of 0.7 adopted by Steele et al. (1998), and well within their errors. It is also in good agreement with the value of ~ 0.75 obtained by Giovanelli et al. (1980) from IUE observations of the λ2200 bump.

2.3.1.2 Using photometry

Lyuty and Zaĭtseva (2000) found a minimum $W_{\lambda H\alpha}$ of 2.2Å on November 6 1998, in agreement with the W_λ expected for an emission free O9.7III star (Peppel, 1984). Figure 2.21 at this value gives a value for the disc free m_V of 9.46 ± 0.02. The same procedure for m_K gives 8.40 ± 0.15, in agreement with the value of 8.50 ± 0.02 found in Section 2.6 by effectively extrapolating the disc area to zero.

Using $A_K = 0.36E(B-V)$ (Fitzpatrick, 1999) gives $A_K = 0.288 \pm 0.029$ and an unreddened $m_K = 8.21 \pm 0.04$. Similarly $A_V = 3.10E(B-V) = 2.48 \pm 0.25$, giving an unreddened $m_V = 6.98 \pm 0.25$ and $(V-K)_0$ index of -1.23 ± 0.25.

The results of Koornneef (1983) suggest that the colour indices, for example (V-K), of giant stars differ considerably from dwarves and supergiant, suggesting that these might be used to resolve the issue of the luminosity class of HDE245770. But more recent work (Wegner, 1994; Winkler, 1997; Ducati et al., 2001) based on much larger samples of stars yields colours that differ little between luminosity classes, as might be expected. Using the spectral classification of O9.7e (Steele et al., 1998), these works give (V-K) indices for class V (III) of -0.77 (-0.73), -0.94 (-0.92) and -0.99 (not given) extrapolating by half a subclass in two cases. Only the last of these values is compatible with the derived $(V-K)_0$ index, suggesting that the reddening has been overestimated. The intrinsic $(V-K)_0$ of Ducati et al. (2001) is probably the most accurate as it is based on a far larger sample of stars (3946) than the previous works. Inverting the procedure we can estimate the reddening using

$$(V-K)_0 = [9.46 \pm 0.02 - 3.10E(B-V)] - [8.50 \pm 0.02 - 0.36E(B-V)]$$

$$E(B-V) = 0.71 \pm 0.02$$

very close to previously published results and marginally outside the value derived in Section 2.3.1; the value for reddening derived from IS lines in this work is slightly higher than most previous estimates though Lyuty and Zaĭtseva (2000) list three

further measurements of 0.8, 0.80 and 0.82 ± 0.04 from the literature.

The observed system (B-V) at disc-loss (ie JD 2450800, Figure 2.4, see also Table 2.6) is 0.40 ± 0.01. An O9.7V (III) has an intrinsic $(B-V)_0$ of -0.265 (-0.24) interpolating from Wegner (1994), yielding E(B-V)=0.665 (0.64). Some other works, mostly earlier, give bluer $(B-V)_0 \sim 0.29$, yielding reddenings marginally more compatible with the IS line value and indeed other previous estimates, though the discrepancy is small and within the error bars of all but the IS line value derived here. Note also that the reddening is sufficiently large that a 5% error in W/E(B-V) given in Jenniskens (1994) could reconcile the differences. Combining these measurements gives E(B-V)=0.70 ± 0.04. Thus the intrinsic colour appears to be $(B-V)_0 = -0.30 \pm 0.04$. Assuming $R = 3.10$, the de-reddened $m_V = 7.29 \pm 0.12$.

2.3.1.3 Distance to A0535+262

The generally accepted distance to A0535+262 is $\sim 2kpc$ (Steele et al., 1998). Interpolating between classes O9.5III and B0III in Table 6 of Vacca, Garmany and Shull (1996) (henceforth VGS96) gives an $M_v = -5.39$ and distance modulus of $\mu = 12.68 \pm 0.12$ or $3436 \pm 200pc$. The calibration of Schmidt and Kaler (1982) yields -5.23, in agreement with the results of Martins et al. (2001) regarding the overestimation of luminosities in VGS96 due to their neglection of line blanketting. The distance is thus reduced to $3190 \pm 170pc$, somewhat higher than previous measurements, but in agreement with the 3kpc found by Lyuty et al. (2000) and scarcely larger than the 2600 ± 400pc by Janot-Pacheco et al. (1987).

Similarly, for a dwarf (V) classification, VGS96 gives $M_v = -4.27$ while Schmidt and Kaler (1982) gives $M_v = -4.47$ for classes IV-V. Adopting the same correction to the VGS96 result mentioned above, we derive a distance of $1900 \pm 100pc$.

Zorec and Briot (1997) provide a calibration of $E(B-V)/A_V$ for eight divisions of galactic longitude. A0535+262 lies at the juncture of zones 5 and 6, for which

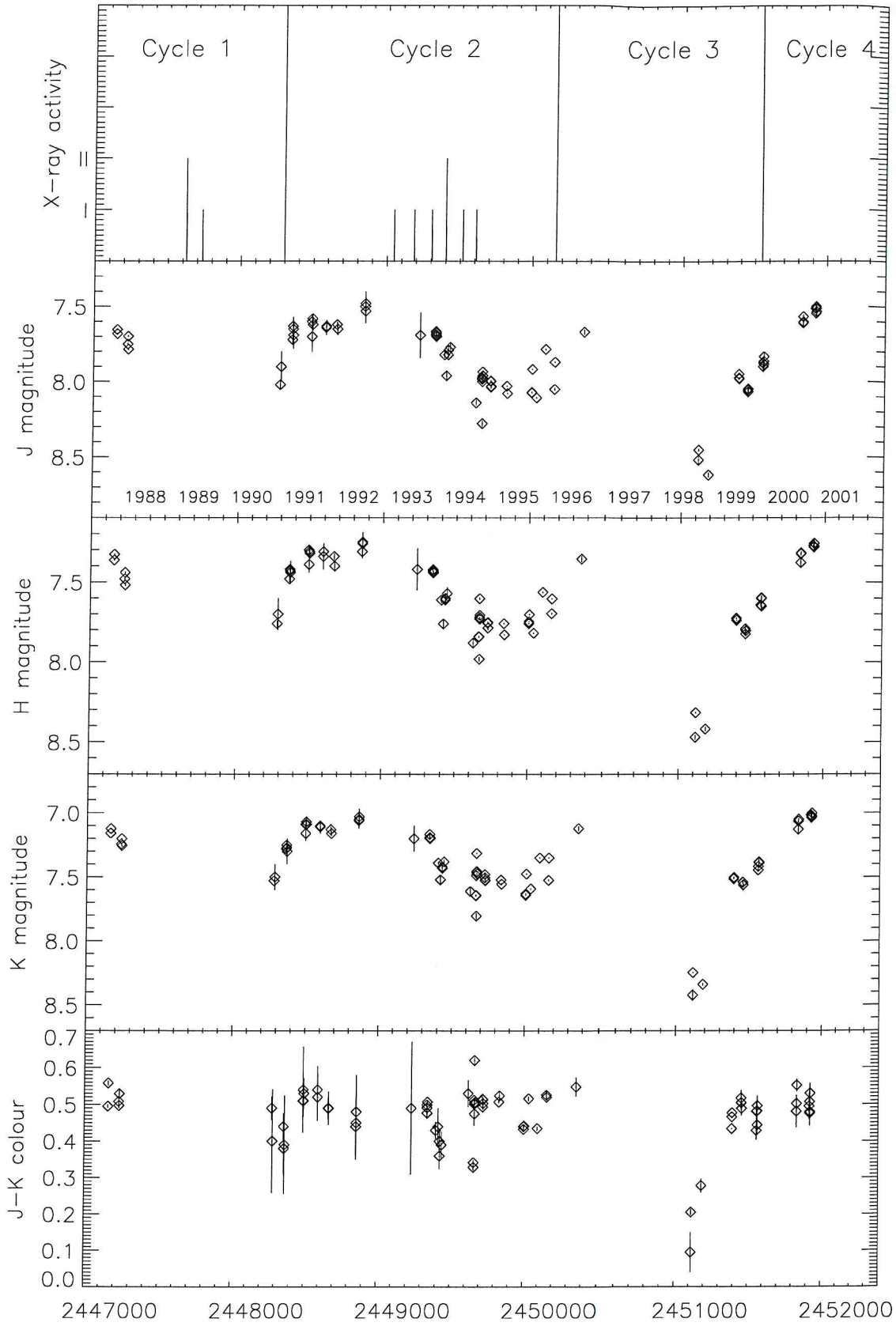

Figure 2.2: $m_{J,H,K}$ and $m_{(J-K)}$ photometry in A0535+262.

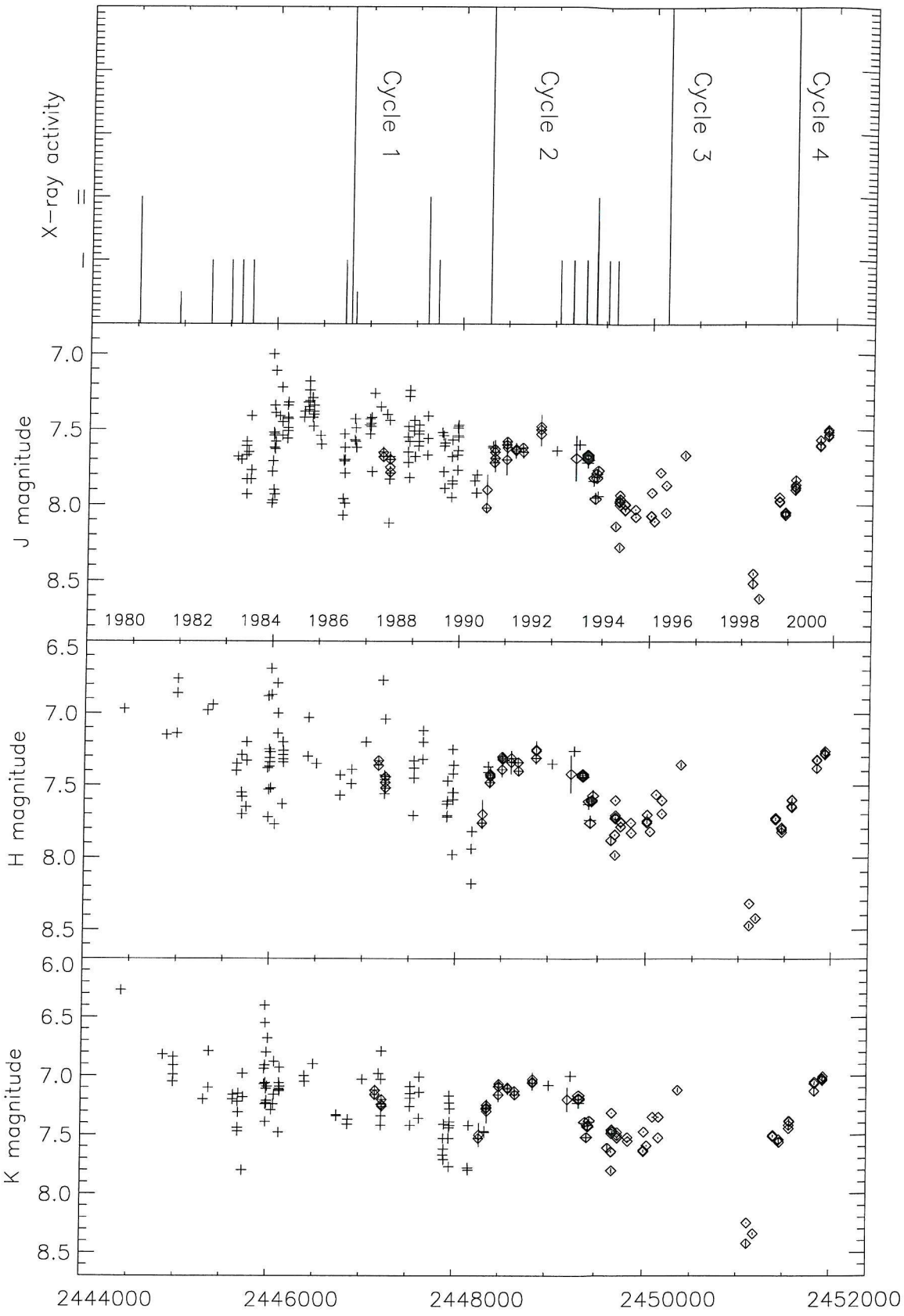

Figure 2.3: JHK photometry including CRAO data (Clark 1997).

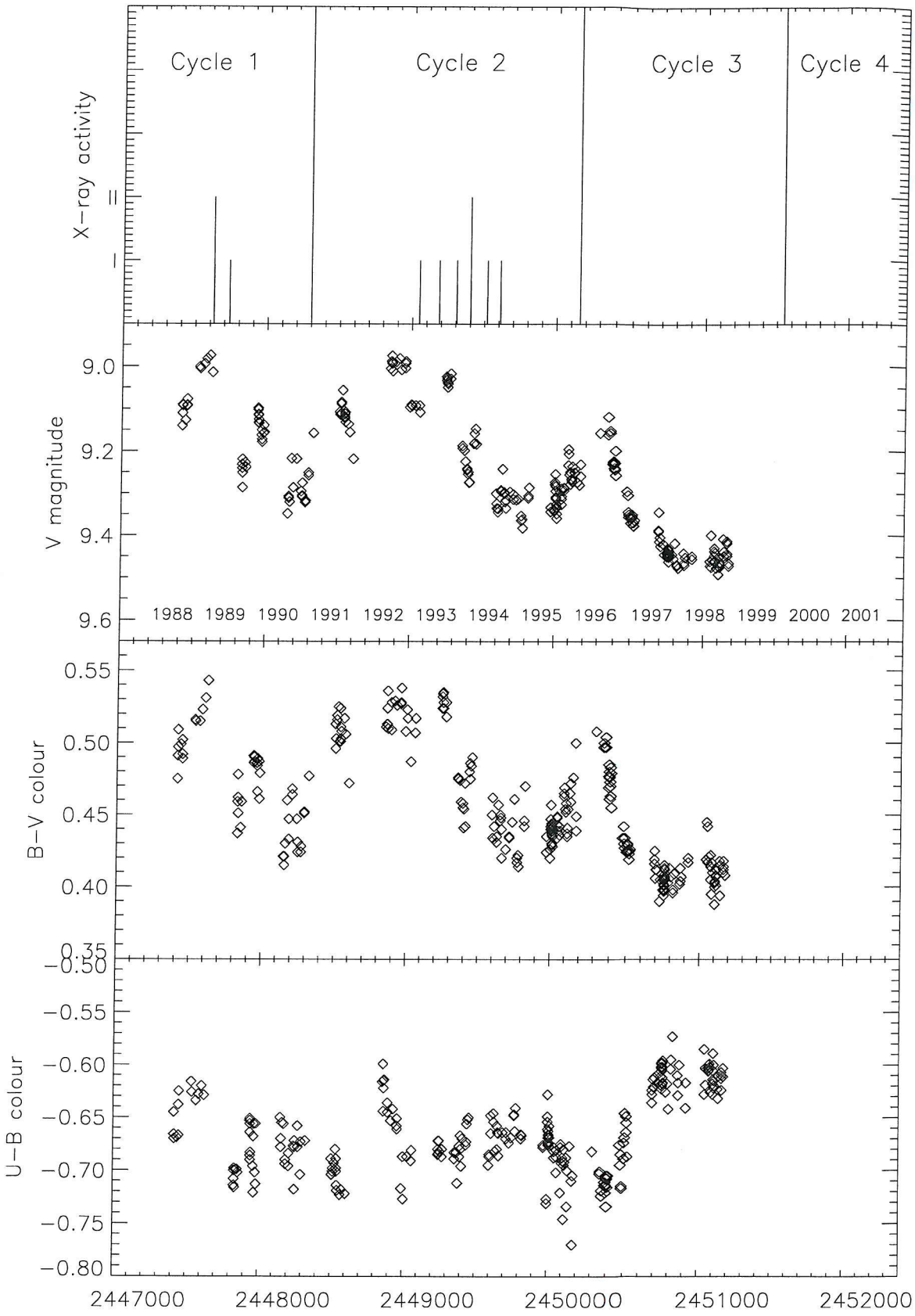

Figure 2.4: UBV photometry from Lyuty and Zaĭtseva (2000).

the mean expected distance at $E(B-V) = 0.70 = 2820$pc, confirming that the calculated colour excess is of the expected magnitude. Though E(B-V) as a function of distance is necessarily an approximate calibration, this argues for a luminosity class III calibration as opposed to V.

Interestingly, the galactic latitude of $-2.64°$ implies a position 147pc below the galactic plane, compared with a scale height for B/Be stars of $h_z \sim 66-70pc$ (Zorec and Briot, 1997; Slettebak et al., 1997). This may be evidence for the expected runaway nature of the system as a HMXRB (van Oijen, 1989) (also see Section 1.6.1).

2.3.2 IR photometry

In general, the JHK lightcurves from 1987 to 2001 (Figure 2.2) show the types of long period variations typical of Be stars, changing on timescales of several hundreds of days. No general description is given here as the changes are discussed throughout the text, in particular Section 2.6.4. One point that will be made is that throughout the large changes in IR excess, the colour index (J-K) remains constant, indicating optically thick emission (Dougherty et al. 1994, hereafter D94) and the domination of the IR colours by the disc emission. The apparent change in disc (J-K) at the transition from cycle 1 to 2 and in the midst of cycle 2 (simultaneous with the March 1994 Type II X-ray event) is discussed in Section 2.6.5.1.

2.3.2.1 IR excess quantisation

A startling observation from the JHK time series plots (Figure 2.2) is that there appears to be a preference for distinct levels of emission intensity; for H these are at approximately magnitudes 7.65 and 7.3. Henceforth these faint and bright levels are referred to as A and B respectively. The histograms in Figure 2.5 show the

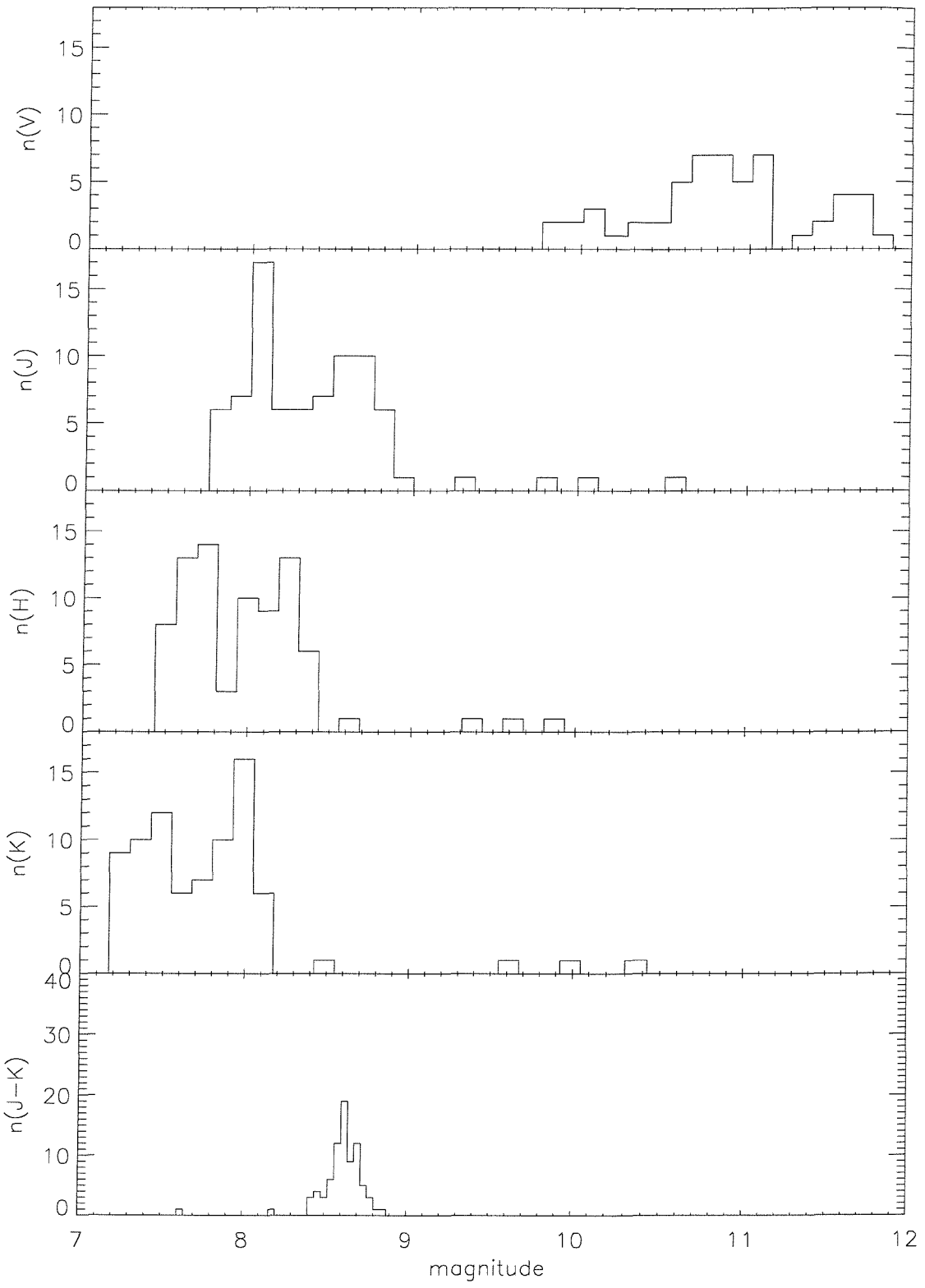

Figure 2.5: Histograms of TCS JHK photometry, and the V band data of Lyuty and Zaitseva (2000). Stellar flux has been subtracted. Bin width=0.125 for VJHK and 0.04 for (J-K). (J-K) is offset by +8 magnitudes.

photometry with the stellar flux subtracted. A bimodal distribution is clear in JHK with peaks separated by $\sim$ 0.6 magnitudes; this is larger than the overall system flux variation as the photospheric component is assumed to be constant. In V the distinction is less clear, though the time series shows distinct levels are separated by constantly changing intermediate points which confuse the histogram structure. The histogram binning is course due to the limited numbers of points, but must necessarily be so to get reasonable statistics in each bin.

In order to cause a change in the IR luminosity between these states, one of three effects could be at work

- Changing T. However, this would alter (J-K) (Figure 2.5), so is probably not the case.
- Changing ρ leading to changing optical depth. But only if optically thin throughout, as if partially optically thick (J-K) would change (D94) and if fully optically thick no change in photometry would be seen.
- Changing disc area. If isothermal would leave (J-K) unchanged as observed.

The disc is almost certainly not optically thin (Dougherty et al., 1994; Negueruela et al., 1999), thus the changing disc area appears most likely; the (J-K) colour index is constant at all times except for during disc-loss when the stellar flux dominates.

This form of behaviour is unexpected, but the work of Okazaki and Negueruela (2001) provides a natural explanation. Their work establishes that in BeXRBs tidal interations between the disc and NS truncate the disc at resonant radii where the NS orbital period is an integer multiple of that of the outer disc (see Section 1.7). For A0535+262 they expect (using reasonable estimates of the viscosity and temperature) that truncation should predominantly occur at the 4:1 and 5:1 resonances, depending upon the viscosity. When the disc is truncated at the 4:1 resonance, the extremities of the disc are slightly outside the Roche lobe of the primary (Figure

1.12) allowing mass transfer at periastron and Type I outbursts, whilst a slight decrease in the viscosity causes the disc to reduce to a more stable truncation at the 5:1 resonance, heralding a cessation of X-ray activity in the absence of substantial disc disturbances.

A natural consequence of this is that the emitting area will increase in proportion to :

$$\frac{Area_1}{Area_2} \alpha \left(\frac{r_1}{r_2}\right)^2 \alpha \left(\frac{p_1}{p_2}\right)^{4/3} \tag{2.2}$$

assuming Keplerian motion and the approximation that $r_{inner} = 0$, i.e. the disc extends to the centre of the star.

Thus a change from 4:1 to 5:1 truncation involves a disc area decrease by a factor of 1.3465. Assuming optically thick emission and an isothermal disc, this will produce a 0.323 magnitude drop in the circumstellar contribution, though of course the observed drop will be smaller as it includes the stellar contribution. The possibility that we are witnessing truncation occurring at different radii is thus a distinct possibility. The precise resonances between which the system is changing is unclear due to the breadth of the peaks in JHK distribution. A change from 3:1 to 4:1 would cause a 0.416 magnitude shift, also compatible with the data. If the disc were moving between several different radii the observed distribution of JHK would be a pattern of peaks separated by $(4/3)^{(4/3)}$=0.416 mags, $(5/4)^{(4/3)}$=0.323 mags, $(6/5)^{(4/3)}$=0.264 mags etc. moving from brighter to fainter fluxes. However none of these magnitude gaps are as large as we observe. The approximation of a constant source function (arising from isothermality) is obviously suspect, but if as expected the temperature and luminosity of the disc declines with radius this would reduce the ratio further.

Allowing for the size of the star as a 'missing' part of the disc makes little differ-

State	V	J	H	K	K_{disc}
1972-80,C	$\sim 8.85 \pm 0.1$[1]	~ 7.34[2]	~ 7.02[2]	~ 6.71[2]	~ 6.94
Bright,B	9.05 ± 0.05	7.6 ± 0.1	7.35 ± 0.1	7.1 ± 0.1	7.45 ± 0.1
Faint,A	9.35 ± 0.02	8.0 ± 0.15	7.75 ± 0.15	7.5 ± 0.15	8.05 ± 0.15
Discloss	9.44[3]	8.49[4]	8.39[4]	8.34[4]	≥ 10

Table 2.5: Magnitudes and observed range of the four observed flux states. 1:Using m_B photometry (Lyuty et al. 2000) and $(B-V) = 0.55$, 2: 11-13/12/1976, Persi et al.(1979), 3: JKT 15/12/1998, 4:TCS 27/10/1998.

ence. However, it appears from this work (Section 2.4.2.1) and that of Rivinius et al. (2001) that cavities of several stellar radii are frequently observed in Be discs, and the surface area of these are not negligible compared to the size of a disc truncated at (for example) 5:1 or 4:1. Rivinius et al. find that excepting periods shortly after mass transferring outbursts, the disc inner radius in η Cen lies at $\sim 3.1R_*$. If one calculates the ratio of disc areas after subtracting this region one finds results compatible with observations. In Figure 2.6 the ratio of areas at (n:1):([n-1]:1) are plotted for $r_{inner} = 1 \rightarrow 5R_*$, assuming $M_* = 21.8M_\odot$ and $R_* = 14.7R_\odot$ (VGS96). Large ratios occur both when flipping between resonances at low n, when r_{outer} is changing rapidly, and at high n when $r_{outer} \sim r_{inner}$. Thus we have found unexpected verification of the 'inner cavity' observations.

On this level the data are not precise or abundant enough, and the model too approximate, to verify absolutely which resonant radii are involved. However, Okazaki et al.'s conclusion that only the 4:1 and 5:1 radii are important combined with a $\sim 4R_*$ cavity provides an excellent fit to the observed flux ratio. Indeed, given the spectroscopic evidence in the literature it would be suprising if there were not a cavity separating the photosphere and disc inner edge (see Section 2.4.2.1).

Lyuty and Zaĭtseva (2000) present a thorough synopsis of the photometric history of A0535+262 since 1898 (reproduced in Figure 1.14). It can be seen that though the period covered in this work, from 1987 to 2001, has amongst the brightest photome-

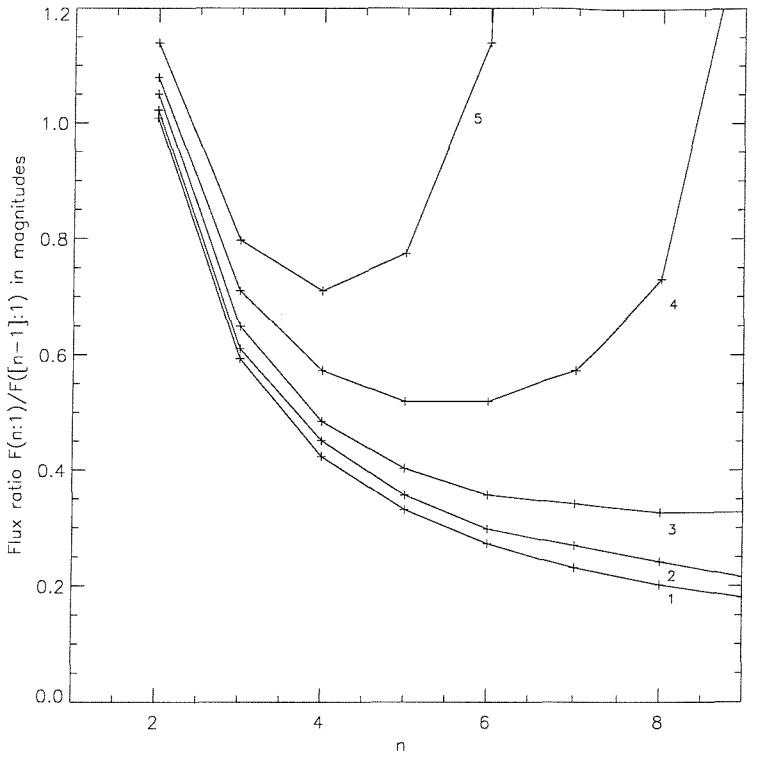

Figure 2.6: Modelling of flux ratios F(n:1):F([n-1]:1) of optically thick isothermal discs with a central cavity $R_{inner} = 1 \rightarrow 5R_*$, where $R_* = 14.7R_\odot$ (III).

try on record, between 1975 and 1980 the system was even brighter (state C). Persi et al. (1979) present IR photometry obtained during this period on 11-13/12/1976, in which $K = 6.71 \pm 0.02$: Subtracting the stellar flux leaves a disc magnitude of 6.942, 0.46 ± 0.1 magnitudes brighter than the bright state of $m_{K(disc)} = 7.4$ seen from 1987-2001. Additional photometry obtained in adjacent months shows m_K brighter still by 0.1-0.2 magnitudes. de Loore et al. (1984) also present photometry from this period; they measure $m_{2.3\mu}(\simeq m_K) = 6.54 \pm 0.02$ on 15/10/1978. These fluxes are considerably outside the observed range for state B (Table 2.5). Lyuty and Zaĭtseva (2000) also present *luminosity normalised* $W_{\lambda H\alpha}$ values from this time showing extremely large values of $\sim -40\mathring{A}$ (equivalent to ~ -20Å).

These observations suggest the existence of a further state (designated C), larger than the discs observed from 1987-2001. A disc truncated at the 3:1 resonance will be rapidly disrupted as it lies well outside the primary lobe at periastron, so it seems likely that state C is truncated at 4:1, with the 1987-2001 states B

and A at the 5:1 and 6:1 respectively. As Figure 2.6 shows, the flux ratio from $6:1 \rightarrow 5:1 \simeq 5:1 \rightarrow 4:1$ enabling this scenario to include all 3 observed states.

If then we are observing truncation at 3 different commensurabilities, the viscosity of the disc must be changing through a greater range than predicted by Okazaki and Negueruela to allow truncation to occur at the 6:1 radius.

A further observation is that the brighter level of emission in the TCS dataset (B) exhibits greater fluctuations than the lower state (A), both in IR and Hα. As the radius remains almost constant for a given resonant truncation, as is born out by simulations (Section 1.7), this suggests that the conditions in the outer disc are varying; it may be that the disc is not completely optically thick at large radii enabling greater variability. A further possibility is that because the outermost regions of a 4:1 disc are outside the primary lobe at periastron (Okazaki and Negueruela, 2001), the outer disc almost certainly becomes disrupted at periastron in this state, and probably to a lesser extent at 5:1 and possibly 6:1. In this scenario the fainter states are expected to exhibit smaller fluctuations. It seems probable that the K band excess is optically thick in order to provide the stability of the magnitude states.

The brightness of A0535+262 in JHK is critical to this discovery. If other systems display similar behaviour, the proximity of the levels prohibits their observation without photometric errors $\leq 0.05 - 0.1$ magnitudes.

2.3.2.2 Temporal association with X-ray outbursts

When the disc outer radius makes a quantum leap inwards (change from state C to B or from B to A) the material present between those radii must be relocated. It is interesting and provocative to note that a photometric change of this nature occurred (as seen in m_K) between JD 2449344 (22/12/1993,state B) and 2449401 (18/2/1994, state A). In m_V fading started between 2449274 (13/10/1993)

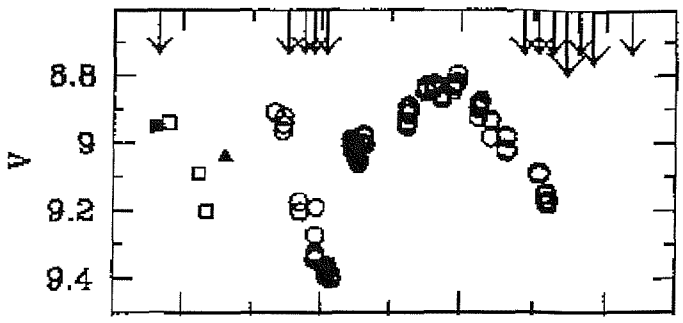

Figure 2.7: Correlated V band photometry and X-ray activity in 4U1145-619, from Stevens et al. (1997).

and 2449359 (6/1/1994), and state A was unequivocally reached between 2449457 (14/4/1994) and 2449596 (31/8/1994). The greater length of variability in V as opposed to K is interpreted as being due to the greater optical depth in K desensitising the photometry to small variations in disc structure.

The last recorded Type II outburst was detected by BATSE from Jan 28 to Mar 20 1994 (Finger et al., 1996). The timing of this outburst, precisely at the time of the optical state change strongly suggests the possibility that this giant outburst was triggered by accretion of disrupted material previously resident between the 5:1 and 6:1 resonances.

Clark et al. (1999) in discussing the long term photometric variations of A0535+262, noted that X-ray outbursts seemed to occur after a period in which the optical light curve was fading, an anticorrelation also observed for 4U 1145-619 (Stevens et al. 1997) shown in Figure 2.7. Clark suggested that this represented an episode in which disc material was lost radially, with X-ray emisison triggered by the interaction of this material with the NS. However, this suggestion was rejected in favour of the traditional 'shell ejection from the primary' scheme. This connection is discussed further in Section 2.6.4.

Looking in detail at the this truncation event shows that it was not simply a straightforward jump in outer radius. The patchy m_V photometry covering the early stages of this event shows a rapid decline followed slightly over 100 days later

by another over the same range, a (partial?) recovery presumably having occurred in the interim. It is tempting to envisage successive orbits of the NS partially removing material until full truncation has occurred (see Section 2.6.6). Interestingly this sequence of repeated fadings and brightenings is simultaneous with the succession of Type I outbursts which occurred either side of the Type II event.

Such a connection between long-term (months-years) photometric changes and X-ray events has not received a great deal of attention in the literature, with most work expecting to observe short optical flares associated with enhanced stellar mass-loss prior to an outburst.

Further work in this area is to be found in Section 2.6 onwards which broadens the exploration of these phenomena to include spectroscopic ramifications.

2.4 Optical emission line spectroscopy

2.4.0.3 Refutation of shell features

It has been suggested (Piccioni et al., 2000; Lyuty and Zaĭtseva, 2000) that the Hα line profile shown by HDE 245770 shortly after disc-loss (late 1998 to early 1999) is evidence of the system entering a shell phase; such an observation would be significant as it would imply an inclination $i \geq 80°$. They note the presence of an 'absorption core' at the line centre. Whilst this more than meets the traditional criterion set out for a shell spectrum (not only is there a central reversal, but the line centre lies beneath the continuum) it arises from confusion regarding the true nature of this line profile. Because Keplerian discs viewed at $i > 0°$ are expected to be double peaked and thus to show a central reversal in their emission features, it is not lack of emission at the line centre but rather *absorption* that defines a shell star. Thus when disc emission is weak, for example 11/1/1999 (Figure 2.8), the line centre

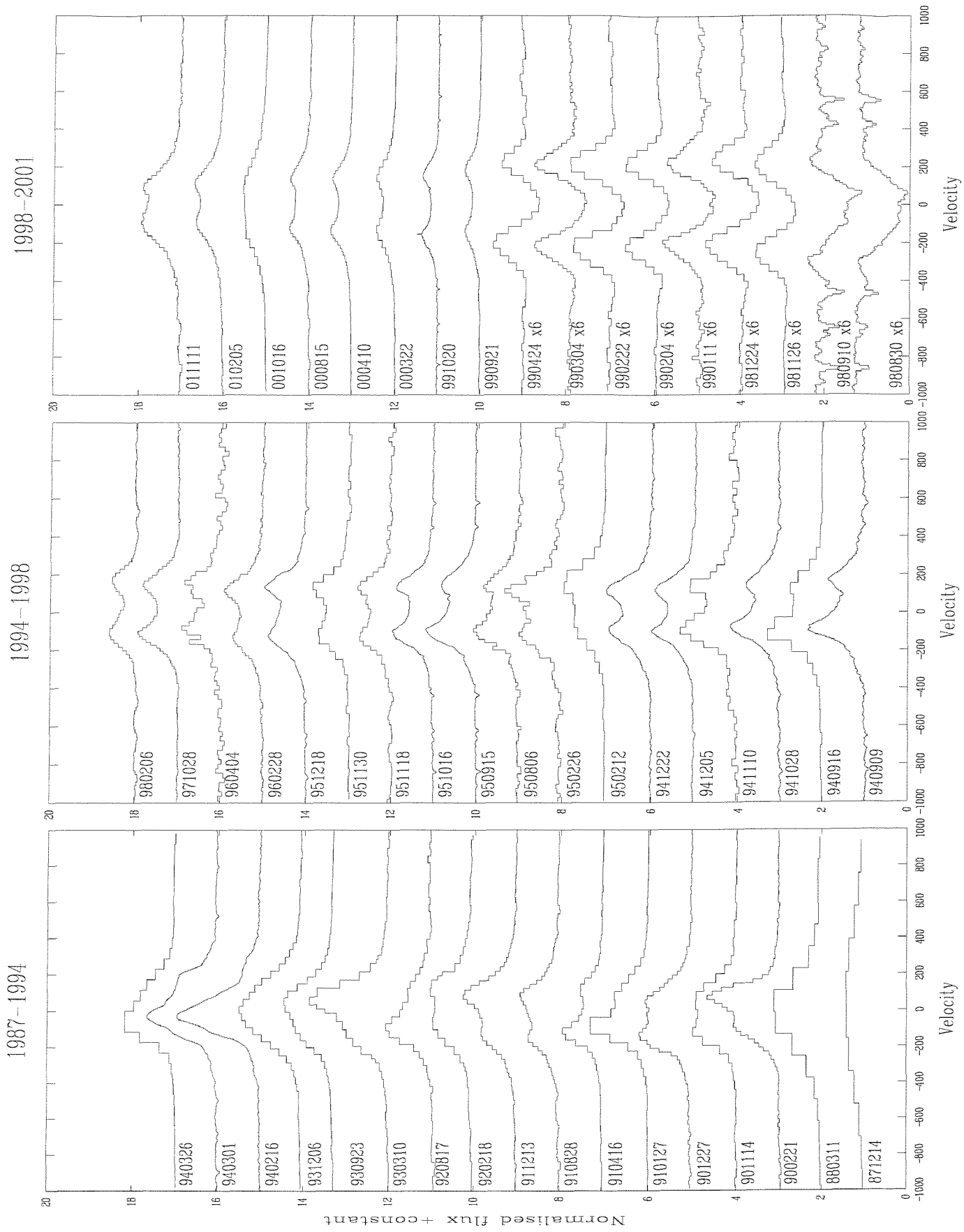

Figure 2.8: Representative HDE 245770 Hα profiles. Note 6$\times$ scaling of spectra around disc-loss.

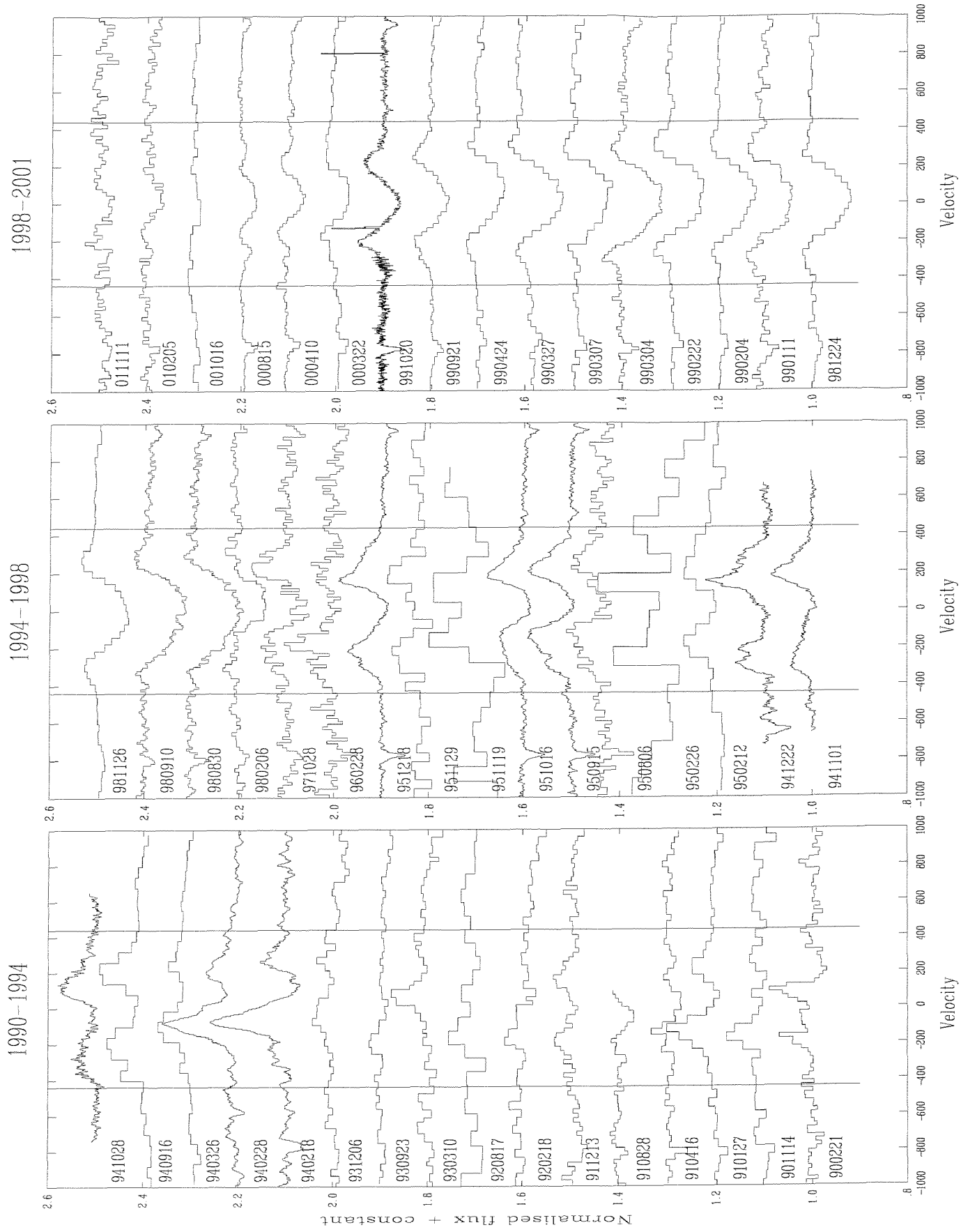

Figure 2.9: HDE 245770 He I 6678Å profiles.

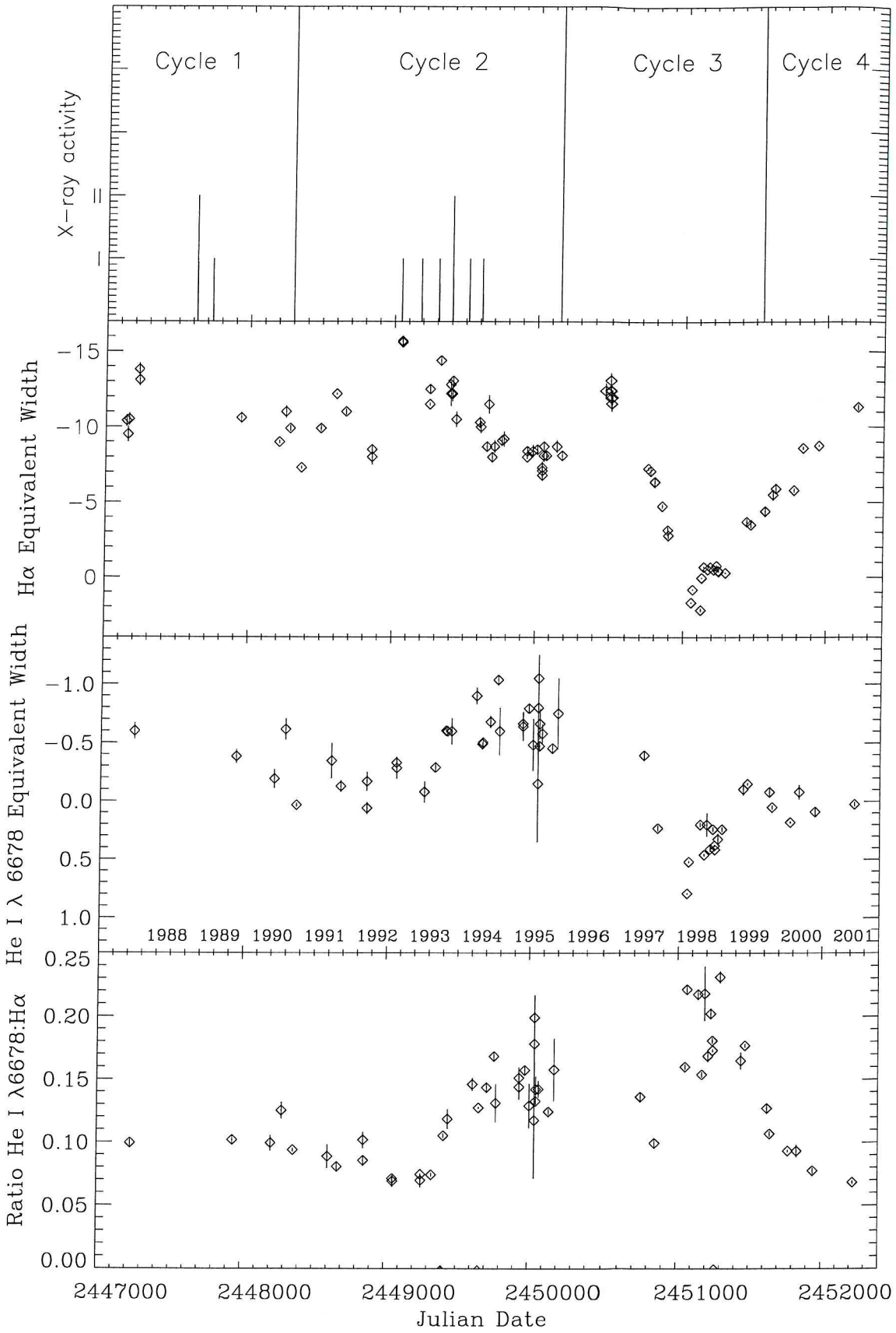

Figure 2.10: Hα and He I λ6678 W_λ data from 1987 to 2001, and the ratio He I:Hα.

has scarcely above the intensity of the underlying photospheric absorption. The width of this apparent 'absorption feature' belies its nature however; true shell stars have extremely narrow absorption cores (FWHM$\leq 50\,\mathrm{km\,s^{-1}}$) due to the minimal motion along the line of sight, whereas the gap between two quasi-Gaussian peaks is considerably broader (see Figure 1.1), presenting a 'shell' feature with FWHM$\approx 300\,\mathrm{km\,s^{-1}}$.

Furthermore, the inclination of the Be star is shown to be $\approx 40°$ in Section 2.6.2, explaining why shell profiles have never been observed in this system. This misinterpretation probably arose from the low resolution of Piccioni et al.'s spectra, and additionally illustrates the benefits of viewing each spectrum in the context of those preceeding and following it so that features can be correctly interpreted; with this ability the 'absorption core' can be seen to be the expected dip between emission wings on either side (see Figure 1.3).

2.4.1 V/R variability

As has been previously observed (Clark et al., 1998) A0535+262 displays V/R cycles on a timescale considerably shorter than most Be stars (eg $\gamma\ CasP \sim 5 \pm 1$years (Telting et al., 1993)). Clark et al. found a period of $\sim 1\ year$, which can be seen in Figure 2.11. A consensus has emerged (Clark et al., 1998; Larionov et al., 2001) that, in common with Be stars in general, such cycles are attributable to the evolution of non-axisymmetric distributions of material over time.

From MJD 48200 to 49850 approximately 3 cycles can be observed in both Hα and He I, yielding a period of 550 days. Following this a cycle is completed in 330 days (up to MJD 50180). Figure 2.10 shows that the initial long cycles occurred during a time of low He I:Hα W_λ ratio, when the disc in the (large) state B; the second faster period corresponds to stronger He I and weaker Hα, and the smaller state A. Confirming this trend is the observation of a 120 day V/R cycle (Figure 2.12),

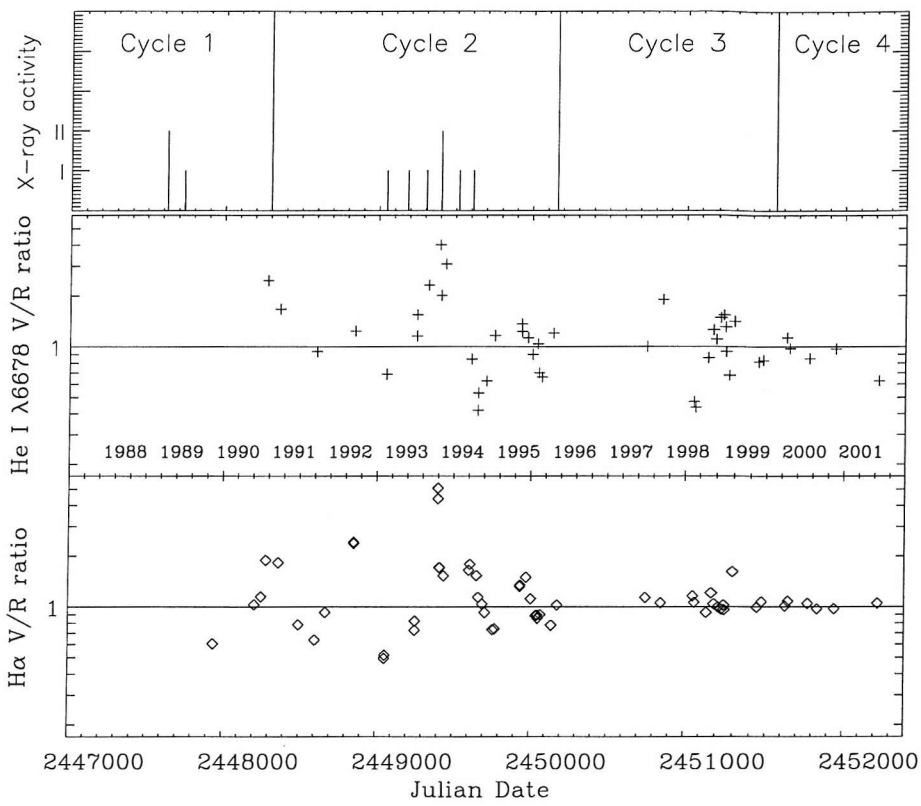

Figure 2.11: V/R oscillations in Hα and He Iλ6678. Log scales are employed.

visible only in He I between MJDs 51160 and 51280, when the disc was reforming after it's mid-1998 disc-loss, and was significantly smaller than typical (see Figure 2.15). Interestingly, X Per also displayed some rapid quasicyclic V/R variations following it's 1990 disc loss (Clark et al., 2001), which quickly lengthened to a more typical period as the disc recovered.

The Hα and He I V/R oscillations track each other quite closely throughout the dataset except for these months following disc-loss, when Hα shows little V/R activity while He I is quite strongly perturbed. Such differential V/R behaviour of Hα and He I has been reported before in A0535+262 (Clark et al., 1998a). This appears to represent an asymmetry, possibly a GOAO, confined to the inner disc at a time when the entire disc was relatively small. There is no suggestion of this asymmetry affecting the disc in any other way; for example the disc expansion throughout this period was linear (Figure 2.15).

Thus there appears to be a relationship between the period and the radius of the

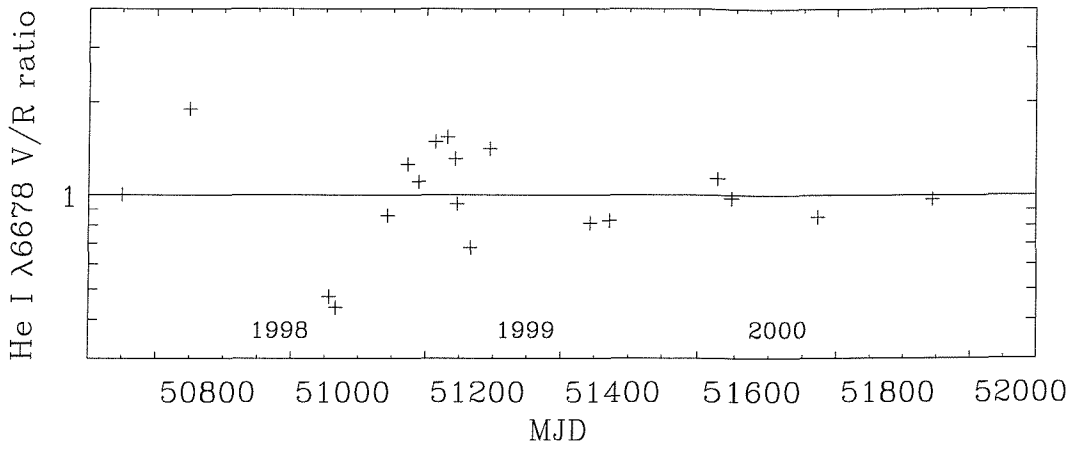

Figure 2.12: Rapid V/R oscillations in He I λ6678 around MJD 51200 following disc reformation.

disc. According to work on GOAOs (Okazaki, 1991) the period is in part a function of the outer disc radius; in general BeX systems should show shorter periods due to truncation (Reig et al., 1997). Unfortunately there is insufficient data following the 120day cycle to verify whether the period increased in step with the gradual growth of the disc.

Hao et al. (1996) found an optical periodicity of 508 days, which could be due to the V/R cycle. It is expected that V/R oscillations show in the continuum if they also affect the overall $W_{\lambda H\alpha}$ (LSI +61 235 shows a correlation between JHK and V/R (Reig et al., 2000)). The global variations in disc emission dominate the photometry on these timescales however, masking most V/R-photometric coupling.

The onset of V/R variations in 66 Oph have been attributed (Hanuschik et al., 1995) to the presence of a critical density above which viscous instabilities can grow. This suggests that the bulk disc has not recovered to the density it possessed prior to disc-loss, particularly in view of the presence of disturbances in the inner disc which should readily seed disturbances further out.

During the Type II outburst of 1994, the V peak at $\sim -50\,\mathrm{km\,s^{-1}}$ appeared to

strengthen greatly to give the two largest V/R ratios recorded here, both in Hα and He I. Although it appears to broadly fit in with the ongoing V/R cycle, it is something of a coincidence that this should be simultaneous with the strongest X-ray activity over the period. Okazaki and Negueruela (2001) found that for systems with moderate eccentricity, such as A0535+262, accretion from the disc can only occur when the disc is heavily perturbed from it's symmetrical state, a state which can naturally produce V/R variations. It appears that strong V/R variations were occurring thoughout the 1993-1994 X-ray activity cycle, declining somewhat afterwards, but in the absence of more thorough spectral coverage a causal link between the strongly perturbed disc and the X-ray outbursts can only be suggested. The possibility that the peak may have been *induced* by the X-ray activity is all the more intriguing. Note that this anomalous V peak and the resultant small ΔV_{peak} is also the cause of the abnormally large orbital radii derived at this epoch (Figure 2.20). More peculiar observations from this epoch are described in Section 2.6.5.1.

2.4.2 Multiple disc phenomena in He I

The phenomenon of emission line outbursts is discussed in Section 1.2.4.2. For reasons mentioned there, such phenomena are well observed in the He I lines, for example He I λ6678. Due to it's spectral proximity to Hα this line has the major benefit of being included in most of the archive spectra, and has previously revealed multiple discs in X Per (Tarasov and Roche, 1995), μ and η Cen amongst others.

A number of spectra of HDE 245770 obtained during 1994 and 1995 clearly show the presence of 4 peaks, mostly as 2 pairs of V and R peaks (Figure 2.9). Unfortunately from an analytical point of view fitting a line profile with 5 components (broad emission peak, indicating the broad level of emission arising from the entire disc, and 2 pairs of V,R peaks) is frought with difficulties and uncertainties. The fact that the peaks are also significantly non Gaussian creates problems. Exceptionally high R spectra of excellent S/N are a prerequisite, and few of these are available.

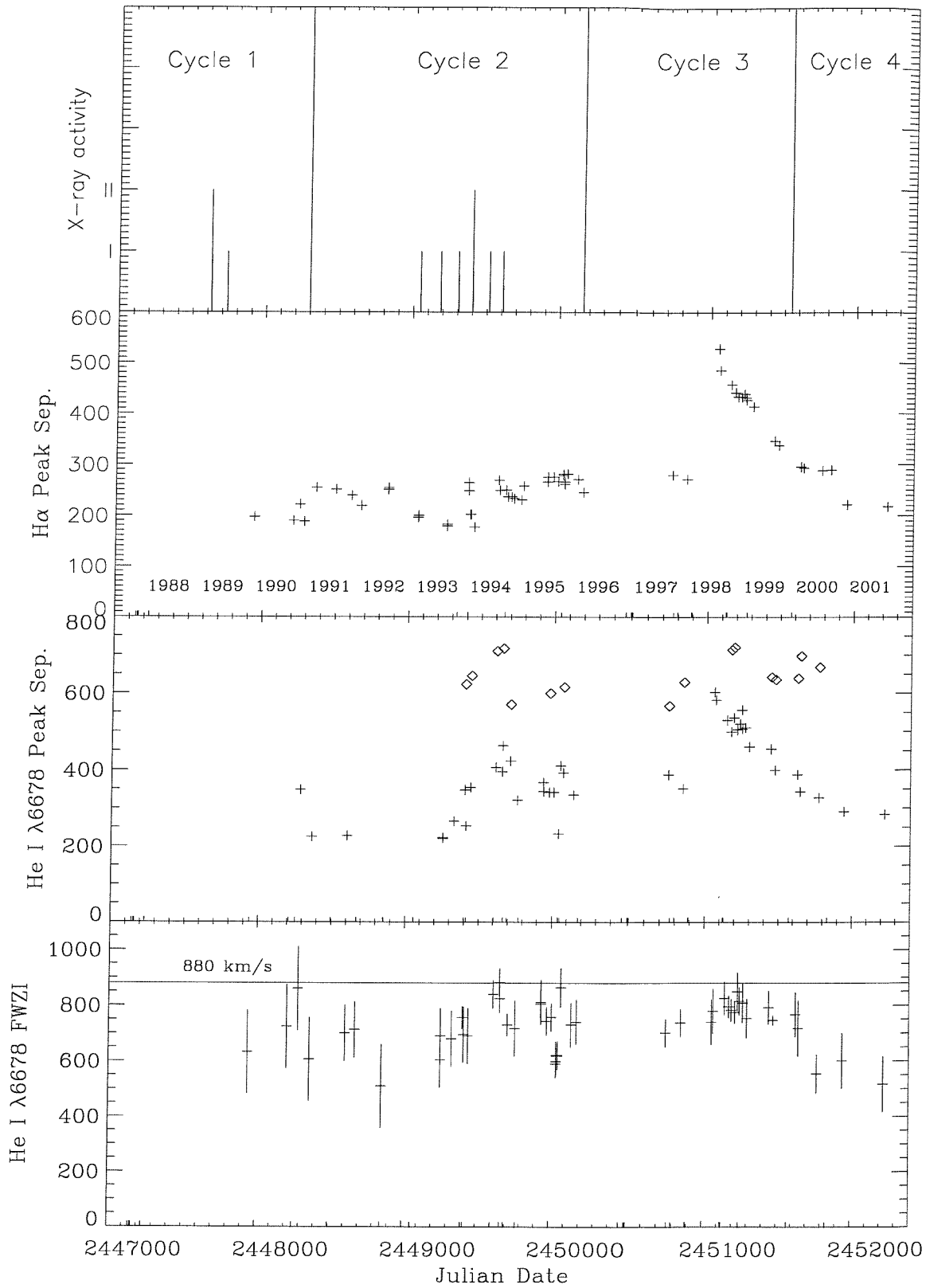

Figure 2.13: ΔV_{peak} of Hα and He I λ6678 and observed maximum velocities of He I in km s^{-1}. A single V-R pair fitted to the profile is plotted as +, whilst o denotes additional high velocity components.

Thus velocities for these high velocity structures are available for only a few spectra.

Figure 2.13 shows in the middle panel the velocity separation ΔV_{peak} of the V-R pairs observed. Instead of forcing the line profile to be decomposed into 2 V-R pairs, a single V-R pair has been fitted to the profile, measuring the 'bulk' material, and any obvious additional components determined subsequently.

Upon close inspection, few if any of the high S/N and high R spectra show He I profiles consistent with a simple uniform disc. Whilst this is often an excellent approximation, there almost invariably are quasi-symmetrical structures in the line wings indicative of radial density variations. Such structures are only detectable at low radii where the Doppler shifts are sufficient to move them well away from the line centre, but there is no reason to conclude that they are restricted to these regions. Thus the double disc points shown in Figure 2.13 should be considered to be only a fraction of those present over time, and indeed correspond only to the epochs of high resolution spectra. This appears to support the proposition that episodic outbursts are extremely common in early type Oe/Be stars (Rivinius et al., 2001). In Section 2.5.2.3 this is discussed further in the context of the 1998 disc-loss episode.

2.4.2.1 Central cavities

The lower panel in Figure 2.17 shows the ΔV_{peak} of the He I λ6678 line peaks in terms of it's W_λ. It can be seen that whilst a range of W_λ exist for typical velocities, this range declines for higher values, approaching zero at the maximum observed ΔV_{peak} for He I - (W_λ 0.792 $\pm$ 0.005, 30/8/1998), where the outer radius of the bulk emission approaches the inner radius. This can be seen to occur at 610 $\pm$ 20 km s^{-1}. Again using the value of 880 km s^{-1} (Figure 2.13) for the maximum observed Keplerian velocity, we thus derive a ratio of $\frac{r_1}{r_2} = (\frac{v_2}{v_1})^2 = 2.08 \pm 0.13$ for the inner radius in terms of the minimum radius at which emission is observed. Thus the inner

cavity is probably of the order of $2.5 - 3R_*$, depending upon assumptions about the minimum radius at which detectable emission is occurring.

The presence of a central cavity can be understood in the framework of episodic mass flow combined with a viscous decretion disc. The radial dependance of the viscous timescale means that reaccretion of material from the inner disc happens much more rapidly than changes that affect the entire disc, and indeed accretion must occur in the absence of angular momentum transfer to the disc, as occurs between mass loss episodes.

2.4.3 IR spectroscopy

Compared to the large numbers of optical spectra in the BeX archive, relatively few IR spectra are available. Additionally those available are of lower resolution such that only W_λ parameters are obtainable. No detailed analysis has been undertaken, other than to verify that broadly the behaviour of the IR HI lines mimics that of the optical Balmer, as with the IR and optical He I lines. The special case of IR spectra obtained around disc-loss is discussed in Section 2.5.2.2.

Zaal et al. (1995) found that IR HI lines should be a more sensitive indicator of low density circumstellar discs than the traditional Balmer lines; τ *Sco* (B0.2Ve) has shown Brα emission while Hα remained in absorption. This is interpreted by Zaal et al. as due to the lower continuum level in the IR allowing weak emission to show through. This does not appear to be born out by the disc loss IR spectroscopy presented here, which show Brγ in absorption, though these spectra were obtained only 5 days after the lowest recorded $W_{\lambda H\alpha}$ of 2.2Å.

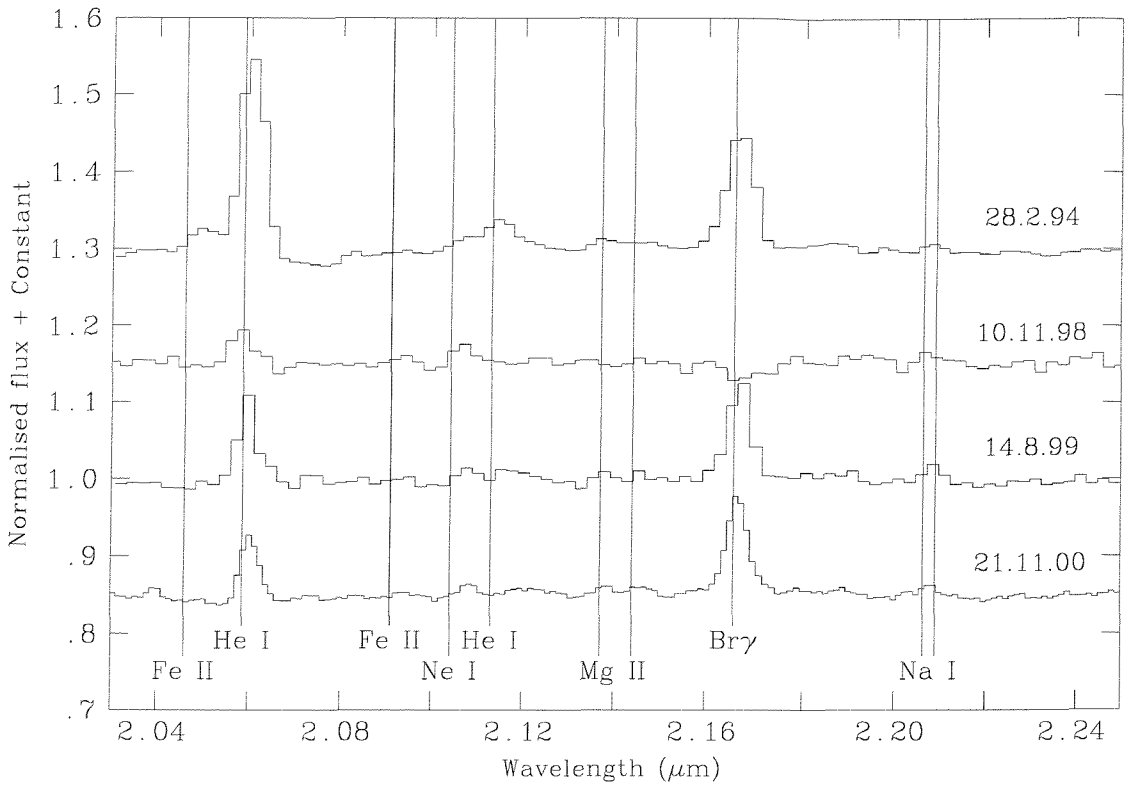

Figure 2.14: CGS4 K band spectra; before, during and after disc-loss.

2.5 The 1998 disc-loss episode.

The most remarkable event to have occurred in the A0535+262 system during the period covered by the dataset presented here is the dissipation of the circumstellar disc that occurred in 1998. The event is characterised by the shift of all parameters that mark HDE245770 as a Be star toward values expected for B stars. In practice this involved a fading in all photometric wavebands (possibly excepting U), and the disappearence of emission in spectral lines, both optical and IR. The only possible explanation for this is a (not necessarily complete) dissipation of the equatorial circumstellar material. The longterm context within which this disc-loss occurred is discussed in Section 2.6.4.

	15 Dec 1998 JKT	27 Oct 1998 TCS	Jan 1999 SAAO	26 Nov 1987 CRAO	29 Dec 1987 TCS
B	9.85		9.92	9.58	
V	9.44		9.46	9.04	
R	9.12		9.13	8.28	
I	8.83		8.80	7.83	
J		8.49	8.62		7.65
H		8.39	8.42		7.36
K		8.34	8.34		7.16

Table 2.6: Comparison of optical/IR photometry at the near discless state of late 1998/early 1999 with the typical state B of Jan/March 1991. CRAO BVRI data from Clark (1997).

2.5.1 Photometry

Comparison of October 1998 JHK photometry with archive data (this work and Clark et al. 1998b) showed that a marked fading in all three wavebands had occurred since the previous observation in March 1996, the decrease in m_K being 0.8 magnitudes (Figure 2.2). The system had also become bluer, the J-K colour index decreasing by approximately 0.3 (Figure 2.2, bottom) as the disc excess became optically thin in J and K. These data illustrate that the (J-K) colour index is an excellent indicator of disc-loss.

A good example of a 'typical' system state can be seen in Nov/Dec 1987 (chosen because there exists quasi-simultaneous UBVRIJHK photometry and spectra). At this time the disc was in a characteristically strong emission state with J and K magnitudes of 7.65 and 7.16 respectively (Table 2.6). On 27-28 October 1998 these magnitudes were 8.49 and 8.34, i.e., the fluxes in these bands had fallen to 46% and 34% of their 1987 values. These percentages are close to the $I_*/(I_* + I_{disc})$ emission fraction as determined from Roche et al. (1993) for X Per, deduced after

this similar system suffered a disc-loss event in 1990 which saw its IR fluxes fall in a similar manner. The lower, bluer colour index reflects the greater relative contribution of the hot B star flux. These results demonstrate the loss of the bulk of the infrared emission from the circumstellar disc around HDE 245770. Additionally, BVRI magnitudes from disc-loss data sets are significantly fainter than seen historically, consistent with the loss of the disc contribution, and the commencement of a 'faint state'.

BVRIJHK were all found to be fainter than at any stage since discovery as an X-ray source.

2.5.2 Spectroscopy

In order to monitor the expected rebuilding of the disc, spectra were acquired as frequently as possible following the October 27^{th} 1998 JHK observation; most spectra are from INT and WHT service requests.

The KPNO spectrum from August the 30^{th} 1998 (Figure 2.8) shows Hα in *absorption*, a state unseen in any observation since the recognition of HDE245770 as the optical counterpart to A0535+262 in 1975. Following similar episodes in X Per (Clark et al., 2001) and 4U0115+63 (Negueruela et al., 2001) this is clear evidence of a disc-loss episode, or 'faint state'. However W_λ reveals some emission to be present, and additional spectra and published W_λ from around this time (Figure 2.15) reveal the emission to have increased by September before reaching it's lowest recorded value of 2.2Å on November 5^{th}. Only 5 days later the line is barely in absorption (0.04Å), and by November the 25^{th} a quasi-steady state was reached at $\sim -0.6\mathring{A}$ which ended between April the 24^{th} and Sept the 20^{th} 1999.

All Hα profiles following the early 1998 gap in coverage display weak double peaked emission either side of photospheric absorption below the continuum, with

quasi-symmetrical emission wings at unusually large velocities of $\pm 200 - 300\,\mathrm{km\,s^{-1}}$. The separation gradually declined as the disc expanded (Figure 2.13). The absorption core of Hα is consistent with the assertion from IR photometry that the disc has lost much of its emission and presumably mass; it reveals a strongly depleted disc outwards of several stellar radii. This demonstrates the equal effectiveness of IR excess and Balmer line emission for probing the extent of the disc in the broadest sense.

Though weaker than in pre-disc-loss spectra, He I 6678$\mathring{A}$ emission wings rapidly appeared at a greater fraction of their historical intensity than did those of Hα. This suggests that the very innermost disc has a higher fraction of its pre-loss density than the regions slightly further out giving rise to the Hα peaks. Similar behaviour is seen in the IR lines.

The assumption of a predominantly kinematic explanation of the line profile, combined with the overall low IR luminosity, implies the existence from approximately November 1998 until a time between April and September 1999 of a rapidly rotating and thus small inner disc. Such a small radius is to be expected of a young disc which has had insufficient time to propagate material outwards (Rivinius et al., 2001). This emerging inner disc appears similar in nature to the rapidly forming inner disc observed in X Per in February 1995 (Tarasov and Roche, 1995).

Interestingly $W_{\lambda H\alpha}$ declined over a much longer timescale than the concurrent shift in JHK emission, which occured quite distinctly and rapidly (Figure 2.15). This could be due to the fact that the IR thermal Bremsstrahlung of a parcel of gas depends (to a first approximation) upon $V\rho^2 = m\rho$ whereas optically thin Hα flux depends only upon m, so a spatially dispersing cloud of circumstellar material of a given mass would cease emitting detectable IR excess long before it's line emission disappeared. Thus it is possible that, as has been suggested for the 1994 truncation event, much circumstellar material was not re-accreted by the Be star but (temporarily?) dispersed within/around the system. However, the limited ΔV_{peak} data

from the midst of the $W_{\lambda H\alpha}$ decline shows a normal state A disc radius (Figure 2.20); in the case of the 1994 truncation/Type II event much of the Hα emission lay at the line centre, suggesting a location far from the Be star. This is also not seen in the decline to disc-loss. Therefore it appears that the material was re-accreted (Porter, 1999) rather than dispersed, with density declining in-situ. The lack of X-radiation centred at this event (JD$\sim$2450450, Figure 2.24) also argues for this.

2.5.2.1 Measurement of $v \sin i$ and ω

The almost purely photospheric spectra obtained at this time allow determination of the stellar $v \sin i$. Following Mazzali et al. (1996) blue end He I lines were used due to their intrinsically narrow FWHMa, using the spectra obtained at the WHT on 24/12/1998. The preferred line (narrow and scarcely contaminated by emission) at 4713.20Å yields a $v \sin i$ of 251 $\pm$ 5 km s^{-1}, whilst the intrinsically broader λ4471,λ4922 lines give 254.2 km s^{-1} and 261.3 km s^{-1} respectively. The instrumental broadening was determined from arc lines to be 120 km s^{-1}, yielding a deconvolved stellar $v \sin i$ of 220.4 km s^{-1} at λ4713, and 224 (232) km s^{-1} for λ4471 (λ4922). Thus a value of 225 $\pm$ 10 km s^{-1} is adopted. This compares with the published value of $v \sin i$= 250 $\pm$ 15 km s^{-1} (Wang and Gies 1998), who did not have the advantage of spectra uncontaminated by emission.

Using $i = 40°$ (Section 2.6.2) we find a rotational velocity of 350 $\pm$ 15 km s^{-1}. Extrapolating the v_{crit} of Porter (1996) by one half-subclass to O9.7(V), we determine $\omega = \frac{v}{v_{crit}} = 0.64$; such a value is typical for shell stars (where $v \approx v \sin i$). Note that this also argues against a substantially higher inclination, which would reduce ω below the expected range for Be stars of 0.6-0.8. If a giant (III) classification is adopted, then by using the $\frac{R_{*(V)}}{R_{*(III)}}$ ratios of VGS96 we obtain $\omega = 0.84$. This is still consistent with the measured range of ω for shell stars, but argues for a larger inclination ($\sim 51°$) to conform with the canonical $\omega = 0.7$.

2.5.2.2 Disc loss IR spectra

Several previous IR spectra of A0535+262 have been presented (Clark et al., 1998b; Clark et al., 1999b) showing the system exhibiting typical Be/BeXRB spectra. Figure 2.14 presents 2.03 - 2.25μm excerpts from a typical K band historical spectrum, the 'disc-loss' spectrum from 1998 November 10, and 2 subsequent spectra illustrating the resumption of normality. Regarding the disc-loss spectrum, the Brγ 2.16 μm feature can be seen to have gone into absorption (W_λ=2.3 Å), although the He I 2.058 μm feature is still weakly in emission (W_λ=-2.8 Å).

Clark & Steele (1999) present K band spectra of a sample of 66 Be stars; in *all* of those spectra whenever He I 2.058μm emission is present it is accompanied by Brγ emission. It is clear therefore that A0535+262 was in a highly unusual state at this time. These observations support the conclusion from optical spectroscopy that a small disc existed at this time, the extent of which is sufficient to emit a close-to-normal He I line (normally emitted at small radii anyway (Stee et al., 1998)) but not significant Brackett and Balmer emission.

In order to observe the He I 2.058μm (1s2s – 1s2p, ^{1}S – ^{1}P^0) line in emission, the circumstellar disc must have appreciable density in order that the optical depth at 584Å can be large enough to prevent de-excitation of the upper 1s2p state via the substantially more favoured (1s^2 – 1s2p, ^{1}S - ^{1}P^0) 584Å transition (Clark, private communication). In most objects, this upper state is populated by recombination from He II(Clark et al., 1999b). Whilst this appears unlikely to be the case, as He IIis not observed in emission in *any* Be stars (Clark, 1997), the conditions in a reforming disc at very small radii may be atypical of Be stars in general (ie hotter), and thus this mechanism may be enhancing the line strength.

It can therefore be seen that the He I 2.058μm emission indicates that a dense environment is required. This implies that disc reformation was taking place by early November 1998.

The observed resumption of Brγ emission by 14 August 1999 verifies the recovery of the disc to a typical state by this time.

2.5.2.3 Discrete mass ejections

It has been suggested (Hanuschik et al., 1993) that the influx of material into the circumstellar discs of Be stars is dominated by discrete episodes of mass transfer, particularly towards earlier spectral classes (Rivinius et al., 2001). Rivinius et al. (1998a) describe excellent quality observations of repeated He I outbursts in μ *Cen*, and subsequently put forward a case for such events occurring at the superpositional maxima of several non-radial pulsational modes.

This episodic nature is observed in A0535+262 during the disc-loss phase, as $W_{\lambda H\alpha}$ rose and subsequently declined at least once before consistent recovery began (Figure 2.15). m_V photometry reveals brightenings coincident with the increases in $W_{\lambda H\alpha}$, at JD 2451050 ± 20 and 2451150 ± 20. Additionally, as discussed below, the Keplerian bulk radius of both Hα and He I declines suddenly at 2451250, explicable best as a further outburst. Thus a pattern of repeated outbursts at intervals of $\sim$ 100days is suggested. If real the similarity of this recurrence period with the orbital period is probably coincidental, the pulsational properties of the Be star determining the period.

Following the August 30^{th} datum, $W_{\lambda H\alpha}$, $W_{\lambda HeI}$ and m_V show evidence for rapid increases followed by gradual declines on timescales of 100-200 days. This period is similar to the 100 days predicted by Hanuschik et al. (1993) for the timescale of material being re-accreted by the Be star μ *Cen* after an ejection event, from which point onward the radial movement of material in the disc is governed by viscosity. For μ *Cen* they observed cycles of rapid brightening (2-5 days) and slower fading (20-80days) very similar to that observed here on a slightly longer timescale. Alternatively, the continuing expansion of the disc at this time (Figure 2.15) suggests

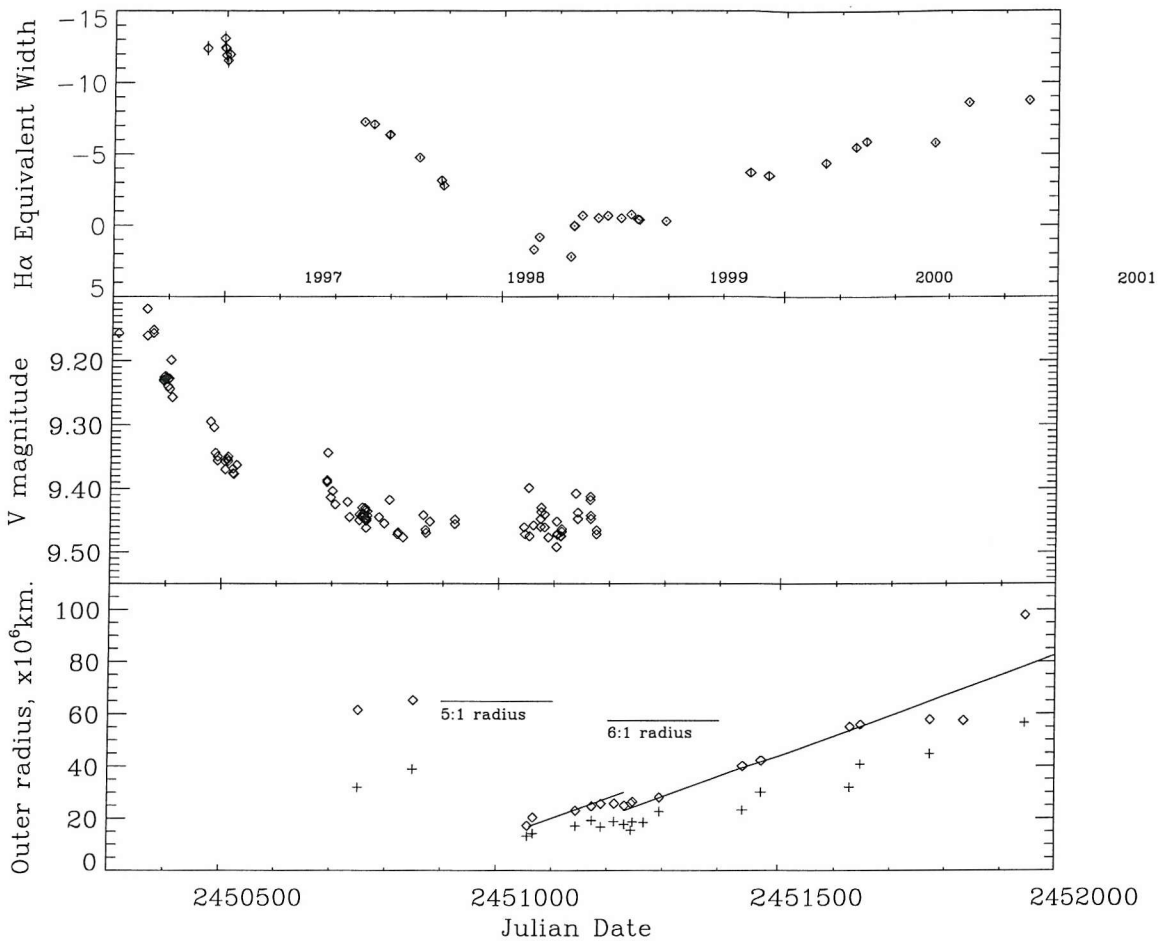

Figure 2.15: $W_{\lambda H\alpha}$ and m_V around the 1998 disc-loss. Lower panel shows outer disc radius in Hα(o) and He I (+) assuming i=40° and $M_* = 21.8 M_\odot$.

that the declines may be attributable to the disc expanding and cooling rather than to re-accretion.

It thus appears that even during disc-loss, the processes that lead to disc formation are continuing. The probable presence of a residual disc throughout disc-loss is thus supported. However, in the absence of information regarding the 'usual' frequency and amplitude of such events it is not possible to conclude whether the disc-loss was caused by changes in the B star (perhaps NRP amplitudes) or by external factors (see Section 2.6.4).

The He I and Hα outburst that led to the regrowth of the disc presents an excellent opportunity to observe the radial expansion velocity. However, if the regrowth was

punctuated by a further large outburst, such that enhanced peaks appeared in the spectra at large velocities, the overall peaks may move outward somewhat reducing the observed expansion velocity and making the value derived here a lower limit. Indeed there exists a slight increase in velocity at 2451250 (visible clearly in He I in Figure 2.13), presumably due to a subsequent outburst. The expansion can be fitted as linear with an offset at this time, with an expansion of $894 \pm 50 ms^{-1}$ in Hα (plotted). Of particular interest is the halt in expansion when r_{outer} reaches the region of the 5:1 and 6:1 resonances, further encouraging the truncation paradigm. The expansion to state B appears to end the cycle roughly 6 months earlier than the previous two (see Section 2.6.4). Though somewhat speculative, this could be due to a higher temperature of the entire 'fresh' disc leading to higher viscosity, whereas in previous cycles the material had been in the disc for some years.

The expansion in He I is far less linear and is probably influenced by changing conditions in the inner disc too much to be useful in this context.

2.5.3 Comparison with X Per

The phenomenon of disc-loss has been observed in numerous isolated Be stars, as well as in the BeXRBs X Per (Clark et al., 2001), 4U0115+63 (Negueruela et al., 2001), A0535+262 (Haigh et al., 1999), γ *Cas* (Norton et al., 1991), GX304-1 (Corbet, 1986) and 4U1145-619 (Stevens, 2000). Spectral coverage is available for all except 4U1145-619. Bearing in mind the limited temporal coverage of most BeXRBs spectroscopically, and the short time for which most have been known (30 years at most), it seems probable that most if not all BeXRBS experience episodes of disc-loss. Coverage for most of these events is sparse, and consist mostly of an Hα spectrum in absorption bracketted by emission some months either side.

X Per underwent a very similar disc loss episode in 1990 (Roche et al., 1993; Clark et al., 2001), and through 1991 passed through similar spectroscopic phases, strongly

suggesting that the events seen in A0535+262 were by no means unusual. In fact, a detailed comparison of the Hα line profile evolution in X Per reveals a near identical event. However, the standstill of several months during which $W_{\lambda H\alpha}$ was static in A0535+262 was not seen in X Per, which showed a much more linear recovery. A possible role of the NS is suggested, as the NS orbit is essentially the only difference between A0535+262 and X Per. It seems that A0535+262 underwent a disc loss event typical of BeXRBs. However, a detailed comparison awaits further work.

2.6 Analysis and correlation of observational parameters

As has been stated frequently elsewhere, it is the goal of astrophysicists to derive quantitative measurements of their subjects from observational data. In order to examine precisely what properties of the system are being measured by different observational parameters (e.g. $W_{\lambda H\alpha}$, IR photometry, He I ΔV_{peak}) it is instructive to examine their relationships to one another. Furthermore, combining various observables reveals behavioural subtleties not directly visible in either component dataset.

2.6.1 Density profile

2.6.1.1 m_K

Huang (1972) found that ΔV_{peak} of a line profile provides the outer disc radius. If the IR excess is occurring from an isothermal optically thick disc (or simply one of constant surface brightness) delimited by the same outer radius seen in Hα, the dependance of the IR flux on the Hα ΔV_{peak} is simply

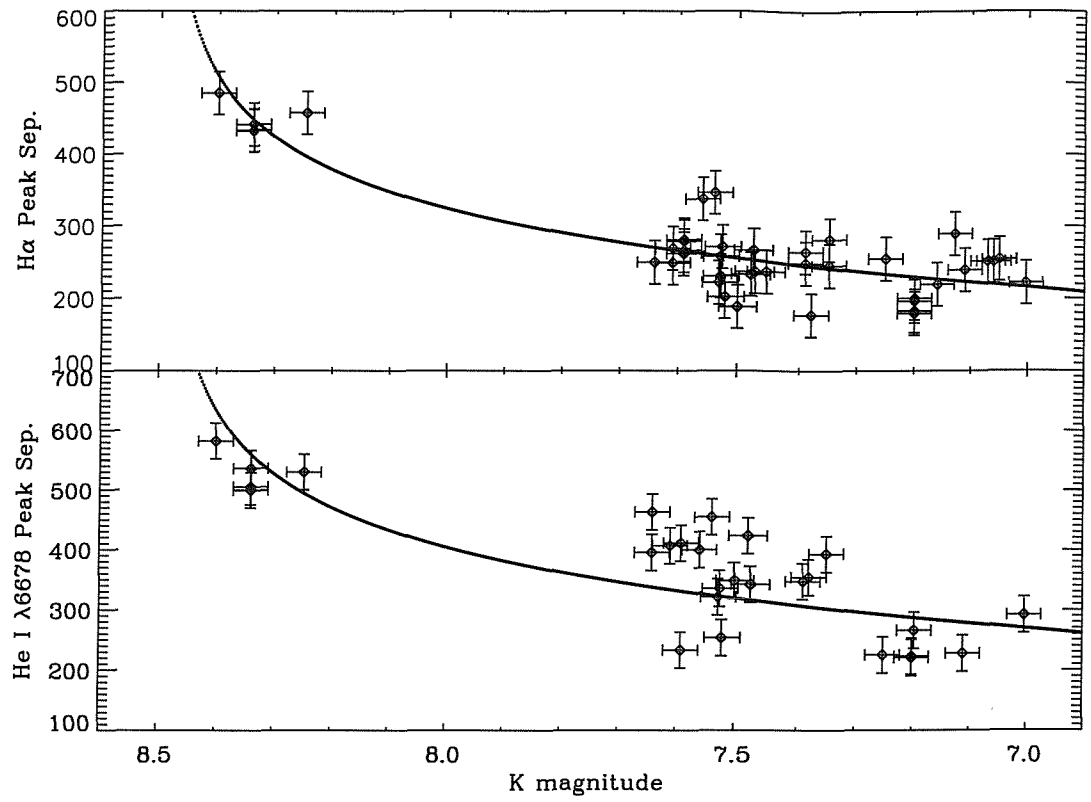

Figure 2.16: Modelling of m_K flux excess as an optically thick isothermal disc of radius $r_K = r_{H\alpha}, r_{Hei}$.

$$Flux = \alpha\left(\frac{2^4}{\Delta V_{peak}^4} - \frac{2^4}{\Delta V_{inner}^4}\right) + \beta \tag{2.3}$$

with α measuring surface brightness and β the stellar flux. ΔV_{inner} is taken to be $610\,\mathrm{km\,s^{-1}}$ (Section 2.4.2.1). Fitting this curve to the data provides a measurement of the stellar $m_K = 8.50 \pm 0.02$ (Figure 2.16). The reasonable fit suggests that the assumptions are valid approximations. However, given that we have considerable evidence that the disc is optically thick at least some of the time at K and shorter wavelengths, the constancy of the fit strongly suggests optical thickness in K at all times as suggested by the constancy of (J-K).

Errors in measurement of ΔV_{peak} can account for the deviation from the fit. Note that, as expected, the radius derived from the He I λ6678 line provides a poor correlation due to the emission from small radii frequently overwhelming that from the outer disc and invalidating the prediction of Huang (1972) that ΔV_{peak} measures

the outer radius.

2.6.1.2 Hα

If we denote the Hα flux per unit disc area as A(r), the total disc Hα flux will be

$$Flux = 2\pi \int_{r_{inner}}^{r_{outer}} A(r) r dr \tag{2.4}$$

Figure 2.17 uses equation 2.4 and various radial dependances of the surface density $A(r)$ to predict the equivalent width of Hα in terms of ΔV_{peak}. $W_{\lambda H\alpha}$ is multiplied by the estimated continuum (m_R) flux, determined from m_K by assuming the additional ff/bf component has a constant (R-K) colour, the value of which was determined using disc-loss photometry. This yields a line flux independant of the continuum, normalised to the continuum level at disc-loss.

If the Hα emission is optically thin (see Section 2.6.3), then A(r) provides an indication of the surface density. The vertical scatter suggests that the disc is not fully optically thick at Hα, or is subject to strong perturbations. It can be seen that the assumption of constant surface brightness (r^0) overpredicts the Hα line flux, with the best fit exponent to $A(r) \propto r^m$ being $m = -3/2 \pm 1/2$. This compares with a predicted surface density for an infinite viscous decretion disc of r^{-2} (Okazaki, 1998).

The implicit assumption though that the disc, at any given size, is identical to that subset of a larger disc is almost certainly flawed. Combined with the unknown optical depth effects, the only firm conclusion that may be drawn is that large discs have lower mean surface brightness in Hα than small discs, as would be expected.

For He I there is practically no correlation whatsoever, demonstrating the variability of the He I zone relative to the overall disc. Equivalent width is of course

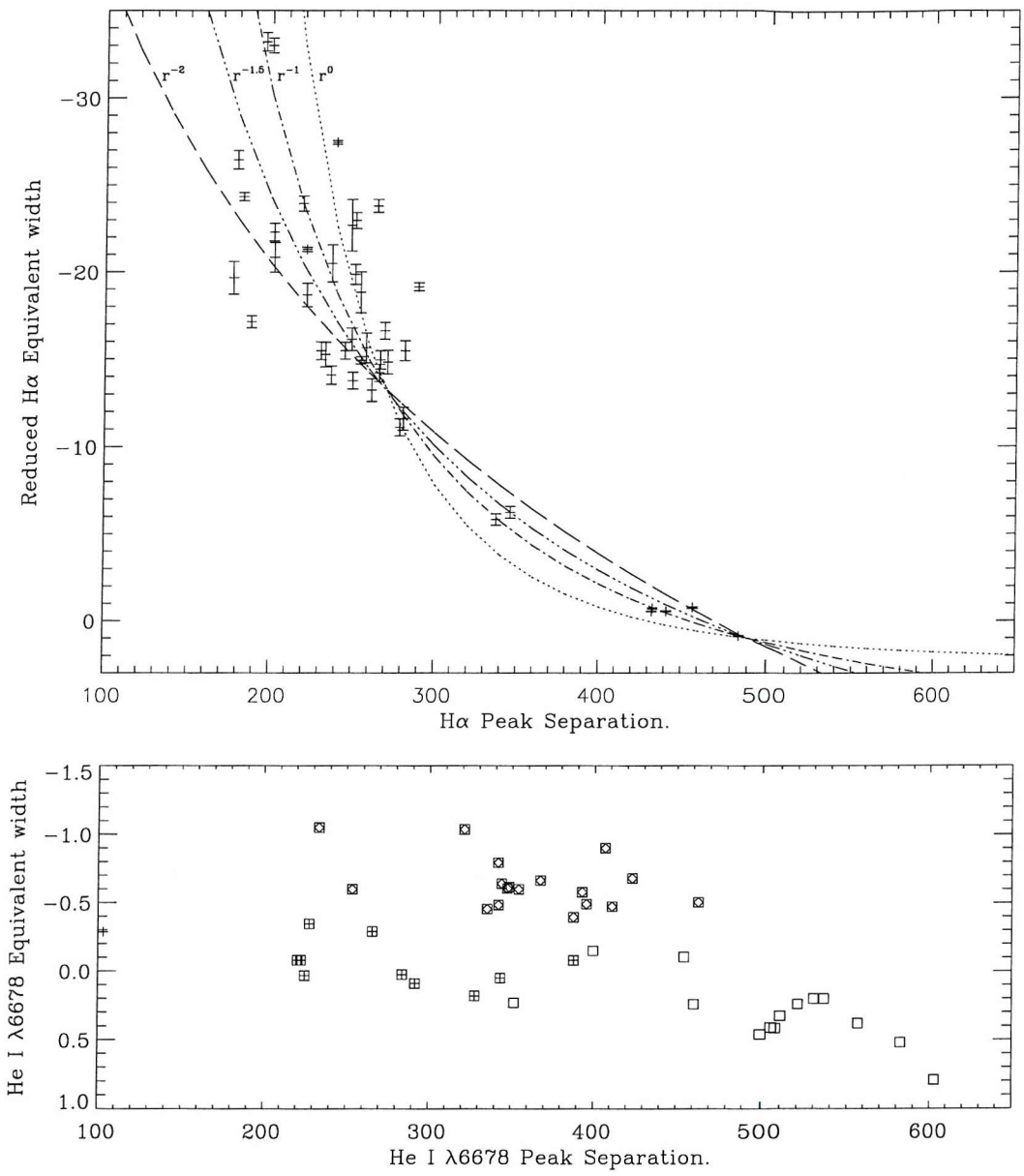

Figure 2.17: W_λ of Hα and He I against their respective ΔV_{peak}. $W_{\lambda H\alpha}$ has been divided by estimated continuum level determined indirectly from m_V, and normalised to a disc-loss continuum. For He I, squares with crosses are from the bright photometric state B, squares with circles are from the faint state A and squares are others, mostly from disc-loss. Errors are in measured W_λ, and do not include errors in normalisation. $W_{\lambda HeI}$ has not been normalised. Fitted curves show radial surface brightness functions of the form $A(r) \propto r^{-m}$.

reduced by associated enhanced continuum emission, so large W_λ values will not be proportional to the line flux, but this effect is not sufficient to explain the scatter. The data have been divided into those from the bright and faint photometric state and others, mostly around disc-loss. The large disc of state B shows a larger radius but weak emission, whereas state A shows greater compactness and approximately twice the line flux (allowing for photospheric absorption), demonstrating the effect of stronger truncation in enhancing the disc at small radii.

2.6.2 Constraining i

In order to derive the most information possible from the kinematic data yielded by spectroscopic studies it is clearly necessary to know the mass, inclination and if possible the stellar radius R_*. Whilst authors have disagreed with regard to the spectral type, the range given in recent literature is small, ranging from 09.5 to B0 (Steele et al., 1998 and references therein) in spectral type and III-V in luminosity class, with the modal classification being O9.7IIIe (Steele et al., 1998).

Several authors have derived wide-ranging masses for the primary based on luminosity, spectral class and orbital motion considerations: 9-17$M_\odot$ Janot-Pacheco, Motch & Mouchet (1987), 10-20$M_\odot$ Clark et al. (1998a), 8-22$M_\odot$ Wang & Gies (1998), $30 \pm 4 M_\odot$ Reig et al. (1997).

Wang and Gies (1998) derived constraints on the orbital inclination of the A0535+262 system, incorporating an orbital solution based upon pulse timing by Finger et al. (1994). Wang and Gies apply a lower limit of 26° based upon observed *vsini* compared to theoretical critical velocities, which are somewhat uncertain. The inherent assumption that the orbit and Be rotation are coplanar is unfortunately also not certain as supernova kicks can alter the neutron star orbit considerably (Lai, 2000); indeed, evidence is presented in Section 2.6.6 that the equatorial plane and NS orbit *are* tilted. Their stated result is $i = 26 \rightarrow 40°$, corresponding to $M_* = 20 \rightarrow 7 M_\odot$.

However, using VGS96 masses $M_{spec} = 21.5 - 23.4 M_{\odot}$ (from the spectroscopic classification) and $M_{NS} = 1 - 2 M_{\odot}$ yields an inclination of $26 \pm 0.5°$. Additionally, a value of $40 - 60°$ has been derived (Janot-Pacheco et al., 1987) using X-ray and optical data.

2.6.2.1 Using the maximum He Iλ6678 velocity

The maximum observed orbital velocity from observations of He I λ6678 (Figure 2.13) can be used to limit the inclination of the Be star. Applying the criterion that $r_{Kep} \geq R_*$ gives

$$\frac{R_*}{M_*} \leq sin^2 i \frac{G}{v_{max}^2} \tag{2.5}$$

which is plotted in Figure 2.18. Ratios of R/M are taken from VGS96 and Schaerer and de Koter (1997) who tabulate masses and radii for luminosity class III and V stars. Though later work incorporating line blanketting (Martins et al., 2002) has revised the VGS96 temperature/luminosity scale upon which masses and radii depend, the effects cancel to first order for radius and M_{spec}. Fortunately the mass and radius are weak functions of Sp/L class in this region, making the ratio R_*/M_* constant to first order over several subclasses around O9-B0 for class III and V stars.

The observed limit at $v \approx 440 \pm 20\,\mathrm{km\,s^{-1}}$ (Figure 2.13) is taken to represent the Keplerian velocity at $r \approx R_*$, and thus the correct inclination lies at the intersection of the appropriate R/M line and the $sin^2 i$ function, or beneath it if the material is significantly above the photosphere.

The inclination thus derived may in fact be an underestimate; Be stars, and rapidly rotating stars in general, have frequently been found to be overluminous (or undermassive) (Lamers et al., 1997), which if a general trait raises the ratio R/M

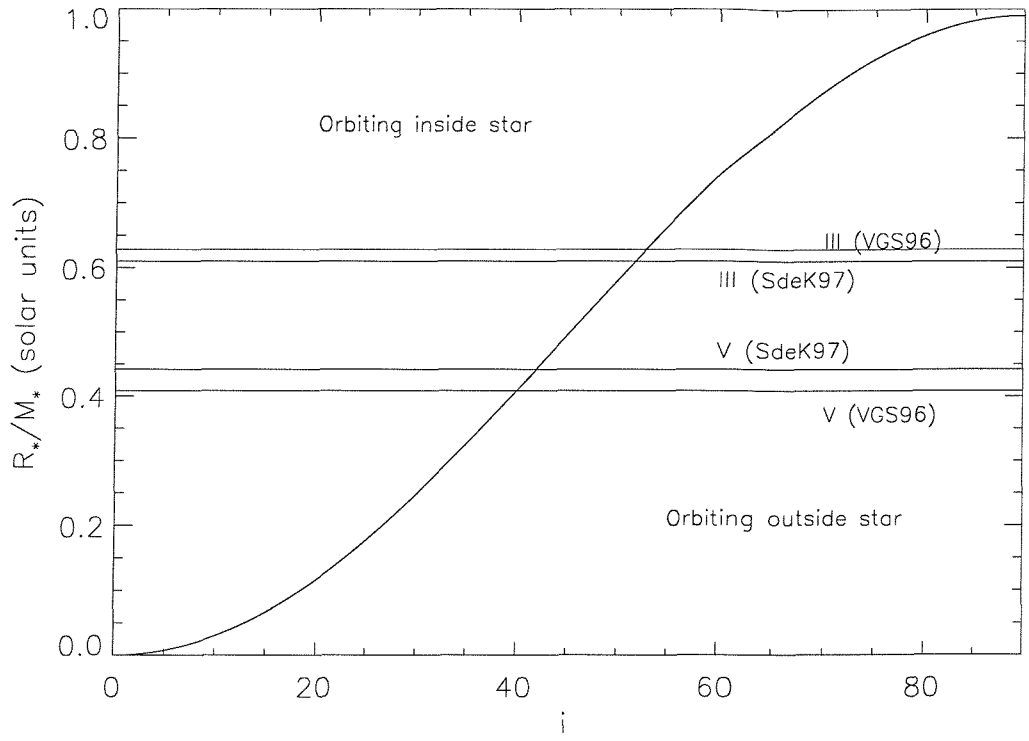

Figure 2.18: Further constraints on the inclination i of HDE 245770. The ratio R_*/M_* measured in solar units must lie below the curved line (equation 2.5, $v_{obs} = 440\,\mathrm{km\,s^{-1}}$). Values of R/M are shown for luminosity classes III and V. SdeK97 = Schaerer and de Koter (1997), VGS96 = Vacca et al. (1996).

further (Gies et al. 1998 discuss this for ϕ Per). Additionally the large value of $\omega = v_{rot}/v_{crit}$ (Wang and Gies 1998 find $\omega = 0.44$) requires that the star be a significantly oblate spheroid (possibly the same phenomenon), increasing the equatorial radius.

The probable inclination range thus derived is dependant upon the luminosity class. For giants, we obtain $i = 52 - 57°$ allowing for a 10% excess in R/M, and similarly for dwarves a range of $i = 39 - 45°$. These values are hard to reconcile with that of Wang and Gies which requires $i \sim 27°$ if $M_* \sim 20M_\odot$ and $M_{NS} = 1.4M_\odot$. The explanation almost certainly lies in a tilted NS orbit.

Stellar mass Using VGS96 values for M_{spec}, M_* changes by just $\sim 8\%$ over the range O9.5-B0V, and the same fractional change is observed for O9.5-B0III. Interpolating to O9.7Ve (O9.7IIIe) we obtain a mass of $20.15M_\odot$ ($23.4M_\odot$). In the absence of further discriminatory knowledge the mean value of $21.8M_\odot$ is used, in good agreement with previously published results.

2.6.2.2 Using the resonant truncation

As opposed to He Iλ6678 which is dominated by emission at small radii (Stee et al., 1998) the Hα line is emitted by most if not all of the disc (confirmed below), and thus it's ΔV_{peak} represents the Keplerian velocity at r_{outer}. The truncation paradigm informs us of, at a given time, the orbital period p for the disc's outer edge and thus by measuring the velocity $v_{Kep} = \frac{v_{obs}}{sini}$ where $\Delta V_{peak} = 2v_{obs}$ we can derive the orbital radius r_{outer}.

$$r_{outer} = \frac{v_{obs}p}{2\pi sini} \tag{2.6}$$

In turn this gives a measure of the stellar mass M_* as a function of inclination, given that the product of the orbital velocity and orbital period yields the radius. Equating r_{outer} to the radius in equation 2.1 gives

$$i = sin^{-1}\left(\left[\frac{v_{obs}^3 p}{2\pi G M_*}\right]^{1/3}\right) \tag{2.7}$$

which is plotted in Figure 2.19.

For the purposes of this work the precession invoked in Section 2.6.4 will be ignored and the disc's orbital motion assumed to be in the equatorial plane. In practice the tilt angles are unlikely to dramatically change the results obtained here.

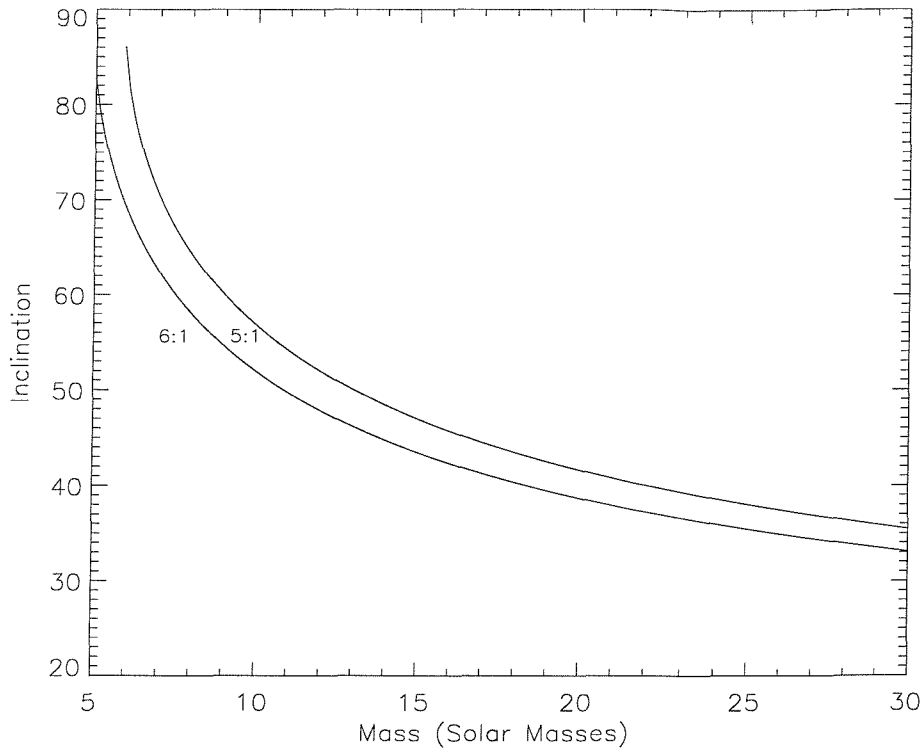

Figure 2.19: i vs. $M_*/M_\odot$ for possible resonances of state A. Note 6:1 is favoured by theory and observation, discussed in Section 2.3.2.1.

The case of state A following the $B \rightarrow A$ transition of March/April 1994 is studied as is presents an understood state with numerous high quality spectra. The observed Hα ΔV_{peak} (Figure 2.13) is taken to be $275 \pm 10\,\mathrm{km\,s^{-1}}$. As discussed in Section 2.3.2.1 this is probably truncated at the 6:1 resonance giving $p_{orb} = 18.5$ days, though i vs. M_* is also plotted for the 5:1 commensurability. 5:1 is probably excluded however on theoretical grounds (Okazaki and Negueruela, 2001), as it would require state C to correspond to 3:1, well outside the Be star Roche lobe at periastron. Using the spectroscopically determined mass of $21.8 M_\odot$ yields 40.2° at 5:1 and 37.4° at 6:1, though it is a weak function of mass. An inclination of $\sim 40°$ degrees thus appears most likely, and is used throughout this work. Referring back to the previous method of determination (Section 2.6.2.1) this result appears to exclude a luminosity class III type, unless the theoretical spectroscopic masses are in excess by a factor of 1.5→2 (depending upon the commensurability). A dwarf classification is thus suggested.

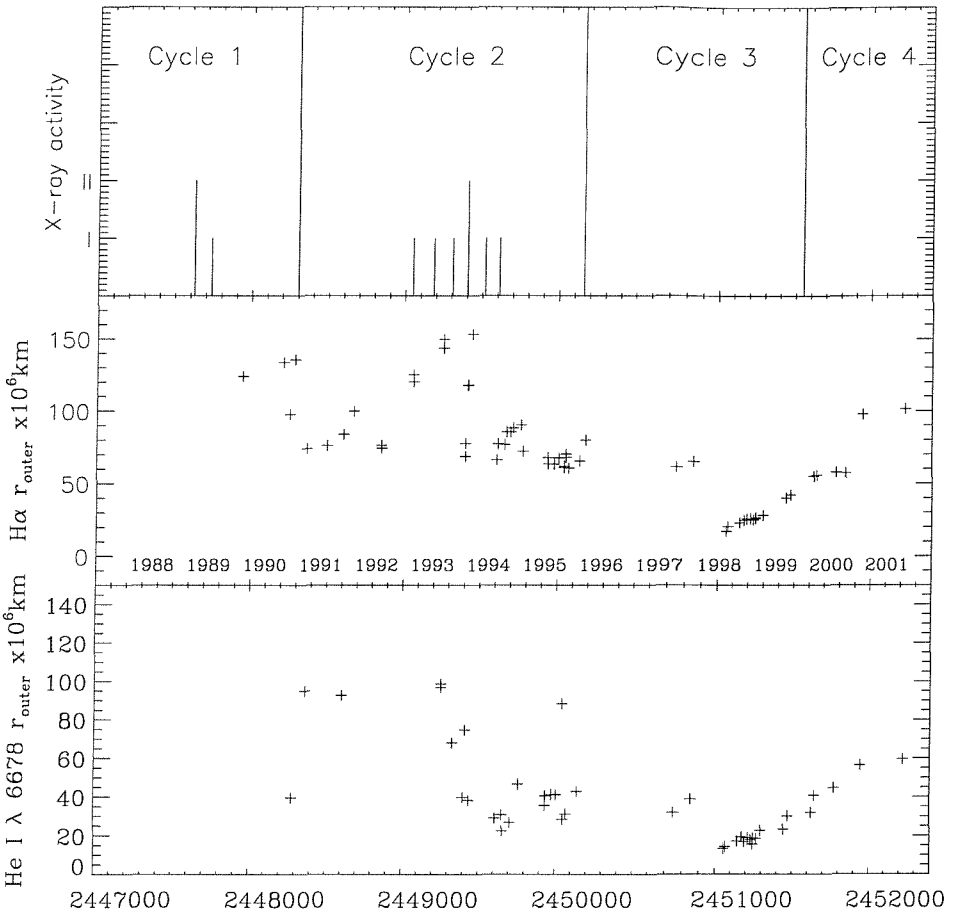

Figure 2.20: Outer radius for Hα and He I λ6678, using $M_* = 21.8M_\odot$ and $i = 40°$.

Returning to equation 2.6, $r_{outer} = (5.44 \pm 0.37) \times 10^{10}m$ assuming a 6:1 truncation. Using VGS96 radii this is $9.2R_*$ (V) or $5.3R_*$ (III).

Stee and Bittar (2001) found that for typical Be stars the Hα emitting region was bounded at $18R_*$, thus the disc is fully within this region at both states A and B ($\frac{r_B}{r_A} = (\frac{n}{n-1})^{2/3} = 1.13$ where n=6) as required by the disc modelling in Section 2.6.1 and others. While in general Hα ΔV_{peak} provides a measurement of disc radius, at times of significant perturbation such as would appear to accompany X-ray activity and the state A$\rightarrow$B transition ending cycle 1 this measurement is less reliable.

This would appear to support one of the conclusions of Okazaki (Section 1.7) that truncated discs have flatter density profiles (see also Section 2.6.1) due to material piling up at r_{outer} (Okazaki and Negueruela, 2001). Indeed it would appear that

the discs in BeXRBs are affected so profoundly that their radial density functions scarcely resemble those of isolated Be stars.

The assumption that He I λ6678 is only emitted by the central parts of the disc can also be investigated; Stee et al. (1998) found that $r_{outer}(\mathrm{He\,I}) = 2.3R_*$. Figure 2.20 shows the calculated He I outer radius. Whilst there are several datapoints above 60 Mkm, the earlier points in particular may be due to poor S/N spectra. It appears that for most epochs, and all of those for which high quality spectra are available, the He I zone is considerably smaller than the Hα zone (Figure 2.15). The apparently large He I radii determined around the 1994 X-ray activity are probably spurious, due to anomalous V-R peaks seen at this time (see Section 2.4.1). Furthermore many photospheric profile-subtracted spectra show evidence for a great deal of emission at much smaller radii than r_{outer} (low gradient profile edges), even if some emission is present to larger radii. Additionally, it may be that in A0535+262 we see a larger than typical He I region (Section 2.4.2.1) because of it's early spectral class relative to those stars considered by Stee et al. (1998).

Overall the success of these methods supports the interpretation of the Hα ΔV_{peak} as a direct measure of the outer radius (Huang, 1972), despite concerns that the outer disc may be too faint to detect in Hα (see, for example, Clark et al. [2001]).

2.6.3 Magnitude vs. W_λ diagrams.

Diagrams of m vs. W_λ (Figures 2.21 and 2.22) are extremely informative regarding the behaviour of A0535+262. As discussed later in Section 2.6.4, during each cycle of activity within the 1987-2001 dataset the system makes one clockwise loop in this parameter space, first increasing in $W_{\lambda H\alpha}$ in the bright state, and then decreasing in $W_{\lambda H\alpha}$ through the fainter state. Note that only quasi-simultaneous data are shown ($T_{sep} < 30 days$) except for in the midst of steady photometric states where 50 days has been used.

The disc appears to be optically thick in K to it's outer edge, as (for example) the simple dependance of m_K excess on the truncation radius, and the modelling of IR emission in Figure 2.16 has shown. However, $W_{\lambda H\alpha}$ displays variability within each state. This W_λ variability cannot be fully attributable to a constant line flux on a changing continuum, as the change in R continuum within state B is ~ 0.2 magnitudes, while $W_{\lambda H\alpha}$ changes by a factor of ~ 2 from -8Åto -15Å. The disc is almost certainly partially optically thick in the Hα continuum, and so $W_{\lambda H\alpha}$ cannot be used as a rigourous tracer of disc mass, though it probably reflects in a broad sense the changing mass within the disc (Hα emission arises from the entire disc, Section 2.6.2.2). The variability noted in fitting $W_{\lambda H\alpha}$ as a function of ΔV_{peak} (Figure 2.17) also suggests that much of the disc is optically thin in Hα.

Where the disc is optically thick in Hα, much of the Hα emission may be arising from a layer above the disc at a higher temperature, so as to avoid the flux limitations imposed by optical thickness. Such a mechanism has been invoked by Hony et al. (2000) to account for line emission from small radii in γ Cas. They suggest that temperatures in the region from which much of the line emission arises may be 30% higher than in the disc. This is in keeping with the ideas of Rivinius et al. (2001) who suggest that the low density high velocity 'polar' wind observed in the UV arises from ablation of the disc 'surface' by the stellar flux, with a corresponding thermal gradient. Some of the Hα emission may also arise from material stripped from the disc by NS interactions, which would become stronger as truncation approached and the system moved to the right in this parameter space. However, this matter is somewhat speculative and very much unresolved at this stage.

It thus becomes apparent that the horizontal bands of points at constant m_K in Figure 2.21 represent constant disc sizes whilst $W_{\lambda H\alpha}$ varies within these fixed size discs. Looking at the chronological order within these distributions reveals that points towards the RHS where Hα is stronger occur just prior to truncation to smaller radii, whilst expansions to larger discs occur when Hα is weak at the LHS of the distribution. This pattern underlies the observed clockwise motion in this

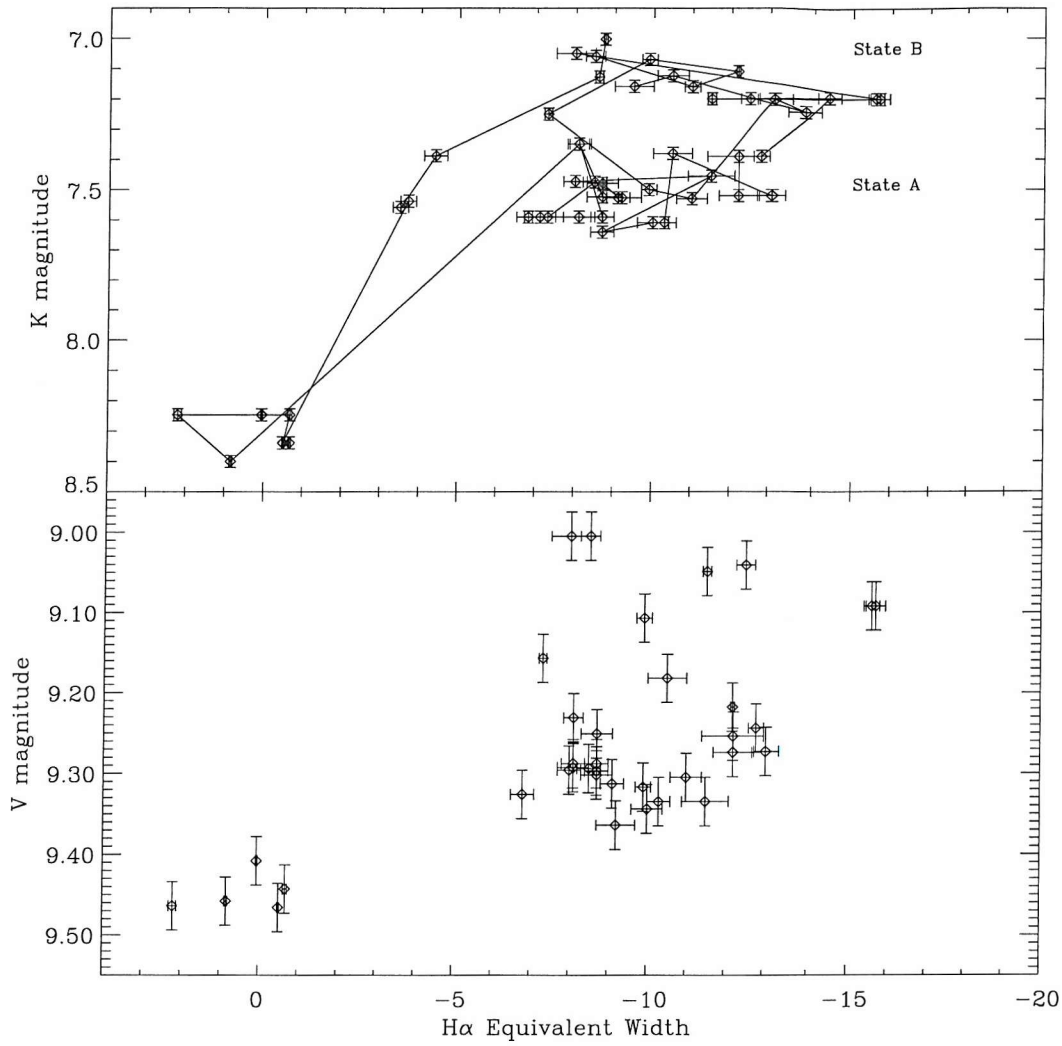

Figure 2.21: Correlation of m_K and m_v with $W_\lambda(\mathrm{H}\alpha)$. States A and B lie across the centre and top respectively.

plane.

Whilst it appears from Figure 2.21 that a small $\sim 10\%$ decrease in Hα emission occurs following truncation (at $W_\lambda \approx -13\mathring{A}$, state $B \rightarrow A$) the decrease in line *flux* is somewhat greater due to the declining continuum. If the decrease in R, which is effectively the Hα continuum, following truncation is taken to be approximately the same as in V (0.3 magnitudes, Table 2.5) then the transition to state A can be seen to be accompanied by a decrease in line flux to $\sim$ 70% of the pre-loss flux, comparable to the decrease in JHK excess.

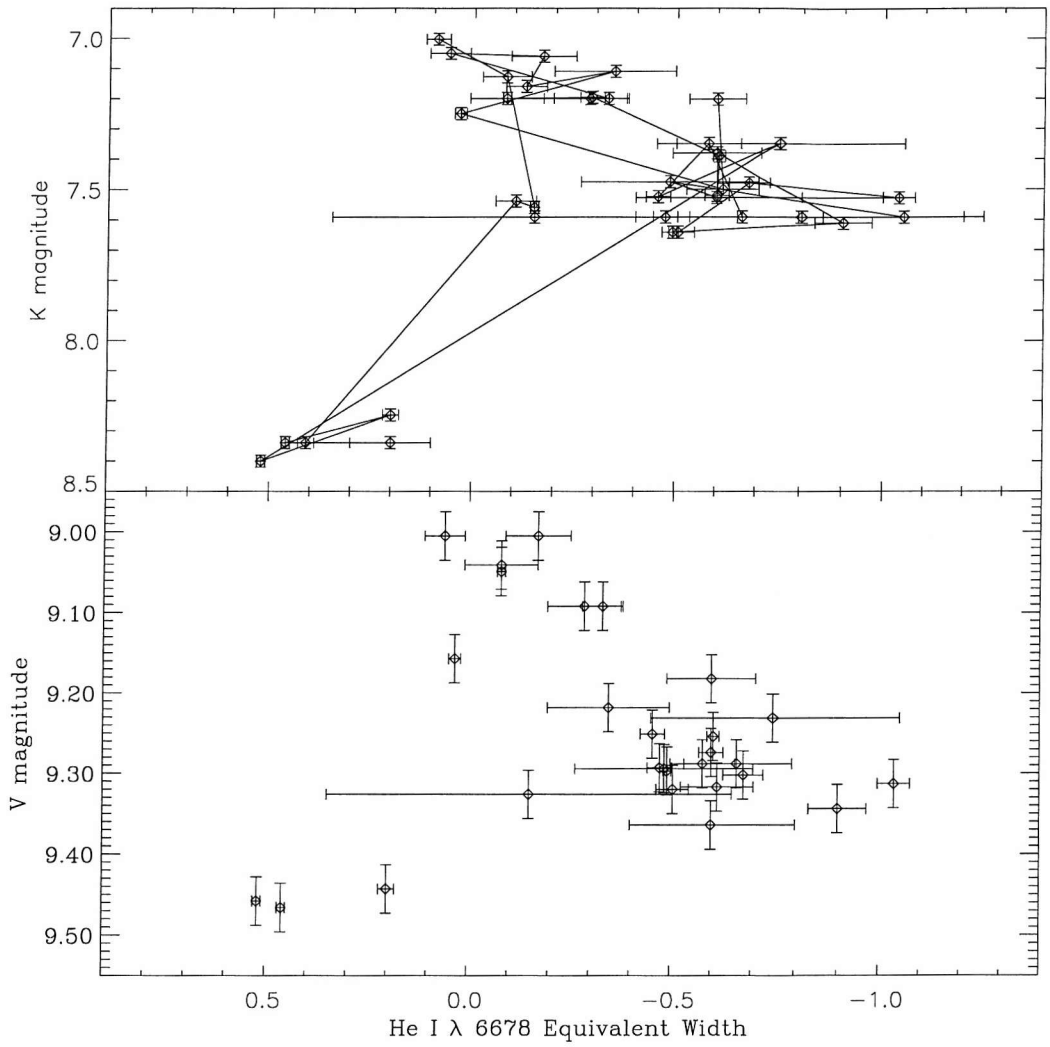

Figure 2.22: Correlation of m_K and m_v with W_λ(He I λ6678). State B lies at upper left and A to the right.

Additional behaviour is observed in the path followed through disc-loss of W_λ (He I λ6678) (Figure 2.22). The IR faint state is characterised by a strong He I λ6678 line ($W_\lambda \sim -0.8 \pm 0.3$) while the IR bright state is weaker ($W_\lambda \sim -0.1 \pm 0.2$). Why should a disc in the bright IR state (inferred as truncation at a larger radius) display weaker He I emission? Indeed, the brightest $m_K = 7.0$ is simultaneous with the weakest He I line outside of disc-loss. It seems that not only does truncation affect the outer edge of the disc, but in preventing material propagating outwards further, more remains at the small radii which emit in the He I lines. Thus here we have evidence that the NS's effects are felt indirectly even at the innermost edges of the disc. This supports the findings that X Per and A0535+262 have amongst the densest discs measured in Be systems in general (Telting et al., 1998), and that BeXRBs have discs twice as dense as isolated Be stars (Zamanov et al., 2001).

In the data from 1987 to 1998, preceeding the disc-loss event, the disc made 6 switches between states. In the two months between the spectra of 931206 and 940216 the $W_{\lambda H\alpha}$ dropped slightly from -14.4 to -12.2 (both bright) whilst m_K dropped into the faint state. This exact pattern is also observed between 880311 and 901227, a slight but still bright decline in Hα accompanied by a change in m_K to the faint state, though unfortunately data is too sparse to specify exact dates.

Between these times, the 910416 dataset is of particular interest. At this datum the only direct transition between the faint and bright states with spectral coverage can be seen, as the 1998 transition passed through a lower disc-loss state and the 1996.5 transition was very rapid and poorly observed excepting m_V. Preceeded 80 days earlier by $m_K = 7.5$ and followed by $m_K = 7.07$ 134 days later, at this date $m_K = 7.25$, perfectly intermediate, and the only point lying in the region between the states in Figure 2.21. Also of note is that this change occurred whilst $W_{\lambda H\alpha}$ was relatively weak at -7.3Å. Thus this seems to be a perfect instance of the disc being 'caught in the act'.

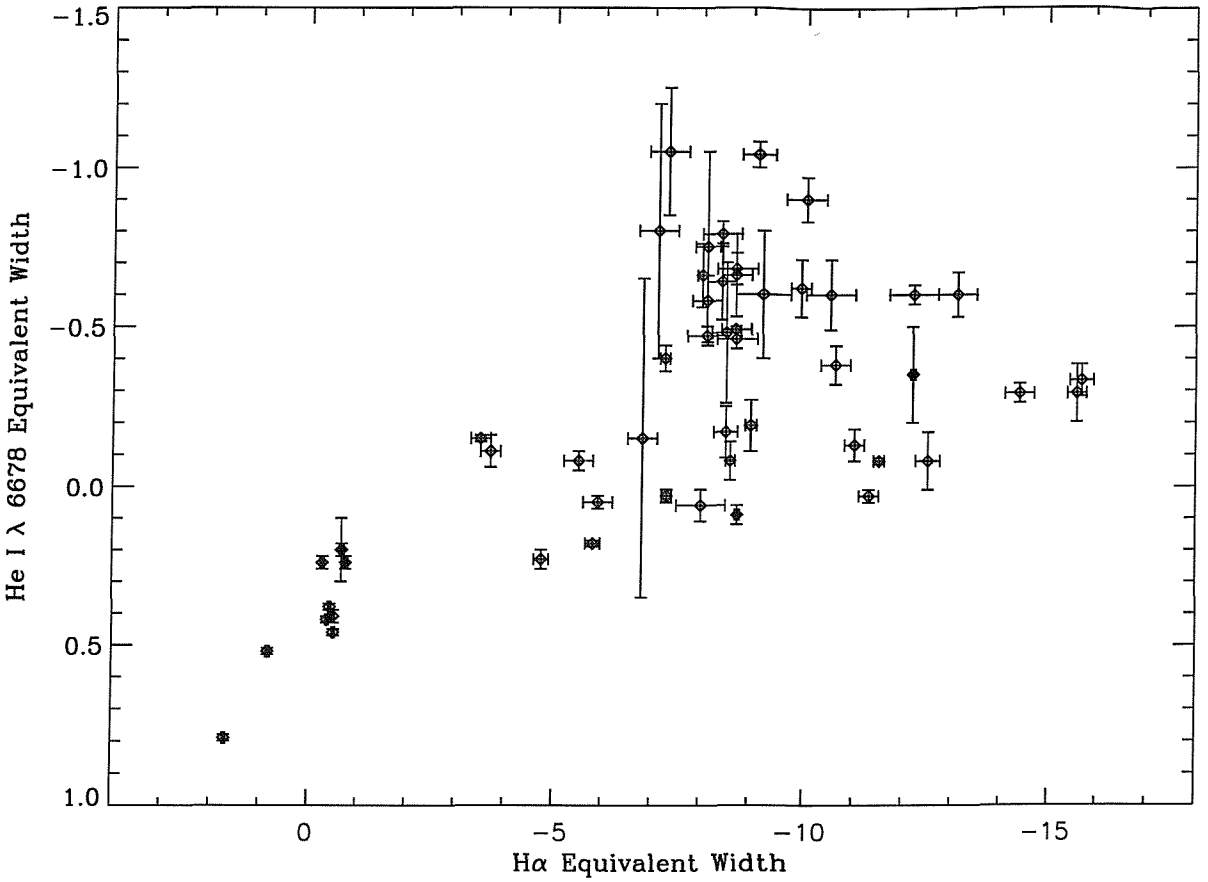

Figure 2.23: Correlation of Hα with He I λ6678 W_λ from all spectra, 1987-2001.

2.6.4 Cycles of activity

As discussed in Section 1.7 Negueruela et al. (2001) discuss cycles of activity in the BeXRB 4U0115+63 including disc-loss, subsequent re-growth, truncation, warping, precession, Type II outbursts and subsequent dispersion and the start of a new cycle. The analysis of the trajectory of A0535+262 in the magnitude vs. $W_\lambda$parameter space shows that similar (if not identical) cycles are also occurring in this system.

In 4U0115+63 the cycles are defined to commence with the disc-loss episodes, of which several have been observed. The A0535+262 system appears considerably less prone to disc-loss; only one episode has been definitively observed (in 1998) whilst long term photometry suggests that the previous loss occurred in $\sim 1948 \pm 3yrs$ (Lyuty and Zaĭtseva, 2000). However, the 1998 disc-loss occurred just prior to the system entering state B and beginning a new cycle as defined here, so it appears

that Negueruela et al.'s 4U0115+63 cycles are the in step with those used here for A0535+262.

Figure 2.21 shows $W_{\lambda H\alpha}$ plotted against m_K (and m_v), with points connected in chronological order. We observe a scatter of points corresponding to the disc-loss state (at lower left), and the relatively smooth rise afterwards. Note that the structure visible represents real variability and not measurement errors; whilst some points are close together and a trajectory is visible, some changes are clearly taking place on a considerably shorter timescale than the sampling period (e.g. the bright state of mid-end of 1996 is not shown due to lack of K photometry). Some large gaps are due to periods when the system was not observed due to its proximity to the sun, it's ecliptic latitude being only a few degrees. Though the dataset is incomplete, the timescales of these changes are long enough that no change in state could have been missed since 1987. Note that using the expansion velocity measured following disc-loss, $T_{6:1\rightarrow5:1} \approx$135 days at 894ms^{-1}.

Cycle 1 1987.0-1991.4 The CRAO $m_{J,H}$ photometry (Figure 2.3) shows the cycle beginning with a brightening from $A \rightarrow B$ at 2446800 $\pm$ 150 (end 1986$\rightarrow$ start 1987). $W_{\lambda H\alpha}$ gradually increased to $\sim$ 14Å by 1989, when a jump to state A occurred poorly documented in JHK. Sparse V photometry suggests the start of a decline on 7 Apr 1989, well underway by November. A Type II outburst occurred on April 8,followed by a Type I. $W_{\lambda H\alpha}$ declined until the end of the cycle in 1991.4.

Cycle 2 1991.4-1996.2 At 1991.4 (2448300 $\pm$ 100) the system abruptly brightened in m_K(A$\rightarrow$B), and Hα recommenced it's gradual increase from $-10 \rightarrow -15$Å. Hα and He I V-R velocity separation declined gradually, showing the bulk of material moving outwards. Again the jump to state A is simultaneous with a Type II outburst bracketted by a series of Type I outbursts (see Section 2.3.2.2). Smaller disc causes increase in ΔV_{peak} with fading in m_K. He I ΔV_{peak} and maximum veloc-

ity increase also. Apparent decline in $(J-K)_{disc}$ (Section 2.6.5.1). $W_{\lambda H\alpha}$ declines until Nov.1995, V shows start of state B at 2450060 $\pm$ 30 (Dec. 1995), m_K shows an intermediate flux at 2450160 (Mar 1996) and m_V firmly at state B luminosity by 2450311(Aug 1996).

Cycle 3 1996.2-2000.1 Hα intensified rapidly through state B to strong W_λ=-12Å. State A began at $\sim$ 2450450(Dec 96) with rapid m_V decline. No x-ray activity seen, ASM limit $<$ 0.004 Crab (Figure 2.24, Section 2.6.6.1). Hα rapidly declines, state A $m_V \sim 9.35$ until 2450689(Aug 1997) from which it declines to photospheric by 2450800$\pm$50(Dec 97). Hα strong but rapidly declining until 2451056 (Aug 1998).

Cycle 4 2000.1-2001 onwards $m_{J,H,K}$ brighten above state A by Jan 2000(2451565), the next photometry $m_K = 7.128$ in Oct 2000 showing a robust state B. Hα increased smoothly to -11.3Å by Oct 2001. As of January 2001 $m_K = 7.00$, at the bright end of state B, typical of it's early stages. Assuming the mean duration of 4.4 years this cycle will end at 2004.5.

Thus cycles 1,2 and 3 lasted 4.4,4.8 and 3.9 years respectively, with a mean of 4.36 years. Truncation to state A took place after 2.3,2.8 and 0.7 years. The shortness of state A in cycle 3 can be seen as part of a longer term trend toward weaker discs and lower emission in all respects since the peak in the late 1970s. It will be interesting to see how cycle 4 progresses, and whether the disc will perhaps be even weaker this time around or whether the system will return to the robust discs of the 1970s-early 1990s. The disc has however remained in state B for 1.0 years (as of Jan 2001) with $m_K = 7.00$, typical of the early stages of this state. As Figure 2.21 shows, previous descents to state A have occurred from $m_K \approx 7.20 \pm 0.05$, suggesting that thus far this cycle is as robust as any of the previous three. Lyuty et al. (2000) wrote shortly after the 1998 disc-loss event that it represented the conclusion of an active 30 year period in A0535+262. However, reports of the death of A0535+262 appear to be

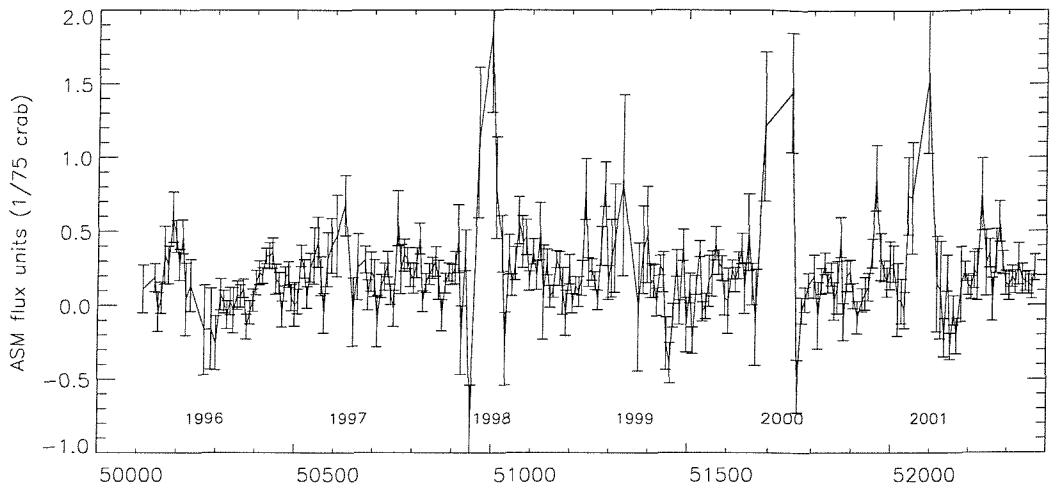

Figure 2.24: XTE ASM flux history of A0535+262. Data are binned at 8 day intervals. Apparent yearly 'flares' are bad data around solar conjunction.

exaggerated and certainly premature; no terminal decline appears imminent.

2.6.5 Comments on cyclical behaviour

Interestingly, at the start of cycle 3 $W_{\lambda HeI}$ can be seen to be lagging behind the changes in other system parameters, remaining high at -0.75Å at JD 2450177 when photometry reveals the disc to be in mid-expansion to state B. This is to be expected, as it takes time for the disc to reach an equilibrium state in which the inner regions have adjusted to expansion of the outer regions.

If we interpret an increase in $W_{\lambda H\alpha}$ within a luminosity state as an increase in the quantity of material in the disc (fully consistent with other findings), a picture emerges. Considering the disc following disc-loss, at the beginning of the cycle a new disc forms at lower than typical ρ and rapidly expands to the large disc state, as evidenced by the weak $W_{\lambda HeI}$ (material free to propogate radially), intermediate $W_{\lambda H\alpha}$ (moderate quantities of plasma) and bright m_K (large size). Though not monotonic, the disc gradually increases in mass (increase in $W_{\lambda H\alpha}$) whilst retaining it's approximate configuration. m_K remains bright, He I remains faint, and Hα gradually increases. When Hα reaches $\sim -14\mathring{A}$, a change in state is observed

JD (approx.)	Date	1-10keV Flux (Crabs)	Type	Disc state
2442533.5	1975 May 1	3.0	II	
2442726.5	1975 Nov 10	0.3	I	
2443284.5	1977 May 21	0.5	I	
2443500.5	>1977 Dec 23	0.5	I	
2443610.5	1978 Apr 12	0.5	I	
2443726.5	1978 Aug 6	0.4	I	
2443950.5	>1979 Mar 18	0.25	I[5]	
2444517.5	1980 Oct 5	1.5	II	*C*
2444950.5	1981 Dec 11-13	<0.1	MO	
2444951.5	1981 Dec 13	0.2	$3.^h5$ flare[10]	
2444963.5	1981 Dec 23-26	<0.1	MO	
2445289.5	1982 Nov 16	0.2	I	
~2445507	1983 Jun	?	I [8]	
2445617.5	1983 Oct 10	0.5	I	
2445732.5	1984 Feb 1	?	I[2]	
~2446167	1985 Apr		MO[8]	
2446498.5	1986 Mar 9	0.0022	MO	A?
2446506.5	1986 Mar 17	<0.005	MO	A?
2446735.5	1986 Nov 1	0.78	I[4]	$A \rightarrow B$
2446846.5	1987 Feb 20	0.025	MO,weak flare[3]	B
2447625	1989 Apr 8	0.6	II[1]	$B \rightarrow A$
~2447735	1989 July	?	I[8]	$B \rightarrow A$

Table 2.7: X-ray events in A0535+262, 1975-1989. For description see next Table.

JD (approx.)	Date	1-10keV Flux (Crabs)	Type	Disc state
~2448276	1991 Jan		MO[8]	$A \rightarrow B$
~2448386	1991 May		MO[8]	$A \rightarrow B$
~2448496	1991 Aug		MO[8]	B
~2448606	1991 Dec		MO[8]	B
~2448717	1992 Apr		MO[8]	B
~2448827	1992 Jul		MO[8]	B
2449049	1993 Mar		I[6]	B
2449186	1993 July 17		I[6]	B
~2449307	1993 Oct-Dec		I[7]	B
2449403	1994 Jan 28-Feb 19	1.4	II[1]	$B \rightarrow A$
~2449519	1994 Jun	?	I	A
~2449611	1994 Sept	?	I	A
$\geq$2449721	1995 Jan$\rightarrow$2001		MO[9]	$A \rightarrow disc-loss \rightarrow B$

Table 2.8: X-ray events in A0535+262, 1989-2001. MO=Missing Outburst. $B \rightarrow A$ indicates occurrence during a state B to A transition. Data to 1987 Feb 20 from Table 4 of Motch et al. (1991). 1: Larionov et al. (2001),2: Giovannelli et al. (1984), 3: Giovannelli et al. (1987), 4: Giovannelli et al. (1986), 5: Sims and Fraser (1979), 6:Wilson et al. (1993), 7: Finger et al. (1994)., 8: Clark et al. 1999, 9: Negueruela et al. (1999), 10: de Loore et al. (1984).

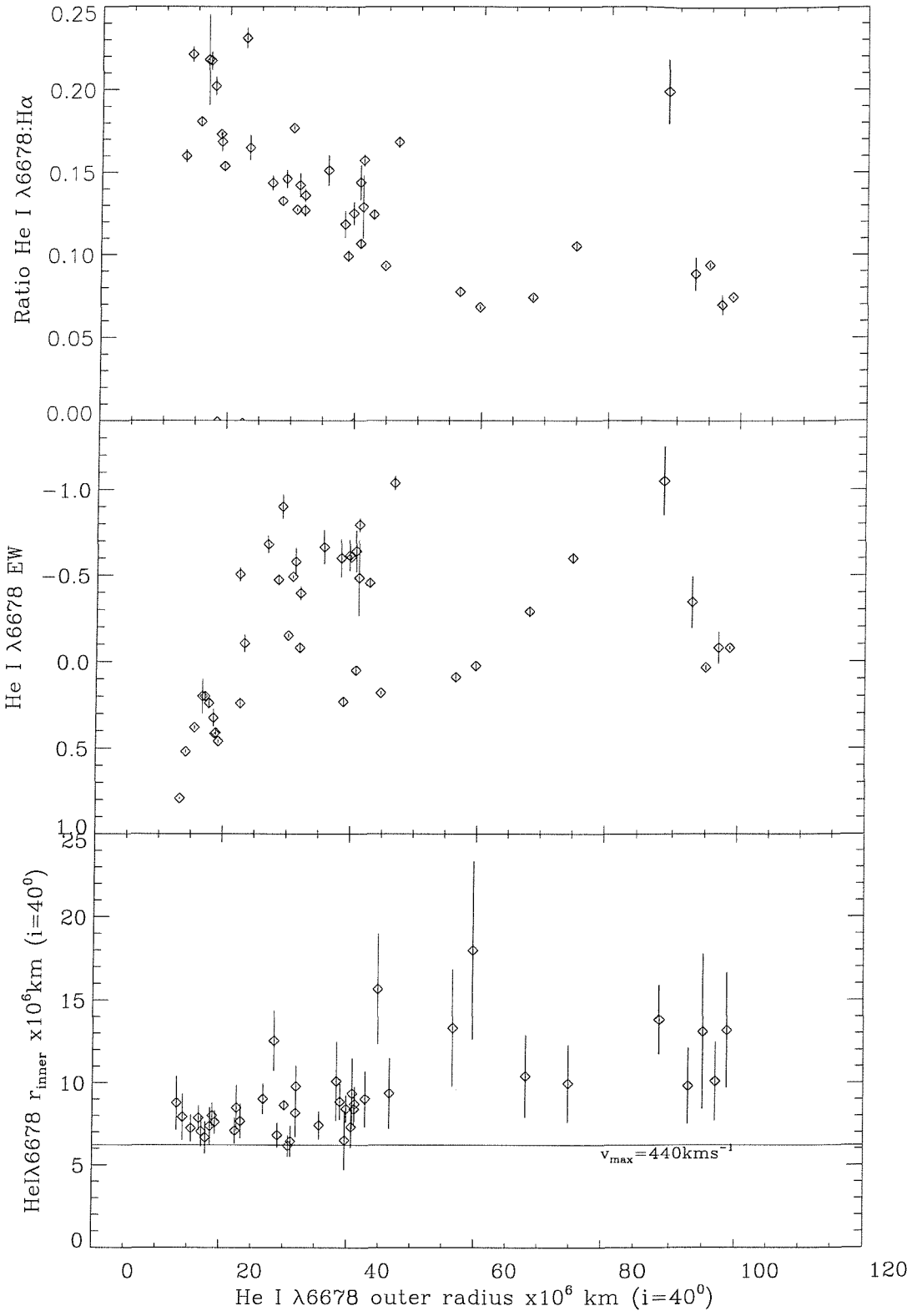

Figure 2.25: Various He I parameters in terms of the He I zone outer radius.

in which the disc contracts (fainter m_K) and more material is found at small radii (stronger $W_{\lambda HeI}$). Following the 1989 fading, $W_{\lambda H\alpha}$ declined (possibly representing the dispersion of material already lost from the disc) whilst $W_{\lambda HeI}$ remained strong until at $W_{\lambda H\alpha}\sim 8\mathring{A}$ the disc expanded to it's larger state again; the motion in the plane is continuous and at some times extremely rapid.

Following the disc-loss episode, when the equatorial disc rebuilt in 1999-2001 it continued the expected trajectory into a bright state, much as it would be expected to have done if the disc-loss had not occurred. Thus the disc-loss event represents a temporary hiatus at best, without affecting the longterm evolution of the disc. If the cycles described here are identical to those described by Negueruela in 4U0115+63, disc-loss episodes, while dramatic, are merely part of the longterm cycle and do not represent anything more dramamtic.

Clark et al. (2001) plot m_V vs. $W_{\lambda H\alpha}$ for a similar length dataset of X Per, during which much variability is observed. However, no well-defined flux states are visible and the movement is parameter space appears more erratic than in A0535+262. This is probably due to the much larger NS orbit influencing the Be disc considerably less, and it's lower eccentricity. Okazaki (Section 1.7) notes that truncation at resonant orbits is much more effective with eccentric orbits. It thus seems that X Per does not display the same cyclical behaviour as A0535+262.

The He I:Hα ratio (Figure 2.10) ratio has the analytical advantage (over just $W_{\lambda HeI}$) that changes in the continuum level alter both W_λ to the same degree and are thus eliminated. It also removes the dependance (seen in $W_{\lambda HeI}$) upon the bulk disc density, and is thus a good probe of the fraction of material located within a few R_*. Figure 2.25 shows that this ratio inversely tracks the He I bulk radius, showing that the mean He I velocity is larger when a greater fraction of material lies at small radii.

It can be seen that the ratio starts a rapid climb in the weeks after the 1994 Type

II X-ray outburst and the associated reduction in the truncation radius. Superficially this appears similar to the He I outbursts described by Rivinius et al., but there is an important difference. True He I outbursts are characterised by emission appearing first at very high velocities (ie orbiting close to the photosphere) and moving steadily *outwards* (Figure 2.13) towards lower velocities. This is exactly what is observed at the end of 1998 when the disc rebuilt from the inside out following disc-loss, making this a true outburst. Conversely the 1994 event is characterised by a slow *decrease* of orbital radius as the line strength builds; the event is occurring from the outer disc inwards. This is also shown in Figure 2.13 where the maximum orbital velocity is seen to gradually increase at the 1994 event; the inner edge of detectable material is moving inwards. This is further evidence that the truncation events lead to enhancement of the inner disc. It is also perhaps confusing that of the two types of events that lead to enhancement of the innermost disc, the events dubbed 'outbursts' have nothing to do with X-ray events whilst the other does.

Thus Figure 2.22 displays some of the most critical findings regarding A0535+262. In addition to clearly displaying the two states, it additionally shows that the bright/large state is accompanied by a decrease of material at small radii. The NS is affecting the *entire* disc.

Whether the truncation radius moving inwards actually forces material inwards is by no means required. Simply inhibiting the outward flow of plasma and thus increasing its surface density in the outer disc could provide sufficient resistance to prevent a modest supply of new material from moving outwards as usual thus enhancing the inner regions.

2.6.5.1 IR excess colour changes

The (J-K) colour index shows a significant transient decline immediately following the March 1994 Type II X-ray event (Figure 2.2), corresponding to the state B→A

truncation event. Though several other datapoints lie below the typical system colour of J-K=0.5, only this epoch appears to be a significant result, and the simultaneity with known system-wide changes makes it worthy of further investigation. The most thorough study of the effect of Be disc parameters on IR excess is due to D94. They present calculated colour excesses $CE(K-L)$ for ranges of several parameters each plotted for a range of base densities ρ_0; it is assumed here that the (J-K) colour will emulate the qualitative behaviour of (K-L).

Clearly such a transient event must be caused by similarly transient system properties, and thus cannot be due entirely to, for example, the change in truncation radius. It must also be noted that the global system JHK magnitudes at this time lay entirely within normal ranges for the transition between states B and A, thus a greater photospheric contribution is not the cause.

The approximation of an infinite disc is clearly not appropriate in a BeXRB, largely because truncation enables the entirety of the disc to be optically thick in JHK. However, it seems probable that unusually large amounts of material were present outside the reduced truncation radius at this time, imitating the distribution of material in a disc of lower n at equilibrium, in order for accretion to occur. Figure 7a of D94 shows that such a situation would actually cause an increase in CE, counter to observations, as the shorter wavelength J becomes optically thin and drops out before the longer K. The probable lower temperature of these outer regions (Figure 7g, D94) would only raise the CE further. Thus these effects, if occurring, must be negligible.

An intriguing possibility is that we may be seeing emission from a temporary accretion disc around the NS, contributing flux with a lower colour index. The Type II outburst was detected from JD 2449380 to 2449432, with large $\dot{P}$ and a strong 20-100mHz QPO for most of this duration (Finger et al., 1996). These are extremely persuasive arguments for an accretion disc, though they do not necessarily restrict it's existence to these times. Anomalous (J-K) colours lie between 244940[illegible]

and 2449440, though this interval reflects observational timings with 57 and 182 day intervals before and after. This simultaneity of this unique set of datapoints within the 14 year dataset with the only clear signature of an accretion disc in the system is however encouraging.

To explain the lack of a system *brightening* the additional flux from this feature must have been obscured by the large decline in the Be disc flux at this time. The (B-V) colour also shows a coincident and rapid 0.04 magnitude increase, but the presence of many other fluctuations within the UBV photometry should be noted. Lyuty and Zaĭtseva (2000) noted that their work has shown no evidence for an optical flux contribution from an accretion disc, but this work analysed the entirety of their long dataset rather than specifically searching at times when an accretion disc was known to exist. Further anomalous spectroscopic observations from this time are discussed in Section 2.4.1.

2.6.5.2 Possible changing disc temperature

A clear observation in Figure 2.21 is that at the commencement of state B $m_K = 7.05$, which declines to $m_K = 7.25$ prior to the $B \rightarrow A$ state transition. If we assume a constant geometry and approximate the K flux to the Rayleigh-Jeans tail of a black-body curve where $I \propto T$, this implies a 20% temperature reduction or $\sim 2500K$ at $T_{disc} = \frac{1}{2}T_* \approx 15000K$.

The formation of a new disc uses high temperature photospheric material, whilst the 'explosive events' and possible magnetic phenomena which have been invoked to explain the insertion of material into orbit will probably raise the temperature higher. However many works on Be discs have used $\frac{1}{2}T_*$ successfully, indicating that temperatures of $\sim 15000K$ are typical of discs in thermal equilibrium. Hony et al. (2000) found a lower temperature of 9700K for γ *Cas*, though in this case the hypothesised large orbit will allow more contribution from large radii; the method also

ignores optically thick regions. The viscosity of accretion/decretion discs is known to be proportional to temperature (Okazaki and Negueruela, 2001), suggesting that the high temperature of fresh material may enable propagation of the disc to large radii, before cooling reduces viscosity to the point that the disc is unable to support itself against tidal perturbations and it collapses to a smaller resonant state. However, a more probable scenario is described below.

2.6.6 Precession of the circumstellar disc

In folding 354 UBV photometry datapoints from 1983 to 1998, Larionov et al. (2001) found only a 103 day periodicity, detected at more than 99.9% confidence. This photometric periodicity was also found by Hao et al. (1996) and Clark et al. (1999a) (Figure 2.28). Figure 2.26 shows the m_V photometry of Lyuty et al. (2000) from state A in cycle 2 (31/8/1994-10/1/1996) folded at the 103.0 day period. This data was selected as it exhibits no long-term fluctuations, probably due to a higher disc density in state A generating a larger fraction of emission in optically thick regions. The PDM software, which is ideal for finding non-sinusoidal modulations, finds a best fit period of 103.0 ± 0.5 (Figure 2.27) depending upon the number of PDM bins used (5-10). The small number of data points (55) limits the resolution possible and makes the result dependant upon input parameters beyond this resolution. An identical analysis was undertaken replacing the magnitudes with white noise but retaining the temporal characteristics to exclude the possibility of this detection being a sampling artifact. The 103.0 day period is detected at approximately 11σ and is thus credible.

If the global ff/bf excess was modulated at this frequency, one would expect a somewhat larger variation in JHK, where most of the flux originates in the disc. The JHK photometry from the same period was folded identically, and any such modulation can be limited to a full amplitude of $\leq 0.3mag$. Unfortunately this is too coarse to permit the colours of the modulation to be usefully constrained, and

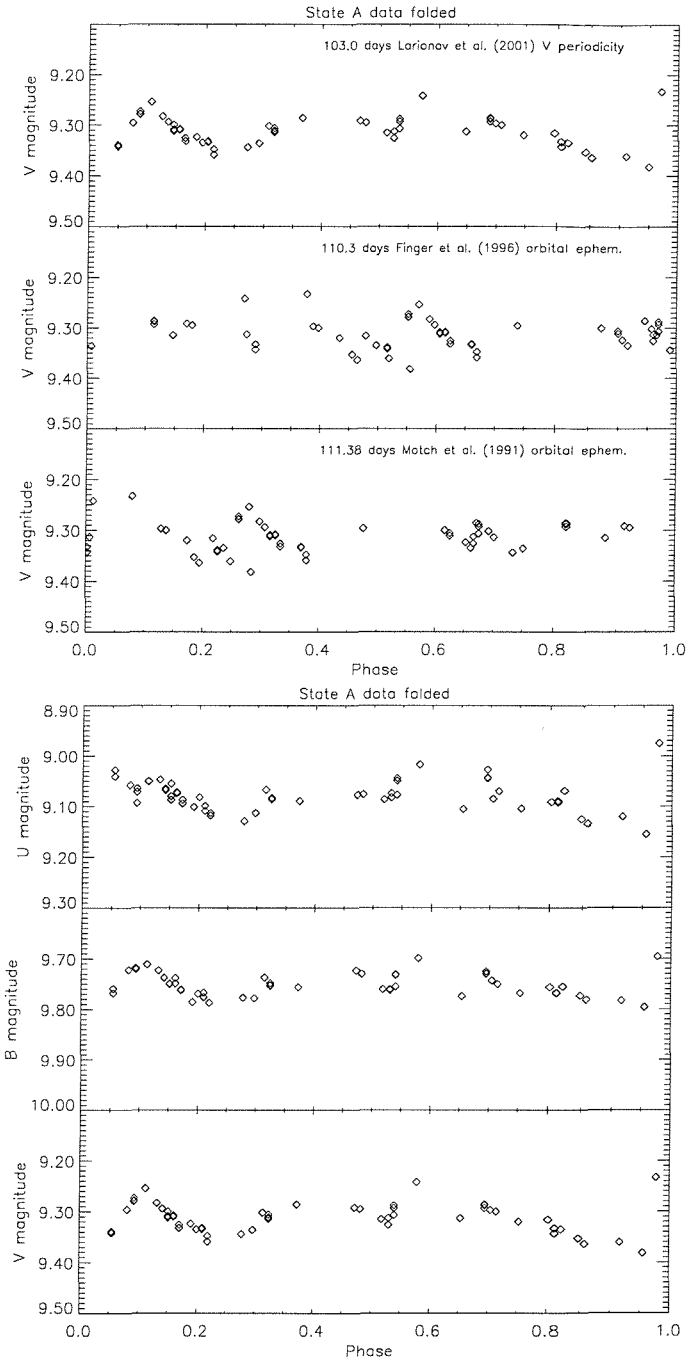

Figure 2.26: Top: m_V photometry from state A of 1994-5 folded at the two best orbital periods and the detected beat period. Bottom: UBV photometry folded as m_V in upper panel.

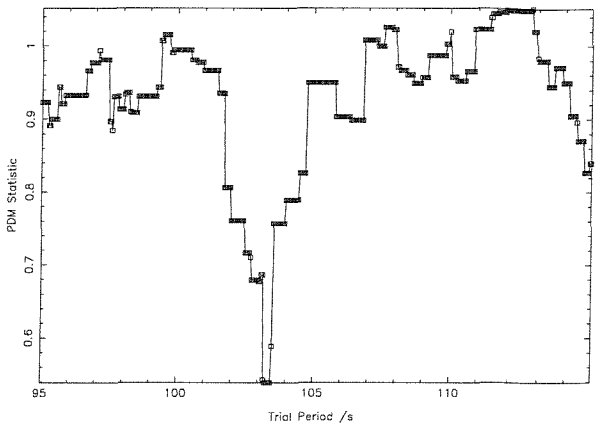

Figure 2.27: PDM periodogram of m_V photometry from state A of 1994-5. Resolution is 0.05 days, using 5 PDM bins. Includes 103 and 111 day periods.

thus to locate the origins of the variation. Folding UBV together however shows the same modulation in B at a lower amplitude, and scarcely detected at all in U. This suggests the modulation indeed arises in the ff/bf emission, and not in a NS accretion disc which would be expected to be much hotter.

This period is in agreement with the 102.83 found by Larionov et al. (2001) who hypothesise that this correponds to a beat period with a 1400 day precession period present either in the accretion disc around the NS or in the warped decretion disc. A 1400 day photometric period is well established in the system (Figure 2.28) having been detected in every published m_V period search, and was present back to at least 1980 (Lyuty et al., 1989) further confirming the stability of the precession, assuming a common origin. The 17 month baseline (4.8 103day periods) further suggests that this is not a quasi-period, and is rooted in periodic phenomena. No such modulation was found in the photometry covering the disc loss period, suggesting that the disc is unaffected by the NS at the small radii characteristic of the disc at that time.

Assuming a beat period of 103.0 ± 0.5 days and an orbital period of 111.0 ± 0.5 gives a precession period of 1430 ± 180 days or 3.92 ± 0.50 years. This value is clearly close to and compatible with the mean cycle length of 4.36 years evaluated over cycles 1,2 and 3. This equivalence strongly suggests that these two periods are

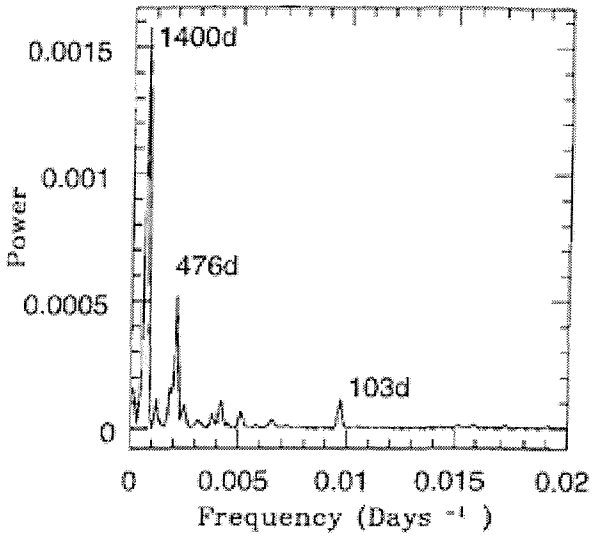

Figure 2.28: Results of a period search of long-term V band photometry. From Clark et al. (1999a). Note 103 and 1400 day periods.

in fact measuring the same cyclical phenomenon, probably the precession period of the warped decretion disc (see below, and Figure 2.29). The 103 day period is thus analogous to the widely known 1.6 day photometric beat period observed in Her X-1 between the 1.7 day orbital period and 35 day precession period (Wijers and Pringle, 1999).

It thus appears that the cycles are intimately linked to the precession of the Be disc. Such a connection makes sense if one considers that as the disc precesses, the separation of the disc's outer edge from the NS will change considerably, and with it the strength of the tidal interactions. Thus the observation that disc disruption occurs at a certain phase of precession makes sense. Whether or not the NS orbit and Be disc are coplanar also strongly affects the strength of the resonant coupling.

If we interpret the $\sim$ 1400day period as the precession of a decretion disc in the opposite sense to the NS orbit (Ogilvie and Dubus, 2001) thus giving a beat period less than the orbital period, then a 103 day interval corresponds to a recurring location of the NS relative to the disc plane. The m_V photometry analysed here commenced 3 weeks following the last recorded X-ray outburst in Sept 1994, thus this

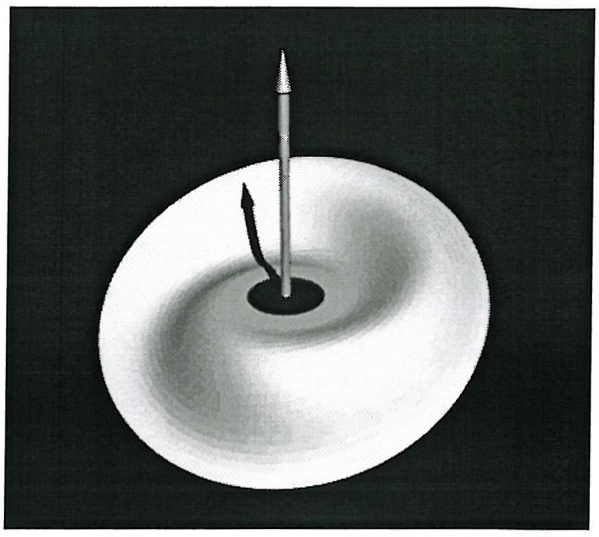

Figure 2.29: A warped precessing disc, Figure 7 from Wijers and Pringle (1999).

scenario shows that NS/disc interactions are occurring even in the absence of X-ray activity. Precession occurs in a retrograde sense with respect to the Keplerian disc motion (Ogilvie and Dubus, 2001); this precession has been shown to be retrograde with respect to the NS orbital motion, confirming the expectation that the disc rotation is also in the same rotational sense as the NS orbital motion.

The possibility of the site of the brightening being the NS seems remote because of the large 0.1 magnitude range of the variations, and the absence of X-ray activity. However, the periodic distortions generated in a Be disc by periastric tidal forces seen in the simulations by Okazaki (Figure 2.30) increase the disc area temporarily and will thus increase optically thick emission; one of his key results was that '(for high eccentricities) orbital modulation in continuum is more remarkable'. Okazaki plots the expected continuum modulation for 4U0115+63 showing a 0.03 magnitude modulation for optically thin ff/bf emission. Thus the greater amplitude observed here could be attributable to the effects of optically thick emission and substantially different system parameters.

One would not expect this 103 day cycle to continue for the entire precession period because after several orbits phase 0 would instead correspond to apastron,

though still to a plane crossing, and the former apastron phase would lie at periastron. The aparent presence of a second peak 0.5 phases from the main peak may be evidence of this apastron→periastron drift.

Periastron passages (Okazaki, private communication) trigger spiral structure to form for ∼1 week, and under some circumstances this structure can cause accretion and outbursts after a few days. Thus the possibility of this observed brightening being related to the so-called shell-ejection events observed several days prior to X-ray activity (Lyuty et al., 1989) is intriguing. The traditional view of a shell of material ejected from the star and accreting directly onto the NS (Demartino et al., 1989) makes little sense in the framework of a viscous decretion disc, where density fluctuations take some time to propagate through the disc and reach the outer edge (Rivinius et al., 2001).

Precession of the Be disc also provides an explanation for the observed decrease in m_K flux through state B, as the inclination of the disc to the line of sight changes, thus eliminating any need to invoke temperature changes (Section 2.6.5.2). If the cycles are as intimately linked to precession as they appear to be, the orientation of the disc in successive cycles will be identical.

Lyuty et al. (1989) present photometry from 1972 to 1988 and note that the 1400 day periodicity was lacking before 1980. In view of the apparent absence of a decretion disc before the late 1960s, it seems possible that the precessional amplitude has built up steadily following the initial formation of a decretion disc in the star's equatorial plane.

The hypothesis that the disc truncation occurs as a function of a 1400 day precessional cycle (certainly it's azimuthal angle, hence the cyclical behaviour described here) could then partially explain why the disc achieved such large $W_{\lambda H\alpha}$ and bright photometric states in the 1970s, before the varying orientation of the precessing disc enabled truncation to become more effective. This trend towards stronger NS/disc

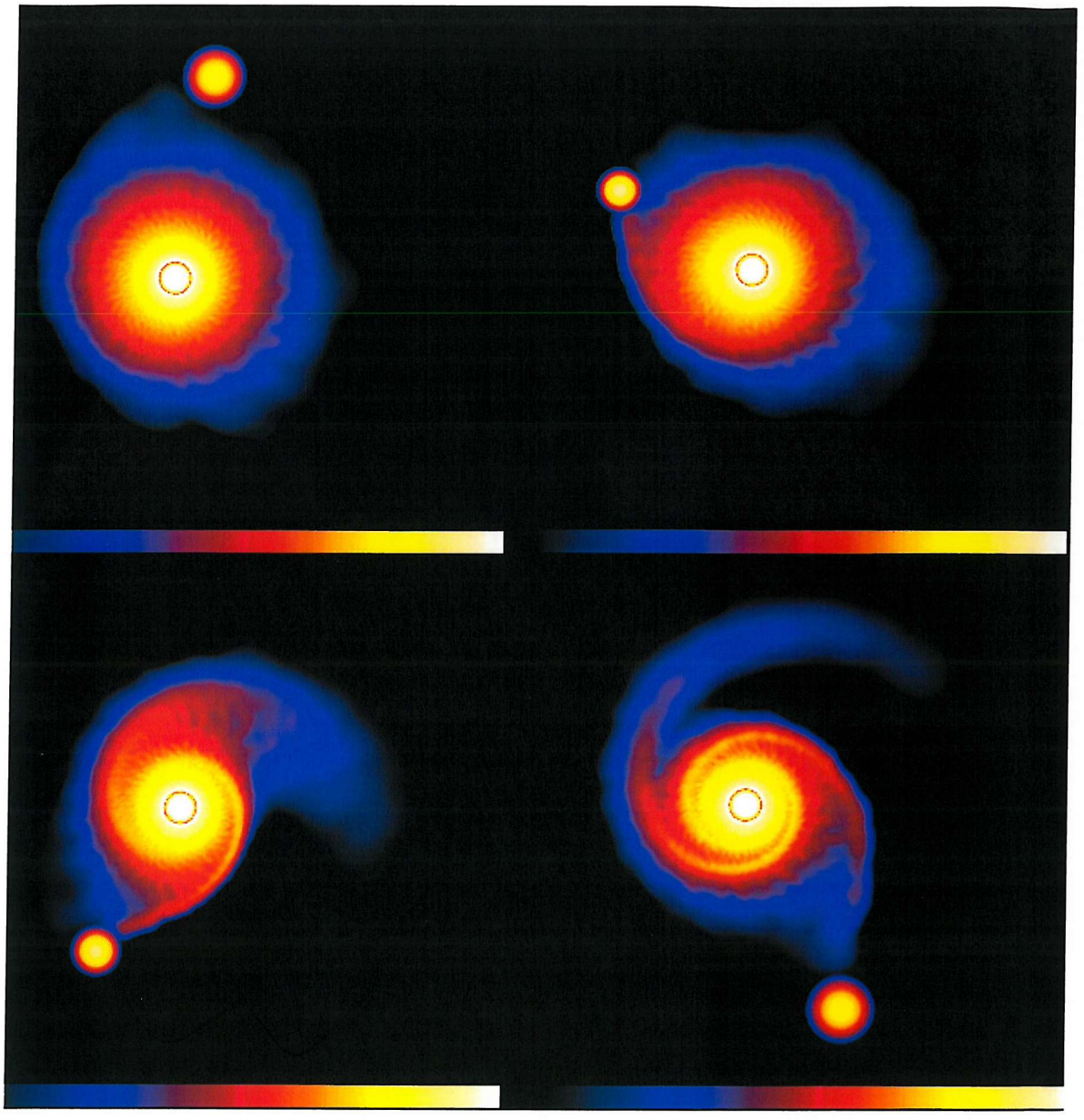

Figure 2.30: 4 frames from simulation by Okazaki (2001) for 4U0115+63 (P=24.3 days,e=0.34,B0Ve) showing disruption of Be disc at periastron and temporary formation of spiral arms.

interactions as the disc tilt increases has thus caused the most recent cycle to culminate in disc-loss, and it seems likely that the current cycle will also include disc-loss. Perhaps the disc tilt will increase until no emission is observed at all, and the system returns to the non-emission state it held for most of this century. This hypothesis requires that a tilted residual disc remains preventing the formation of new equatorial disc. Eventually the remaining disc is completely disrupted, and a new disc will form in the equatorial plane as happened in the late 1960s.

This interpretation additionally explains why at no time did the disc completely dissipate during the disc-loss period. The role of the central star in this process is thus reduced to supplying material whilst the interaction of the precessing disc and NS governs the disc state and X-ray phenomena. The disc-loss did not correspond to the star faltering in it's outbursts of material, thus high velocity emission wings are visible at all times in the spectra.

Periods of around 4 years have been reported for other BeXRBs. The cycles in 4U0115+63 reported by Negueruela et al. last 3-5 years, and 'quasi-cyclic Be star envelope variations' have been invoked to explain the 4 year modulation in the amplitude of the periodic radio outbursts in LSI+61°303 (Gregory et al., 1989). Hummel (1998) reported shell-Be-shell transitions in γ *Cas* at 1450 $\pm$ 150 days. which he attributed to a precessing circumstellar disc. Clark et al. (2001) also shows that X Per has exhibited disc-loss and disc 'low states' separated by intervals of 5 and 6 years.

These systems have widely varying orbital parameters (particularly γ *Cas*) but similar Be stars so far as temperatures, masses and ω are concerned, suggesting that the precession *period* has more to do with the properties of the oblate Be star than the third body, though the presence of a tilt between the equatorial plane and the disc is possibly induced by the NS.

2.6.6.1 Additional connections with X-ray events

Unlike the behaviour in cycles 1 and 2, the Oct. 1980 Type II outburst occurred during state C, the CRAO dataset from Jan 1980 until Dec 1980 showing $m_V = 8.9 \pm 0.04$. No state change occurred until some months after the event. However this can be understood, as the 4:1 resonance hypothesised to characterise state C is marginally outside the Be star Roche lobe (see Section 2.3.2.1) enabling mass transfer without a change in truncation radius (Okazaki and Negueruela, 2001). This may indeed be the mechanism behind many of the X-ray outbursts during the bright photometric state of the 1970s. As has been noted (Lyuty et al., 1989) even the quiescent X-ray flux of A0535+262 was elevated from 1975-1980; the identification of this epoch with a 4:1 truncation (state C) could permit strong 'leakage' at perihelion even in the absence of outbursts.

The question remains of why some transitions lead to X-ray activity while others do not (see Section 2.6.4). A possible factor is that though the disc truncation occurring midway through each cycle occurs at a specific precession phase, this phase angle will change by $\sim 25°$ each orbit. To take a simplistic viewpoint, it may be that whether the NS lies precisely in the disc plane at the time of critical precession phase determines whether we see a Type II outburst or not. The 1996 truncation occurred very early in the cycle, and no X-ray activity was seen (Figure 2.24, discussed in Section 2.5).

Importantly, truncation would appear to be the cause of the X-radiation and not vice-versa, as truncation commences before the X-ray emission.

The 1993-94 series of X-ray outbursts are expicable as occurring from the beginning of the truncation process and continuing until it was completed. V/R variability (Section 2.4.1) around this time suggests that the mechanism of density-wave induced overflow suggested by Okazaki and Negueruela (2001) may have been the trigger for the 1993-4 activity. m_V shows rapid variations during this period (Figure

2.4, Section 2.3.2.2) suggesting disruption of the disc and revealing that truncation is not an instantaneous event, taking at least 2 orbital cycles to complete, and doubtless varying in detail from cycle to cycle. Additionally the data suggest that optical depth is lower in m_V than m_K, as m_K shows far less variation during the truncation process; such a lower optical depth at shorter λ is expected.

This same effect of outbursts bracketing disruption is visible in the 1989 data. The 1986-87 X-ray outbursts are harder to explain, occurring as they do around a transition from state $A \rightarrow B$. Clearly this framework is far from complete.

2.7 Comparison with 4U0115+63

The sparsity of spectral data presented by Negueruela et al. (2001) prohibits a detailed analysis of the disc behaviour during cycles except in the broadest terms. Type II outbursts are observed to occur before/during/after bright single peaked phases, corresponding to large disc radii. In a general sense this is also true of A0535+262, though the spectra remain two peaked. The explanation of this, the warping of the disc to an essentially face-on configuration, requires an extremely large disc tilt in order to also permit shell spectra. A0535+262 shows far less evidence of such large amplitude tilting, which may be explicable by different NS orbital properties.

Critically Negueruela et al. do not observe different flux states, and thus do not see varying truncation, probably due to the poorer quality photometry. Whereas this work interprets X-ray activity as being due to material lost from the disc, primarily around truncation, encountering the NS Roche lobe, Negueruela et al. suggest that the warped disc can 'overwhelm' truncation and impinge upon the NS orbit. Furthermore, they explain that we only see Type II outbursts when Hα is single peaked because by chance when the system is configured for X-ray activity

our line of sight is face-on to the disc. A simpler explanation, that the single peaked spectra inform us of a large disc in a state favourable for mass transfer, seems more likely.

A further significant difference is that we interpret the disc precession as occurring throughout the cycles, rather than just before each Type II outburst as Negueruela et al. discuss in 4U0115+63. It seems likely that this constant precession also occurs in 4U0115+63. 4U0115+63 exhibits Type II outbursts 1-2 yrs after disc-loss, as does A0535+262. It seems possible that the shell phases observed in 4U0115+63 could be due more to part of a global precessional cycle that is occurring continuously, as has been invoked here for A0535+262, rather than a temporary precession that occurs only for part of each cycle. Certain phases of precession could position the outer edges of the disc in the line-of-sight causing shell features. Alternatively, the fact that these shell lines occur approximately simultaneously with Type II outbursts could also be attributable to the dispersion of the material lost from the disc which did not encounter the NS. Such shell phases are not seen in A0535+262 because of the lower inclination. Overall these aspects of their framework appear to provide a poorer explanation than the picture described here for A0535+262.

Whilst few if any other BeXRBs have been observed with the scrutiny reserved for A0535+262, there are suggestions that the cyclical behaviour described here is widespread. As observed in A0535+262, Reig et al. (1997) confirm that 4U0115+63 exhibits Type II outbursts at the time of maximum $W_{\lambda H\alpha}$, as does A1118-616. Figure 2.7 shows identical behaviour for 4U1145-619. It seems probable that these are all examples of the same mid-cycle behaviour.

2.8 Summary

A review of the activity and variability displayed by A0535+262 over the past 15 years, since the commencement of regular monitoring, has been undertaken. The range of the emission characteristics shown over this time, including a disc-loss episode, has enabled the relationships between the primary observables (m_K, $W_{\lambda H\alpha}$etc.) to be characterised. The disc-loss episode itself has enabled a new determination of the interstellar reddening (as has an analysis of DIBs) and a unique chance to observe a reforming disc and it's properties: rapid V/R cycles, a low expansion velocity and evidence for episodic disc renewal were seen. The system inclination, a matter of considerable disagreement, has been shown to be in the range 40-50° by two methods, both of which exploit the long run of data available, and one of which makes use of the truncation paradigm which has recently revolutionised the study of BeXRBs.

A0535+262 has been shown to display quantised IR excess flux states, which are interpreted as the first observational verification of the variable truncation scheme proposed by Okazaki and Negueruela (2001). The simultaneity of X-ray activity with transitions between states strongly suggests a broad mechanism for outbursts, one in which material stripped from the disc during the reduction of truncation radius is thereafter accreted by the NS. Furthermore these states and changes between states are shown to be linked to a probable 1400day precession period which appears to dictate the global, cyclical, behaviour of the system. Such a framework appears to be exportable to other BeXRBs.

Chapter 3

Observations of the unusual BeXRB AX J0051−733

3.1 Introduction

The source that is the subject of this Chapter, AX J0051−733, lies in the Small Magellanic Cloud, a region of space that is extremely rich in HMXRBs (see Section 1.9). It was reported as a 323s pulsar by Yokogawa & Koyama (1998) and Imanishi et al (1999). Subsequently Cook (1998) identified a 0.7d optically variable object within the ASCA X-ray error circle. The system was discussed in the context of it being a normal HMXRB by Coe & Orosz (2000) who presented some early OGLE data on the object identified by Cook (1998) and modelled the system parameters. Coe & Orosz identified several problems with understanding this system, primarily that if the photometric modulation is arising from ellipsoidal variations then its true period would be 1.4d and it would be an extremely compact system. Additionally, the combination of the pulse period and such a binary period violates the Corbet relationship for such systems (Corbet, 1986).

Date	UTC	Filter	Exposure (seconds)
1996 Oct 2	23.50	Hα	1000
1996 Oct 3	00.12	R	100
	00.15	V	200
	00.20	B	300
1999 Jan 19-25	-	V	200

Table 3.1: SAAO 1.0m telescope CCD imaging observations.

This Chapter reports on extensive new data sets from both OGLE and MACHO, as well as a detailed photometric study of the field. The results reveal many complex observational features that are hard to explain in the traditional BeXRB model.

3.2 Observations

3.2.1 Photometric

Images containing the X-ray error circle of AX J0051−733 were acquired on the 2nd October 1996 from the 1.0m reflector at SAAO. The Tek8 CCD was used in conjunction with the 3× Shara focal reducer. The resultant image covered 519 × 519", at a scale of 1.05″ pixel^{-1}. Observations were made through standard BV(R)$_c$ and Hα filters (Table 3.1). Instrumental signatures were removed using IRAF. The standard star E950 was used for photometric calibration.

Further continuous 200 second observations in V only were made from January 19-25th 1999, again using the 1.0m reflector at SAAO. The Tek8 CCD was used giving a field of 179″ at a pixel scale of 0.35″ pixel^{-1}. Instrumental signatures were removed using IRAF and STARLINK software, with aperture photometry performed using scripts based upon STARLINK routines. Instrumental magnitudes were corrected to

Date	UTC	Wavelength Range (Å)	Dispersion (Å/pixel)
1999 Nov 1	02.41	3600-5900	1.00
2000 Sep 15	02.41	3600-5900	1.00
2000 Oct 22	02.41	3600-5900	1.00

Table 3.2: AX J0051–733 ESO spectroscopic observations.

the standard system using observations of E region standards.

3.2.2 Spectroscopic

Spectra were obtained from the ESO 1.52-m telescope at La Silla Observatory, Chile, using the Boller and Chivens spectrograph with the no: 33 holographic grating, covering the range from the classification region $(4000 - 5000\mathring{A})$ up to $\sim 5900\mathring{A}$. See Table 3.2 for details of these observations.

3.3 X-ray source location

As will be seen from the photometric results presented below, it is critical to establish the correct optical counterpart to the X-ray pulsar. In particular, it is vital to clearly link the ASCA source to an optical object, and other ROSAT X-ray sources may, or may not be relevant (because no pulsations have been detected from ROSAT objects). Figure 3.1 illustrates the somewhat complex situation associated with this object. In this Figure the large dotted circle indicates the original ASCA X-ray position and uncertainty from Imanishi et al (1999). Within this error circle lie the much smaller error circles of the ROSAT sources RX J0050.8-7316 (Cowley et al., 1997) and RX J0050.7-7316 (Kahabka, 1998). Subsequently, the position of the ASCA error circle was refined to the large solid circle shown in the Figure (Imanishi

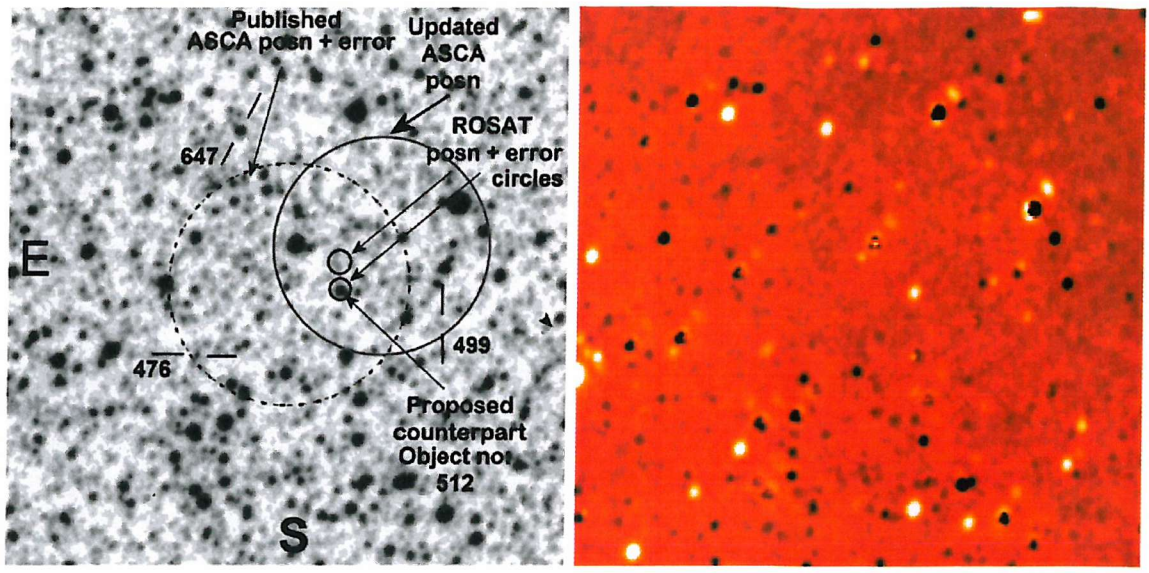

Figure 3.1: Left: Finding chart for AX J0051-733 covering a field of 4 x 4 arcmin created using an optical V band image from this work. The northern ROSAT circle refers to RX J0050.8-7316 and the southern one is that of RX J0050.7-7316. Right: Continuum subtracted Hα image of the same field. Positive images are Hα emission line objects, including Be stars. However, note ghost images to the upper right of bright stars.

2001, private communication).

Within the ROSAT error circle for RX J0050.7-7316 and the revised ASCA circle for AX J0051−733 lies an obvious optical object that has been proposed as the counterpart to both of these X-ray objects (Cowley et al., 1997; Schmidtke and Cowley, 1998; Coe and Orosz, 2000). It is a blue star exhibiting variability which strongly suggests that it is a Be star companion to the X-ray pulsar. This object also shows a strong 0.7d optical modulation (or possibly twice that value) which could be associated with a binary period of the system (Cook, 1998; Coe and Orosz, 2000). However, this period is very short for a HMXRB and the modulation signature atypical of that seen from such objects.

Consequently, it was felt necessary to revisit the linking of this optical object with

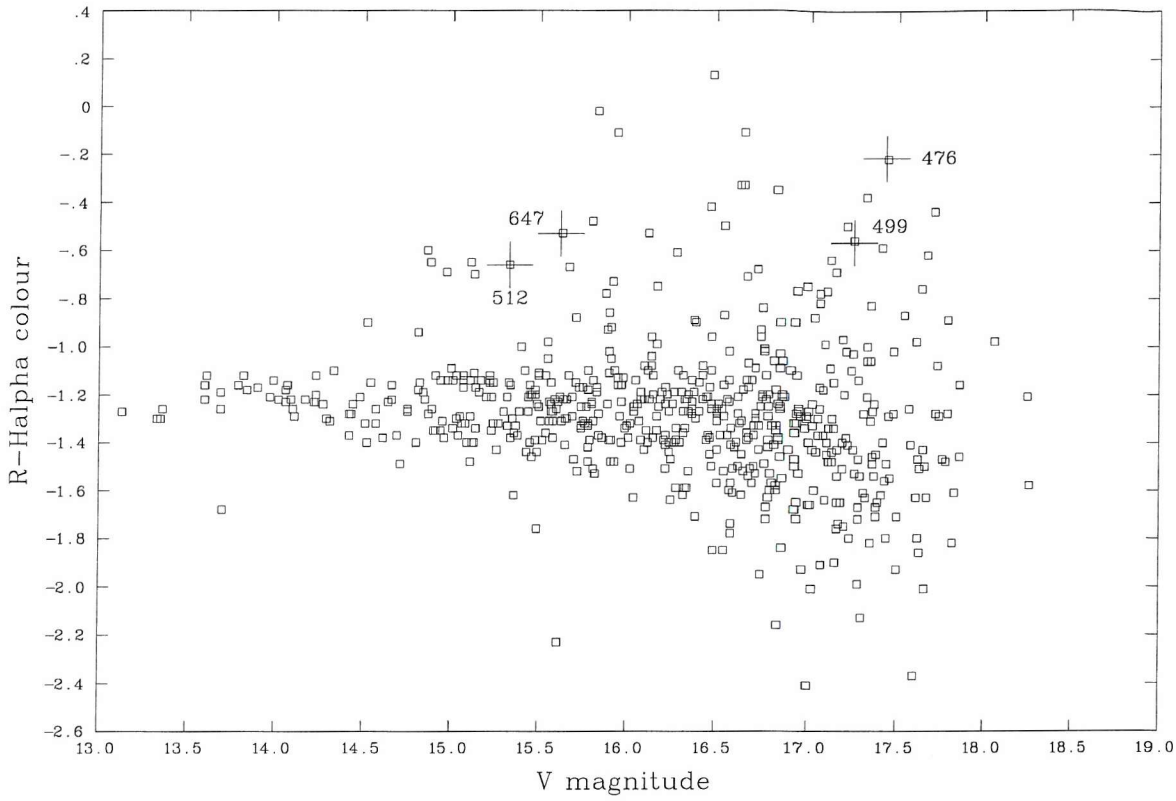

Figure 3.2: Colour-magnitude diagram for a region of 8 x 8 arcmin around the reported X-ray positions for AX J0051−733. A total of approximately 900 objects are shown in the plot. Indicated by numbers are the only 4 objects that both lie close to the X-ray positions, and have a strong Hα component. All other objects either lie too far away, or have weak Hα emission.

the ASCA pulsar to make sure that some other candidate was not more appropriate within the X-ray error circle.

3.4 Optical & IR counterpart search

From these CCD frames a R-Hα colour index was created and this was plotted against the V band flux for the ~800 objects detected.

ID	V	B-V	V-I	J	K
476	18.70	1.00	1.08	-	-
499	17.21	-0.08	0.15	-	-
512	15.44	-0.03	0.17	15.3	14.8
647	15.69	0.07	0.26	16.5	15.9

Table 3.3: Optical photometric values taken from the OGLE database and IR values from the 2MASS survey.

On the assumption that our optical counterpart was likely to be a Hα bright system, all the objects in the top third of the colour-magnitude plot were examined and their location in the field identified. Only four such objects were determined to be in, or close to, the ASCA error circle. These are numbered 476, 499, 512 and 647 in Figure 3.1 (object no: 512 is the proposed counterpart to the ROSAT sources). All the other objects with an R-Hα index ≥ -1.0 lie well away from the region of interest.

The average B, V &I colours of these four objects were extracted from the OGLE database and are presented in Table 1. In addition, IR magnitudes for two of the objects are also presented that were extracted from the 2MASS survey data base, the other 2 candidates were too faint to be detected in that survey.

The selection of the primary target, no: 512, is supported by the continuum subtracted Hα image shown in Figure 3.1. This source is the brightest Hα emitting star in the ASCA error circle, and it's appearance is typical of Be stars in such images. The formation of such images is described in Section 4.4.1.

To confirm the nature of Object 512 as a B or Be star, the optical spectra described in Section 3.2.2 were obtained. Since no obvious variations were seen between the spectra obtained at different epochs they were combined to increase the signal-to-noise ratio. The resulting spectrum is presented in Figure 3.3. In this Figure our spectrum is compared to that of the B0.5V standard 40 Per. Object 512 is

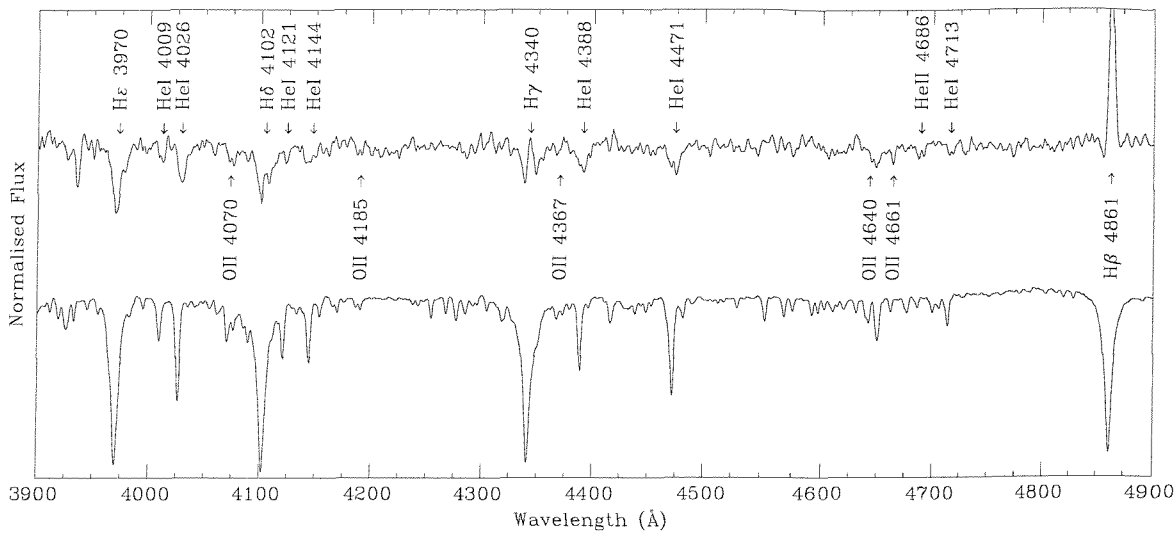

Figure 3.3: Blue spectrum of Object 512 (upper spectrum) compared to a B0.5V standard at a similar resolution. Note the presence of relatively strong Na II λ3934Å in the spectrum of Object 512, presumably of interstellar origin.

obviously a Be star, with Hβ and Hγ in emission and several other lines affected by emission components. The presence of weak He II λ4686 Å places the object close to B0V (Walborn and Fitzpatrick, 1990). Though several O II lines are present, C IV λ4650 Å is surprisingly weak or absent. The relatively weak Si III and Si IV lines seen in 40 Per are not easily detectable in object 512, which is compatible with the lower metallicity of the SMC, but unexpected in view of the rather strong O II lines.

3.5 OGLE and MACHO data

The field of AX J0051-733 lies within the areas covered by both the OGLE [1] and MACHO [2] monitoring programmes. Hence excellent photometric coverage exists for

[1] http://sirius.astrouw.edu.pl/ ogle

[2] http://wwwmacho.mcmaster.ca

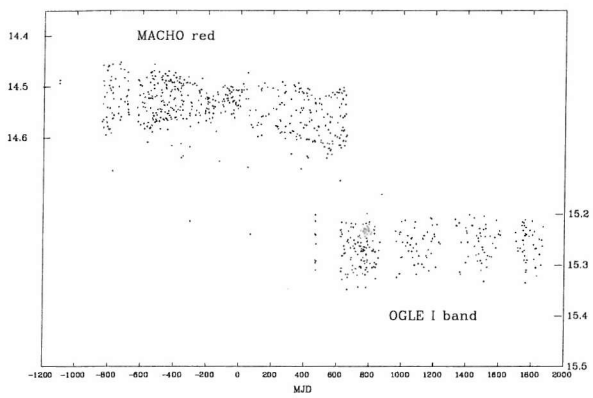

Figure 3.4: Approximately 7 years of photometric observations of the proposed counterpart to AX J0051-733 taken from the MACHO and OGLE data bases. The date axis has MJD = JD - 2450000. In both cases the magnitude scale is indicated, though the MACHO one is described as "approximately R".

the brighter counterparts for a total of nearly 7 years.

Detailed I band photometry was obtained from the OGLE data base for objects numbered 499 (no significant variability), 647 (some evidence for long term changes comparable to the length of the data set) and 512. As Cook (1998) and Coe & Orosz (2000) have already shown from subsets of the OGLE/MACHO data, this object exhibits a strong clear sinusoidal modulation at $\sim$ 0.7d. The combined OGLE and MACHO data set for this object is presented in Figure 3.4.

Though the precise modulation is not obvious from this Figure, it clearly shows the varying amplitude of the modulation over the data set. If the total data set is analysed for periodic behaviour, then a period of 0.70872d is determined using a Lomb-Scargle analysis. However, this period is the average of the data, because if one splits up the data set into $\sim$ 150d samples a slightly different period is found for each one.

Figure 3.5 illustrates the Lomb-Scargle power spectrum for one such subset of

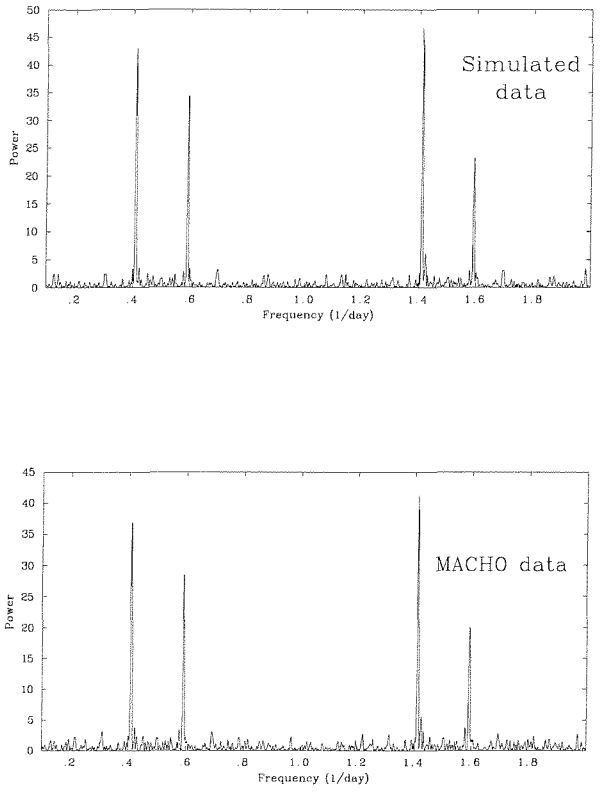

Figure 3.5: Comparison of a Lomb-Scargle power spectrum for a ~150d section of MACHO data (lower panel) and a simulated data set (upper panel). The simulated data set consists of a pure sine wave with the same window function as the raw data (see text for more details).

data. To check on the aliasing with the Nyquist frequency and the effects of the window function, a simulated data set was created. This data set consists of a single sinewave with period and amplitude determined from the original data sampled with exactly the same temporal structure as the original data. As can be seen by comparison between the two power spectra in Figure 4, there is no significant difference. Thus the conclusion is that there are no other frequencies present in the original data set.

The shape of the modulation was determined by folding one of the MACHO and OGLE data sets at the determined period for that data set. The result of this is

illustrated in Figure 3.6. Lightcurves from four different filters are shown in this Figure. In the case of the V band, the OGLE data are rather sparse since this is not their main filter, and so the data have been supplemented by observations taken over several nights from the SAAO 1.0m in January 1999 and 2000. Since this data set is not as uniform as the other 3 bands the individual results are presented in the phase diagram rather than a folded light curve. Overall, from this Figure, the extremely sinusoidal nature of the modulation is very clear.

The topmost curve in Figure 3.6 is a measure of the colour of the object obtained by subtracting individual MACHO blue measurements from their red measurements taken on the same night. If the colour data are also subjected to the same Lomb-Scargle analysis, then the same period emerges from the data, but the depth of modulation is clearly very small.

Perhaps the most important result to emerge from the combined OGLE/MACHO data set is the period history. Figure 3.7 illustrates this by showing the periods determined from the 12 individual data sets. From this Figure one can clearly see that the period is changing by a significant amount over the 7 years. The simplest interpretation of the period change is a linear one, and from such an assumption a value of 13.5s/year is found. More complex changes, for example a sinusoidal modulation with a period of ~3600d, may be speculated upon but are not required by the data as yet.

The upper curve in Figure 3.7 shows the result of fitting a sine wave to each individual data set and determining its amplitude. Though there is clear evidence of amplitude variation by ~40% from both this Figure and Figure 3.4, it is not obvious that there is any significant pattern to the change.

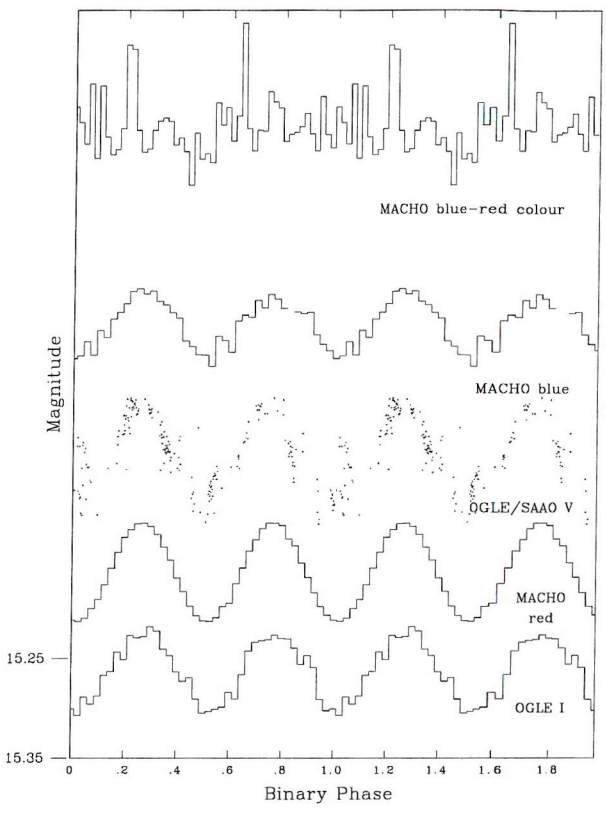

Figure 3.6: The lightcurves obtained by folding a ~150d sample of MACHO and OGLE data at the period of 1.4174d. Because the OGLE V filter coverage is very sparse it has been amalgamated with the SAAO observations in this band. The magnitude scale on the left only refers to the OGLE I band data, all the other photometric bands have been arbitarily shifted upwards by a constant amount to fit conveniently on the Figure. In each case the data sets have been phase shifted to coalign with the OGLE I band data set (see text for further details). The uppermost curve shows the colour information obtained from the same MACHO data set used to construct the light curve in the Figure.

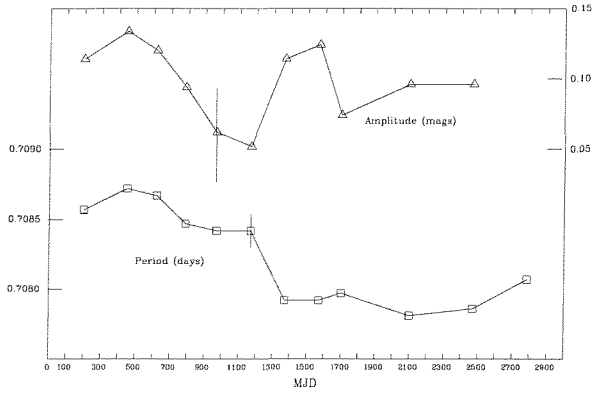

Figure 3.7: The lower curve shows the period history determined from the combined MACHO and OGLE data sets. If the variability is caused by ellipsoidal variations in a binary system then we should expect the true binary period to be twice the value indicated on the left hand axis. The upper curve shows the amplitude of a sine wave fitted to each data block. In both cases a typical error bar is indicated. The time axis has MJD = JD - 2449000.

3.6 Discussion

3.6.1 Optical candidate

In trying to establish the optical counterpart to the ASCA pulsar one must keep in mind that the ROSAT source is too weak to have shown any detectable pulsations. Thus putting the ROSAT source aside for the moment, the most objective approach is to just look at the colour-magnitude diagram (Figure 3.2). This diagram reveals just two objects inside the best ASCA positional error circle - nos. 512 and 499. The other two objects lie in, or very close to the original ASCA circle, but are now significantly less attractive as counterparts. Object 499 is very faint compared to all other known counterparts to HMXRBs in the SMC, which typically have $V \sim 15 - 16$. Its colours and the presence of Hα in emission suggest a B3-4Ve star - a somewhat later spectral type than most other BeXRB systems. Its OGLE

lightcurve reveals nothing of interest and it is not a detectable IR source in the 2MASS data. Hence it cannot be a strong contender for the counterpart to AX J0051−733.

On the other hand, Object 512 has $V = 15.4$ and a significant IR flux at $J = 15.3$. Both of these make it look like a classic counterpart to a BeXRB system. If we compare this object to another SMC X-ray pulsar system, 1WGA J0053.8−7226 (Buckley et al., 2001), we find it is extremely similar. In 1WGA J0053.8−7226 we have $(B - V) = -0.06$ compared to -0.03 in Object 512, and $(J - K) = 0.62$ compared to 0.51 in Object 512. The reddening found for many other SMC counterparts to BeXRB systems is ~ 0.25 (a combination of extinction to the SMC plus local extinction and extra flux due to cirumstellar material). Applying this to the observed values for Object 512 given in Table 1 leads to an identification for the spectral type of B0III-V. Thus even before one considers the *ROSAT* source, one is led inexorably to Object 512 being the prime candidate for the optical counterpart to AX J0051-733. The presence of a convincing *ROSAT* source at the same position adds significant extra weight to this conclusion.

The optical spectrum of Object 512 presented in Figure 3.3 is no later and perhaps slightly earlier than the comparison standard. From the colours presented in Table 1 and assuming $(B-V)_0 = -0.26$ (Wegner, 1994), this results in an extinction value of $E(B-V) = 0.23$, which confirms the number used above in interpreting just the photometry. Assuming standard reddening, $A_V = 0.71$ and a distance modulus to the SMC $(M - m) = 19.0$, the absolute magnitude for Object 512 is $M_V = -4.3$, which is in rather good agreement with a spectral type in the B0-B0.5V range.

3.6.2 Optical modulation

The strong sinusoidal optical modulation of Object 512 is challenging to interpret in terms of a traditional BeXRB model. Firstly, the expected binary period of AX

J0051−733 based on the Corbet diagram (Corbet, 1986) is 100–200d. Secondly, a binary period of just 1.4d involving a Be star implies an extremely tight orbit – the Keplerian orbital radius would be $\sim$ 14 solar radii and the B0 star has a size of $\sim$ 8 solar radii. Thirdly, if the period is really decreasing at a rate of 13.5 s/year then this implies (Huang, 1963) a mass transfer of 10^{-5} $M_{\odot}$/year for mass transfer between an $18M_{\odot}$ Be star and a $1.4M_{\odot}$ NS – which is not only much larger than that typically observed in HMXRB systems ($\lesssim 10^{-8}$ $M_{\odot}$/year in most cases), but would also imply a much higher X-ray luminosity unless the accretion mechanism is extremely inefficient at converting gravitational potential into X-rays.

Mass transfer rates of this magnitude are deduced to exist in the EB binary system β Lyrae which is changing its $\sim$ 13d orbital period at a rate of 19s/year (van Hamme et al., 1995). In this case the change is to a longer period with the mass transferring from the smaller B6-8 star to the more massive Be star. In our case, the mass would be flowing in the opposite direction, i.e. from the more massive object to a less massive one. The optical lightcurve of β Lyrae is similar to the one presented here for Object 512, but with the notable difference that in β Lyrae the two minima are not of the same depth.

In fact the symmetry of the light curve is much more suggestive of a W UMa type system. Unfortunately, the observed period of 1.4d is much greater than any such reported system in the SMC (Rucinski, 1997). The maximum observed period is 0.8d and our period is well off the end of the distribution. In addition, it is perhaps worth noting that the predicted $(V-I)$ colour obtained from the distribution of such objects and our binary period of 1.4d is +0.026, but from Table 1 it can be seen that the observed $(V-I)$ for Object 512 is 0.17. Even allowing for interstellar extinction this further adds to it being unlikely that this system is of this class.

The possibility of a blended variable star plus Be star can be considered. At the SMC's distance, such superpositions are quite feasible. For example, a chance superposition of Be star (to give the observed colours) plus Cepheid or RR Lyrae (to

give the optical modulation). However, all of these models can be ruled out because of either the magnitude of the period, or the depth of modulation, or the shape of the lightcurve. Additionally the PSF is identical to that of field stars, placing tight constraints on the alignment.

Interestingly the optical modulation is somewhat similar to the short periodic modulation seen by (Balona, 1992) in Be stars in the cluster NGC330 in the SMC. In this case Balona attributes this modulation to surface features on the rapidly rotating objects. However, how the period of such objects could change on a timescale of years is not clear, unless the star is in a very wide binary system. It is possible that the data in Figure 3.7 could be fitted to ~10 year sinusoidal modulation, but then the orbit of the NS would be so distant from the Be star that it hard to see how accretion could ever occur. In addition X-ray outbursts have been detected 3 times over 2 years from this system (Laycock, private communication) making such a long orbit unlikely. Perhaps further optical data may clarify exactly what the shape of the period change is on such timescales.

3.6.3 A triple system?

We are left with no convincing traditional scenario to explain all the observational data. It is very hard to see how the orbital period change seen in Figure 3.7 could possibly be caused by mass loss from a normal B0 star at a rate of 10^{-5} $M_{\odot}$/year. Another possibility perhaps worth considering is that AX J0051−733 is a triple system – Be star plus another star in a tight 1.4d orbit, and the NS in a highly eccentric 100−200d orbit around the pair. Such a system could not only be intrinsically very stable since most of the mass is concentrated in the inner binary pair, but the transfer of angular momentum from the inner binary to the orbit of the NS might also explain the evolution of the orbital period.

Eggleton & Kiseleva (1995) derive a critical parameter X_o^{min} for a stable triple

system, which is the period ratio between the outer and inner orbits. For a system to be stable it is required that the ratio of the orbital periods be greater than X_o^{min}. If we assume that our inner 1.4d binary consists of a B0V star (M=18$M_\odot$) and a 1$M_\odot$ star, while the third outer body is a 1.4$M_\odot$ NS, then this parameter X_o^{min} = 17. Assuming that the outer orbital period is approximately given by the position of AX J0051−733 on the Corbet diagram and has a value of $\sim$ 100days, then this criterion is easily satisfied.

Bailyn & Grindlay (1987) provide a formula for the rate of change of size of the major axis of such a tight binary (their Equation 7). Using their relationship, and assuming one of the binary partners is the observed BO star, then it is possible to predict the rate of change of orbital period as a function of the mass of the other star in the inner binary. For masses of the order 15-20$M_\odot$ the predicted period change is $\sim$10 s/year. This number is in good agreement with the observed value of 13s/year and suggests that the inner binary may, in fact, consist of two very similar B-type stars. This, of course, would not present any problems to the observed photometric or spectroscopic parameters of the system. Even assuming that the two stars contribute equally to the luminosity of the system would mean that their intrinsic magnitudes are $M_V = -3.5$, still compatible with B0.5Ve. Furthermore, the Eggleton & Kiseleva criterion remains comfortably satisfied for such a system. A possible problem raised by such a scenario though would be the minimal space remaining within the inner binary for a Be disc.

However, the evolution of this system would have to have been very different from a classic BeXRB system. In particular, the NS progenitor has probably evolved without any mass-transfer to either of the objects in the inner binary. Consequently it must have been much more massive in order to have reached its current state so long ahead of the other stars in the system. Clearly this solution for AX J0051−733 is also not without challenges.

3.7 Summary

Detailed optical observations and analysis have been carried out of the proposed counterpart to AX J0051-733. The most likely counterpart has been identified on the basis of its colours and Hα emission. However this object is revealed to have a strong 0.7/1.4d modulation from long-term MACHO and OGLE observations. Furthermore this strong period is shown to be changing at a rate of 13.5s/year. It is hard to reconcile all these observations with the classic BeXRB model and further studies of this system are required.

Chapter 4

The nature of the BeXRB XTE J0111.2–7317

4.1 Introduction and background

The X-ray transient XTE J0111.2–7317 was first detected by the Proportional Counter Array (PCA), flying on the RXTE X-ray observatory, on October the 29th 1998 (Chakrabarty et al., 1998a; Chakrabarty et al., 1998b) in the 2-10keV band. Further confirming observations came from the BATSE instrument on CGRO which detected the source in the 20-50 keV band (Figure 4.1). RXTE All Sky Monitor (ASM) data provide a clear detection for $\sim$ 100days, from early November 1998 until the end of January 1999 (Figure 4.2).

The observed temporal, flux and spectral characteristics are typical of BeXRBs. The detection of pulsations at 32 seconds further strengthens this hypothesis. In addition the source location is coincident with the SMC, the assumption of membership permitting an absolute luminosity to be calculated. Whilst towards the upper end of the typical flux distribution, peaking at approximately $2 \times 10^{38} ergs^{-1}$, it is

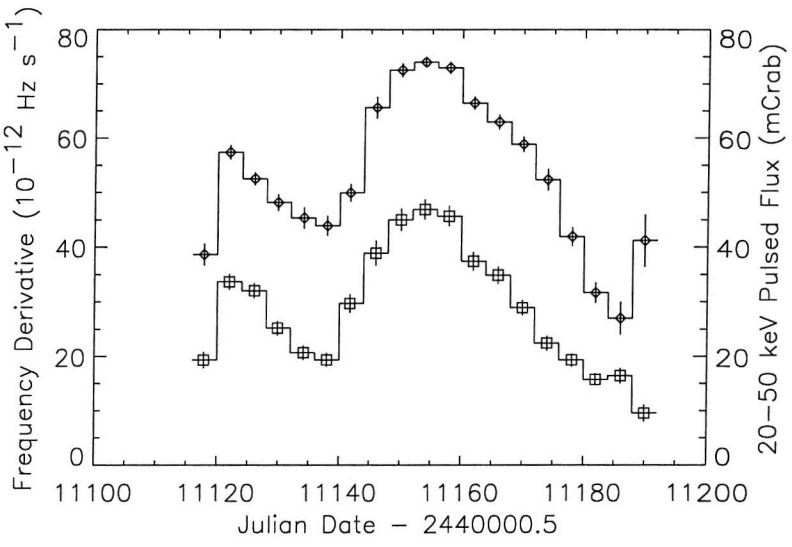

Figure 4.1: XTE J0111.2–7317 20-50 keV BATSE frequency derivative (top) and flux.

consistent with a giant (Type II) outburst from a BeXRB. The luminosity calculated from the period derivative compared to the observed flux (Figure 4.1 places it at unequivocally in the SMC (Wilson, private communication).

Clearly optical and IR study of the optical counterpart to a system such as this is enormously enlightening as to its nature. The first step is the identification of such a star; conveniently the small error circle enables the entire region to be imaged in a single CCD frame. This was done by us on January the 24th (Table 4.1), but unfortunately spectroscopy of the two brightest objects (Israel et al., 1999) on January 19th 1999 established a Be star located at R.A. = 1h11m08s.4, Decl. = -73o16'46" (1" uncertainty) as the likely optical counterpart before we were able to reduce our data.

Though in many ways typical of the growing population of known SMC BeXRBs (see Section 1.9), this system has proved particularly interesting, and to some extent unique, because of it's location in a small region of nebulosity (Figure 4.10), the nature of which is clearly of considerable interest. If a SNR the size of 3.1pc, using

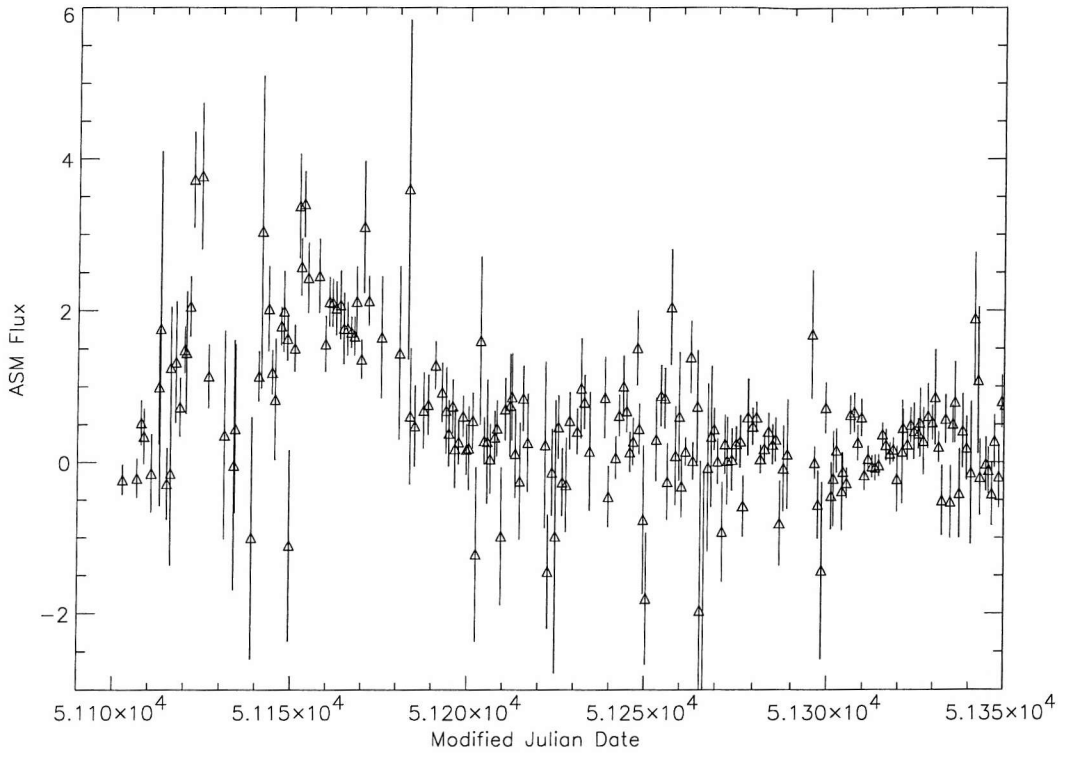

Figure 4.2: XTE J0111.2–7317 2-10 keV RXTE ASM flux history.

the diameter-to-age relationship $D = 0.9t^{2/5}$ (Clark and Caswell, 1976), implies an age of 120yrs. The typical expansion velocity of 10000 km s^{-1}(Chevalier, 1977) for Type II SNe implies an age of $\sim$ 300years. Such a young BeXRB would be of particular interest. This matter is analysed in Section 4.4.

Throughout this work XTE J0111.2–7317 refers both to the X-ray source and to the optical counterpart.

4.2 Observations

4.2.1 Optical imaging/photometry

Images containing the X-ray error circle of XTE J0111.2–7317 were acquired on the 21st and 24th of January 1999 from the 1.0m reflector at SAAO. The Tek8 CCD was used giving a field of 179″ at a pixel scale of 0.35″ pixel^{-1}. Observations were made through standard UBV(RI)$_c$ and Strömgren-Crawford uvbyβ filters (Table 4.1). Instrumental signatures were removed using IRAF and STARLINK software, with aperture photometry performed in GAIA. Instrumental magnitudes were corrected to the standard system using observations of E region standards. The photometric measurements are contained in Table 4.4.

Further Wide Field Imager (WFI) images of the field were extracted from the ESO archive. The WFI is a focal reducer-type camera which is permanently mounted at the Cassegrain focus of the 2.2-m MPG/ESO telescope at La Silla, Chile. The detector is a mosaic of 4 × 2 4096 × 8192 CCDs with 0.24″ pixels. These observations targeted a different object, but because of the huge 34′×33′ field XTE J0111.2–7317 was also imaged (Table 4.2). Unfortunately dithering of the pointing to eliminate inter-chip gaps led to XTE J0111.2–7317 falling outside the field of view on some images. Useful images in [SII], Hα, [OIII] and a continuum regions close to Hα were de-archived. Preprocessing was performed using STARLINK software.

Further photometric points have come from Covino et al. (2001) and the DENIS survey.

Date	UTC	Filter	Exposure (seconds)
1999 Jan 21	20.15	R	100
	20.17	V	200
	20.22	B	200
	20.26	I	100
	20.29	U	300
	20.40	Hα	1000
	20.59	y_s	400
	21.07	b_s	500
	21.16	$H_{\beta W}$	500
	21.26	$H_{\beta N}$	1000
	21.43	v_s	600
	21.55	u_s	1800
1999 Jan 24	22.08	V	200
	22.14	Hα	2000

Table 4.1: SAAO 1.0m telescope CCD imaging observations.

Date	UTC	Filter	Exposure (seconds)
1999 July 26	09.02	Hα	300
	09.10	Hα	300
	09.17	Hα	300
	09.24	Hα Continuum	180
	09.40	[OIII]	300
	09.48	[SII]	300

Table 4.2: Archive ESO 2.2m telescope CCD imaging observations.

Date	UTC	Wavelength Range (Å)	Dispersion (Å/pixel)
1999 Jan 9	21.15	6250-6900	0.75
1999 Jan 9	21.53	6250-6900	0.75
1999 Jan 10	20.44	3700-5400	1.50
1999 Nov 3	02.41	3600-5900	1.00

Table 4.3: XTE J0111.2–7317 spectroscopic observations.

4.2.2 IR photometry

The infra-red JHK photometry (4.4) was obtained using the Mk III photometer on the Radcliffe 1.9metre telescope at the South African Astrophysical Observatory (SAAO), Sutherland. The date of these observations, January the 8th 1999, is only 13 days prior to that of the optical data and so may be regarded with caution as simultaneous.

4.2.3 Spectroscopy

Optical spectra were taken of XTE J0111.2–7317 in January 1999 from the 1.9metre Radcliffe telescope at SAAO. The grating spectrograph was employed with the SITe CCD detector.

An additional spectrum was obtained at the ESO 1.52m telescope at La Silla, Chile, on November the 3rd 1999. The Boller and Chivens spectrograph was used with the no: 33 holographic grating, covering the range from the classification region $(4000-5000\mathring{A})$ up to $\sim 5900\mathring{A}$. The slit was oriented in a NW-SE line to encompass the brightest parts of the nebulosity. See Table 4.3 for details of these observations.

4.3 Optical studies of XTE J0111.2–7317

4.3.1 Photometry

4.3.1.1 Optical

The discovery of an optical counterpart (Israel et al., 1999) was confirmed by our work (Coe et al., 2000) and has been reiterated more recently (Covino et al., 2001). This ID work was based upon detecting Hα (or to a lesser extent Hβ) emission from the system, which must additionally possess the photometric properties of late O to early B stars. Figure 4.3 shows a V band image from our SAAO 1.0m observations showing the X-ray positional uncertainty (30″ radius error circle) and optical counterpart.

An accurate spectral classification based upon photometry presents the usual problems regarding uncertain interstellar reddening, circumstellar excess and the disagreement between various authors regarding the luminosities and temperatures of OB stars.

Based upon the observed correlation of m_V against $W_{\lambda H\alpha}$found for A0535+262, the derived nebulosity subtracted $W_{\lambda H\alpha}$of 16.5Å(Section 4.3.2) suggests a ff/bf colour excess of CE(B-V)$\approx$ 0.35 $\pm$ 0.15 (Figure 2.21) and a photospheric m_V = 15.68 $\pm$ 0.15. We thus derive $M_V = -3.32 \pm 0.2$, allowing for a 0.1 magnitude error in μ_{smc}.

The Martins et al. (2001) estimate of the line-blanketting (at SMC metallicities) induced correction to VGS96 magnitudes is +0.15 magnitudes, giving an expected $M_V = -3.95$ at B0.5V and -3.84 at B1V. The 0.575 magnitude discrepancy between these values and observation hints at interstellar extinction; using R=2.72 $\pm$ 0.21 (Bouchet et al., 1985) an $E(B-V) \approx 0.2$ is suggested (or alternatively the unlikely

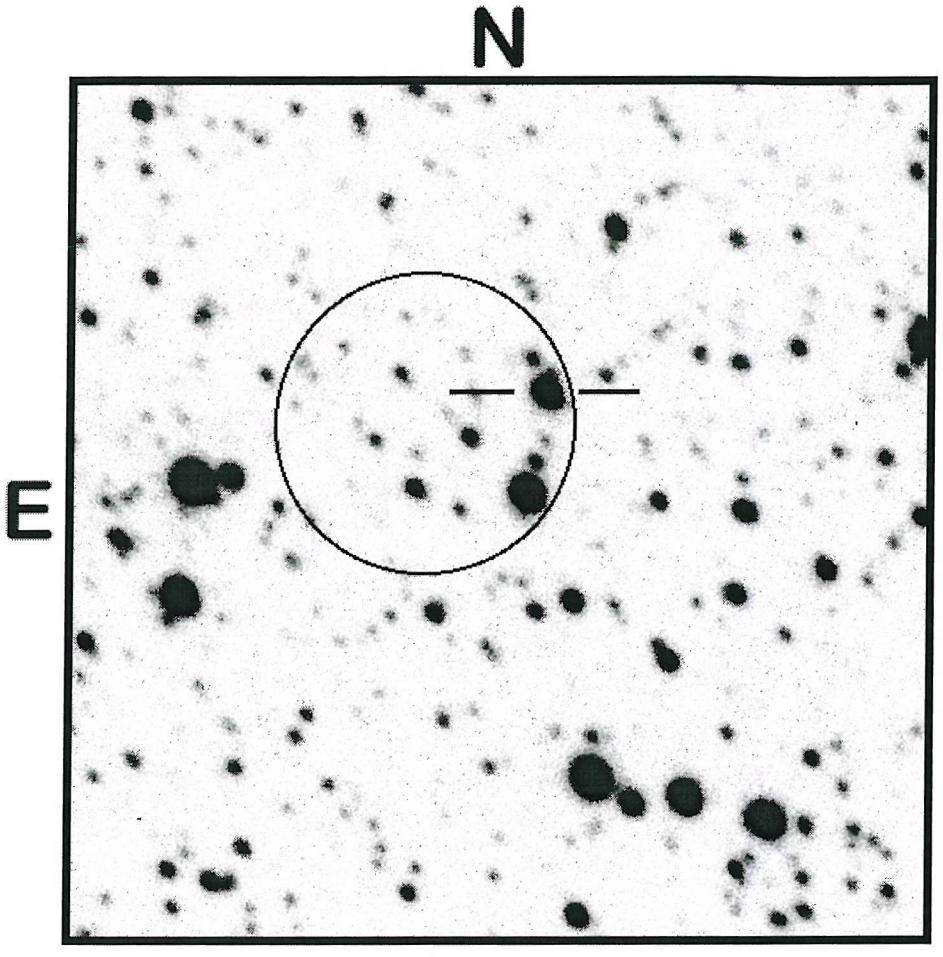

Figure 4.3: V band SAAO 1.0m image of the field containing the source XTE J0111.2–7317 (marked) and the X-ray error circle (30″ radius) from the RXTE satellite. The field of view is 3 x 3 arcminutes.

classification of $\sim B6$). However, in view of the commonly encountered variations in published OB star luminosities, this is by no means certain. Note however that a luminosity class of V is required.

Figure 4.4 shows the photometry listed in Table 4.4 converted to fluxes using the conversion factors of Bessel et al. 1998 (UBVRIJHK) and Fabregat and Reig 1996 (uvby). Effective wavelengths for filters are from Bessel et al. 1998, Bessel 1990 (UBVRIJHK) and Gray 1998 (uvby). The data shown have not been de-reddened - rather the model atmospheres plotted have had reddening applied to them to provide fits to the data. Because the effective wavelengths of the V (5450Å) and y (5460Å) filters are so close, the fluxes measured at this point may be combined to produce an error-weighted mean flux density of $2.679 \pm 0.05 \times 10^{-15} erg/cm^2/s/\AA$ at 5450Å, or m_V of 15.33 ± 0.02. This provides the normalisation.

The spectral classification of Covino et al. (2001) of B0.5-1Ve ($T_{eff} \approx 30,000K$ is plotted with reddenings of E(B-V)=0.2 and 0. Regarding the optical photometry, the E(B-V) of 0 provides a significantly poorer fit to the data than does 0.2. Additionally, a higher reddening of ~ 0.3 eliminates any IR excess up to m_J, which is certain not to be the case.

In addition to the observed colour index of $(B-V) = -0.08 \pm 0.02$, the transformation of Strömgren photometry to Johnson colours (Turner, 1990) gives $(B-V) = -0.01 \pm 0.03$. Wegner (1994) gives $(B-V)_0 = -0.23$ for B0.5-B1V, yielding E(B-V)=0.20 including circumstellar reddening. In A0535+262, correlations of $W_{\lambda H\alpha}$with (B-V) suggest a circumstellar E(B-V) contribution of 0.05-0.1. Thus the estimated interstellar reddening is E(B-V)=0.10-0.15.

Overall, these results strongly suggest that a moderate degree of interstellar reddening is occurring along the line of sight. A value of E(B-V)=0.1-0.2 is at the high end of the normal distribution for the SMC, hinting that XTE J0111.2–7317 is associated with an enhanced ISM.

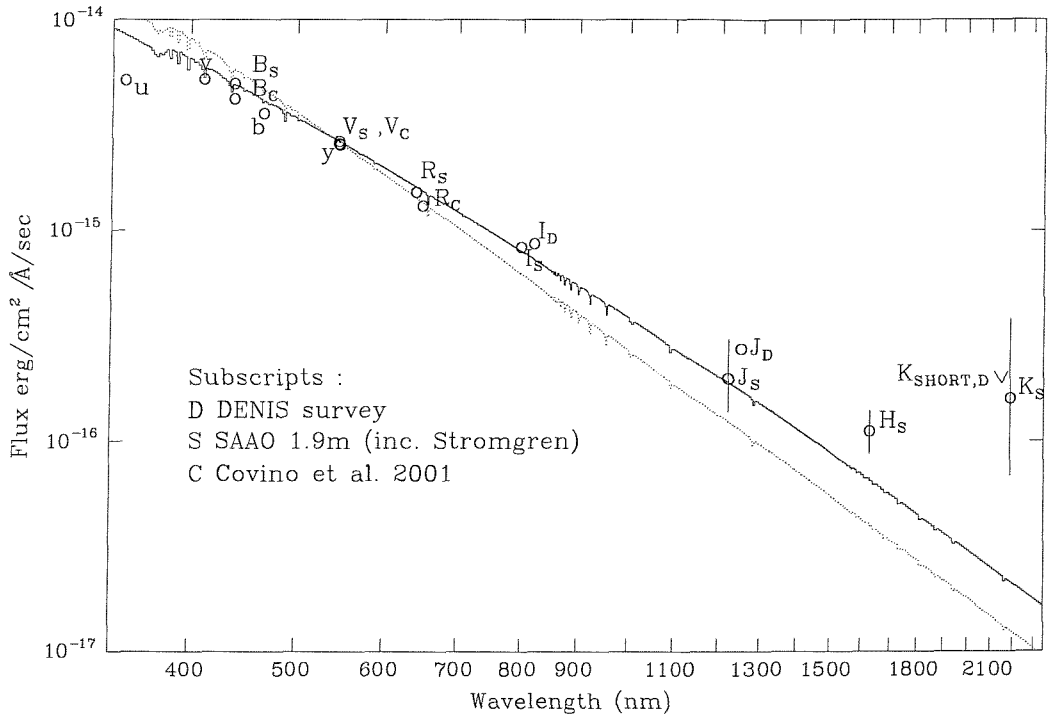

Figure 4.4: All available photometry with superimposed B1V Kurucz continuum reddened with E(B-V)=0.2 (continuous) and E(B-V)=0 (dotted).

4.3.1.2 IR

Because of the faintness of the target the JHK photometric errors are large, but the data are precise enough to see an excess of luminosity over that expected from purely photospheric emission (Figure 4.4). The J and H magnitudes, and thus (J-H) colour, are typical of MC BeXRB systems with similar Hα strength (J-H$\sim 0.3-0.4$) but m_K is significantly brighter than expected; whereas $H-K \sim 0.2-0.3$ might be expected, the measured $H-K = 1.6 \pm 0.96$.

A search through the 2nd release of the 2MASS catalogue, which includes the SMC, frustratingly revealed the source to be located on a gap in the coverage, presumably due to a problem with the relevant images. There are no plans to release any more 2MASS data before the final release which is still some months away. Additionally the DENIS IR catalogue has yielded I and J measurements but not K_S, because of it's faintness. This in itself suggests that the SAAO measurements may be inaccurate, as DENIS is complete to $K_S = 13.25$ and almost so at the $K_S \sim 13.5$ level (C. Loup. private communication). Clearly better IR photometry is required; however a JHK imaging request on IRIS2 at the AAT which will provide this data has yet to be carried out.

Plotting the IR colours on Figure 1 of Gummersbach et al. (1995) places XTE J0111.2–7317 squarely in the region inhabited by B[e] systems, well away from the Be and MS stars. This separation arises from the SED of B[e] systems becoming dominated by thermal dust emission from K redwards; this strongly alters the H-K colour whilst leaving the J-H similar to that observed in Be systems. Unfortunately the errors are considerable.

This link became all the more significant with the discovery of [OIII] emission spatially coincident with XTE J0111.2–7317 (see Figure 4.7), as forbidden line emission is a trait of most types of B[e] star.

Whilst the B[e] phenomenon is most widely associated with supergiant systems (Lamers et al., 1998) with $logL_*/L_\odot \sim 5-6$, such characteristics have been found to exist in stars of considerably lower luminosity ($logL_*/L_\odot = 4$) than formerly was believed, at least in the MCs (Gummersbach et al., 1995). Gummersbach et al. include 4 B[e] stars in this work extending down to the luminosity of XTE J0111.2–7317. Recently, the former BeXRB system 1H 0521+37 has been investigated (Clark et al., 1999b) and found to have IRAS colours consistent with emission from cold dust, and thus reclassified as unclB[e], following the classification scheme of Lamers et al. (1998) as it is insufficiently luminous to fit the sgB[e] category. It is however of similar luminosity to the XTE J0111.2–7317 system, and if the curious IR characteristics of XTE J0111.2–7317 are confirmed may well prove to be related, making a third B[e]XRB system. Clark et al. note that only 3 Be stars are known to display cool dust emission, and these are possibly nascent stars with dusty discs allied to β Pictoris, Vega and the Herbig Ae/Be stars, and thus probably evolutionarily distant from the necessarily older BeXRBs.

Much work has been expended on MC B[e] systems, for the usual reasons that the MCs are at a known distance and extinction whereas these uncertainties plague galactic studies. However, it is worth noting that the [OIII] emission detected from this system is barely spatially extended at the levels typical of ground-based spectroscopy; without the more detailed study presented in Section 4.4.4.4 this may not have been noted. It seems a possibility that some of the [OIII] emission associated with B[e] systems may in fact more closely resemble the compact nebula we have observed in this system than the much smaller 'extended circumstellar discs' described in the literature.

As will be discussed later (Section 4.4.5), the nebulosity associated with this system could be interpreted as a bowshock; such objects are strong emitters in the IR due to the presence of dust (as with planetary nebulae), to the extent that many have been found through their IRAS 60μm emissions (Noriega-Crespo et al., 1997b). Thus a possibility exists that the anomalously bright m_K could be attributed to dust

Band	8 Jan 1999 SAAO	21 Jan 1999 SAAO	19 Jan 1999 Covino et al.2001	2 Sept 1996 DENIS
B		15.24±0.01	15.42±0.05	
V		15.32±0.01	15.36±0.03	
R		15.37±0.02	15.29±0.03	
I		15.31±0.01		15.27±0.02
u		15.90±0.02		
v		15.56±0.02		
b		15.53±0.01		
y		15.44±0.02		
J	15.54±0.34			15.19±0.10
H	15.08±0.25			
K	13.48±0.93			>13.25

Table 4.4: Optical and IR photometry of XTE J0111.2–7317.

emission from the bowshock. The other possible classifications of the nebula, SNR and HII region, are both also expected to possess some IR flux. Thus the nebulosity as a source of this unexplained excess cannot be ruled out. Unfortunately the system is too distant to be resolved or even detected by IRAS, particularly as there are strong sources close by.

4.3.2 Spectroscopy

The only significant features detected in the initial examinations of the SAAO optical spectroscopic data were strong Hα and Hβ emission lines, as expected for a BeXRB. The measured equivalent widths were -27 ± 0.3Å for Hα (Israel et al. 1999 found -21Å) and -3.8 ± 0.2Å for Hβ. However, a considerable fraction of this emission is contamination from the nebular emission which crosses the stellar spectrum (see Figure 4.6). Because the nebulosity is brightest close to the star, the

sky/background subtraction carried out as a standard procedure in the spectral reduction does not remove such contamination. The nebular [SII] lines at 6716$\AA$ and 6731$\AA$ contaminate the stellar spectrum in the same way. All published equivalent widths to date (Covino et al.2001, Coe et al.2000) have been skewed by this effect.

Figure 4.5 shows the Hα region of the SAAO XTE J0111.2–7317 spectrum. Inspection of the images (Figure 4.6) shows that while the nebular contamination is fully contained in a band 5 pixels wide ($\sim 2.1\AA$ or $97\,\mathrm{km\,s^{-1}}$), the true circumstellar emission is considerably broader at $\sim 400\,\mathrm{km\,s^{-1}}$, typical for Be stars. Thus whilst the measured $W_\lambda$is certainly an overestimate, there is no doubt that intrinsic circumstellar emission exists. A two component Gaussian fit to the line profile was performed within the DIPSO/ELF package using the measured FWHM of the nebular contamination (from a spatial position adjacent to the star) to robustly remove it (Figure 4.5). This fit assigns $61 \pm 4\%$ of the line flux to the broader circumstellar disc (conventional Be) component, producing an intrinsic $W_{\lambda H\alpha}$of 16.5±1.1Å.

The Doppler shift of the broad circumstellar component of Hα is recessional at $170.8\pm9.3\,\mathrm{km\,s^{-1}}$(visible in Figure 4.5) which agrees well with the systemic value of $166\pm3\,\mathrm{km\,s^{-1}}$(Feast, 1961) for the SMC. Not only does this confirm membership of the SMC (never really in doubt because of the X-ray flux and photometry) but it also places a constraint on the system's radial velocity relative to the local ISM of $2.5 \pm 12.5\,\mathrm{km\,s^{-1}}$. Accurate Doppler shifts for all of the lines detected from the surrounding nebulosity are in Table 4.5.

The other bright star within the error circle was also observed but did not show any evidence of Hα in emission. This is also evident from its appearance in Figure 4.10 where it appears in negative below the white Be counterpart; an explanation of these images is in Section 4.4.1.

Regarding a classification based upon spectroscopic features, this has been done by Covino et a. (2001) based upon superior spectra, and their conclusion of B0.5-1Ve

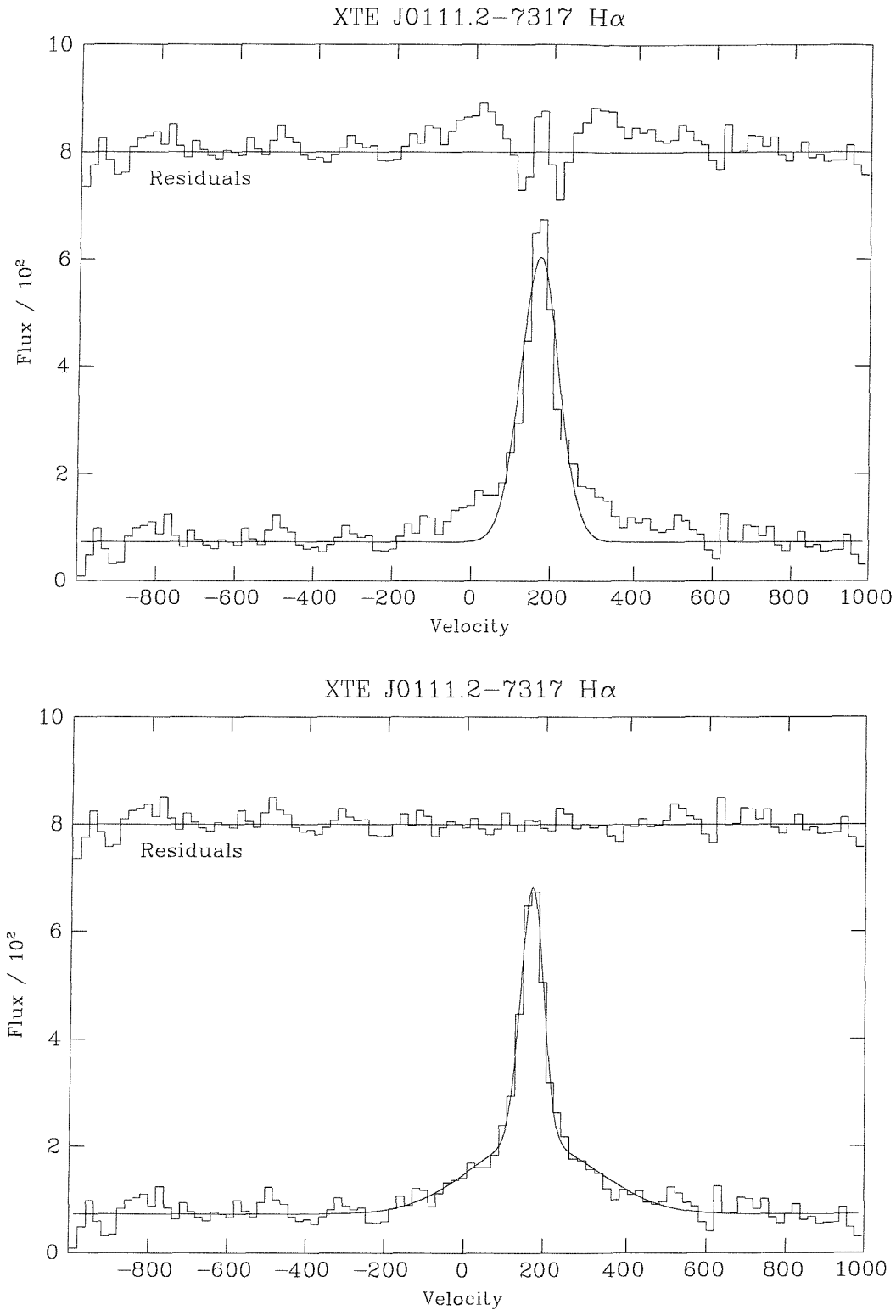

Figure 4.5: Hα region of SAAO XTE J0111.2–7317 spectrum with 1 and 2 component Gaussian fits.

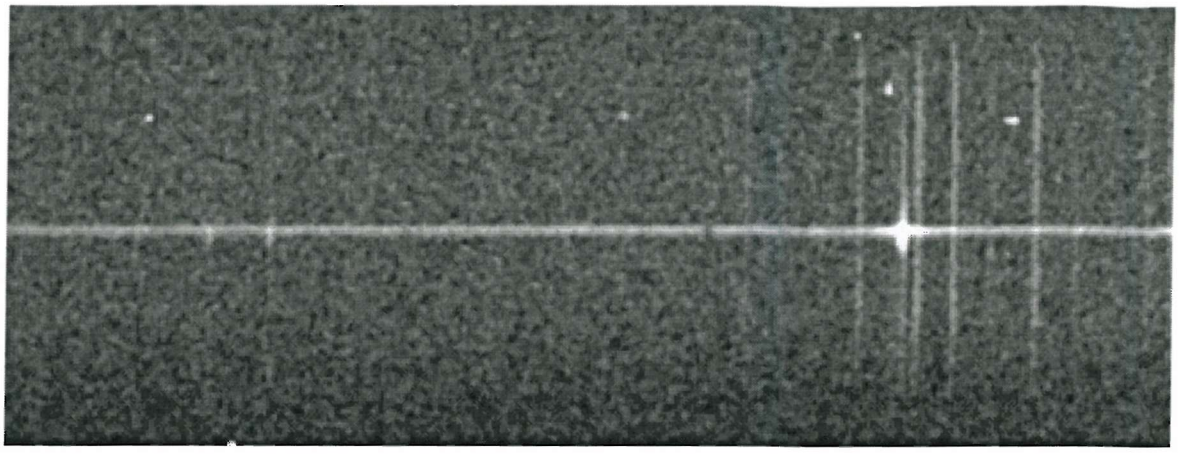

Figure 4.6: Part of the preprocessed, co-added spectrum of XTE J0111.2–7317 showing Hα (at right) and S[II] (two lines on the left) emission just beneath the stellar continuum. Telluric sky lines and cosmic ray events are also seen.

is unchallenged by this work.

Spectra (Figure 4.7) show lines at 4959Å and 5007Å, attributed to [OIII] emission. Such forbidden line emission is typical of most nebulae but uncharacteristic of the relatively dense circumstellar environment of Be stars. A search through the spectra of 11 other LMC/SMC BeXRB spectra in the Southampton database, and several galactic systems (including X Per and A0535+262) found no other systems with features at this wavelength, as expected if it arises from [OIII] emission. Section 4.4.4.4 shows that this feature results from the superposition of nebular emission.

4.4 Nebulosity

The SAAO images of the field of XTE J0111.2–7317 were acquired on the 21st of January 1999 with a view to identifying the counterpart from its expected Hα excess

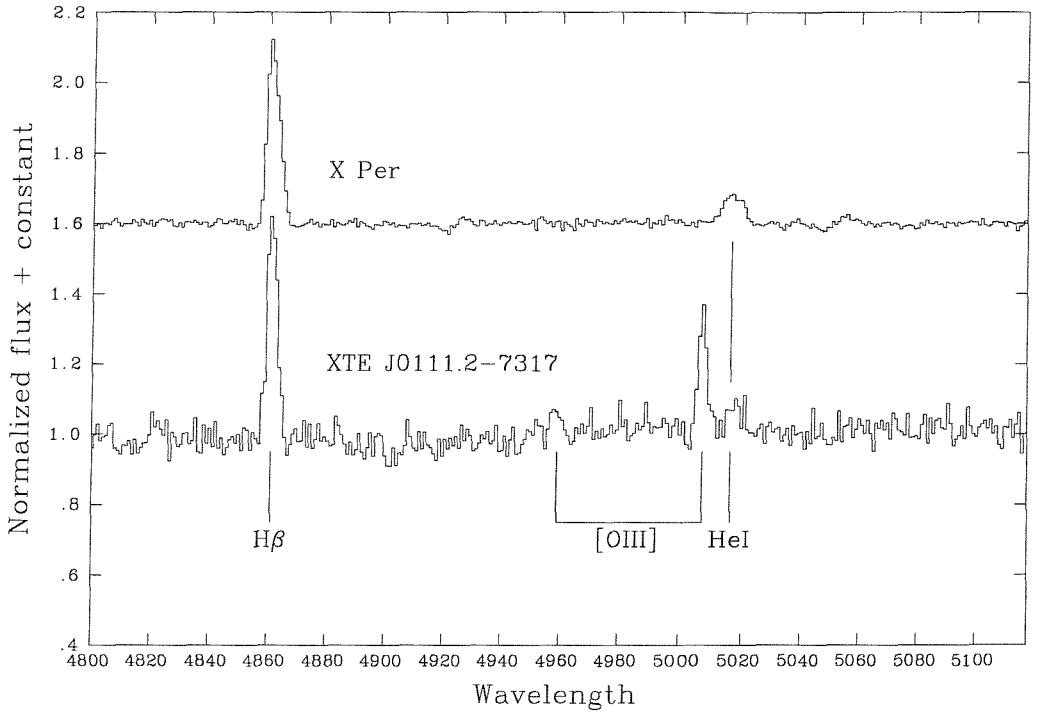

Figure 4.7: The 4800–5050$\AA$ region of the ESO spectrum of XTE J0111.2–7317 showing Hβ, [OIII] and HeI emission lines. The same range of a spectrum of the classic BeXRB X Per from the same observing run is shown for comparison. The XTE J0111.2–7317 spectrum has been shifted by $-165\,\mathrm{km\,s^{-1}}$ to the heliocentric rest frame.

and optical colours. Unexpectedly though, initial inspection of a 1000 second raw Hα image at the telescope showed faint nebulosity extending to $\sim 10''$ around a star within the error circle. This star was shortly thereafter (February 1st) proposed as the optical counterpart (Israel et al., 1999). Nebulosity was visible only in Hα (and not Hβ) images, so a further 2000 second Hα exposure was acquired on January the 24th.

4.4.1 The MERGE script - imaging faint nebulosity.

The low surface brightness of the nebulosity, and the presence of faint field stars superimposed upon it and nearby, combine to make a morphological interpretation difficult. The upper panel of Figure 4.9 shows the Hα image of XTE J0111.2–7317, and though the nebulosity is clearly visible, it is unclear whether some of the brighter patches are stars or enhanced nebular emission. However, because the Hα filter bandpass is effectively a subset of the broader R filter, the stellar continuum emission present in the Hα images can be largely removed using an R band image. To perform these tasks the C-shell script 'MERGE' was written.

Essentially, the continuum flux present in the Hα image is modelled using a scaled, registered and convolved R band image, and then subtracted. Selection of a star in both Hα and R images enables a comparison to be made regarding registration and image FWHM. The convolution of the sharper image to match the PSF of the poorer image accounts for the fact that whilst the Hα images are generally less sharp and frequently exhibit guiding errors due to their lengthy duration, in general no two images possess sufficiently similar PSFs that simple subtraction will not leave excessive artifacts. The transforming PSF is derived by deconvolving the inferior (usually Hα) PSF with the superior using the STARLINK MEM2D routine. Convolving the sharper image with the resultant transformation PSF yields images with nearly indistinguishable PSFs, which can then be subtracted without leaving the artifacts which would otherwise mask faint detail.

Some scaling must be applied to the continuum image before subtraction; the software either does this by equating the flux from a user-defined non-emission star in both images, or by a using a pre-defined ratio. Though selection of a field star can make this scaling factor somewhat arbitrary, its precise value has little to no significant effect on the final image unless one selects an emission line star as reference, which leads to over subtraction of the continuum image. It also enables rapid results to be obtained.

The output images from this script reveal sources of Hα emission as positive images, whilst non emission-line stars subtract out completely leaving only regions of enhanced photon noise and (usually) weak artifacts. This script frequently reveals Hα regions invisible on the unmodified Hα images, and also clearly shows stars with Hα emission, mostly Be stars (Figure 4.8). It is thus also of use in swiftly determining the probable optical counterparts of BeXRBs with error circles of a few arcminutes. See Figures 4.9 and 4.10[lower panel] to see the results of this process. The final result shows that the emission is smoother than would appear from the Hα image alone, though two slightly brighter features are weakly visible to the SSW (lower right). Confirmation of these comes from the lower resolution, but slightly deeper SAAO images (Figure 4.10[upper panel]).

4.4.2 Image characteristics

Initial analyses of the nebula used CCD imaging from the SAAO 1.0m reflector (see Table 4.1) which provided the 'first look'. Though images were obtained in all Strömgren and Johnson filters and Hα, only the Hα image shows nebulosity (Figure 4.9, top). Though Hβ emission is present (Table 4.5), it is apparently too weak to register in the image, due both to the large amount of continuum also transmitted and to the poor response of the CCD in the blue.

However these data were to some extent superseded by archival images from the

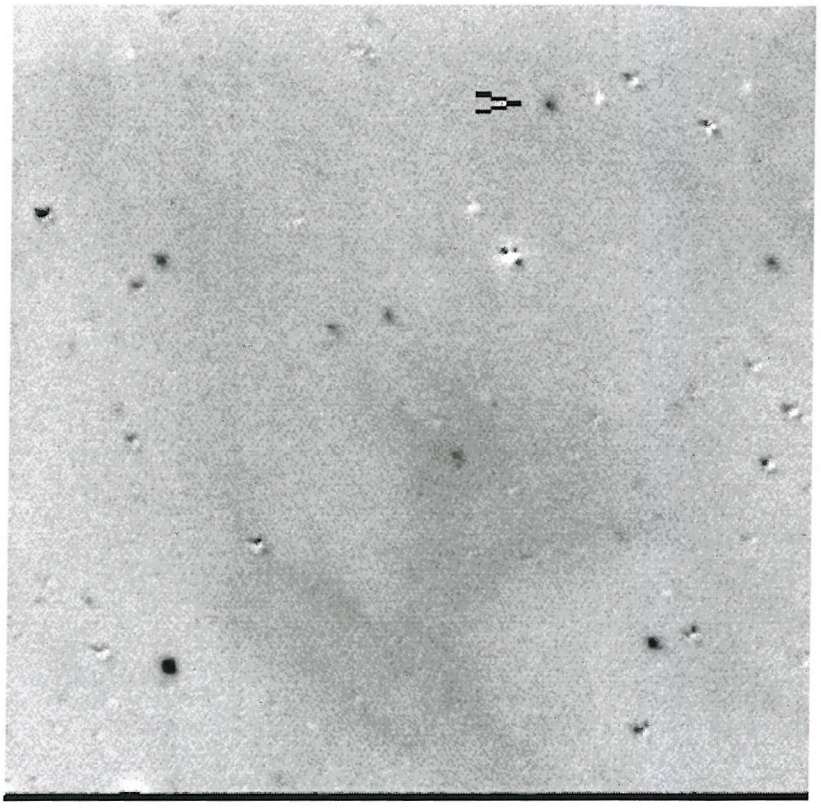

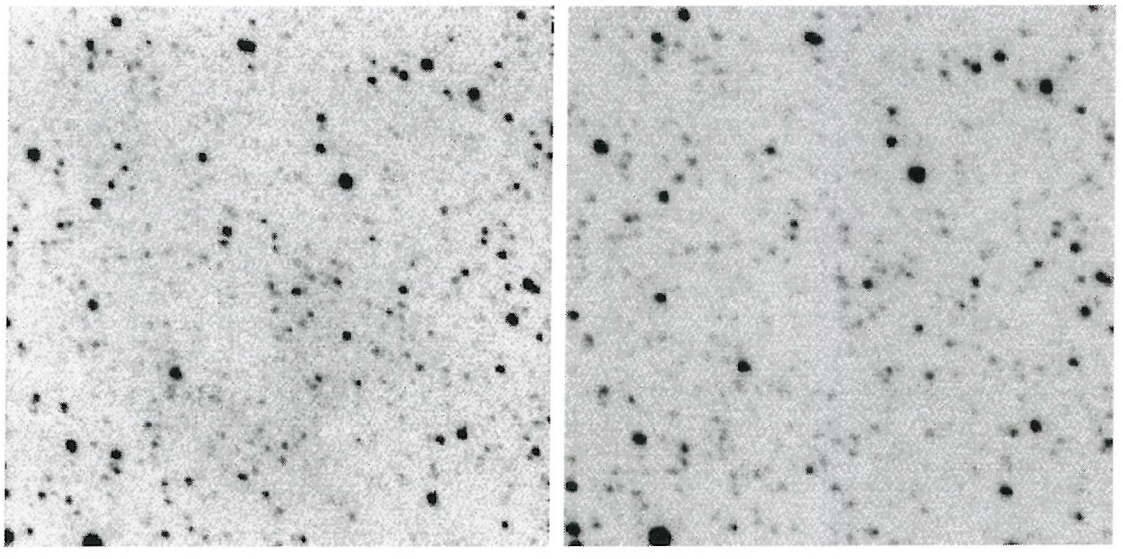

Figure 4.8: MERGE output of AX J0049-732 showing field nebulosity. North is up, field is $3' \times 3'$. Lower panels are Hα(left) and continuum/R(right). Positive (black) images are emission line sources. The marked object is currently favoured as the optical counterpart (Coe, private communication), but no definitive ID has been made.

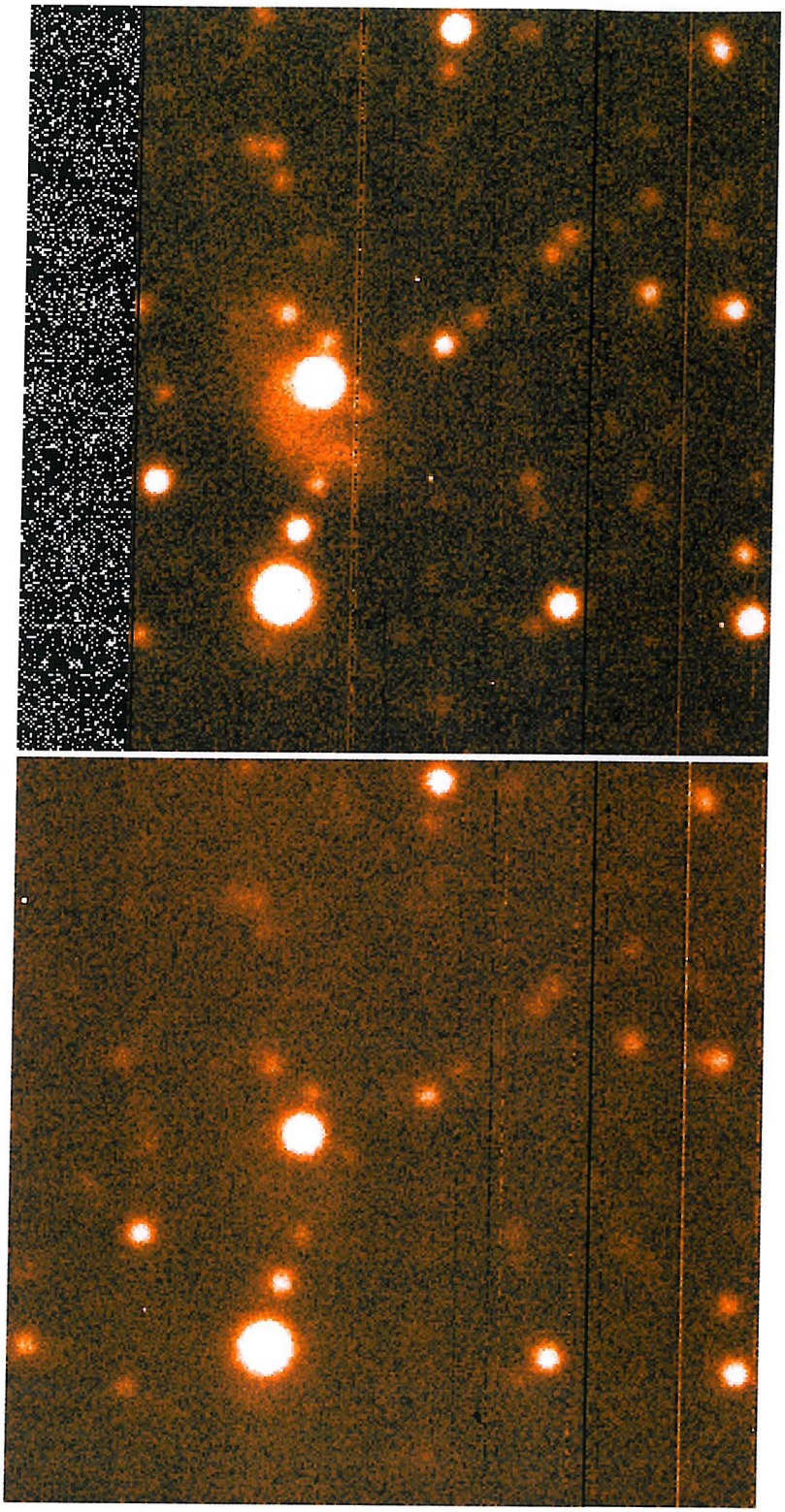

Figure 4.9: Hα and adjacent Hα continuum images from the ESO La Silla 2.2m archive data. Bright and dark lines are due to bad CCD columns.

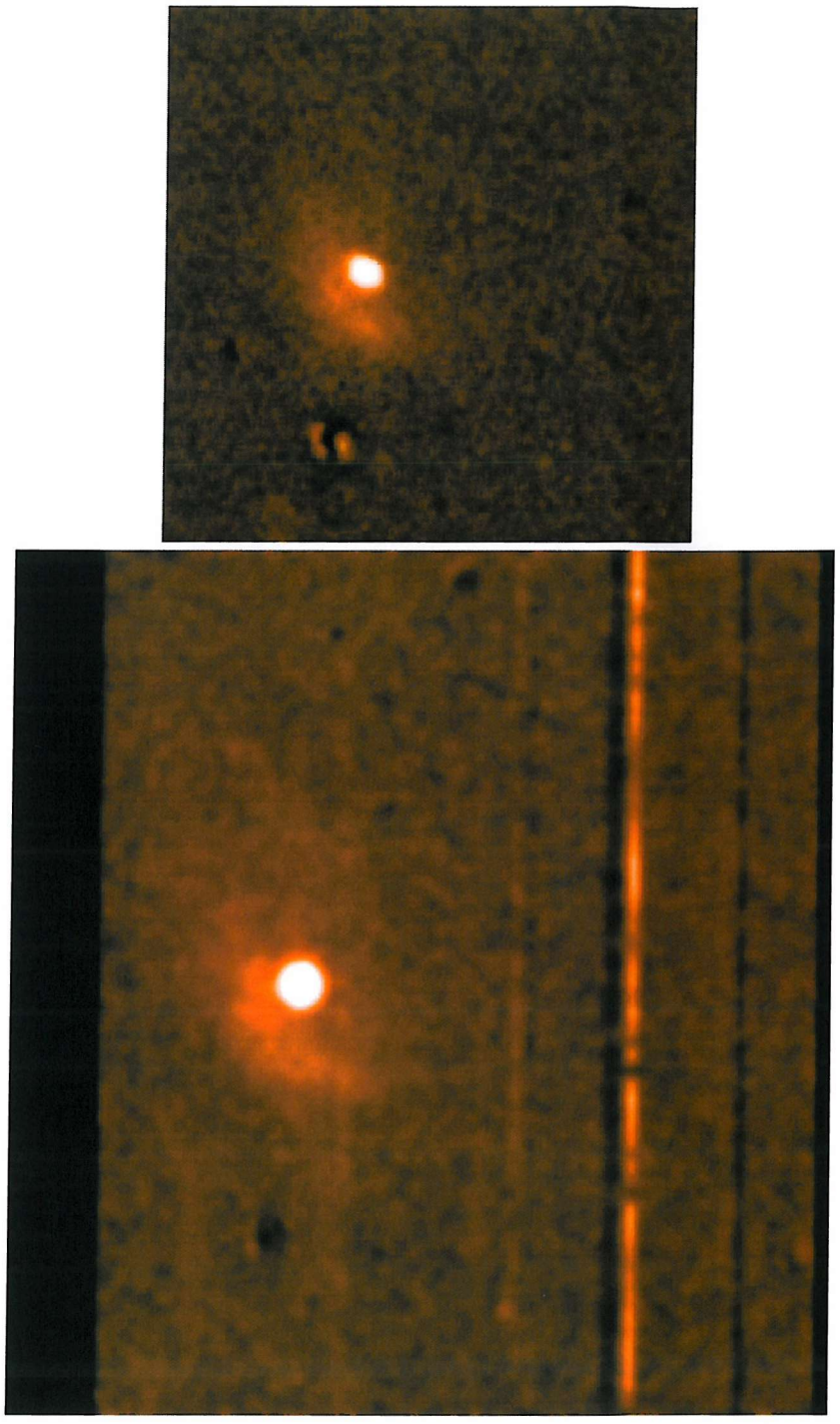

Figure 4.10: Continuum subtracted Hα images of the region around XTE J0111.2–7317. Upper panel SAAO 1.0m images, lower panel images from ESO La Silla 2.2m archive, smoothed with a $\sigma = 1''$ Gaussian filter. Bright and dark lines are due to bad CCD columns.

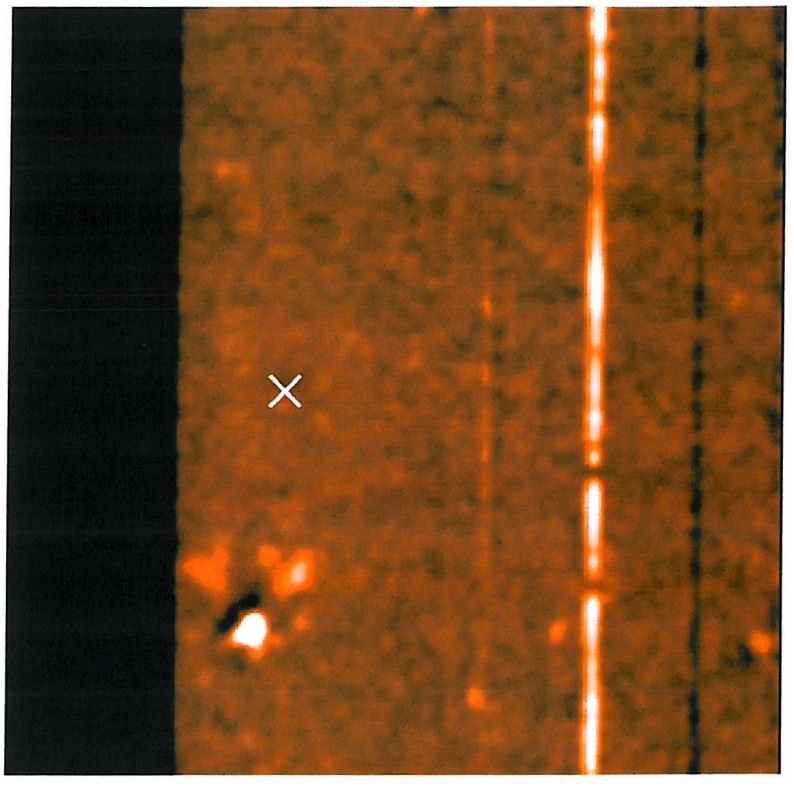

Figure 4.11: Continuum subtracted [SII] image of the region around XTE J0111.2–7317. Smoothed with a $\sigma = 1''$ Gaussian filter. The Be star is located with a white cross. Images from the ESO La Silla 2.2m archive data. Bright and dark lines are due to bad CCD columns. Extensive artifacts are visible around the lower field star.

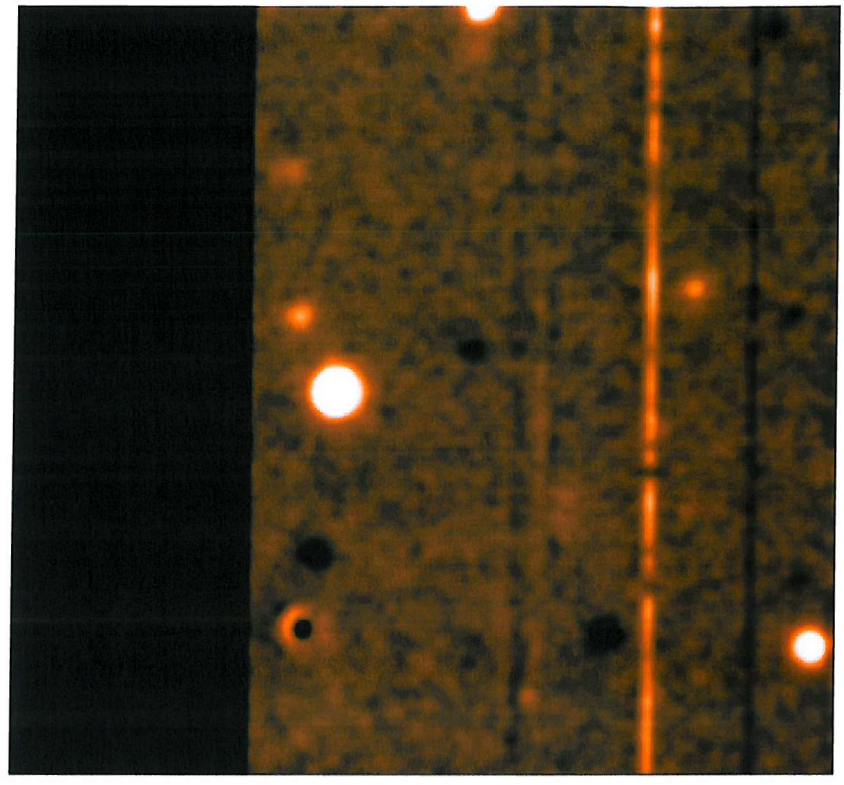

Figure 4.12: Continuum subtracted [OIII] 5007Å image of the region around XTE J0111.2–7317, which is the bright source left of centre. Smoothed with a $\sigma = 1''$ Gaussian filter. Images from the ESO La Silla 2.2m archive data. Bright and dark lines are due to bad CCD columns, whilst positive and negative star images result from the undesirable necessity of using of a 6650Åcontinuum image. The ring shape towards the bottom of the image is an artifact left after subtraction of a bright field star.

ESO 2.2m telescope (Table 4.2) due to their superior depth and resolution. Images in Hα, Hα continuum, [OIII] and [SII] were dearchived, but again only Hα clearly displayed nebulosity (Figure 4.10). The MERGE script (Section 4.4.1) was used to remove continua for both the [SII] and [OIII] images (Figures 4.11 and 4.12). Unfortunately only Hα continuum images were available to model the continuum component; this was not a problem with [SII] (at $\lambda\lambda$ 6717,6731 c.f. Hα at λ6563) because of the minimal spectral separation, but the [OIII] λ5007 continuum was not adequately represented by the Hα continuum image, thus leaving significant stellar images and preventing the detection of the small [OIII] nebula (Section 4.4.4.4). The FWHM of XTE J0111.2–7317 was measured both in the un-subtracted and post-MERGE [OIII] images and found to be consistent with the other field stars. [SII] (Figure 4.11) appears to show extremely weak emission coincident with Hα.

Thus analyses of the structure of the nebula in the light of these species had to be undertaken spectroscopically (Section 4.4.4.4).

Of the possible nebular types considered the simplest is a conventional HII region, photoionised by XTE J0111.2–7317. A second possibility is that the nebula is an SNR. In view of the association with the BeXRB system, it would be extremely interesting to identify the SNR corresponding to the formation of the system's neutron star. This would, amongst other things, enable the system's age to be determined.

Another possibility which exists is that the nebulosity is a bowshock. Such structures (Figure 4.22, Vela X-1) arise when ram pressure due to supersonic motion of a star confines it's expanding wind. The head or apex of the structure defines a point where the momentum of the expanding stellar wind balances that of the oncoming interstellar medium. Bowshocks are commonplace around OB runaway stars (see Section 1.6). Indeed, according to the standard theory of BeXRB formation, such systems MUST be runaways. Therefore bowshocks could be commonplace around BeXRBs. The nature of the nebula is discussed in Section 4.4.5.

4.4.3 Spectral data

4.4.3.1 Nebular spectrum extraction

No nebulosity had been observed when the SAAO spectra were taken so the exposures were calculated to properly expose for the Be star. However subsequent examination of the raw spectral images reveals weak nebular emission lines offset to one side of the stellar continuum; this one-sidedness stems from the asymmetrical morphology of the nebulosity.

Two spectra of the source were acquired, the second because the intended star largely missed the slit on the first. However both contained strong nebular features, and so were co-added. The exposures were sequential and as a pair were bracketted by arc exposures; no wavelength shift was detectable. All further reduction took place on this co-added image, a subset of which is shown in Figure 4.6. This section of the image contains Hα at 6563$\AA$ and the two [SII] lines at 6716$\AA$ and 6731$\AA$; no other emission lines are seen in the entire image, which covers $\sim$ 6200$\AA$ to $\sim$ 6900$\AA$.

The SAAO blue exposure similarly shows only very weak nebular Hβ emission. In view of the existence of a far higher S/N blue spectrum from La Silla, no further work was undertaken on the blue SAAO spectrum.

Thus the STARLINK task EXTRACT was used to extract the region immediately adjacent to the star including these emission features; sky subtraction was from a region 10 pixels below. Whilst sky subtraction was used to identify and reject telluric and other non-nebular lines, actual measurement used subtraction of a constant background to significantly reduce noise. This also enabled telluric lines to be used as wavelength standards, for example the 3.682Å separation of telluric Hα from it's SMC component provides a highly accurate velocity. Care was taken to exclude any stellar (including Be circumstellar disc) flux. Table 4.5 lists the nebular emission lines obtained from the SAAO red and ESO blue spectra.

Species	λ ($\AA$)	Rest λ ($\AA$)	Flux per " ($10^{-16} erg/cm^2/s$)	Velocity ($\mathrm{km\,s^{-1}}$)	FWHM ($\mathrm{km\,s^{-1}}$)
ESO blue 3600–5900$\AA$					
[OII]	3728.12 ± 0.14	3726.16	25.3 ± 3.7	145.3 ± 10.8	176 ± 20
[OII]	3730.91 ± 0.14	3728.91	37.4 ± 4.0	148.4 ± 10.8	176 ± 20
Hγ	4343.10 ± 0.43	4340.47	10.0 ± 2.7	169.7 ± 29.4	217 ± 60
Hβ	4864.31 ± 0.10	4861.33	17.7 ± 1.3	172.0 ± 6.0	189 ± 19
[OIII]	4961.89 ± 0.23	4958.91	2.8 ± 1.2	168.1 ± 13.6	171 ± 39
[OIII]	5009.82 ± 0.23	5006.84	7.7 ± 1.4	166.4 ± 13.5	170 ± 39
SAAO red 6180–6930$\AA$					
Hα	6566.28 ± 0.02	6562.76	150.5 ± 3.5	168.3 ± 8.3	66 ± 2
[SII]	6720.03 ± 0.06	6716.47	25.1 ± 3.5	163.7 ± 5.7	47 ± 6
[SII]	6734.41 ± 0.06	6730.85	18.0 ± 3.2	163.4 ± 5.7	47 ± 6

Table 4.5: List of observed discrete emission lines from nebulosity around XTE J0111.2–7317. Wavelengths from Allen (1976), Meinel (1965) and Takami et al. (2001).

ESO (La Silla) blue spectra were extracted using the same method.

Dividing the Hα flux density integrated along the slit by the approximate scale of 8″for the object (the exact slit orientation is unknown), one derives a Hα flux density of $\sim 20\times10^{-16} erg/cm^2/s/arcsec^2$, which is close to the value found for the bowshock associated with Vela X-1 (Kaper et al., 1997) of $\sim 10 \times 10^{-16} erg/cm^2/s/arcsec^2$.

Because of the small number of counts from the nebular lines, the extracted spectra are a spatial average over all the nebulosity which fell upon the spectrograph slit. Without higher S/N data this is the only way of extracting spectra of usable quality. Of course, the nature of spectroscopy of an optically thin source across a plane in the sky means that even spectra of a point are actually integrated through the depth of the object, thus this further integration loses little information. However, some work has been done on the spatial distribution of the different emission lines (Section 4.4.4.4).

4.4.3.2 Line fitting

In order to derive the most accurate line fluxes the Emission Line Fitting (ELF) suite within DIPSO was employed. This package allows magnificent flexibility within the fitting procedure; for example, to fit the [OII] $\lambda\lambda$ 3726,3729 line pair it may be specified that the FWHM are equal, and that there is a separation of 2.79$\AA$ whilst leaving the exact wavelengths, line strengths and value of FWHM as free parameters. However in this case the FWHM was specified from measurement of the Hβ line to reduce the number of free parameters and thus errors. The final fit is shown in Figure 4.14.

A full breakdown of all lines measured and their derived parameters is presented in Table 4.5. The velocities are derived from the shift relative to laboratory rest wavelengths, and further corrected to a heliocentric reference frame using the STARLINK program RV. The positive values refer to a movement away from the observer,

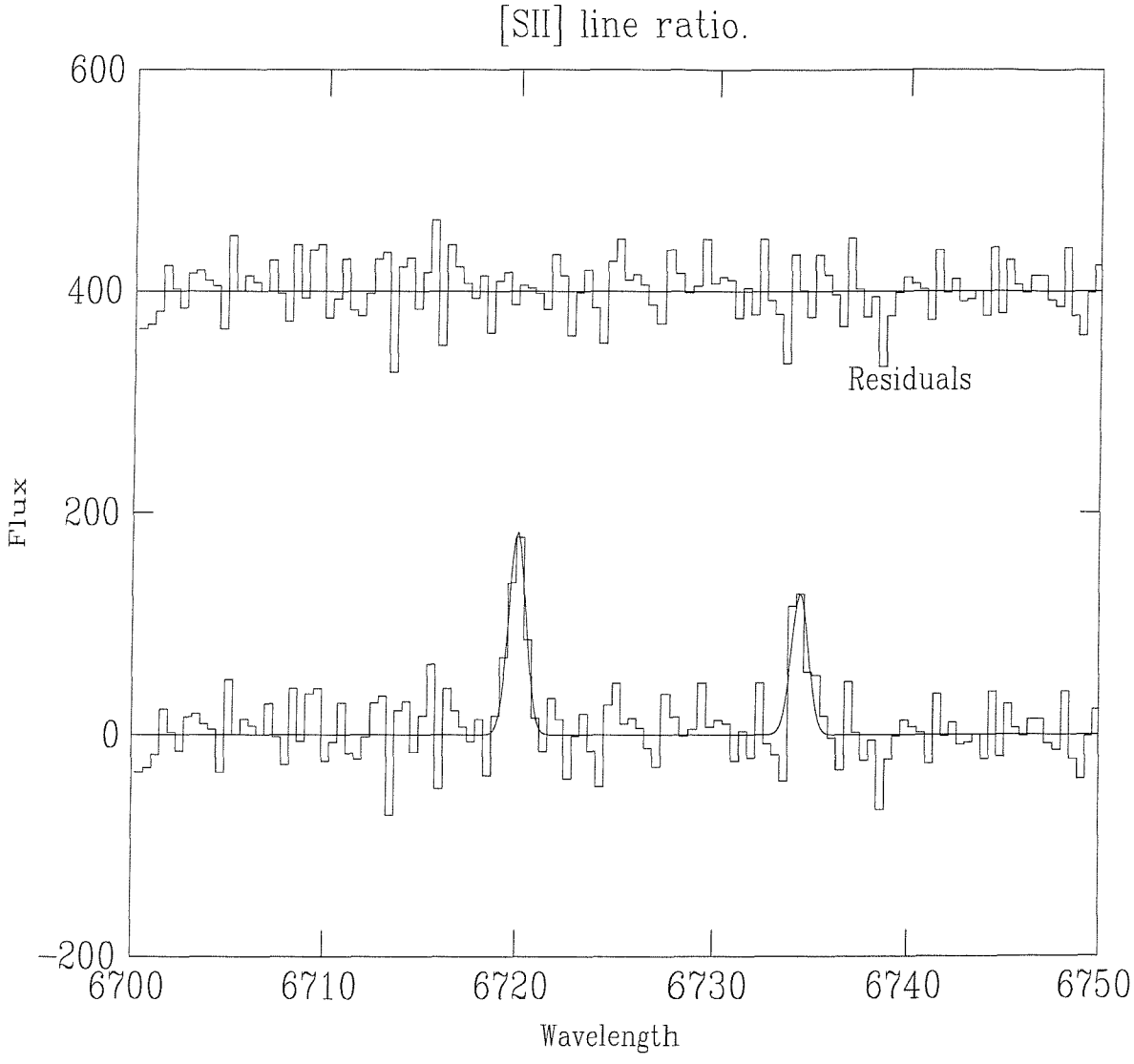

Figure 4.13: Gaussian fit to the [SII] $\lambda\lambda$ 6716,6731 lines seen in the nebulosity around XTE J0111.2–7317.

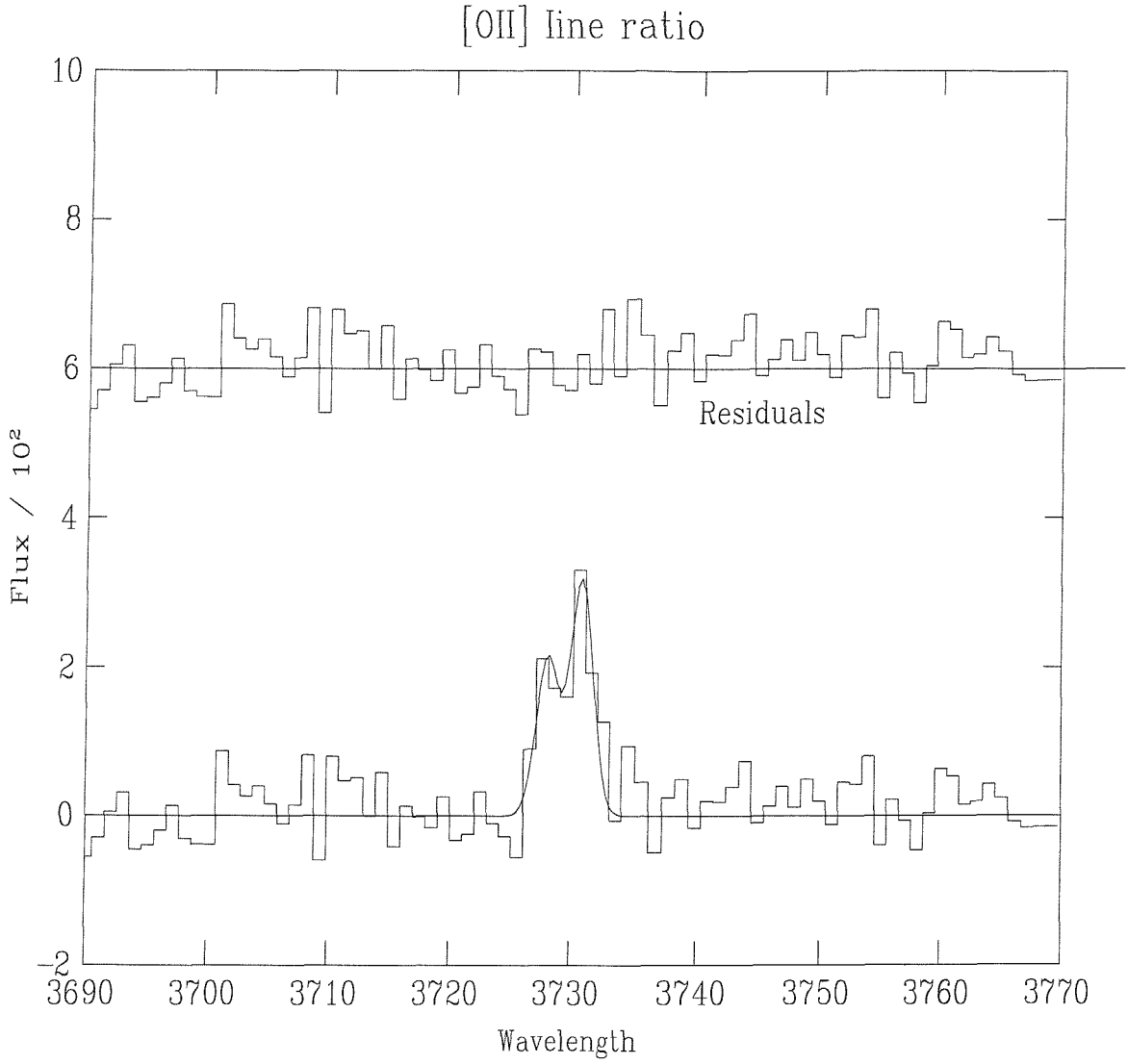

Figure 4.14: Gaussian fit to the [OII] $\lambda\lambda$ 3727,3729 lines seen in the nebulosity around XTE J0111.2–7317.

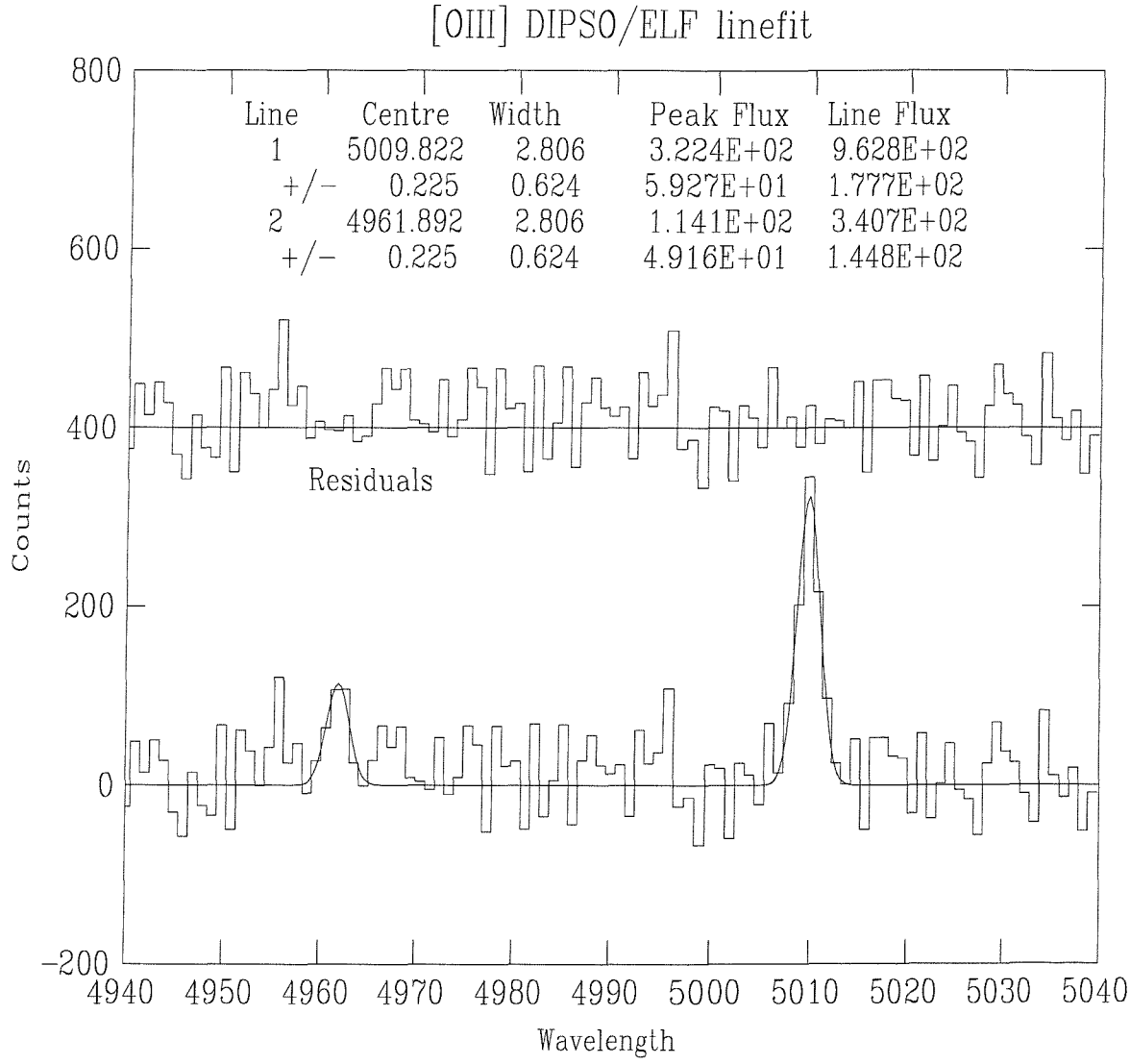

Figure 4.15: Gaussian fit to the [OIII] $\lambda\lambda$ 4959,5007 lines seen in the nebulosity around XTE J0111.2–7317.

i.e. a redshift.

4.4.3.3 Line flux calibration

The presence of the stellar continuum alongside the nebular spectrum allows an absolute flux calibration to be performed. Such calibration is important for establishing reliable line ratios for diagnostic techniques.

The reddened theoretical Kurucz model photospheric spectrum (Kurucz, 1979) fitted in Section 4.3.1.1 was further reddened to allow, crudely but effectively, for the circumstellar reddening. This was normalized using the photometry at B and R for the blue and red spectra respectively. The extracted stellar spectrum was divided into this and fitted with a polynomial yielding the required scaling factor at each wavelength to convert from counts (the units of the line fitting) to $erg/cm^2/s/\AA$. Clearly this calibration technique is dependent upon the Kurucz atmosphere being an accurate model of the true stellar spectrum; possible reasons why this may not be the case are discussed below. Note however that only the shape of the spectrum within each spectral range is important; the normalization, which is performed using photometry approximately in the centre of each range, ensures that the flux density is correct at this point and thus near the mark over the entire spectral range.

A source of uncertainty is implicit in the assumption that the spectrograph slit transmits all of the light, and that guiding errors or other causes do not cause significant losses. Such errors do not reduce the transmission of the nebular spectrum as it is larger than the slit size, and so will cause overestimation of nebular line strengths. Line ratios remain unaffected.

4.4.4 Spectral results

4.4.4.1 Temperature.

The O line strengths (4.4.5.4) constrain the nebular electron temperature to below 25-40,000; in fact standard nebular theory provides a mechanism to maintain the temperature in the range $5 - 10 \times 10^3$. Collisions of high energy electrons with ionised O, Ne, S and Fe excite these ions into the metastable states which subsequently decay by photon emission thereby ridding the nebula of this energy. This mechanism can be seen to be at work from the high intensity of O and S forbidden lines. This effectively limits the electron temperature to 10000K with a mean value of 6700K (Kitchin, 1987). The consistency with which this mechanism has been seen to provide a 'thermostat' controling the temperature of nebulae provides encouragement that it also applies in this case.

4.4.4.2 Nebular Density.

[OII] and [SII] both emit close pairs of optical lines whose ratios are diagnostic of N_e, the electron density (Saraph and Seaton, 1970). Using ratios of lines produced by the same species are especially appealing as uncertainties based on abundance, degree of ionization and the many other variables cancel out. This diagnostic tool is based upon the increasing effect of collisional de-excitation in preventing the emission of a photon by an excited ion in a metastable state, as one considers progressively higher densities. In the low densities encountered in nebulae, collisions of electrons with ions produce very large populations in such long lived states.

$$R = \frac{I(\lambda 6716)}{I(\lambda 6731)} \; or \; \frac{I(\lambda 3729)}{I(\lambda 3726)} \tag{4.1}$$

In a population of S^+ (for example) in the low density limit $N_e \rightarrow 0$, every

excitation into either the $^2D_{5/2}$ or $^2D_{3/2}$ states will eventually decay producing either a λ6716 or λ6731 photon respectively. Thus the relative fluxes of these lines are proportional to the rates at which the corresponding excited upper states are created, which is in the ratio 3/2 for not only the [SII] lines but also [OII] and several other ions (Osterbrock, 1989, p. 132).

$$N_e \rightarrow 0, R = \frac{N_{^2D_{5/2}}}{N_{^2D_{3/2}}} = \frac{3}{2} = 1.5 \tag{4.2}$$

However, at higher densities collisional de-excitations tend to occur before the majority of excited ions can radiatively decay. Thus the velocity of the ions is important, and the measured property is actually $N_e/T_e^{1/2}$; most work assumes a canonical nebular temperature of 10^4K, in agreement with available data for this object. Thus in the $N_e \rightarrow \infty$ case the line fluxes are determined by an additional factor of the ratio of transitional probabilities $A(\rightarrow^4 S)$, or the reciprocal of the ratio of the upper states mean lifetime τ.

$$N_e \rightarrow \infty \ , \ R = \frac{N_{^2D_{5/2}}}{N_{^2D_{3/2}}} \frac{A_{\lambda 6716}}{A_{\lambda 6731}} = \frac{3}{2} \frac{2.6 \times 10^{-4}}{8.8 \times 10^{-4}} = 0.44 \tag{4.3}$$

In the approximate neighbourhood of the critical densities from $10^2 - 10^4 cm^{-3}$ accurate densities may be derived (Figure 4.16), but outside of this range the results are indistuinguishable from either 0 or ∞ on each side of the critical density. The results in Table 4.6 (derived from line fits shown in Figures 4.13 and 4.14) merely place an upper limit of $N_e \leq 200 cm^{-3}$.

4.4.4.3 Line velocities.

The heliocentric velocities of the nebular lines are all consistent with a systemic SMC velocity of 166 km s^{-1}, excepting the [OII] $\lambda\lambda$ 3726,3729Å. However, these lines lie

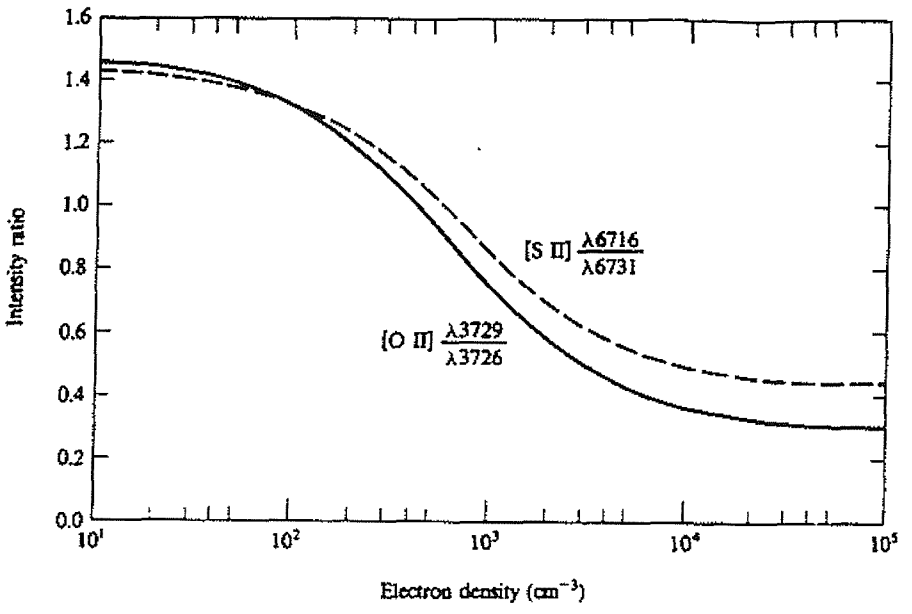

Figure 4.16: Intensity ratios of [OII] and [SII] pairs as a function of ISM density N_e.

at the extreme end of the spectral range where the wavelength calibration is less accurate, so this is not believed to represent a real velocity shift.

The FWHMa are all consistent with instrumental broadening, with values comparable those of the calibration arc lines. The resolution of the blue spectrum is such that structure with a velocity dispersion of up to $\sim 100\,\mathrm{km\,s^{-1}}$could lie unresolved, whereas the red spectrum limits such structure to $\sim 30\,\mathrm{km\,s^{-1}}$. This result argues strongly against a SNR hypothesis for the nebulosity; even 'old' SNR display expansion velocity dispersions of several hundred $\mathrm{km\,s^{-1}}$(Lozinskaia, 1980).

4.4.4.4 Spatial distribution of nebular lines.

The full known extent of the nebulosity is defined by the narrowband Hα image seen in Figure 4.10. Whether this represents the true distribution of material in the structure or is more a reflection of the state of ionization can best be inferred by looking at the distribution of emission from different atoms and ionization states.

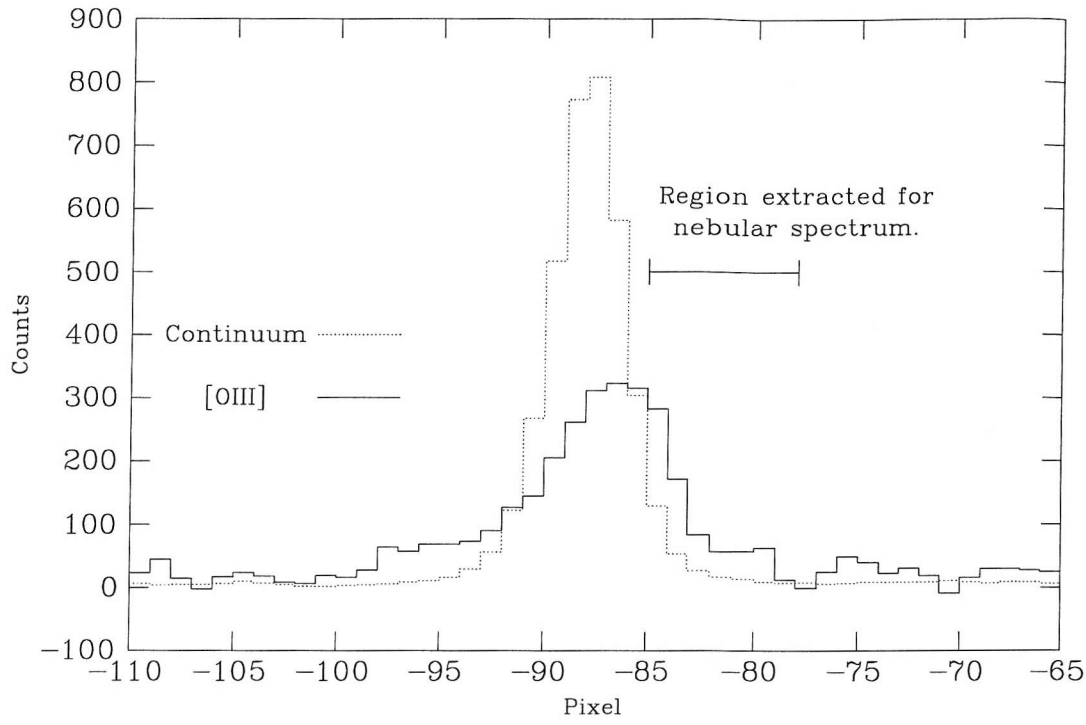

Figure 4.17: Cross section through the full width of [OIII] 5007 emission line. The stellar contribution has been subtracted, and is shown, multiplied by a factor of 0.5, for reference. Profiles have been Gaussian smoothed with $\sigma = 0.7$.

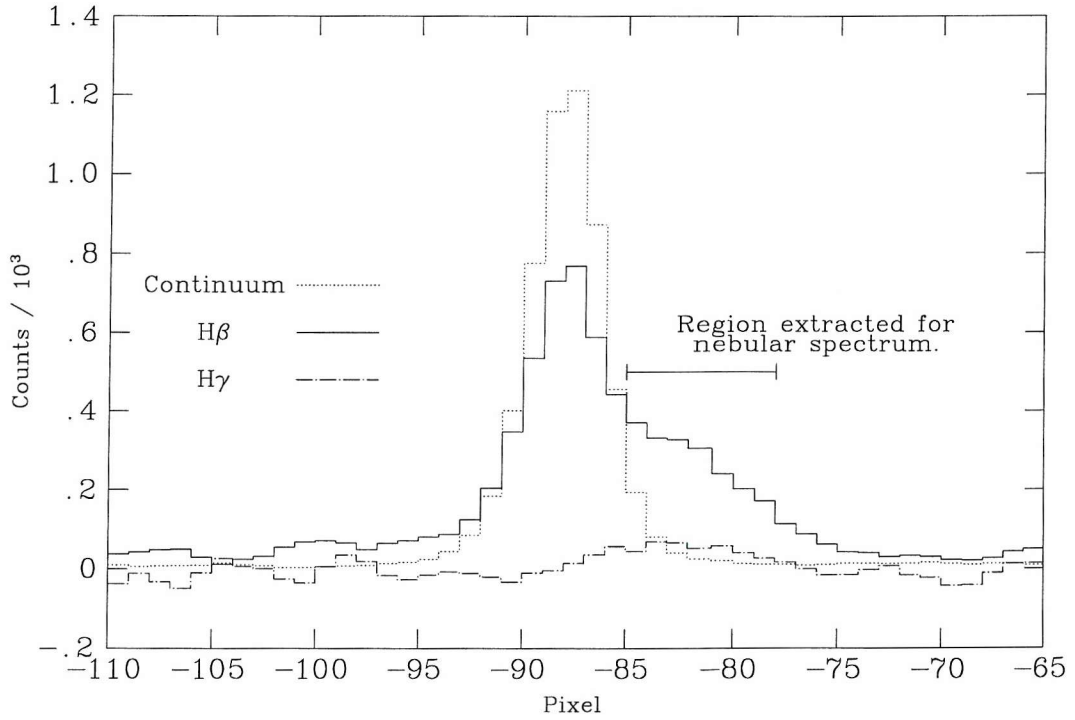

Figure 4.18: Cross sections through the full widths of the Hβ and Hγ emission lines. The photospheric, but not circumstellar disc, contribution has been subtracted, and is shown (multiplied by a factor of 0.75) for reference. Profiles have been Gaussian smoothed with $\sigma = 0.7$.

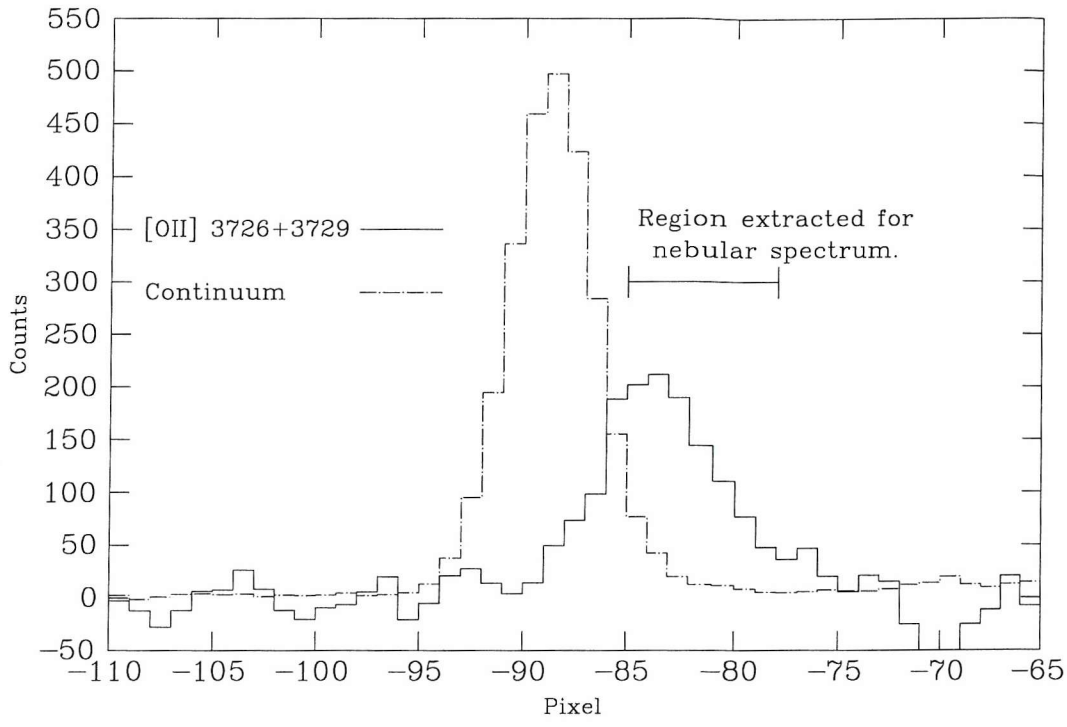

Figure 4.19: Cross sections through the full widths of the [OII] 3726,3729 emission lines. The stellar contribution has been subtracted, and is shown for reference. Profiles have been Gaussian smoothed with $\sigma = 0.7$.

Figures 4.17 to 4.21 show cross-sections along the spatial axis of the spectral images, taken through the mid-point of the detected emission lines with an appropriate width of pixels sampled (mostly 3) depending upon the FWHM. These plots thus show the spatial distribution of emission from each emission line; with the caveat that the central Be star produces a peak at it's spatial location. This arises from both photospheric emission and from the circumstellar disc. An attempt has been made to subtract the stellar contribution by subtracting an extracted profile derived by interpolation of the continua adjacent to each spectral line, in a manner analogous to sky subtraction in conventional spectral reduction. This was relatively successful for those lines which have no photospheric or circumstellar counterpart:[SII], [O II] and [OIII], though [O II] was affected by the rapid non-linearly declining response of the CCD at short wavelengths.

In the case of the Balmer lines the combined spatial profile from the photosphere and circumstellar disc has the same FWHM in the spatial direction as the contin-

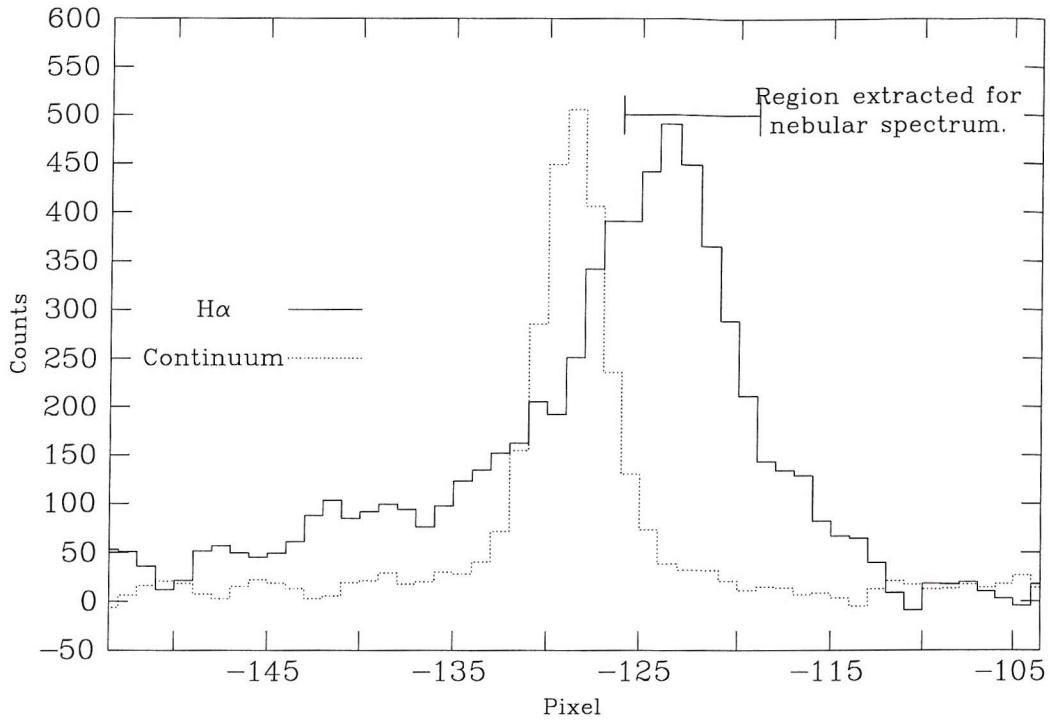

Figure 4.20: Cross section through the full width of the Hα emission line. The stellar and circumstellar contribution has been subtracted, and is shown for reference. Profiles have been Gaussian smoothed with $\sigma = 0.7$.

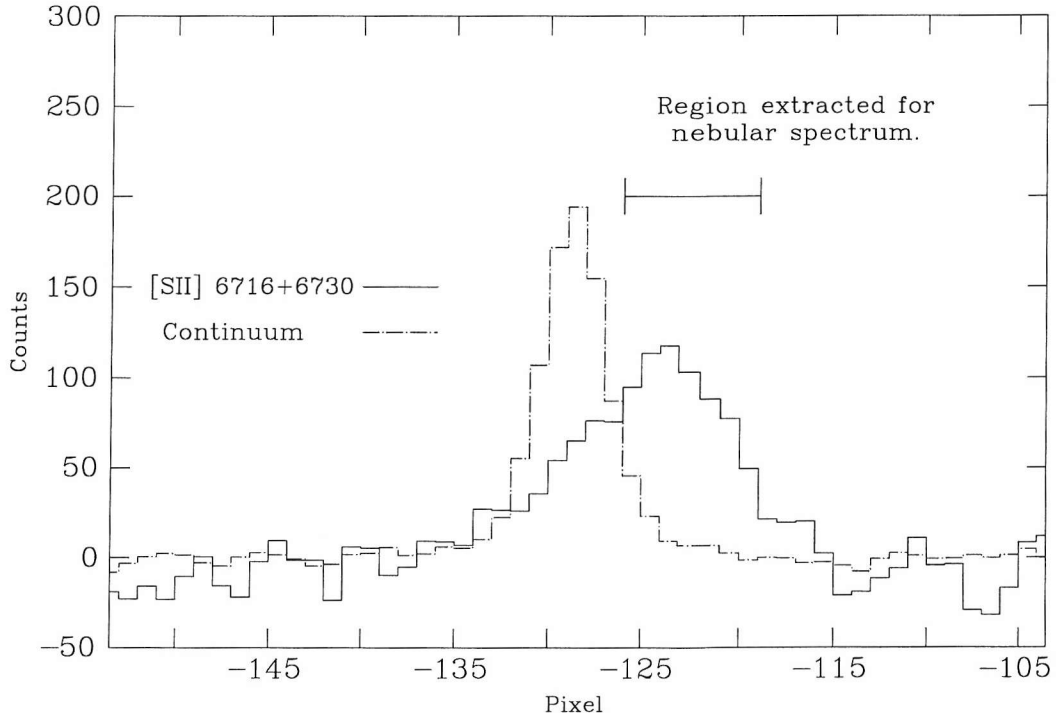

Figure 4.21: Summed cross section through the full widths of the [SII] emission lines. The stellar contribution has been subtracted, and is shown for reference. Profiles have been Gaussian smoothed with $\sigma = 0.7$.

uum, but must be scaled to account for the circumstellar emission. Photospheric and circumstellar contribution to the Hα profile was calculated from the peak intensity of the broad circumstellar Hα component seen in Figure 4.5. This was not possible for Hβ and Hγ due to the lower spectral resolution and weaker circumstellar emission, thus leaving artifacts at the stellar location in the profiles of Hβ and Hγ. Hβ shows emission at the stellar location, whilst Hγ shows very weak (photospheric) absorption.

ESO blue spectrum - [OIII], [OII], Hβ and Hγ The orientation of the slit for these data is through the star and the brightest part of the nebulosity - NW to SE, thus in the context of the bowshock scenario it is usefully aligned along the direction of the standoff distance l.

The [OIII] line was expected as it is observed to be amongst the strongest lines in many nebulae, including other bowshock nebulae (see Figure 4.25), HII regions and PNe.

Narrow band imaging of the field has not produced a detection at [OIII] $\lambda\lambda$ 4959,5007 (Figure 4.12) and in the spectral data it is detected only weakly from the nebular regions brightest in Hβ (compare Figures 4.17 and 4.18). It is however observed as a strong feature from regions much closer to the star itself, to the extent that extraction of the stellar spectrum shows strong features at the aforementioned wavelengths (Figure 4.7), whereas extraction of the neighbouring nebular spectrum detects them only very weakly. This can be understood with reference to Figures 4.17 and 4.18, which show spatial profiles of the Hβ, Hγ and [OIII] emission lines along the spatial axis.

Whilst [OIII] emission peaks close to the stellar location and rapidly drops off, Hβ is observed to considerably larger distances. The [OIII] emission profile is much more symmetric around the Be star, with only minor enhancement in the direction of strongest Balmer emission. Additionally [OIII] is seen from the NW side of the

Be star where there is negligible Balmer emission. Where Hβ and Hγ are brightest there is scarcely any [OIII] emission at all.

Hβ, Hγ and [OII] emission (Figures 4.18 and 4.19) appear to be coincident, though few conclusions can be drawn from the weak Hγ detection. All are seen only to the SE side of the Be star, in a manner totally consistent with the distribution seen from the Hα image in Figure 4.10. Detection from pixels 75.5 to 92.5 implies an angular diameter of 13.9″, or 4.3 pc.

SAAO red spectrum - Hα and [SII] Figure 4.20 shows the distribution of nebular Hα emission. Whilst the exact slit orientation of this observation is not known, the size of the nebulosity appears to be the same as that of Hβ and Hγ, with detection out to slightly larger radii because of the much stronger signal. [SII] appears to trace the Hα exactly.

4.4.5 Nebular classification.

If a spectral classification of B0.5-B1 (Coe et al., 2000; Covino et al., 2001) is accepted, along with the nebular density of $N_e = 10 \rightarrow 200cm^{-3}$ (Section 4.4.4.2), it becomes possible to calculate the Strömgren radius within which a uniform cloud of H is completely photoionized (note this does not apply to the hollow bowshock model) and would be expected to emit Hα. This radius is sensitive to spectral class around B0, in that this classification sensitively determines the Lyman continuum flux Q_0 depending upon the details of the stellar model used. Whilst the statement that 'a B1 star emits only 0.5% the Lyman continuum flux of a B0' (Kitchin, 1987) has been shown to be an exaggeration (Martins et al., 2002), Figure 8 of VGS96 shows a decline in Q_0 by a factor of ~ 10 as one passes from B0 to B1. Vacca et al. 1996 tabulate Q_0 for O3-B0.5V stars, so though one must perform an extrapolation to yield a result for B1, the function is a smooth one and so the result expected to

be accurate.

Incorporating Martins et al. downward revision by 40% of Vacca et al.'s Q_0 one arrives at 4.8×10^{47} at B0.5V and 2.4×10^{47} at B1V. Suitably modifying the derivation of equation 6A.1.10 (Kitchin, 1987), we arrive at the formula

$$R_S = \left(\frac{3Q_0}{4\pi N_e^2 \times 6.5 \times 10^{-15} T_e^{-0.85}} \right)^{\frac{1}{3}} (metres) \tag{4.4}$$

Using the observed nebular radius of 3.05pc requires $N_e = 7.6 cm^{-3}$ at B0.5 or only $N_e = 5.1 cm^{-3}$ at B1V, at the lower end of observed nebular densities, and in agreement with the results of Section 4.4.4.2 using forbidden line ratios. The use of SMC metallicities, reducing line blanketting effects, raises Q_0 and thus requires slightly higher densities, but this effect is only of the order of a few %.

This suggests the scenario that the nebulosity is simply an HII region, perhaps part of a cloud adjacent to and ionized by XTE J0111.2–7317. If so, and considering the fact that the calculated densities are very much at the lower end of the range for HII regions, why is this structure detectable at all? Most OB stars rid their neighbourhood of gas early in their existence via powerful winds. The answer may lie in the fact that as a BeXRB, XTE J0111.2–7317 has a large space motion (van den Heuvel et al., 2000) and has impinged upon a cloud which it has subsequently ionized. If this cloud increases in density towards the south-east (lower left in the images), the slightly smaller radius in this direction can be explained with the Strömgren sphere argument ($R_S = fn(N_H)$), or as an ionization front propogating into the cloud.

4.4.5.1 The bowshock theory

Stellar bow-shocks (Figure 1.11) form from the ram-pressure interaction of the local interstellar medium with the stellar wind; when the star's velocity exceeds the

[OII] 3729:3726	1.48 ± 0.27
[SII] 6716:6731	1.40 ± 0.31
[SII]:Hα	0.286 ± 0.031
Hβ:[OIII]	1.69 ± 0.32

Table 4.6: Diagnostic line ratios from nebulosity around XTE J0111.2–7317.

sound velocity in the ISM material is swept up into a shock front which is detected primarily using one of two techniques: narrowband imaging (mostly Hα) and IR imaging, mostly using IRAS data. Whereas Hα imaging takes advantage of excited H, the IRAS flux (usually most pronounced in the 60μm band) arises from thermal radiation from swept-up dust originating from the star, heated by shock interactions.

The appearance of a bowshock is clearly heavily dependant upon the angle that the star's velocity vector makes with respect to the plane of the sky. Classic parabolic structures such as Vela X-1 and α Cam (Figure 4.22) are seen when the star's motion lies almost entirely within this plane. Less clearly defined structures are more commonly seen, though enhanced brightness on one side, such as is observed in XTE J0111.2–7317, is usually apparent (Noriega-Crespo et al., 1997b).

Thus the morphology of a bowshock is such that the head or apex of the structure is well defined if viewed side-on, enabling a 'standoff distance' l to be determined; there is no sharply defined trailing edge. The size of the structure is thus easily characterised only for side-on specimens, though many less ideally oriented examples have been found (Noriega-Crespo et al., 1997b). In the case of XTE J0111.2–7317, the standoff distance is approximately 3pc (see Section 4.4.4.4),

Comparing the 60μm IRAS image of the α Cam bowshock in Figure 4.22 with the XTE J0111.2–7317 nebula (Figure 4.10) reveals an extremely similar appearance. Both nebulae lie within an approximately parabolic perimeter, and though α Cam itself is not visible in the IRAS image, both stars lie slightly inside the radius of curvature of the nebulosity, agreeing with the theoretical radius of curvature for a

Object	Spectral class	Standoff dist.(pc)	Space vel.($\mathrm{km\,s^{-1}}$)
XTE J0111.2–7317	$B0Ve$[1]	3.0	
Vela X-1	$B0.5Ibe$[2]	0.48	$\sim 50\,\mathrm{km\,s^{-1}}$[8]
α Cam	$O9.5Iae$[3]	5.1[6]	48[7]
0623+71	$CataclysmicVar.$[4]	0.08	$\sim 100\,\mathrm{km\,s^{-1}}$
Betelgeuse	$M2Iab$[5]	0.8	56

Table 4.7: Sizes of some stellar bowshocks and spectral classification of their associated stars. Sources 1:This work, 2:Kaper et al. (1997), 3:Noriega-Crespo et al. (1997), 4:Hollis et al. (1992), 5:Noriega-Crespo et al. (1997), 6:van Buren and McCray (1988), 7:Stone (1979), 8:Comeron et al. (1998)

stellar wind bowshock of $(5/3)l$.

Without doubt a measured space velocity for XTE J0111.2–7317 would be strong evidence one way or the other, but at the distance of the SMC proper motions are beyond the limit of current technology. The radial velocity has been investigated by cross correlating the blue ESO spectrum with that of a velocity standard, but errors of $50\,\mathrm{km\,s^{-1}}$and a result consistent with zero were sufficiently large to preclude any conclusions being drawn, probably because of the low S/N of the spectrum. Studies of specific lines would seem to suggest a limit on v_r of less than $10\,\mathrm{km\,s^{-1}}$(after allowing for the SMC systemic component). The bowshock appears however to be nearly edge on, in which case most of the stellar velocity is oriented in the plane of the sky and a modest or zero v_r would be expected.

Comeron et al. (1998) have performed numerical simulations of bowshocks in a number of cases. One of their findings is that in low velocity cases ($v_* \ll 100\,\mathrm{km\,s^{-1}}$), of which XTE J0111.2–7317 is an example as a BeXRB, the bowshock becomes much thicker as the assumption of instantaneous cooling, implicit in the above equation, fails. The resulting thick layer of hot gas, bounded on one side by the stellar wind, and on the other by the ISM, certainly can explain the broader appearance of XTE J0111.2–7317's nebula compared to that of Vela X-1.

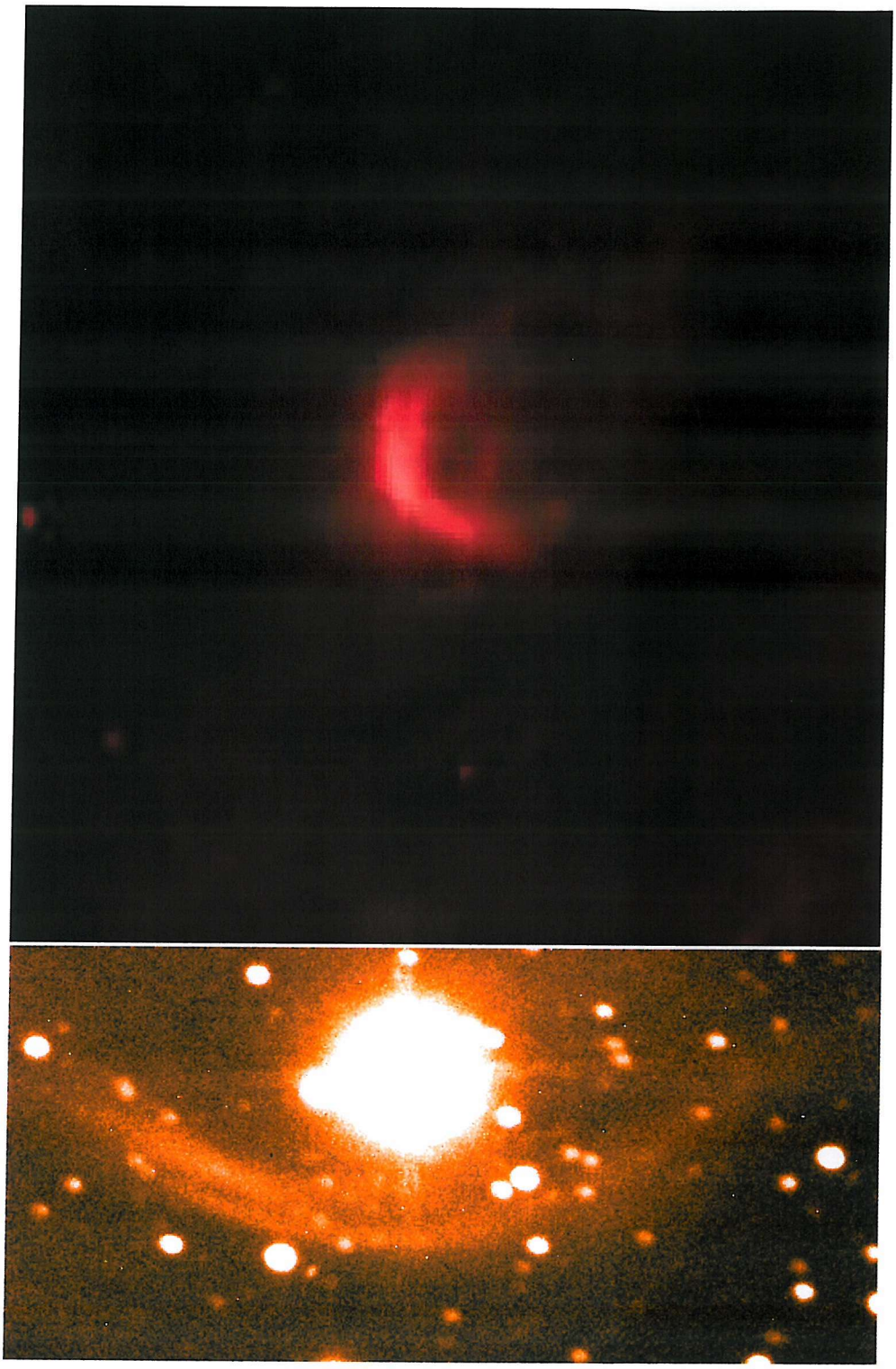

Figure 4.22: Top: 60μm IRAS image of α Cam showing classic bowshock morphology. α Cam itself is not visible, but lies just inside the apex of the shock. Bottom: Hα image of Vela X-1 and it's associated bowshock. Image 5' across.

A second consequence is that peak density occurs at $1.5-2l$, somewhat away than the balance point l predicted by simple momentum balance. Rearranging equation 16 of Raga et al. (1997) to incorporate metallicity dependances (Vink et al., 2001) of $\dot{M}$ and v_W gives the following equation balancing the ram pressure of the ISM with that of the expanding stellar wind at the standoff point, a distance l from the star.

$$N_{ISM} = \frac{\dot{M}_{Z=1} Z^{0.82} v_W}{4\pi l^2 m_H v_*^2} \tag{4.5}$$

Using a solar metallicity mass loss rate of $3 \times 10^{-8} M\odot yr^{-1}$ (Vink et al., 2000), a wind velocity of $1000\,\mathrm{km\,s^{-1}}$, the assumption of a pure hydrogen ISM, system velocity $V_w = 15\,\mathrm{km\,s^{-1}}$ (mean BeXRB velocity), and $l = 3.0pc/(1.5-2)$ requires an ISM density of $0.02 - 0.034cm^{-3}$. This value is low for any ISM, particularly in a gas rich galaxy like the ISM where densities of less than $0.1cm^{-3}$ are uncommon. The assumption of an unusually high wind speed and/or mass loss rate can reconcile this situation, but both seem somewhat unlikely.

Though this is clearly some way from an exact method of calculating the ISM density, it seems safe to conclude that it must be low if we believe the bowshock interpretation. We are therefore led to questioning why this is the only one known around a BeXRB. The requirement of supersonic velocity may be the reason; the typical ISM sound speed of $v_S \alpha N^{1/2} \sim 10\,\mathrm{km\,s^{-1}}$ is only slightly below the mean BeXRB velocity of $15\,\mathrm{km\,s^{-1}}$(van den Heuvel et al., 2000), so perversely it could be only the BeXRB systems travelling through relatively tenuous regions that are capable of producing bowshocks. This is discussed further in Section 4.4.5.5.

The argument in Section 4.4.5 concerning the Strömgren radius around the B star does not apply to such thin shells. Equation 21 of Comeron and Kaper (1998) considers the flow of material into the bowshock to find the required ionizing flux - using the values given above, the flux necessary to fully ionize the material in the

shock front is only $4 \times 10^{42} sec^{-1}$, which is several orders of magnitude less than a B0.5-B1 star provides. Thus we expect to see Hα emission from the bowshock.

Whilst the [SII]:Hα ratio of 0.286 is below the threshold of 0.4 usually accepted as clear evidence of shock excitation, it is significantly above the typical values for photoionized nebulae which mostly lie below 0.2. This suggests the possibility that a combination of photoionization and shock excitation may be at work.

4.4.5.2 Comparison with other bowshock spectra

The discovery and study of bow-shocks around high velocity stars is a relatively new facet of astronomy, with the vast majority of papers on the subject having been published in the last 10 years. Perhaps as a consequence of this, few published spectra exist; spectra of only two other stellar wind bowshocks have been found in the literature. Figure 4.25 shows that of Vela X-1 (Kaper et al., 1997), a super-giant HMXRB system, and also the bowshock of 0623+71 (Hollis et al., 1992), a CV system. Both sources show strong Balmer emission as well as [OIII] and [SII] lines, in common with XTE J0111.2–7317. Additionally the 0623+71 spectra show strong [OII] lines much like XTE J0111.2–7317. The only significant difference is the absence of [NII] lines in the XTE J0111.2–7317 spectra, though the Vela X-1 spectra show them so weakly that if present in XTE J0111.2–7317 at a similar level they would not have been detected. Thus the Vela X-1 nebular spectrum is not significantly different to that of XTE J0111.2–7317, strengthening the bowshock hypothesis.

Essentially the XTE J0111.2–7317 nebular spectra are qualitatively similar to both of the bowshock spectra shown, in particular that of Vela X-1. This is to be expected as the XTE J0111.2–7317 system far more closely resembles Vela X-1 than 0623+71.

Two possible explanations for the differences between these bowshock spectra

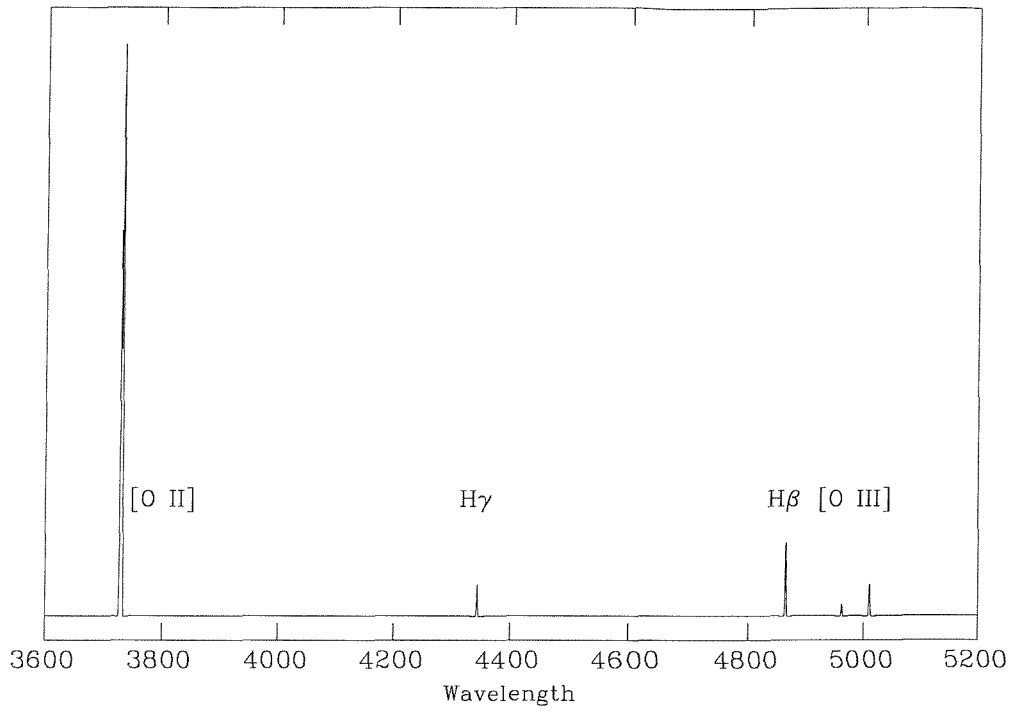

Figure 4.23: Synthesised spectrum of the XTE J0111.2–7317 nebula. Created from fits to all detected lines in the blue ESO spectrum.

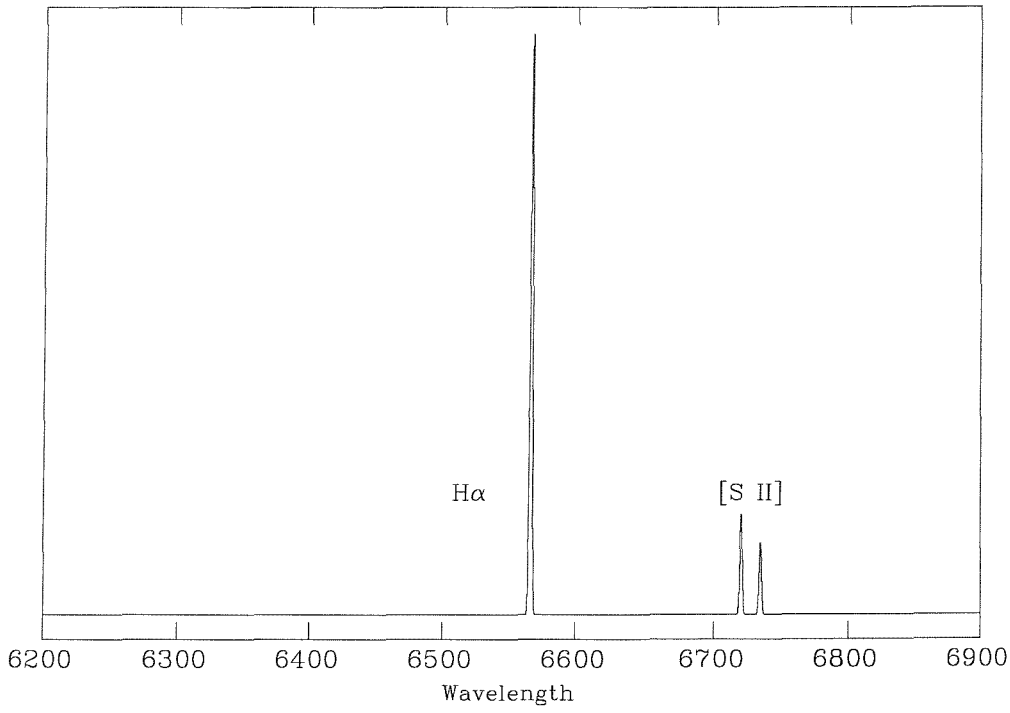

Figure 4.24: Synthesised spectrum of the XTE J0111.2–7317 nebula. Created from fits to all detected lines in the red SAAO spectrum.

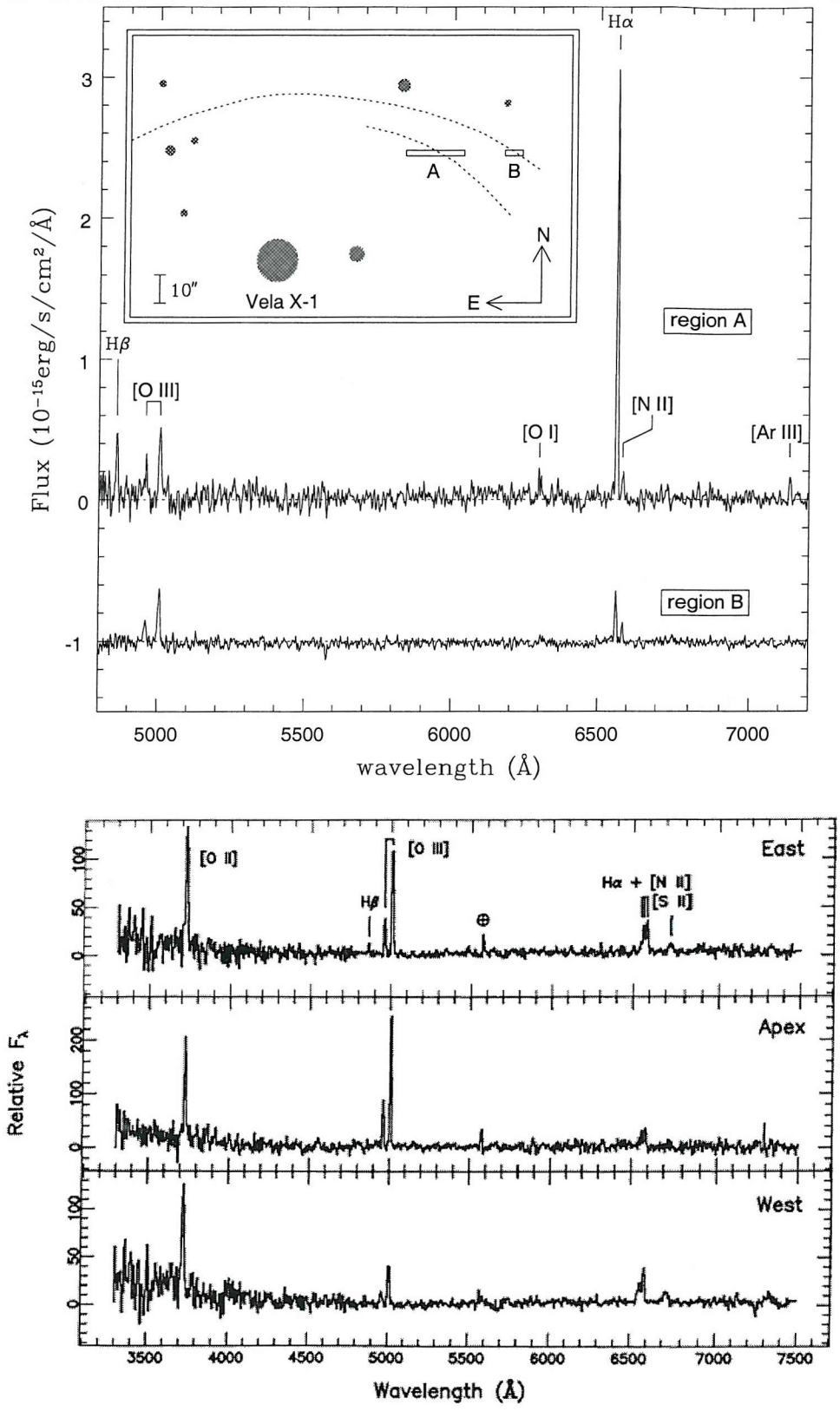

Figure 4.25: Top: Spectra of the Vela X-1 bowshock. Figure 2 from Kaper et al. 1997.Bottom: Spectra at 3 slit positions of the bow-shock around the cataclysmic variable 0623+71, from Hollis et al. 1992

have been found. Firstly, the WDs in CV systems produce much more extreme UV flux than B giants due to their high temperatures, so the balance of ionization is expected to be markedly different. In an ionization front such as the head of a bowshock, the electron temperature can be elevated greatly if the ionizing photons have energies greatly in excess of the required critical value; the excess of energy carried by the photon manifests itself as kinetic energy of the resultant ion/electron pair. This energy is dissipated chiefly by line radiation after collisions with the predominantly neutral or singly ionized species present in the front. Thus WD (as opposed to OB) ionized systems are expected to have greatly strengthened [NII]$\lambda\lambda$ 6548,6583 and [OII]$\lambda\lambda$ 3727,3729 lines (Kitchin, 1987, p.180), as observed in this case.

A second explanation uses the line ratios. As discussed in Section 4.4.5.4, the [SII]:Hα line ratio is a useful diagnostic of shock excitation. Hollis et al. find a ratio of ~ 0.7, well above the usual range encountered in photoionized nebulae, and an almost certain indicator of strong shock ionization. In a similar manner to the mechanism that strengthens [SII] in SNR, this could strengthen the lines of neutral and singly ionized species, as observed.

The presence of [OIII] far from the presumed shock interaction suggests photoionization as the mechanism for it's excitation rather than shock proceses; Noriega-Crespo and Garnavich (1992), in their studies of bowshocks of Herbig-Haro objects, confirm earlier findings (Dopita et al., 1984) that shock velocities of $80\,\mathrm{km\,s^{-1}}$are required to provide sufficient excitation to produce [OIII] $\lambda\lambda$ 4959,5007, and spectra do not reveal such velocities to be present. Bowshock theory also does not predict this order of velocity (see Section 1.6.1).

4.4.5.3 The HII region hypothesis.

A high [OIII]:Hβ ratio is a diagnostic of photoionization from the Be star's UV flux, comparable to the strong [OIII] lines seen in planetary nebulae caused by the white dwarf's UV flux.

Ths observation of a small [OIII] nebula coincident with the central star raises a possible problem for the bowshock theory. If this material truly lies within the larger Hα nebula, it would appear to argue against the bowshock theory, as the interior of it's paraboloidal shell is considered to be empty, excepting the expanding rarified stellar wind. The simulation work of Comeron et al. (1998) allows for some material to pervade this region, but probably not as close to the star as we observe. Therefore in this scenario the [OIII] emission must lie on the surface of this shell. In the 0623+71 shock structure, Hollis et al. point out that the distribution of [OIII] does not correlate well with Hα, but still arises from the bowshock structure. However, in 0623+71, [OIII] emission is patchy, and is undoubtedly associated with the shell. In the case of XTE J0111.2–7317 however, the chances of one patch of emission lying so well centred on our line of sight to the star seem remote - the best explanation for this must be that the [OIII] emission arises physically within the bounds of the Hα nebula, particularly as a Strömgren sphere argument (below) can account for the relative sizes and locations of these features in this scenario.

Section 4.4.4.4 shows that the HII, [SII] and [OII] nebulae are approximately coincident. Whereas this flows naturally from a bowshock theory (one is simply measuring the standoff distance l), it can also be understood in terms of Strömgren spheres. The abundance of elements heavier than He is sufficiently small that their ionization removes negligible photons from the UV flux, so leaving the H Strömgren radius unaffected. The ionization potentials for H, S and O from their ground states are 13.6, 10.36 and 13.6eV respectively, thus the [SII] nebula should be slightly larger than the HII and [OII] nebulae, which should be identically sized, as S can be ionized by photons slightly less energetic than the 91nm limit of O and H, all

of which are absorbed within the H(and O) Strömgren sphere. Figures 4.20(Hα) and 4.21([SII]) leave this point unclear, but they are certainly of comparable radius, $\sim 3.2pc$.

Comparing Figures 4.19 ([OII]) and 4.18 (Hβ,Hγ) shows that, as predicted, these line strengths are observed to the same radius from the star, $\sim 3.0pc$. However, even if [OIII] emission is patchy over the bowshock shell, it should still have approximately the same size. But it does not - Figure 4.17 shows [OIII] emission from the star in pixels 87.5 to 81.5, or only 1.5pc at a scale of 0.82″/pixel. This is exactly what is expected for an OB star ionizing a surrounding uniform gas cloud; all of the few photons capable of ionizing OII to OIII ($h\nu > 35.1eV$) are absorbed within a small radius, thus leaving a more compact [OIII] nebula within the larger HII region.

In view of the abundance of nebulae within 30′of XTE J0111.2–7317, the association with a gas cloud does not cause any problems. SHASSA (Southern H-Alpha Sky Survey Atlas) (Gaustad et al., 2001) shows large HII regions close by and diffuse emission to be extremely pervasive.

The high space velocity which all BeXRB possess could simply have enabled the star to drift into an interstellar cloud and ionize it; it could not have been in this position long as the surrounding gas would have been blown away by the stellar wind. The mean space velocity of BeXRBs of $15\,\mathrm{km\,s^{-1}}$(van den Heuvel et al., 2000) corresponds to 1pc in 11,000 years.

4.4.5.4 SNR hypothesis

Obviously, the presence of the NS in a BeXRB requires there to have been a SN explosion at some stage in the system's evolution. Thus the discovery of a nebula surrounding the system naturally raises the possibility that this may be a SNR, thus enabling the age of the system in its BEXRB state to be reliably estimated and providing verification of the BeXRB formation mechanism. However, spectral

evidence shows that this is not the case.

Even a qualitative comparison of the nebular spectrum reveals that it is much more closely allied both to published bowshock (discussed further in Section 4.4.5.2) and HII region spectra than to a those of SNR. However, several quantitative properties argue powerfully against it being a SNR.

[SII]:Hα ratio This line ratio is a good distinguishing diagnostic between HII regions and SNRs, and is the standard diagnostic used for classifying nebulae in neighbouring galxies where morphology cannot be used (Blair and Long, 1997). With the exception of a handful of extremely low surface brightness HII regions similar to and including the diffuse interstellar gas, the vast majority of such objects have a [SII]:Hα ratio of less than 0.4, and usually below 0.2. This is due to a large fraction of the S being ionized to S^{++}, whereas shock-excited SNRs possess a broader range of ionization and thus greater population of S^{+} relative to S^{++}.

Figure 4.26 shows the position of the XTE J0111.2–7317 nebulosity on a diagnostic diagram showing HII regions and SNRs detected in the spiral galaxy NGC 300 (Blair and Long, 1997). This work was a search for SNR, and the candidate objects plotted all showed enough [SII] emission to merit closer inspection as candidate SNR; most HII regions possess [SII]:Hα ratios of less than 0.2 and were excluded at an early stage. Thus with a ratio of 0.286 XTE J0111.2–7317 lies at the upper end of the distribution of HII regions, suggesting the possibility of a shock heating component in addition to photoionization as the dominant mechanism.

[N II] The [N II] $\lambda\lambda$ 6548,6584 lines which bracket Hα are extremely strong in SNR, frequently rivalling Hα itself. In the case of XTE J0111.2–7317 however, these lines are not seen to a limit of $I_{H\alpha}/I_{[NII]} \geq 15$. Such a line ratio is not seen in SNRs and by itself argues very strongly against a SNR hypothesis, indeed the detection limit exceeds the observed line ratio in any PN, HII region or SNR spectrum encoun-

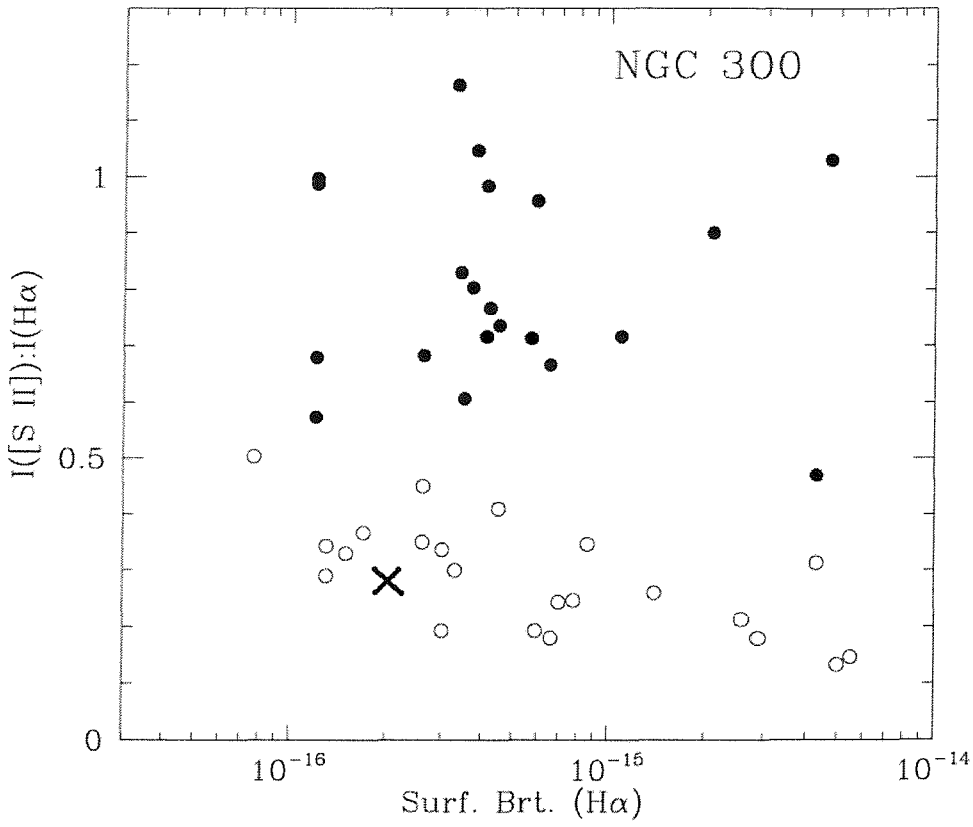

Figure 4.26: The position of the XTE J0111.2–7317 nebulosity on a [SII]:Hα vs. Hα surface brightness plot of SNR candidates in the nearby spiral galaxy NGC 300. Filled circles are SNRs, clear are HII regions. Adapted from Figure 14a, Blair and Long (1997).

tered in the literature. A possible explanation for this could be that the observed emission is from swept up SMC ISM which is of lower metallicity than the predominantly galactic objects studied in the literature; however this explanation would also affect the interpretation of the [SII]:Hα ratio amongst others, and indeed would still have trouble explaining such a profound lack of [NII] emission.

O lines Whilst the temperature sensitive line ratio [OIII] λ5007/[OII] λ3726 + λ3729 appears to be 0.12 from Table 4.5, implying a temperature in excess of 70,000K (Dopita, 1977, Fig. 7) this is strongly affected by the photoionized component at small distances from the star; no [OIII] emission is detected from the shock-front itself implying temperatures below those encountered in SNR. Similarly, whilst the [OIII] λ4363/λ5007 ratio is traditionally used to provide temperatures in SNR, upper limits to the λ4363 line (3×10^{-17}) combined with the [OIII] line strength can only suggest temperatures below 25-40,000K, in the realm more typical of planetary nebulae than SNR. The negligible presence of O^{++} at the shock location in itself betrays temperatures of below 40,000K (Dopita, 1977). Additionally the lack of [O I] $\lambda\lambda$ 6300,6364 places the system well away from the realm of SNR in the diagnostic diagrams of Fesen et al. (1985).

In addition, Section 4.4.4.3 reveals that any expansion velocity is very low, less than a few tens of $\mathrm{km\,s^{-1}}$, well below that expected in a SNR.

4.4.5.5 Search for similar systems.

Using the MERGE script (Section 4.4.1) a search was undertaken for other similar nebular structures associated with (mostly) MC BeXRBs, using SAAO 1.0m Hα and R band imaging data to produce deep Hα images in the same manner that Figure 4.10 was produced. Table 4.8 lists the systems examined in this way.

Much ambient nebulosity is visible in the images (Figure 4.8), but nothing asso-

SMC
AX J0043-737
AX J0049-732
AX J0049.4-7323
1E 0050.1-7247
RX J0051.9-7311
XTE J0052-723
RX J0052.1-7319
RX J0052.9-7158
AX J0058-72.0
AX J0105-722
LMC
RX J0512.6-6717
RX J0531.5-6518
RX J0535.0-6700
RX J0535.8-6530
A 0538-66
Other
Wack 2134
1SAX J1324.4-6200

Table 4.8: BeXRB systems examined for associated Hα nebulosity and bowshock candidates.

ciated with any of the counterpartss (or indeed, any other stars in the fields).

Considering from this point on only the MC sources, anything down to a scale of ~ 1 pc and Hα flux density $\sim 20\%$ of the XTE J0111.2–7317 nebula (which has almost exactly the same Hα surface brightness as the Vela X-1 bowshock) would have been detected. In view of the consistency of the surface brightness of these structures (see Section 4.4.3.1) and typical sizes (see Table 4.7) it seems probable that any other similar structures would have been found. Thus the frequency of such objects in our sample is 1 in 15, or 6.7%. This statistic is in exact agreement with the results of Huthoff and Kaper (2001) who searched for IR bowshocks around 15 *galactic* HMXRBs, and found none except for the well-known case of Vela X-1 (Kaper et al., 1997).

The most thorough search for galactic bowshocks around OB runaways is that of Van Buren et al. (1995), which used IRAS images to reveal bowshock like structures based upon morphology and excess 60μm emission. They found that 58 out of 188 of their target systems, selected by the criterion $v_space > 30\,\mathrm{km\,s^{-1}}$, displayed bowshocks. BeXRBs, whilst runaways, typically have lower velocities of the order of $15 \pm 6\,\mathrm{km\,s^{-1}}$ (van den Heuvel et al., 2000) and are thus less likely to be travelling supersonically. Where both Hα and IRAS data are available, such as for Vela X-1, the morphologies appear identical and are obvious in images. It is unclear however whether the presence of a bowshock in one band requires it's visibility in the other, so these two surveys may not be directly comparable. The effect described by Huthoff and Kaper (2001), whereby many OB runaways are travelling through hot, tenuous superbubbles associated with their OB associations and thus are subsonic despite their high velocities, may also apply to the SMC. The effect will be considerably stronger for BeXRBs with their modest velocities relative to OB runaways, due to the smaller distances travelled since formation. The detection of 0 or 1 bowshocks associated with an SMC BeXRB is thus in agreement with the above observations.

4.4.6 Summary.

The observed characteristics of the nebulosity surrounding XTE J0111.2–7317 have been examined in the context of three possible nebular types: SNR, bowshock and HII region. Of these, the SNR hypothesis is excluded by several line ratios and velocity dispersion. Such properties provide no discrimination between bowshocks and HII regions, but the spatial distribution of line emission from different species matches predictions for an HII region to a high degree, whilst providing only a poor match to the expectations for a bowshock. Overall these results provide good evidence that the nebulosity surrounding XTE J0111.2–7317 is nothing more than a conventional HII region.

The IR excess flux reported as evidence for possible B[e] attributes is explicable either as an instrumental error due to source faintness, or equally likely as IR emission from the nebulosity. Thus, while apparently unique, XTE J0111.2–7317 appears to be a normal SMC BeXRB embedded in a locally enhanced ISM which it has photoionised to create an HII region.

Chapter 5

Conclusions and further work

This work is divided into three Chapters, each of which deals with a *different* BeXRB system. The combination of these three into a single work thus provides a glimpse of the breadth of BeXRB observational research; firstly we have A0535+262, a relatively nearby system which has been intensively studied for 30 years (and longer as a B/Be star), and is therefore understood as well as any BeXRB in the sky. And in AX J0051–733 and XTE J0111.2–7317 we have two recently discovered systems, neither of which are known in great detail but both of which exhibit unusual traits which have been worthy of investigation here. The detail with which we have observed A0535+262 will probably never be afforded to AX J0051–733 or XTE J0111.2–7317, but the processes observed in this nearby system almost certainly inform us of processes occurring in the more distant systems.

Regarding the fundamental system properties of A0535+262, a new determination of E(B-V) has been made by combining an analysis of DIBs and using photometry at disc-loss, giving 0.70 ± 0.04. Furthermore an intrinsic colour of $(B-V)_0 = -0.30 \pm 0.04$, de-reddened $m_V = 7.29 \pm 0.12$ and distance of 2000-3000kpc are obtained. The error on this last result is misleading however, being due almost entirely to the still unknown luminosity class of the primary. This remains

probably the largest unknown regarding the basic system properties; contradictory evidence both for a giant and a dwarf classification has been obtained. Blue end spectra of A0535+262 obtained on 24/12/1998, immediately following the disc-loss, will be analysed to classify the star in the BCD system, using the characteristics of the Balmer discontinuity. At present analysis is hindered by residual emission and the complex continuum shape.

The system inclination is shown to be in the range $40 - 50°$ from comparison of $v \sin i$ with theoretical and empirical rotational velocities, observations of the fastest observed Keplerian orbital velocities, and knowledge of the orbital radius,period and velocity of disc material. Again, a luminosity class would constrain this quantity considerably more rigorously. All of these measurements are in agreement with previous work.

Evidence for fully optically thick emission in K has come through the constancy of (J-K), the quality of fit of m_K derived from the disc-size given by $\Delta V_{peak}(\mathrm{H}\alpha)$, and lack of variability compared with m_V. Regarding determination of disc size, ΔV_{peak} is found to be considerably less reliable than m_K. Just how much of this unreliability is due to noisy/low resolution spectra is unclear, but the value of monitoring these systems spectroscopically would be enhanced enormously by improving the S/N of these data, particularly as regards lines other than Hα; line profiles betray many of a BeXRBs most fascinating secrets. The observation of multiple ring-like enhancements within the circumstellar disc has expanded the number of systems in which these have been observed; it is beginning to look as though high resolution, high S/N He I spectra will show this phenomenon in any early Be star.

The disc-loss episode of 1998 and it's subsequent recovery provided a unique opportunity, regarding both the observation of interesting disc-related (in particular the reforming disc) behaviour and a chance to observe the underlying B star untainted by emission. The short period V/R cycles observed to follow disc-loss match theoretical predictions, and the linearly expanding disc that followed provided an

excellent measure of it's radial velocity. Some evidence supporting discrete mass ejections was also found.

In A0535+262 we have provided the first observational evidence for the variable resonant truncation of Be discs in BeXRBs proposed by Okazaki and Negueruela (2001). This is primarily witnessed through the quantisation of JHK emission, modelling of which also provided evidence for the central cavities which have been described for other systems.

We have observed the dominance of a 1400 day cyclical behaviour in governing this activity, probably the result of a precession of the Be decretion disc at this period. Observed cycles evidenced by varying disc truncation, and diagnosed through line ratios and optical/IR photometry, and the simultaneity of these truncation events with X-ray activity have been extracted from multi-waveband data. The Type II outbursts displayed by this system over the last 15 years both occurred simultaneously with transitions to higher commensurabilities, where the disc shrinks and material is relocated and accretion occurs onto the NS. Some spectroscopic evidence is seen of this mass loss at the 1994 Type II event; photometry and X-ray activity suggest that such transitions between states take place over several orbits. The presence of anomalous (J-K) colours and line profiles from this time strongly hint that the X-ray outburst may have left it's signature in the JHK photometry, and possibly in the He I line profiles.

It would be informative to obtain good (resolution and S/N) archive spectra taken before 1990, ideally during the late 1970s and early 1980s, to shed light upon whether the curent cycles were also occurring then, and whether perhaps truncation was weaker. This should permit a better determination of the cycle period and confirm whether the observed precession period and cycle period are indeed the same; if confirmed, theory will have to show how the precessional period imprints itself upon the disc truncation.

A critical point that has emerged from recent work and is only further compounded here is that BeXRBs are not probes of the circumstellar disc in the traditionally accepted manner. Although the X-ray activity is part of a complete system and BeXRBs undoubtedly inform us of the processes occurring, the NS has far too strong an effect upon the disc to be considered a probe of isolated Be discs.

A full understanding of this baffling system is dragged inevitably closer with the introduction of this framework. Perhaps more importantly, this framework appears to govern the activity of several other, if not all, BeXRBs. A comparison with 4U0115+63 reveals that it's behaviour can be understood as the manifestation of identical processes in a more closely edge-on system.

Looking forward, a more detailed comparison with other systems, in particular 4U0115+63 and systems with good archival photometry, is required. An analysis of the IR photometric history of other BeXRBs in the database to look for quantised behaviour, and lack thereof in isolated Be stars would also represent progress. In particular, such patterns as declining Hα and strengthening He I could be a universal sign of truncation and should be searched for in other similar systems, in view of the general scarcity of long term IR photometry.

The known disc radii obtained in Section 2.6.2.2 can be used to find the luminosity of the disc and thus derive a global temperature in terms of the distance. Further to this constraints upon the colour and luminosity of the possible accretion disc flux will be examined.

A thorough search of the pulse period history should determine whether there are any signs of accretion just prior to disc-loss, and indeed any other times when outbursts were not detected. This should give an indication regarding whether the circumstellar material left the system or was re-accreted (or both).

AX J0051-733 is a superficially ordinary SMC BeXRB, for which optical and IR observations are presented. The relationship between the X-ray source and possible

optical counterparts was discussed, and a previously established likely counterpart confirmed on the basis of excess (Hα-R) flux and astrometry. Spectral classification has shown a good agreement with a B0V standard, in line with the observed range of BeXRB primaries. Long term optical data from over 7 years were presented revealing a near sinusoidal 0.7/1.4d modulation. If attributed to ellipsoidal variations this would place the system in a highly anomalous position on the Corbet diagram, and create problems regarding the necessarily small system dimensions.

This variability displays both amplitude changes and a drift in period which, if due to changes in a binary period, represents unusually rapid evolution. Various models are discussed, none of which are entirely satisfactory. The continued monitoring of this system as part of the ongoing microlensing surveys will in time provide a better picture of the changing photometric period and amplitude, which may improve our picture, but a reasonable understanding of this system appears to be some way off. Studies of intrinsically faint systems such as AX J0051–733 and XTE J0111.2–7317 currently require unrealistic exposure times, even on 2.5-4m class telescopes, to achieve the sorts of S/N needed to investigate the primaries and their circumstellar environment in any kind of detail. The advent of the 10m class SALT at SAAO will hopefully revolutionise studies of distant systems such as these; with it, a radial velocity study of AX J0051–733 could be undertaken to establish what rôle binarity plays in the system, perhaps identifying it as a double-lined spectroscopic binary.

Like AX J0051–733, XTE J0111.2–7317 is a superficially typical SMC BeXRB, but with the peculiarity of being surrounded by an enigmatic nebula, the nature of which is examined. This feature has been shown to be unique in a survey of 15 MC objects. The possibility of this being a stellar wind bowshock with the associated velocity and age information this would have yielded have made this worthy of investigation, as has the further possibility of a SNR identification. The spectral characteristics of this nebulosity eliminated the SNR option based upon line ratios and widths. Photometry suggests extinction higher than typical for the SMC, while

studies of the spatial distribution of line emission from different species strongly suggests a conventional HII interpretation for the nebulosity.

Anomalous IR photometry have suggested the intriguing possibility that this system may possess IR dust emission in common with B[e] systems. The discovery that two other HMXRBs have B[e] primaries make this all the more relevant. However, it appears just as probable that this IR excess may be explicable as IR emission from the nebulosity, or possibly that it is nothing more remarkable than instrumental error. Superior IR imaging photometry, currently awaiting service time on IRIS2 at the AAT, should resolve this dichotomy.

The work that has been undertaken in this thesis, in particular in studying the long term behaviour of A0535+262, surely demonstrates the essential rôle of multi-year, multi-waveband monitoring of such bright systems. Whilst it is undoubtedly possible to learn an enormous amount about some processes with a few nights of excellent data, the forms of variability identified in these pages could not have been seen without quasi-simultaneous spectroscopy and photometry over many years. One only hopes that time allocation commities will continue to be sympathetic to this fact.

Bibliography

Allen, C. W.: 1976, *Astrophysical Quantities*, Astrophysical Quantities, London: Athlone (3rd edition), 1976

Allen, D. A. and Swings, J. P.: 1976, *Astron. Astrophys.* **47**, 293

Alonso, A., Arribas, S., and Martinez-Roger, C.: 1998, *Astron. Astrophys. Suppl. Ser.* **131**, 209

Ankay, A., Kaper, L., de Bruijne, J. H. J., Dewi, J., Hoogerwerf, R., and Savonije, G. J.: 2001, *Astron. Astrophys.* **370**, 170

Baade, D.: 2000, in *ASP Conf. Ser. 214: The Be Phenomenon in Early-Type Stars*, pp 178+

Bailyn, C. D. and Grindlay, J. E.: 1987, *Astrophys. J.* **312**, 748

Balona, L. A.: 1992, *Mon. Not. R. Astron. Soc.* **256**, 425

Balona, L. A.: 2000, in *ASP Conf. Ser. 214: The Be Phenomenon in Early-Type Stars*, pp 1–58381

Bessell, M. S.: 1990, *Publ. Astron. Soc. Pac.* **102**, 1181

Bessell, M. S., Castelli, F., and Plez, B.: 1998, *Astron. Astrophys.* **333**, 231

Blaauw, A.: 1961, *Bull. Astron. Inst. Netherlands* **15**, 265

Blair, W. P. and Long, K. S.: 1997, *Astrophys. J., Suppl. Ser.* **108**, 261

Bouchet, P., Lequeux, J., Maurice, E., Prevot, L., and Prevot-Burnichon, M. L.: 1985, *Astron. Astrophys.* **149**, 330

Briot, D.: 1986, *Astron. Astrophys.* **163**, 67

Briot, D., Robichon, N., and Hubert, A. M.: 1997, in *ESA SP-402: Hipparcos - Venice '97*, Vol. 402, pp 319–322

Buckley, D. A. H., Coe, M. J., Stevens, J. B., van der Heyden, K., Angelini, L., White, N., and Giommi, P.: 2001, *Mon. Not. R. Astron. Soc.* **320**, 281

Chakrabarty, D., Levine, A., Clark, G., Takeshima, T., Wilson, C., and Finger, M.: 1998a, *IAU Circ.* 7048

Chakrabarty, D., Ozaki, M., Paul, B., and Yokogawa, J.: 1998b, *IAU Circ.* 7062

Chevalier, R. A.: 1977, *Ann. Rev. Astron. Astrophys.* **15**, 175

Cioni, M.-R. L., Habing, H. J., and Israel, F. P.: 2000, *Astron. Astrophys.* **358**, L9

Clark, D. H. and Caswell, J. L.: 1976, *Mon. Not. R. Astron. Soc.* **174**, 267

Clark, J., Steele, I., Fender, R., and Coe, M.: 1999, *Astron. Astrophys.* **348**, 888

Clark, J., Tarasov, A., Steele, I., Coe, M., Roche, P., C.Shrader, Buckley, D., Larionov, V., Larionova, L., Lyuty, V., Zaitseva, G., Grunsfeld, J., Fabregat, J., and Parise, R.: 1998, *Mon. Not. R. Astron. Soc.* **294**, 165

Clark, J. S.: 1997, *Ph.D. Thesis, University of Southampton*

Clark, J. S., Lyuty, V. M., Zaitseva, G. V., Larionov, V. M., Larionova, L. V., Finger, M., Tarasov, A. E., Roche, P., and Coe, M. J.: 1999a, *Mon. Not. R. Astron. Soc.* **302**, 167

Clark, J. S., Steele, I. A., Coe, M. J., and Roche, P.: 1998a, *Mon. Not. R. Astron. Soc.* **297**, 657

Clark, J. S., Steele, I. A., Fender, R. P., and Coe, M. J.: 1999b, *Astron. Astrophys.* **348**, 888

Clark, J. S., Tarasov, A. E., Okazaki, A. T., Roche, P., and Lyuty, V. M.: 2001, *Astron. Astrophys.* **380**, 615

Clark, J. S., Tarasov, A. E., Steele, I. A., Coe, M. J., Roche, P., Shrader, C., Buckley, D. A. H., Larionov, V., Larionova, L., Lyuty, V. M., Zaitseva, G. V., Grunsfeld, J., Fabregat, J., and Parise, R.: 1998b, *Mon. Not. R. Astron. Soc.* **294**, 165

Coe, M., Carpenter, G., Engel, A., and Quenby, J.: 1975, *Nature* **256**, 630

Coe, M., Haigh, N., and Reig, P.: 2000, *Mon. Not. R. Astron. Soc.* **314**, 290

Coe, M. J.: 2000, in *ASP Conf. Ser. 214: The Be Phenomenon in Early-Type Stars*, p. 656

Coe, M. J., Buckley, D. A. H., Negueruela, I., Corbet, R. H. D., Reig, P., and Haigh, N. J.: 2000, *AAS/High Energy Astrophysics Division* 32

Coe, M. J. and Orosz, J. A.: 2000, *Mon. Not. R. Astron. Soc.* **311**, 169

Comeron, F. and Kaper, L.: 1998, *Astron. Astrophys.* **338**, 273

Cook, K.: 1998, *IAU Circ.* 6860

Corbet, R. H. D.: 1986, *Mon. Not. R. Astron. Soc.* **220**, 1047

Covino, S., Negueruela, I., Campana, S., Israel, G., Polcaro, V., Stella, L., and Verrecchia, F.: 2001, *astro-ph/0105555*

Cowley, A. P., Schmidtke, P. C., McGrath, T. K., Ponder, A. L., Fertig, M. R., Hutchings, J. B., and Crampton, D.: 1997, *Publ. Astron. Soc. Pac.* **109**, 21

Dachs, J., Hanuschik, R., Kaiser, D., and Rohe, D.: 1986, *Astron. Astrophys.* **159**, 276

Dachs, J., Kiehling, R., and Engels, D.: 1988, *Astron. Astrophys.* **194**, 167

de Loore, C., Giovannelli, F., van Dessel, E. L., Bartolini, C., Burger, M., Ferrari-Toniolo, M., Giangrande, A., Guarnieri, A., Hellings, P., Hensberge, H., Persi, P., Piccioni, A., and van Diest, H.: 1984, *Astron. Astrophys.* **141**, 279

Delgado-Marti, H., Levine, A., Pfahl, E., and Rappaport, S.: 2000, *astro-ph/0004258*

Demartino, D., Waters, L. B. F. M., Giovannelli, F., Bartolini, C., Guarnieri, A., and Piccioni, C.: 1989, in *Two Topics in X-Ray Astronomy, Volume 1: X Ray Binaries. Volume 2: AGN and the X Ray Background*, pp 521–523

Doazan, V., Bourdonneau, B., and Thomas, R. N.: 1988, *Astron. Astrophys.* **205**, L11

Doazan, V., Stalio, R., and Thomas, R. N.: 1982, in *IAU Symp. 98: Be Stars*, Vol. 98, p. 489

Dopita, M. A.: 1977, *Astrophys. J., Suppl. Ser.* **33**, 437

Dopita, M. A., Binette, L., Dodorico, S., and Benvenuti, P.: 1984, *Astrophys. J.* **276**, 653

Dougherty, S. M. and Taylor, A. R.: 1992, *Nature* **359**, 808

Dougherty, S. M., Waters, L. B. F. M., Burki, G., Cote, J., Cramer, N., van Kerk-

wijk, M. H., and Taylor, A. R.: 1994, *Astron. Astrophys.* **290**, 609

Ducati, J. R., Bevilacqua, C. M., Rembold, S. B., and Ribeiro, D.: 2001, *Astrophys. J.* **558**, 309

Eggleton, P. and Kiseleva, L.: 1995, *Astrophys. J.* **455**, 640

Eyles, C. J., Skinner, G. K., Willmore, A. P., Rosenberg, F. D., and Berthelsdorf, R.: 1975, *IAU Circ.* 2774

Fabregat, J. and Reig, P.: 1996, *Publ. Astron. Soc. Pac.* **108**, 90

Fabregat, J. and Torrejón, J. M.: 2000, *Astron. Astrophys.* **357**, 451

Fabregat, J. and Torrejon, J. M.: 1998, *Astron. Astrophys.* **332**, 643

Fabregat, J., Torrejon, J. M., Reig, P., Bernabeu, G., Busquets, J., Marco, A., and Reglero, V.: 1996, *Astron. Astrophys.* **119**, 271

Feast, M.: 1961, *Mon. Not. R. Astron. Soc.* **122**, 1

Fesen, R. A., Blair, W. P., and Kirshner, R. P.: 1985, *Astrophys. J.* **292**, 29

Finger, M. H., Wilson, R. B., and Hagedon, K. S.: 1994, *IAU Circ.* 5931

Finger, M. H., Wilson, R. B., and Harmon, B. A.: 1996, *Astrophys. J.* **459**, 288

Fitzpatrick, E. L.: 1999, *Publ. Astron. Soc. Pac.* **111**, 63

Gaustad, J. E., McCullough, P. R., Rosing, W., and Van Buren, D.: 2001, *Publ. Astron. Soc. Pac.* **113**, 1326

Gehrz, R. D., Hackwell, J. A., and Jones, T. W.: 1974, *Astrophys. J.* **191**, 675

Gibson, B.: 1999, *astro-ph/9910574*

Gies, D. R.: 2000, in *ASP Conf. Ser. 214: The Be Phenomenon in Early-Type Stars*, p. 668

Gies, D. R., Bagnuolo, W. G., Ferrara, E. C., Kaye, A. B., Thaller, M. L., Penny, L. R., and Peters, G. J.: 1998, *Astrophys. J.* **493**, 440

Giovannelli, F., Ferrari-Toniolo, M., Persi, P., Bartolini, C., Guarnieri, A., Piccioni, A., Vandessel, E. L., Burger, M., Deloore, C., and Bisnovatyi-Kogan, G. S.: 1984, in *Fourth European IUE Conference*, pp 439–442

Giovannelli, F. and Graziati, L. S.: 1992, *Space Science Reviews* **59**, 1

Giovannelli, F., Kurt, V. G., and Sheffer, E. K.: 1986, *IAU Circ.* 4284

Giovannelli, F., Kurt, V. G., and Sheffer, E. K.: 1987, *IAU Circ.* 4368

Giovannelli, F., Sabau-Graziati, L., Bernabei, S., and Galleti, S.: 1999, *IAU Circ.* 7293

Giovannneli, F., Ferrari-Toniolo, M., Bartolini, C., Guarnieri, A., Rucinski, S. M., Giangrande, A., Persi, P., and Piccioni, A.: 1980, in *ESA 2nd European IUE Conf.*, pp 159–164

Graff, D. S. and Gould, A. P.: 2000, *Astrophys. J., Lett.* **534**, L51

Gray, R. O.: 1998, *Astron. J.* **116**, 482

Gregory, P. C., Xu, H., Backhouse, C. J., and Reid, A.: 1989, *Astrophys. J.* **339**, 1054

Gulliver, A. F.: 1977, **35**, 441

Gummersbach, C., Zickgraf, F.-J., and Wolf, B.: 1995, *Astron. Astrophys.* **302**, 409

Haberl, F. and Sasaki, M.: 2000, *Astron. Astrophys.* **359**, 573

Haigh, N., Coe, M., Steele, I., and Fabregat, J.: 1999, *Mon. Not. R. Astron. Soc.* **310**, L21

Hanuschik, R. W., Dachs, J., Baudzus, M., and Thimm, G.: 1993, *Astron. Astrophys.* **274**, 356

Hanuschik, R. W., Hummel, W., Dietle, O., and Sutorius, E.: 1995, *Astron. Astrophys.* **300**, 163

Hao, J.-X., Huang, L., and Guo, Z. H.: 1996, *Astron. Astrophys.* **308**, 499

Harmanec, P.: 1998, *Astron. Astrophys.* **334**, 558

Hayakawa, S.: 1981, *Space Sci. Rev.* **29**, 22

Hollis, J., Oliversen, R., Wagner, R., and Feibelman, W.: 1992, *Astrophys. J.* **393**, 217

Hony, S., Waters, L. B. F. M., Zaal, P. A., de Koter, A., Marlborough, J. M., Millar, C. E., Trams, N. R., Morris, P. W., and de Graauw, T.: 2000, *Astron. Astrophys.* **355**, 187

Huang, S.: 1963, *Astrophys. J.* **138**, 471

Huang, S.: 1972, *Astrophys. J.* **171**, 549

Hughes, J. and Smith, R.: 1994, *Astron. J.* **107**, 1363

Hummel, W.: 1998, *Astron. Astrophys.* **330**, 243

Huthoff, F. and Kaper, L.: 2002, *Astron. Astrophys.* **383**, 999

Imanishi, K., Yokogawa, J., Tsujimoto, M., and Koyama, K.: 1999, *Publ. Astron. Soc. Jpn.* **51**, L15

in't Zand, J. J. M., Swank, J., Corbet, R. H. D., and Markwardt, C. B.: 2001, *Astron. Astrophys.* **380**, L26

Israel, G., Stella, L., Covino, S., Campana, S., and Mereghetti, S.: 1999, *IAU Circ.* 7101

Israel, G. L., Campana, S., Covino, S., Dal Fiume, D., Gaetz, T. J., Mereghetti, S., Oosterbroek, T., Orlandini, M., Parmar, A. N., Ricci, D., and Stella, L.: 2000, *Astrophys. J., Lett.* **531**, L131

Janot-Pacheco, E., Motch, C., and Mouchet, M.: 1987, *Astron. Astrophys.* **177**, 91

Jenniskens, P. and Desert, F.-X.: 1994, *Astron. Astrophys. Suppl. Ser.* **106**, 39

Kahabka, P.: 1998, *IAU Circ.* **6854**, 2

Kahabka, P. and Pietsch, W.: 1996, *Astron. Astrophys.* **312**, 919

Kaper, L., Loon, J. T. V., Augusteijn, T., Goudfrooij, P., Patat, F., Waters, L., and Zijlstra, A.: 1997, *Astrophys. J.* **475**, L37

Kitchin, C. R.: 1987, *Stars, nebulae and the interstellar medium. Observational physics and astrophysics*, Bristol: Hilger, 1987

Koornneef, J.: 1983, *Astron. Astrophys.* **128**, 84

Kurucz, R.: 1979, *Astrophys. J., Suppl. Ser.* **40**, 1

Lai, B.: 2000, *astro-ph/0012049*

Lamers, H., Zickgraf, F.-J., de Winter, D., Houziaux, L., and Zorec, J.: 1998, *Astron. Astrophys.* **340**, 117

Lamers, H. J. G. L. M., Harzevoort, J. M. A. G., Schrijver, H., Hoogerwerf, R., and Kudritzki, R. P.: 1997, *Astron. Astrophys.* **325**, L25

Larionov, V., Lyuty, V. M., and Zaitseva, G. V.: 2001, *Astron. Astrophys.* **378**, 837

Leonard, P. J. T.: 1995, *Mon. Not. R. Astron. Soc.* **277**, 1080

Liller, W.: 1975, *IAU Circ.* 2780

Lozinskaia, T. A.: 1980, *Astron. Astrophys.* **84**, 26

Lyuty, V. M. and Zaitseva, G. V.: 2000, *VizieR Online Data Catalog*

Lyuty, V. M., Zaitseva, G. V., and Latysheva, I. D.: 1989, *Soviet Astronomy Letters* **15**, 182

Lyuty, V. M. and Zaĭtseva, G. V.: 2000, *Astronomy Letters* **26**, 9

Maeder, A. and Meynet, G.: 2001, *Astron. Astrophys.* **373**, 555

Manfroid, J.: 1993, *Astron. Astrophys.* **271**, 714

Martins, F., Schaerer, D., and Hillier, D. J.: 2002, *Astron. Astrophys.* **382**, 999

Mathewson, D. S.: 1985, *Proceedings of the Astronomical Society of Australia* **6**, 104

Mazzali, P. A., Lennon, D. J., Pasian, F., Marconi, G., Baade, D., and Castellani, V.: 1996, *Astron. Astrophys.* **316**, 173

Megessier, C.: 1995, *Astron. Astrophys.* **296**, 771

Meinel, A. B., Aveni, A. F., and Stockton, M. W.: 1965, *Catalog of emission lines in astrophysical objects*, Optical Sciences Center Technical Report, Tucson: University Arizona, Optical Sciences Center and Steward Observatory, 1965, 2nd ed.

Mennickent, R. E. and Vogt, N.: 1991, *Astron. Astrophys.* **241**, 159

Motch, C., Stella, L., Janot-Pacheco, E., and Mouchet, M.: 1991, *Astrophys. J.* **369**, 490

Negueruela, I.: 1998, *Astron. Astrophys.* **338**, 505

Negueruela, I., Grove, J. E., Coe, M. J., Fabregat, J., Finger, M. H., Phlips, B. F., Roche, P., Steele, I. A., and Unger, S. J.: 1997, *Mon. Not. R. Astron. Soc.* **284**, 859

Negueruela, I. and Okazaki, A. T.: 2001, *Astron. Astrophys.* **369**, 108

Negueruela, I., Okazaki, A. T., Fabregat, J., Coe, M. J., Munari, U., and Tomov, T.: 2001, *Astron. Astrophys.* **369**, 117

Negueruela, I., Reig, P., Coe, M. J., and Fabregat, J.: 1998, *Astron. Astrophys.* **336**, 251

Negueruela, I., Roche, P., Fabregat, J., and Coe, M. J.: 1999, *Mon. Not. R. Astron. Soc.* **307**, 695

Noriega-Crespo, A. and Garnavich, P. M.: 1992, *American Astronomical Society*

Meeting **181**, 1147

Noriega-Crespo, A., van Buren, D., Cao, Y., and Dgani, R.: 1997a, **114**, 837

Noriega-Crespo, A., van Buren, D., and Dgani, R.: 1997b, *Astron. J.* **113**, 780

Norton, A. J., Coe, M. J., Estela, A., Fabregat, J., Gorrod, M. J., Kastner, J., Payne, B. J., Reglero, V., Roche, P., and Unger, S. J.: 1991, *Mon. Not. R. Astron. Soc.* **253**, 579

Ogilvie, G. I. and Dubus, G.: 2001, *Mon. Not. R. Astron. Soc.* **320**, 485

Okazaki, A. T.: 1991, *Publ. Astron. Soc. Jpn.* **43**, 75

Okazaki, A. T.: 1998, in *IAU Symp. 188: The Hot Universe*, Vol. 188, p. 362

Okazaki, A. T.: 2001, *http://harmas.arc.hokkai-s-u.ac.jp/ okazaki/BeX/sim/*

Okazaki, A. T. and Negueruela, I.: 2001, *Astron. Astrophys.* **377**, 161

Osterbrock, D. E.: 1989, *Astrophysics of gaseous nebulae and active galactic nuclei*, Research supported by the University of California, John Simon Guggenheim Memorial Foundation, University of Minnesota, et al. Mill Valley, CA, University Science Books, 1989, 422 p.

Peppel, U.: 1984, *Astron. Astrophys. Suppl. Ser.* **57**, 107

Persi, P., Ferrari Toniolo, M., and Spada, G.: 1979, in *IAU Symp. 83: Mass Loss and Evolution of O-Type Stars*, Vol. 83, pp 139–142

Piccioni, A., Bartolini, C., Bernabei, S., and et al.: 1998, in *Vulcano workshop 1998: Frontier objects in Astrophysics and Particle physics.*

Piccioni, A., Bartolini, C., Bernabei, S., and et al.: 2000, in *ASP Conf. Ser. 214: The Be Phenomenon in Early-Type Stars*, p. 569

Porter, J. M.: 1996, *Mon. Not. R. Astron. Soc.* **280**, L31

Porter, J. M.: 1999, *Astron. Astrophys.* **348**, 512

Priedhorsky, W. C. and Terrell, J.: 1983, *Nature* **303**, 681

Puxley, P. J., Beard, S. M., and Ramsay, S. K.: 1992, in *DATA ANALYSIS WORKSHOP - 4TH ESO/ST-ECF GARCHING P. 117, 1992*, p. 117

Quirrenbach, A., Bjorkman, K. S., Bjorkman, J. E., Hummel, C. A., Buscher, D. F., Armstrong, J. T., Mozurkewich, D., Elias, N. M., and Babler, B. L.: 1997, *Astrophys. J.* **479**, 477

Quirrenbach, A., Buscher, D. F., Mozurkewich, D., Hummel, C. A., and Armstrong, J. T.: 1994, *Astron. Astrophys.* **283**, L13

Raga, A. C., Noriega-Crespo, A., Cantó, J., Steffen, W., van Buren, D., Mellema, G., and Lundqvist, P.: 1997, *Revista Mexicana de Astronomia y Astrofisica* **33**, 73

Reig, P., Fabregat, J., and Coe, M. J.: 1997, *Astron. Astrophys.* **322**, 193

Reig, P., Negueruela, I., Coe, M. J., Fabregat, J., Tarasov, A. E., and Zamanov, R. K.: 2000, *Mon. Not. R. Astron. Soc.* **317**, 205

Reig, P. and Roche, P.: 1999, *Mon. Not. R. Astron. Soc.* **306**, 100

Rivinius, T., Baade, D., Stefl, S., Stahl, O., Wolf, B., and Kaufer, A.: 1998a, *Astron. Astrophys.* **336**, 177

Rivinius, T., Baade, D., Stefl, S., Stahl, O., Wolf, B., and Kaufer, A.: 1998b, *Astron. Astrophys.* **333**, 125

Rivinius, T., Baade, D., Štefl, S., and Maintz, M.: 2001, *Astron. Astrophys.* **379**, 257

Roche, P., Coe, M. J., Fabregat, J., McHardy, I. M., Norton, A. J., Percy, J. R., Reglero, V., Reynolds, A., and Unger, S. J.: 1993, *Astron. Astrophys.* **270**, 122

Rosenberg, F., Eyles, C., Skinner, C., and Willmore, A.: 1975, *Nature* **256**, 628

Rucinski, S. M.: 1997, **113**, 407

Saraph, H. E. and Seaton, M. J.: 1970, *Mon. Not. R. Astron. Soc.* **148**, 367

Schaerer, D. and de Koter, A.: 1997, *Astron. Astrophys.* **322**, 598

Schmidtke, P. C. and Cowley, A. P.: 1998, *IAU Circ.* 6880

Sims, M. R. and Fraser, G. W.: 1979, *IAU Circ.* 3339

Slettebak, A., Wagner, R. M., and Bertram, R.: 1997, *Publ. Astron. Soc. Pac.* **109**, 1

Smith, M. A.: 2000, in *ASP Conf. Ser. 214: The Be Phenomenon in Early-Type Stars*, p. 292

Stee, P. and Bittar, J.: 2001, *Astron. Astrophys.* **367**, 532

Stee, P., Vakili, F., Bonneau, D., and Mourard, D.: 1998, *Astron. Astrophys.* **332**, 268

Steele, I., Negueruela, I., Coe, M., and Roche, P.: 1998, *Astron. Astrophys.* **297**, L5

Stella, L., White, N. E., and Rosner, R.: 1986, *Astrophys. J.* **308**, 669

Stevens, J. B.: 2000, *Ph.D. Thesis, University of Southampton*

Stevens, J. B., Reig, P., Coe, M. J., Buckley, D. A. H., Fabregat, J., and Steele, I. A.: 1997, *Mon. Not. R. Astron. Soc.* **288**, 988

Stone, R. C.: 1979, *Astrophys. J.* **232**, 520

Struve, O.: 1931, *Astrophys. J.* **73**, 94

Takami, M., Bailey, J., Gledhill, T., Chrysostomou, A., and Hough, J.: 2001, *astro-ph/0103311*

Tarasov, A. and Roche, P.: 1995, *Mon. Not. R. Astron. Soc.* **276**, L19

Telting, J., Waters, L., Roche, P., Boogert, A., Clark, J., de Martino, D., and Persi, P.: 1998, *Mon. Not. R. Astron. Soc.* **296**, 785

Telting, J. H., Waters, L. B. F. M., Persi, P., and Dunlop, S. R.: 1993, *Astron. Astrophys.* **270**, 355

Torrejon, J. M., Fabregat, J., Bernabeu, G., and Alba, S.: 1997, *Astron. Astrophys.* **124**, 329

Turner, D. G.: 1990, *Publ. Astron. Soc. Pac.* **102**, 1331

Vacca, W. D., Garmany, C. D., and Shull, J. M.: 1996, *Astrophys. J.* **460**, 914

Vakili, F., Mourard, D., Stee, P., Bonneau, D., Berio, P., Chesneau, O., Thureau, N., Morand, F., Labeyrie, A., and Tallon-Bosc, I.: 1998, *Astron. Astrophys.* **335**, 261

van Buren, D. and McCray, R.: 1988, *Astrophys. J., Lett.* **329**, L93

van Buren, D., Noriega-Crespo, A., and Dgani, R.: 1995, **110**, 2914

van den Heuvel, E. P. J.: 1983, in *Accretion-Driven Stellar X-ray Sources*, pp 303–341

van den Heuvel, E. P. J., Portegies Zwart, S. F. B. D., and Kaper, L.: 2000, *Astron. Astrophys.* **364**, 563

van Hamme, W., Wilson, R. E., and Guinan, E. F.: 1995, **110**, 1350

van Oijen, J. G. J.: 1989, *Astron. Astrophys.* **217**, 115

Vink, J. S., de Koter, A., and Lamers, H. J. G. L. M.: 2000, *Astron. Astrophys.*

362, 295

Vink, J. S., de Koter, A., and Lamers, H. J. G. L. M.: 2001, *Astron. Astrophys.* **369**, 574

Walborn, N. R. and Fitzpatrick, E. L.: 1990, *Publ. Astron. Soc. Pac.* **102**, 379

Wang, Z. X. and Gies, D. R.: 1998, *Publ. Astron. Soc. Pac.* **110**, 1310

Waters, L. B. F., Marlborough, J. M., van der Veen, W. E. C., Taylor, A. R., and Dougherty, S. M.: 1991, *Astron. Astrophys.* **244**, 120

Wegner, W.: 1994, *Mon. Not. R. Astron. Soc.* **270**, 229

Wijers, R. A. M. J. and Pringle, J. E.: 1999, *Mon. Not. R. Astron. Soc.* **308**, 207

Wilson, R. B., Finger, M. H., Gibby, L., and Fishman, G. J.: 1993, *IAU Circ.* 5833

Winkler, H.: 1997, *Mon. Not. R. Astron. Soc.* **287**, 481

Yokogawa, J. and Koyama, K.: 1998, *IAU Circ.* 6853

Yokogawa, J., Paul, B., Ozaki, M., Nagase, F., Chakrabarty, D., and Takeshima, T.: 2000, *astro-ph/0003251*

Yudin, R. V.: 2001, *Astron. Astrophys.* **368**, 912

Zaal, P. A., Waters, L. B. F. M., and Marlborough, J. M.: 1995, *Astron. Astrophys.* **299**, 574

Zamanov, R. K., Reig, P., Martí, J., Coe, M. J., Fabregat, J., Tomov, N. A., and Valchev, T.: 2001, *Astron. Astrophys.* **367**, 884

Zaritsky, D., Harris, J., Grebel, E. K., and Thompson, I. B.: 2000, *Astrophys. J., Lett.* **534**, L53

Zickgraf, F.: 2000, in *ASP Conf. Ser. 214: The Be Phenomenon in Early-Type Stars*, p. 26

Zorec, J. and Briot, D.: 1991, *Astron. Astrophys.* **245**, 150

Zorec, J. and Briot, D.: 1997, *Astron. Astrophys.* **318**, 443

Chapter 6

Acknowledgements!

Anyone who knows me will confirm that without Malcolm Coe's encouragement, cheerful supervision and subtle goading this work would still be a far off dream (nightmare?) and I'd be on a beach somewhere. I haven't made it easy, so I'd be a cad if I didn't express my profound gratitude! Cheers Malcolm.

In a similar vein, Simon Clark has been a source of sage advice and wisdom throughout, and has frequently gone out of his way to offer help and guidance when under no obligation to do so. And like me he shows an incautious disregard for the conventionally accepted limits of the coiffeur's art.

There are a lot of spectra in this thesis, and if you took them out it just wouldn't be the same. So a rousing cheer please for Don Pollacco and the good people at the ING Service Programme, Douglas Gies, Luisa Morales and Pierre Maxted for understanding just why A0535+262 is *so* important. And if anyone else is off observing, I've still got a stack of finders.

There have been occasions, just one or two, when I've tested the patience of those around me during the last few months (years?). Taj, without your relaxed, calming almost Buddha-like influence I'd never have understood the whole cup of tea and a

benson philosophy or heard the tunes of ninja's, and certainly wouldn't have spent half as much time on the physics roof whinging.

To the massed ranks of Soton Astro, both past and present, you've been a great bunch so take a lesson from me and stop publishing so much. In particular those with whom I've shared this magical office, steeped in history, and who have tolerated my faults and LaTeX queries. All the best Pablo, Rach, Silas, Edouardo, Luisa, Carolyn, William and ....Jimbo, you thanked me, and now it falls to me to return the honour. It was indeed a trip, as they all were. Thanks for letting me inherit your chair and the best bit of real estate in 4075.

To all of my family, I hope you don't mind having supported my 28 year dalliance with the education system. Thanks for, well, everything!

To my men of action; Matt, Gilleth, Scifi, Mumbly, Tracy (sorry) and the rest of you for taking me surfing a thousand times, often at a reduced rate; for sharing freezing dawnies, roast chickens in the car, swiss rolls, hangovers, drop-ins, 1ft Highcliffe and going right on lefts.

Phil, how I can have such trust in and respect for a man with 10,000 dead things in his bedroom is a mystery but there you go. Thanks for being a great mate all this time. Typhis pungens!

Lena, you've been a source of calm, happiness and friendship in a generally disturbing world, and long may it be so. Thanks for being around. Similarly Hugh, you've taken my mind off the heavens with talk of melancholy, renaissance perversions and splenneticke bile.

Jenny, word's definitely fail me here but you've been an outright goddess and a pillar of strength throughout this, dare I say it, ordeal. Quite why I'll probably never know, but for now I'll just say a huge thanks for everything.

Can I go home now?